Preparation, Characterisation and Application of QTC Inks

By

Qi Meng

Submitted in accordance with the requirements for the degree of
Doctor of Philosophy

The University of Leeds
Department of Colour and Polymer Chemistry

September, 2015

The candidate confirms that the work submitted is his/her own and that appropriate credit has been given where reference has been made to the work of others.

Acknowledgements

I would never have been able to finish my thesis without the guidance from my supervisor and group members, the help from my friends and the support from my family.

I would like to express my deepest gratitude to my supervisor, Prof. Long Lin, for his excellent guidance, caring, patience and providing me with an excellent atmosphere for doing research. I would like to thank Long for giving me such an amazing opportunity to study in the University of Leeds during my PhD. His knowledge, encouragement, optimism and enthusiasm have been of utmost importance.

I am grateful to Peratech Ltd. for the financial support enabling me to carry out this study. I would like to thank Mr David Lussey and Dr. Adam Graham for the supervision of the study during the first two years. My gratitude goes to Mr David Lussey for his support, encouragement, approval, guidance and numerous fruitful conversations during the supervision.

I would like to thank all the people from the Department of Colour and Polymer Science. I would like to say a sincere "thank you" to Prof. Jim Guthrie, who patiently and carefully corrected my bad writing. I would like to thank Dr. Algy Kazlauciunas's kind help and suggestions for all the technical analysis, SEM, TGA and DLS. I want to thank Dr. Saminu Magami for his support, encouragement, spirit and kindness. Also, I would like to thank Dr. Mohammed Ali for his advice and help. I would like to thank my PhD company, Sam Hill, for his optimism, friendliness and chats. I also want to thank other group members, Andy Brown, Dr. Wajiha Abbasi, Xujun Luo, Leighton Jones and Peng Huang. It would not have been such a lovely group without them.

I would like to thank all the friends that I met in the UK, especially Dr. Yuhan Zhao, Dr. Yunwei Wang, Chantal Smyth and James Dawson for all the happiness and memories.

Finally, I would like to say a big "thank you" and "I love you" to my parents. They are always supporting me and encouraging me without any conditions.

Abstract

Quantum Tunnelling Composites (QTC) have attractive mechanical-electrical properties and have found applications in a number of advanced technologies such as the touch-sensitive finger-tips on the gloves of the NASA space suits. There was a demand to apply QTC materials to consumer products such as credit cards, *via* a conventional printing process. The challenge, however, was that QTC materials only functioned properly at high solid loadings (thus very high viscosity) and as thick films. Hence, the aim of the study described in this thesis was to develop a series of QTC inks that would be printable *via* conventional printing technologies such as screen printing, meanwhile, these inks would be potentially applied as an electrical switch in the RFID card, sportswear, games and *etc.* To date, several screen printable functional inks, each containing a combination of conductive spiky-like nickel particles, three grades of semiconducting titanium dioxides particles and a range of water-based binders, have been formulated and used to study the electrical properties of the QTC inks. Relevant experimental designs, interpretation of the property-composition relationships, modelling of the electrical-mechanical properties and a strategy for the optimisation of the QTC inks, are all presented in this thesis.

When QTC materials are quiescent, the metal particles are well separated from each other. This leads to the QTC material behaves as an insulator. An increase in applied compression on the QTC material results in a lower electrical resistance through it. This is because the electrons from the metal particles can "hop" from one to the other with or without touching. This is known as "quantum tunnel effect", arising because the nickel particles can build a high electric charge field on the spike tips.

Detailed in this thesis, are a series of comprehensive investigations of the pressure-sensitive response of a printed film, and the contribution of each component to the formulation in terms of printability, electrical property, rheology, thermal stability and the mechanical properties. It was found that the printed film behaved as an insulator in the absence of external compression, even when the nickel filler content was well above the expected percolation threshold. The electrical resistance of the printed film decreased, up to 10 orders of magnitude, with an increase in external compression. This dramatic resistance variation was

explained by the quantum tunnelling mechanism and percolation mechanism, which were mainly dependent on the nickel loading, the distribution of the nickel particles and nickel aggregates, the morphology of the nickel particles and the elasticity of a polymer matrix. Furthermore, it was found that at least one grade of titanium dioxide could be used to reduce the sensitivity of electrical resistance of the printed film.

Moreover, a model of the response of the electrical properties an external compression of the printed QTC films has been successfully developed. This permits quantification of the relationship between the electrical properties and the structure of the composite. This model was most applicable to the printed composite film for the prediction of the electrical-mechanical properties of the nickel particles randomly dispersed in a polymeric matrix.

Table of Contents

List of Tables

List of Figures

List of Equations

List of Abbreviations

QTC	Quantum Tunnelling Composite
RFID	Radio-frequency identification
LCD	Liquid crystal display
TFT	Thin-film transistor
AMOLED	Active matrix organic light-emitting diode
ITO	Indium Tin oxide
PV	Photovoltaic
FET	Field effect transistors
PVP	Poly(vinylpyrrolidone)
ICP	Intrinsically conducting polymer
CPC	Conductive polymer composites
PPV	Poly(p-phenylene vinylene)
EMT	Effective medium theory
GEM	General effective medium
LNB	Links-Nodes-Blobs
PVP-S	Poly(1-vinyl pyrrolidone-*co*-styrene)
PET	Poly(ethylene terephthalate)
PTFE	Poly(tetrafluoroethylene)
IPA	Isopropyl alcohol
PSE1	Silicone modified polyurethane emulsion
PSE2	Poly(disiloxane) emulsion
PIP	Poly(isoprene)

Chapter 1. General introduction

Recent advances in the field of printed electronics have enabled a significant revolution in electronic technology to take place. Printed electronics cover a series of printing methods, for fabrication of electronic devices on a variety of substrates. Printing processes, especially screen printing, reduce the costs of manufacture, the number of processing steps and contamination of the environment dramatically, compared with traditional electronic fabrication processes [1]. These electronic devices or parts are lightweight, small and thin, flexible, cheap and disposable [2]. However, despite recent developments in printed electronics, the technology is still not sufficiently advanced. The use of printed electronics in daily life is expected to increase in value to more than $300 billion by 2030 [3-6]. Printed electronics have seen application in a variety of areas. Examples include mobile devices, e-readers, flexible displays, sports equipment, apparatus and sportswear, healthcare technologies, toys, games and security products [9-13]. Hence, the combination of an efficient printing process and improved electronics technologies is envisaged to facilitate an increase in the productivity and value in the use of such materials.

Quantum Tunnelling Composite (QTC) materials were invented by Lussey in 1996 and commercialised, in 2006, by the UK-based company, Peratech Ltd. [7]. A QTC is an elastic material that is designed to be extremely sensitive to a large number of different types of mechanical pressure that can be applied either directly or by remote manipulation [8]. When QTC materials are quiescent, they behave as electrical insulators. When mechanical pressure is applied, a change is effected and the materials become electrically conductive. With such properties, QTC materials have the potential to be employed in a vast range of applications commercial, industrial and scientific, including switches or sensors. One of the more widespread applications of QTC materials is in wearable electronics as a switch. Contemporary applications include the newly designed Samsung Navikey mobile telephone for menu navigation [9], radio-frequency identification (RFID) chip security protection [10], and applications as tactile sensors for robotic hands [11-13] used by NASA [14].

1.1 Printed electronic devices

The printing of fabricated objects has the potential to revolutionise the electronic applications of nearly every consumer good, due to a number of inherent benefits [15, 16]. They can be used in a vast number of areas, such as conductors [16], semi-conductors [15], dielectrics [17], luminescent [18], electrochromic [19], electrophoretic [20] and other functional materials. With these various applications, electronic technology is emerging our daily life, such as small games on the packages [21], intelligent displays on the magazines and bendable E-book readers [4].

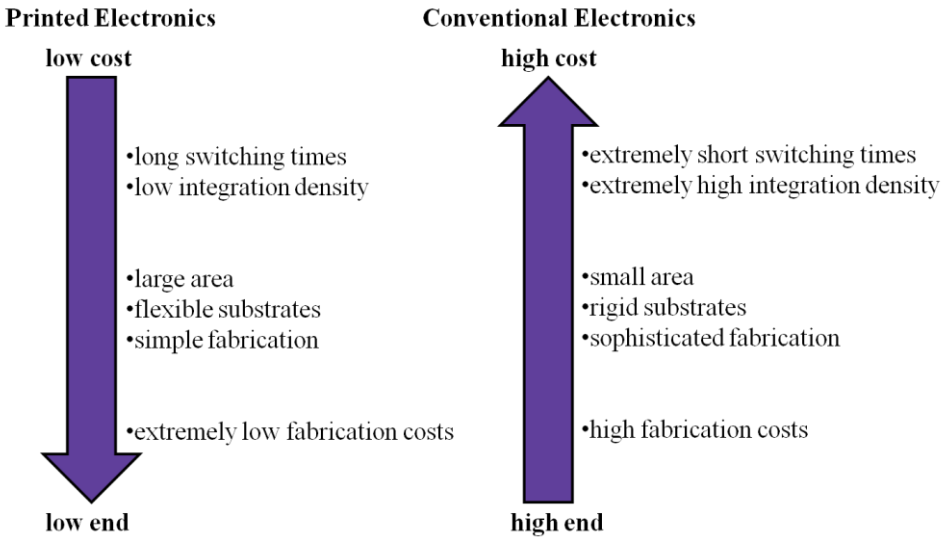

Figure 1.1 Printed electronics and conventional silicon-based electronics as complementary technologies [2]

Printed electronics are not a replacement for conventional silicon-based electronics, however, they are anticipated to open a new area of low cost printed circuits and also it acts as a complementary technology to conventional silicon-based electronics. Figure 1.1 compares printed electronics with conventional electronics [2]. Electronic devices are usually fabricated using carbon-based or organic materials, rather than traditional expensive and complex to produce silicon-based or inorganic materials [22-24]. Thus, the uses of printed materials in the production of printed electronics lead to significant advantages over traditional electronic fabrication processes, *e.g.* low production costs, large-area electronics,

greater productivity, more rapid printing process, superior resolution and a reduced environmental impact [15, 25-27].

1.1.1 Predicted growth of printed electronics market

The printed electronics market mainly consists of lighting, sensors, photovoltaic integrated displays and smart packaging. The predicted bright future for printed electronics has clearly attracted a number of industries, such as BASF, Dow Corning, DuPont Microcircuit Materials, Evonik Fujihilm Dimatix, Henkel, InkTec Co Ltd. Thin Film Electronics, NovaCentrix, Soligie, Ceradrop and so on. Printed electronics enter into new, diverse applications, for instance, in consumer goods, in healthcare products, electronics, media, mobility and architecture. IDTechEx, market researchers, estimated that the market for printed, flexible and organic electronics will grow rapidly to $35 billion in 2020 and $300 billion by 2030 [6]. Figure 1.2 displays the predicted growth of major components for the printed electronics' market from 2015 to 2021 [28].

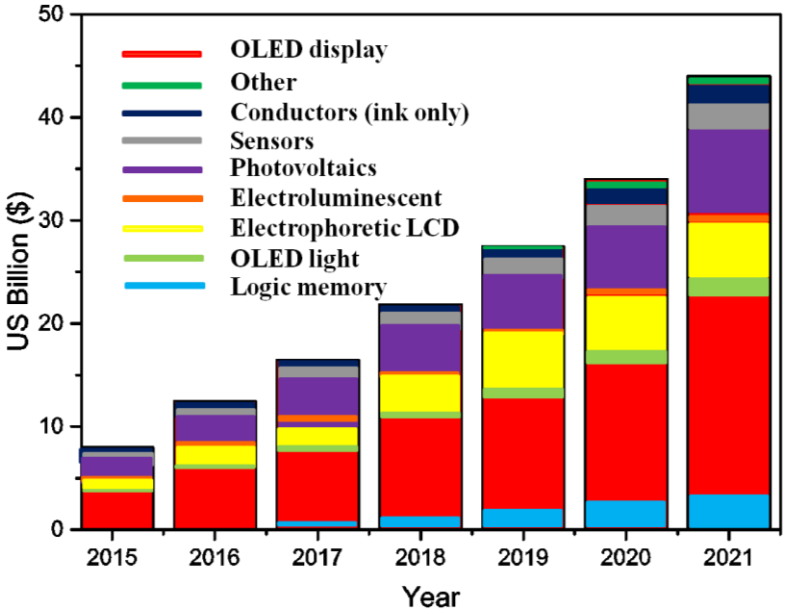

Figure 1.2 The growth of major components for the printed electronics' market from 2015 to 2021 by IDTechEx Market research [28]. Each colour represents a key application in printed electronic market

Figure 1.3 shows the growth of flexible applications based on printed electronics technologies from 2015 to 2020. As can be seen, the world market for

flexible electronics applications should be significantly greater by 2020 than it was in 2015, particularly with respect to OLED lighting system and displays, sensors and electronic papers [29].

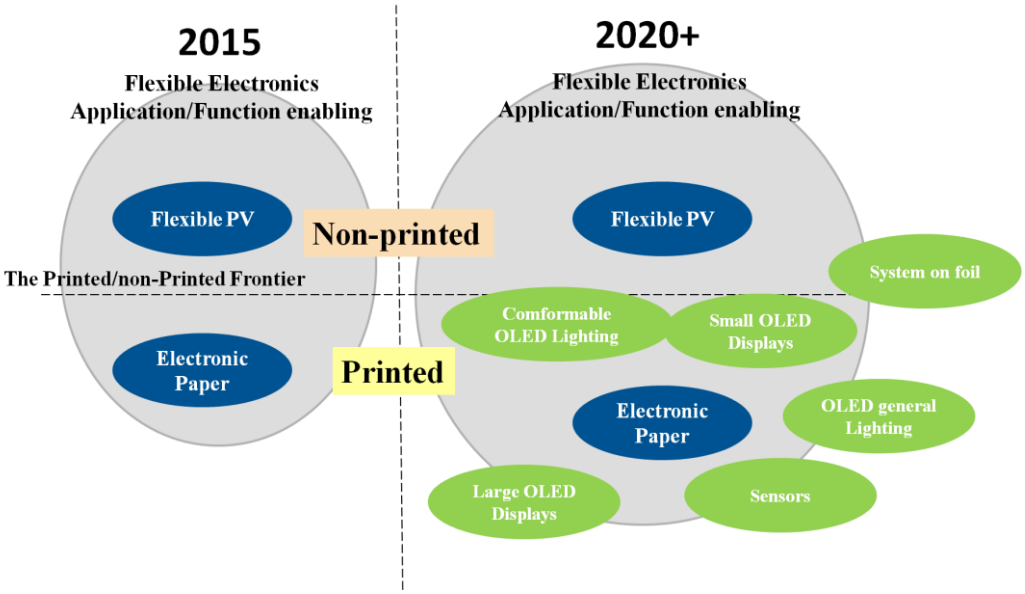

Figure 1.3 Landscape for the growth of applications using printing processes for flexible electronics from 2014 to 2020 [29]

1.1.2 Advantages and challenges of printed electronics

Printed electronics can provide simple, large-area, flexible, lightweight and low cost electrical products. Printed electronics can effectively reduce the manufacturing costs due to the additive and non-vacuum used in the technology, and meanwhile the large-area and few steps procedure. Furthermore, printing can be used to apply on fragile substrates without contacting [4, 5].

Conventional semiconductor electronics technology is usually based on higher temperature evaporative inorganic metals, *e.g.* silicon and metal oxides. Conventional process usually has more patterning steps than printed process, *i.e.* film deposition, resistive coating, drying, exposure, etching, resist strip and rinse. However, printing process usually contain printing and drying [5]. Several current printing processes are extremely productive and cost-efficient compared to the conventional procedures in the manufacture of silicon-based electronics. Furthermore, the versatility of the printed substrates in printed electronics can be

varied from paper and carton board, plastics, textiles and ceramics that do not have to be flat surfaces. Traditional silicon-based printing electronics usually use paper as a base. Printed electronics are usually fabricated as a flexible and thin product. However, silicon-based electronics are hardly ever able to achieve these qualities.

Nowadays, over 100 million electronic units are discarded annually in the UK alone. This results in one of the greater growing waste issues. In order to prevent ecological consequences, the choices of green materials will become more significant in the future. Printed electronics can be produced to be biodegradable or adaptable to disposal by incinerating [30, 31]. Additionally, energy requirement of electronics manufacture and disposal is classified as being an environmental challenge. Printed electronics is not an exception either. Therefore, as the addition printed electronics, more energy will be consumed. In this case, an energy production will continue to rise. Moreover, quality and yield of printed materials need to be carefully controlled. Material properties have to be repeatable and controllable under normal environmental hazards, *i.e.* humidity, wear and tear, sunlight, oxygenation, *etc*.

1.1.3 Introduction to applications of printed electronics

Printed electronics have been developed as an attractive technology to industries and scientists due to their flexibility and their low-cost mass production [4]. Typically, versatile examples of applications using printed electronics are listed and discussed below.

1.1.3.1 Thin-film transistor circuits

Liquid crystal displays (LCDs) have existed for over half a century, attracting the interest of industries and scientists. However, LCD products are still not perfect due to their limited viewing angles, long response time and small area panels. The production of the thin-film transistor (TFT) has changed this situation. The worldwide revenue from the TFT rose from $1 billion in 1989 to approximately $110 billion in 2012 [32].

TFT is a dominant technology that provides large area electronic circuit on the non-conducting substrate. TFT assembles a semi-conducting thin film layer, a

dielectric layer and a metallic layer on the substrate (often glass), which is the most commonly used substrate owing to its high transparency and compatibility with conventional semiconductors. The thin film usually consists of integrated amorphous silicon or polycrystalline silicon [33-35].

Figure 1.4 provides a schematic diagram for the configuration of a TFT which contains three parts, an insulator, a thin semiconducting layer and three electrodes [36]. The source and the drain electrodes are directly in contact with a thin-film semiconductor. The thin-film semiconductor basically works as a capacitor. When a voltage is applied to the gate, the electron charges are induced equally on the insulator. When the charge is inserted into the semiconductor material, a conducting channel is formed through the material. In this case, a current is formed between source and drain [37].

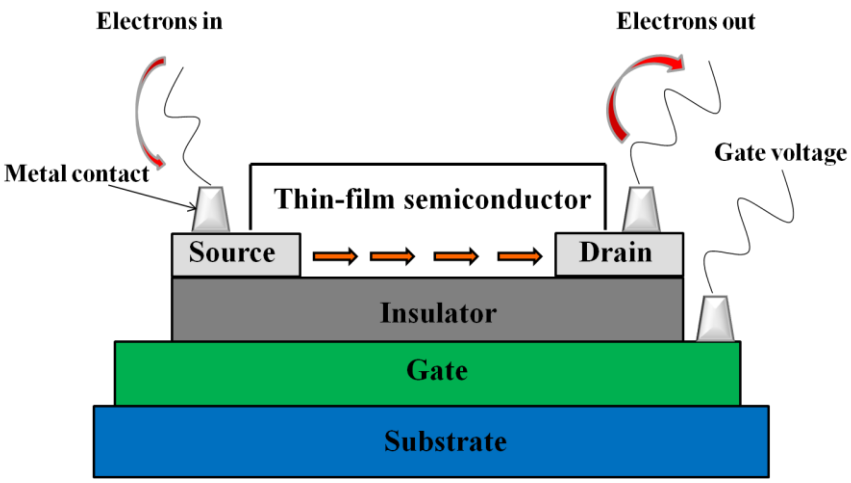

Figure 1.4 Schematic diagram for the configuration of thin-film transistor [37]

Due to their features and benefits, TFTs, have been used in a considerable number of applications. For instance, they are employed in LCDs [38], in digital radiography [39], in medical radiography [40] and in active matrix organic light-emitting diode (AMOLED) screens [41].

1.1.3.2 Displays (e-paper and e-reader and electrochromic)

When considering e-paper technology, the compositions and operations of electronic inks have to be brought into focus. E-paper is fabricated by sandwiching millions of

microcapsules, which contain charged pigment microparticles, between two flexible sheets. These charged pigments are electrophoretic particles that are usually black and white. These black and white microcapsules have opposite charged particles and are dispersed in a clear fluid. When an electric voltage is applied to the microcapsules, the black and white particles migrate in opposite directions. Then, the appearance of either black or white will be seen through the top layer of a clear display [42, 43].

Figure 1.5 gives details of the e-reader displays market share and consumption forecast [44]. It is estimated that the number of e-readers, in Kindle and Sony, will reach $10 billion by 2018. Electronic paper technology has been embedded in the back of credit and debit cards to replace the printed 3-digit Card Verification Value. The codes will be displayed and periodically change on a small screen. This can serve to detect criminals who copy card details [45].

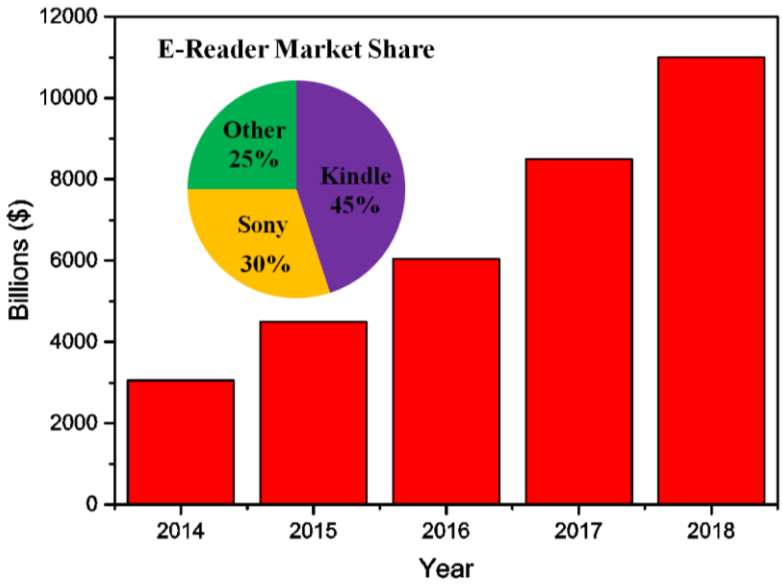

Figure 1.5 The e-reader market share and consumption forecast [44, 46]

Electrochromic devices can alter their optical properties (*i.e.* optical transmission, absorption, emittance and reflectance) when a voltage is applied. The conventional production of electrochromic displays is based on assembling indium, 'sandwiched' electrodes that contain at least one optically transparent electrode, *e.g.* indium tin oxide (ITO) [47]. The manufacture of electrochromic displays has been

commercialised by using printing technology [48, 49]. Electrochromic devices are employed in smart windows, electrochromic mirrors and electrochromic display devices.

1.1.3.3 Touch screens

The touch screen is a technology of an electronic display that is typically pressure sensitive, electrically sensitive or acoustically sensitive. The touch screen system is a new replacement for a primary input device such as a keyboard and/or a mouse. The touch screen is highly resistant to environmental damage. Touch screens can be used in a large number of electronic devices and software.

Ink formulations designed for use with resistive touch screens usually consist of an electrically conductive metal mixed with an electrically resistant polymer. This leads to a variation in the electrical current and voltage [50, 51]. The advantages of resistive touch screens are low cost, multi-touch capability, low power consumption, resistance to environmental changes and the ability to be operated by finger, by glove and by any pointing devices. The products are not as durable as those of other technologies, and can have poor optical quality. Resistive touch screens are usually used in medical displays; signature captures devices and military navigation systems.

Capacitive touch screens are coated with a transparent metallic conductive layer, on whose edges an electrode pattern is printed. The advantages of capacitive touch screens include their long lifetime, extremely precise resolution, excellent optical properties, multi-touch capabilities, ease of integration, reliability and durability, ability to operate under extreme conditions and drift free coordinates with no recalibration required. However, the disadvantages of capacitive touch include their high cost and the fact that they can be operated by fingers only. They are usually used in medical instruments, in signature capture and in aerospace entertainment systems [52, 53].

Surface wave touch screens use mechanical or acoustic waves as the sensing mechanism for the touching panel. All acoustic wave devices generally employ piezoelectric materials to generate the acoustic wave, which registers the position of touch and processes the information to the detector. Surface wave touch screen

panels are the most advancing among the three types. However, these can be damaged by environmental contamination. Acoustic wave sensors are often used in medical devices, in automotive sensors, and in other industrial and commercial applications [54, 55].

1.1.3.4 Photovoltaic devices

A Photovoltaic (PV) system uses semiconducting materials to convert solar energy into electricity directly. The most popular and widely used application that is based on photovoltaic systems concerns solar panels used on building to generate thermal energy, powder station, transport, spacecraft and signals [56].

Figure 1.6 represents the schematic image of a typical photovoltaic cell. There are two types of semiconductors (n-type and p-type) that have different electrical properties configuring and joining together in the cell. The junction between n-type and p-type semiconductors is known as 'p–n junction'. Silicon is usually used in the production of these semiconductors as it conducts electricity. The cell has the ability to absorb sunlight, creating particles with free moving positive or negative charge inside the cell. N-type and p-type semiconductors gather negative charges (electrons) and positive charges (holes), respectively. Thus, when a light or sun is shone to the cell, electricity will flow within the cell, as shown in Figure 1.6 [57, 58].

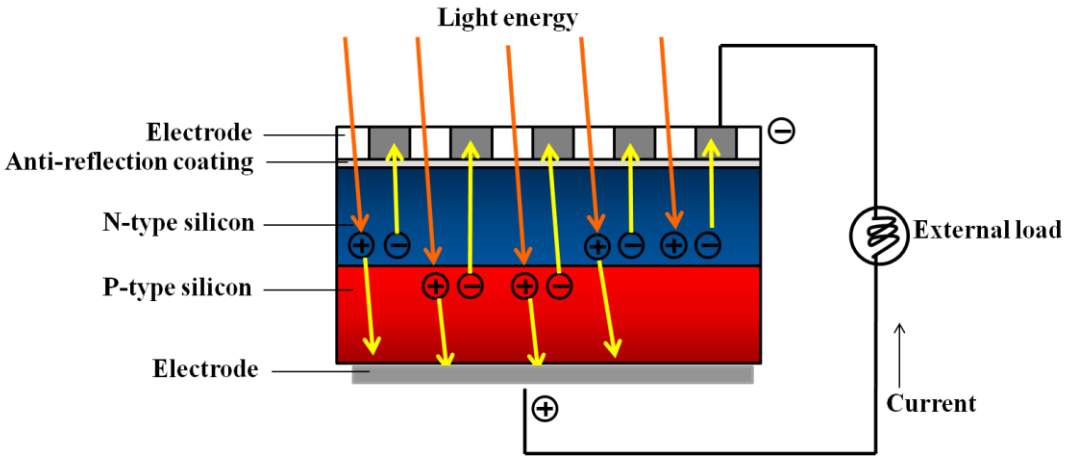

Figure 1.6 Schematic diagram for a photovoltaic cell [57, 58]

1.2 Materials used in printed electronics

Materials used in printed electronics can be classified into two groups, organic materials and inorganic materials. Compared with the inorganic materials, organic materials have a larger share of the printed electronics market [29].

1.2.1 Organic semiconductors or conductive polymers

Organic semiconductor materials are able to provide useful electrical conductivity. They are applied in the manufacture of electronic displays and flexible displays. They are widely used in smartphones [59], tablets [60], TV [61], RFID [62], LED [63], field effect transistors (FET) [64] and e-readers [65].

Organic semiconductors are typically sp^2-hybridised in their carbon bonding structure having the abilities to conduct electrons. The electronic conductivity ranges from 10^{-9} to 10^{3} S/m (between metals and insulators) [36, 37]. Pentacene is one of the more widely used organic polymers in TFTs [66], having the greatest thin film mobility.

1.2.2 Inorganic semiconductors (liquid silicon and metal oxides)

Amorphous silicon is currently the most significant semiconductor that is used in transistors. Silicon is also the second most economically important semiconductor. The benefits of silicon include excellent performance, low cost, ability to be used in various printing types and substrates producing high quality films [67]. Even though it has been reported that the electrical performance of thin films based on organic polymers is quite promising, they still cannot match the performance of silicon-based films for some applications. Also, polycrystalline silicon possesses high carrier mobility and various degrees of crystallinity [68].

Metal oxides, especially transition metals, such as ZnO and its derivatives constitute a large group of inorganic semiconductors that used to be employed in various applications of electronics. These non-stoichiometric metal oxides are usually transparent due to their large bandgaps (>3 eV). Under such a circumstance, invisible electronic displays on windscreens can be developed, when transparent metal oxides are mixed with transparent conductors and dielectrics. These metal oxides are also often applied in TFTs [68].

ITO is one of the more widely used transparent conductors popular because of its high electrical conductivity and optical transparency. The ITO has applications across a large number of products, such as liquid crystal displays, plasma displays, touch panels, flat panel displays, windscreens, OLED, and solar cells [69-71].

1.2.3 Dielectrics

A dielectric material stops the electrons flowing through the system due to its intrinsic lack of a charge-carrying mechanism [72]. The printed dielectric creates an insulating coating that plays an important role in enhancing and protecting the conductive material. For instance, poly(vinylpyrrolidone) (PVP)-based films are usually used as a dielectric coating for printed field effect transistors [25, 73]. Properties of printed dielectric films that have an important effect on the performance of printed electronics, include the thickness, smoothness and capacity properties [74, 75].

1.3 Conductive polymer composites

Conductive polymers can be divided into two parts, intrinsically conducting polymer (ICP) (organic conjugated polymers) and conductive polymer composites (CPCs). Electrically conductive polymer composites containing single or hybrid conductive fillers in an insulating polymer matrix are widely used in recent research and applications. The conductive fillers include graphene, metal powder, carbon fibres, carbon black and conducting polymers such as polyaniline [76-78]. The electrical properties of CPC materials rely on the conductivity, the loading, the particle size, the shape and the distribution of the conductive fillers in the hosting polymer. A range of applications, such as shielding, switching, sensing or heating, is dependent on the electrical resistivity of CPCs, as shown in Figure 1.7 [77]. Accordingly, the electrical resistivity of QTC commercial material ranges from 10^{12} down to 10 Ω, which can vary from insulating to conductive properties [24].

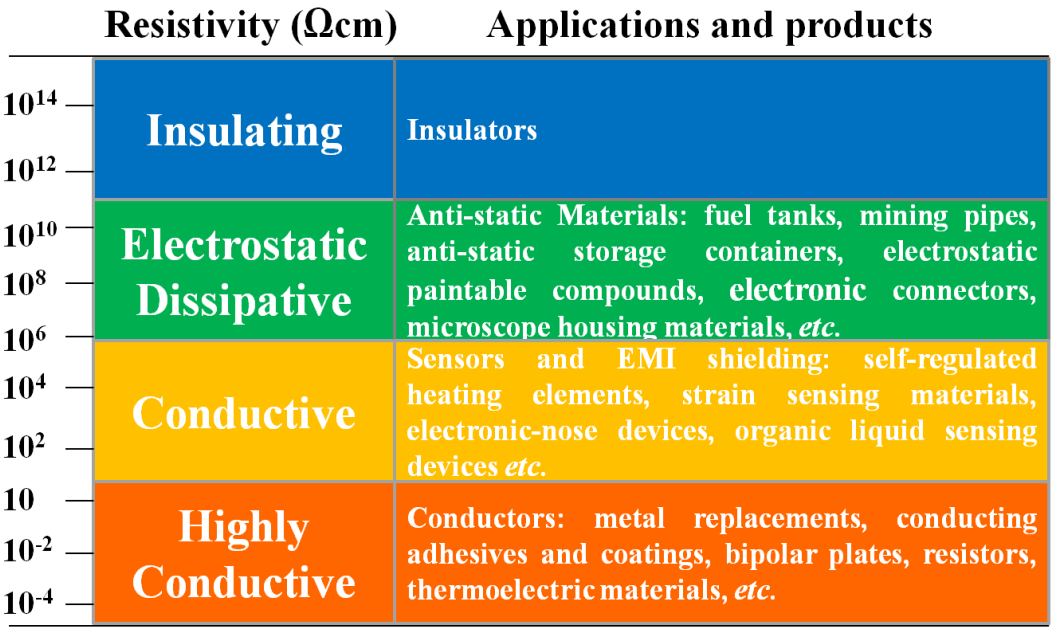

Figure 1.7 Classification of CPCs is based on their electrical resistivity and applications [77]

1.3.1 Pressure sensitive conductive materials

Electrically conductive composites have been studied for over a century. The majority of the composites range from metal-polymer composites containing, for example, copper, nickel, aluminium, iron and silver particles to carbon-containing composites [24, 79].

1.3.1.1 Carbon nanotube composites

Since the discovery of carbon nanotubes by Iijima [80], interest has been shown by the scientific community and industries because of the carbon nanotubes' outstanding properties. Those properties include thermal optical, electrical and mechanical properties. The stiffness and strength of carbon nanotubes are extraordinary. The stiffest carbon nanotube, the carbon fibre, has a Young's modulus of the order of 1 TPa. The Young's modulus of glass fibres is normally approximately 70 GPa [81]. Carbon nanotubes are usually mixed with other materials (*i.e.* polymers, ceramics and metals) to achieve high mechanical properties. Furthermore, one of the more significant characteristics of carbon nanotubes is their electrically semiconducting character or metallic behaviour which

depends on their structure and diameter. It has been reported that the electrical resistance of carbon nanotubes ranges from 0.05 μΩm to 10 mΩm. With such a good conductivity properties, carbon nanotubes, such as carbon black [82], are often used as fillers in the low cost polymers to improve the conductivity. Conjugations of carbon nanotubes with poly(p-phenylene vinylene) (PPV) and its derivatives have displayed electroluminuescent properties that normally are exploited in light emitting diodes and photovoltaic devices [80, 83, 84].

1.3.1.2 Nickel particles in composites

In the last two decades, nickel nanoparticles have attracted much attention from scientists and engineers due to their abundant applications, such as in magnetic inks [85], magnetic storage media and sensors [86], conducting materials [87] and catalysts [88]. Apart from such numerous applications, the manufacturing cost used nickel powder is pretty lowsince the price of the metal powder is normally quite expensive.

Several physical and chemical approaches have been taken to fabricate high quality nickel nanoparticles, including ultrasound irradiation [89], electrochemical methods [90], metal evaporation condensation [91], metal salt reduction [92], polyol methods [93], ultrasonic spray pyrolysis [94] and neutral organometallic precursor decomposition [87, 95]. In general, comparing with physical processes, chemical reduction methods have the benefits of simple to run, easy to control and low cost production [96].

1.4 QTC metal composites

QTC metal composites have greater intrinsic conductivity than carbon-containing composites and have a well-defined morphology [24]. Lussey, in 1996, invented a novel composite material termed a quantum tunnelling composite (QTC) [7].

Quantum Tunnelling Composites consist of a polymer matrix in which metal particles are present. The original target was to create an electrically conductive adhesive. However, this adhesive did not conduct but had a high electrical resistance until some kind of mechanical pressure was applied. When the pressure was applied, electrical conductivity was achieved [97]. Generally, composites

containing low metal filler concentration have slightly greater electrical conductivity than that of the polymer alone. This is because each metal particle is well separated by the insulating polymer. By increasing the metal filler loading, the electrical conductivity of the composites increases slowly. However, the electrical conductivity increases rapidly within a limited range of metal filler content [24]. This is the reason why an electrically conductive adhesive has not been fabricated, yet novel pressure sensitive conductive QTC materials have been created.

1.4.1 Compositions of QTC materials

Nearly all contemporary electronic products contain silicon, which is also used in QTC composites, as a semiconductor. However, the electronic devices that mainly contained silicon are expensive, difficult to fabricate and require clean rooms and precise manufacturing techniques [15, 23, 97]. A typical QTC comprises a mixture of spiky nickel particles, of approximately 1-100 μm diameter, and an elastomeric poly(siloxane) matrix. These fulfil different roles [97]. The nickel particles are coated with a polymer matrix, as shown in Figure 1.8, that have sharp projections on the surface [24, 98]. As a result, the particles themselves do not "communicate" to form chains with each other directly. QTC contains a nickel type 123 and type 287 (supplied by Inco Ltd.), dispersed in a blend of liquid monomers. These nickel-monomer combinations are polymerised to give a flexible and elastic sheet with a thickness of 1-2 mm [24, 97]. The particle size distributions of nickel type 123 and nickel type 287 are in the range of 3.5 to 4.5 μm and 2.6 to 3.3 μm respectively. A silicone based monomer or urethane based monomer is used. Siloxane-based monomers, includet Alphasil 2000 (Alphas Industries Ltd.), Silicoset 153 (Ambersil Ltd.), Silastic T4 (Dow Corning) and RTV6166 (GE Silicones). The urethane-based monomer include F42 (supplied by Techsil Ltd.) [8, 24]. In order to establish a material that reaches or exceeds the percolation threshold, the ratio of conductive filler to polymer matrix, within the solid state formulation should be in the range of 4:1 to 6:1 [7].

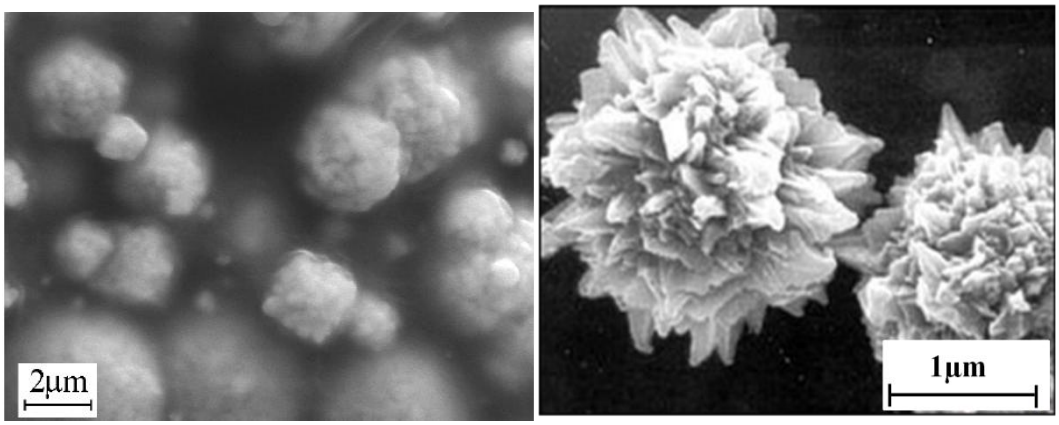

Figure 1.8 SEM image of a QTC material, for which the ratio of silicone monomer to nickel powder was 6:1 and 4:1 by weight [24, 98]

The components of the QTCs can also be blended with small amounts of acicular semiconductor particles, such as Acicular TiO_2, at less than 10 % by weight. As a result, the material displays a large piezoresistive effect, which means that the electrical resistance of the QTC can be extremely sensitive to deformation [97]. "This elastomeric conductive polymer composition displays a large dynamic resistance range and isotropic electrical properties when subjected to distortion forces" [99]. When no pressure is applied, the metal particles are separated and do not interact with each other; the QTC sample behaves as an insulator. In this state, the composition of the QTC material is below the percolation threshold [8, 99, 100]. However, when some form of mechanical pressure is applied, such as compression, stretching, bending or twisting, the composite becomes an excellent conductor. The reason why QTCs display such an unusual property arises from the deformation of the particles. When QTC materials are quiescent, the metal particles are well separated from each other. However, when mechanical pressure is applied, the electrons from the metal particles can "hop" from one to the other with or without touching. This is known as the 'quantum tunnel effect' [7, 24, 97], arising because the nickel particles can build a high electric charge field on the spike tips.

1.4.2 Working principles of QTC materials

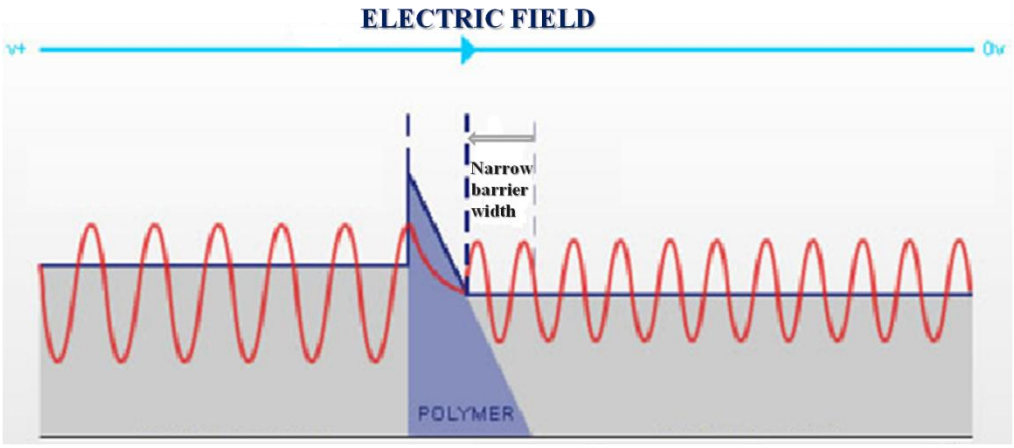

Figure 1.9 Schematic image of QTC material's working principles [101]

Experiments have shown that the resistance of the QTC diminishes exponentially and rapidly with increase in pressure. However, the resistance decreases more slowly at greater applied pressures until it eventually decreases below the residual circuit resistance [24, 97]. This performance of QTCs at lower pressures can be explained by percolation theory. Thus, the effect arises from the aggregations of conductive particles that produce conductive pathways at the percolation threshold. As a consequence, QTC materials possess a large piezoresistive effect. Thus the resistance of the materials is sensitive to the mechanical deformation. As a conductive pathway is established, the conductivity of QTCs increases to a maximum value, when it approaches saturation. At saturation, the composite becomes an insulator. Thus percolation theory fails. The percolation theory proposes a region in which the conductivity performance changes very quickly [24]. The percolation threshold relates to the loading of filler particles at which the minimum value can provide the behaviour of rapidly varying conductivity [100]. As mentioned in 1.4.1, the electrical conductivity increases rapidly within a limited range of metal filler content. This metal filler content gives the percolation threshold of the material. The required loading of the metal filler, at the percolation threshold, is associated with the shape of the filler particles.

In addition, the particle shape of agglomerates has a large influence on the conductivity of a QTC at the percolation threshold. "Values of the volume fraction

of filler at the percolation threshold are observed to range from <1 % for needle-like particles to >10 % for spherical particles" [24, 102]. Thus, QTC inks have the ability to carry high electric current densities due to the spiky tips on their surface, although no metallic routes are established [8, 24]. The resistance of QTCs can vary from 10^{12}–10^{13} Ω to less than 1 Ω under the deformation at room temperature [24].

The piezoresistive effect is different from quantum tunnelling. Figure 1.10 indicates a relationship between the electrical resistance and the amount of stress placed on the piezoelectric material [103, 104]. The most common application of a piezoresistive material is in transistors. Piezoresistive materials are made from semi-conductor materials that usually contain silicon.

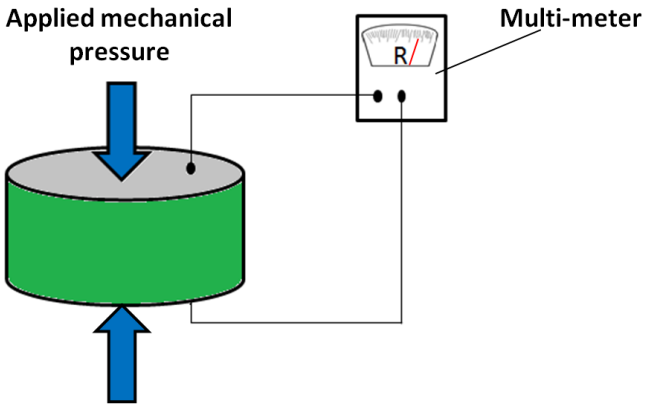

Figure 1.10 Diagram demonstrates how the piezoresistive material works when the pressure is applied [105]

The resistance of the material decreases exponentially with increasing deformation. Such a material can be used up to thousands of times without any observable damage occurring. This is the reason why elastomeric polymer matrices are of great interest in this context. The flexibility and resilience are both dependent on the grade of the poly(siloxane) elastomer, the filler loading and the QTC layer thickness [8, 24, 97].

Compared to other conductive composites, QTCs have a much greater initial electrical resistance. Also, the electrical resistance of a QTC falls with increasing pressure more significantly than that does in other conductive composites, that work by the percolation theory [100, 106, 107], as shown in Figure 1.11. The red line

represents the R-F plot of the first generation of QTC material and the black line represents R-F plot of a typical percolation composite [24, 100].

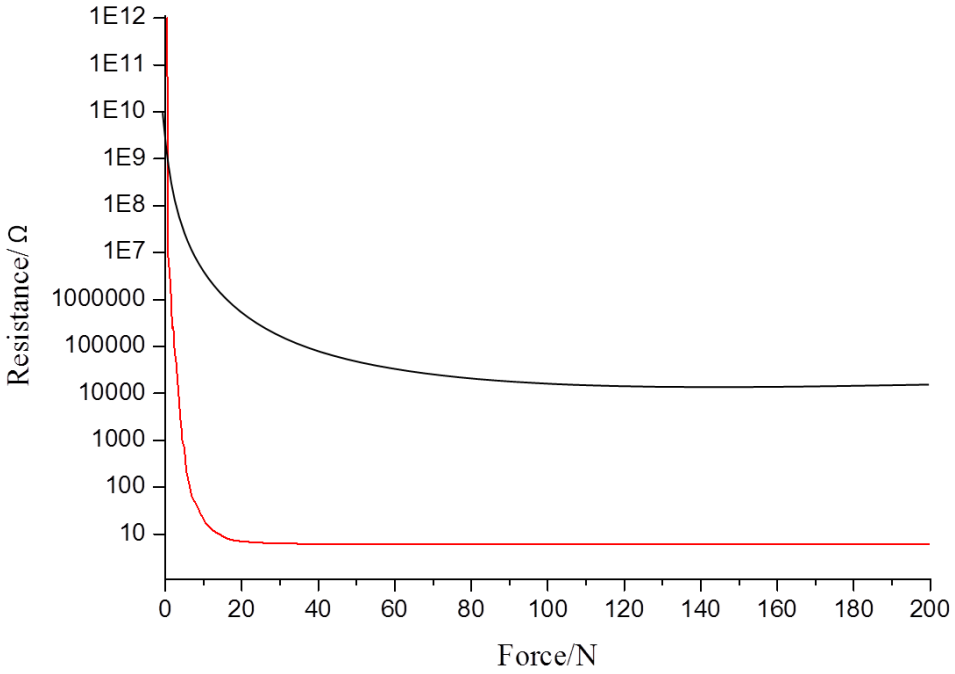

Figure 1.11 Comparison of the resistance and force to the first generation of QTC material and a typical percolation composite [24, 100]

1.4.3 Current Voltage characteristics of QTC material

An explanation of the quantum tunnelling effect by Henri Becquerel in 1896, given on the basis of the Fowler-Nordheim (wave-mechanical) effect has been provided [108]. This describes how the electrons migrate from a metallic conductive surface barrier into the insulator particle array, because of the quantum-mechanical tunnel effect, under the influence of a strong electric field [109, 110]. The performance can be reduced with the removal of the spiky tips of the nickel particles. As a result, the sensitivity of the QTC reduces significantly on deformation. The Fowler-Nordheim effect is responsive and reproducible. However, the mechanism for the thermo-mechanical which enables the use of this type of system as a transducer cannot be rationalised [24, 97]. Furthermore, the nickel particles were fully covered by the polymer matrix, so at high filler concentration, there is no direct contact of the particles and conduction is primarily through electric field across relatively thicker

barriers. This system provides unusual electronic behaviour that is high resistivity above the expected percolation threshold and then an exponential decrease in resistivity over more than 12 orders of magnitude under mechanical deformation.

An applied force should alter the current-voltage behaviour of a QTC from being ohmic at the quiescent state to being non-linear during deformation. Ohmic contact is illustrated by a linear current–voltage (I–V) relationship between two conductors, as shown in Equation 1-1. A hysteresis phenomenon is seen, the nature of which is dependent of the degree of deformation. In this case, the electrical charges are stored in the QTC material as a Fowler-Nordheim effect, which is an unfavourable factor due to its inconsistent deformation. Figure 1.12 shows the nature of the current-voltage characteristics of a sample of a QTC material on being subject to uniaxial compression [7, 24].

$$R = \frac{V}{I}$$

Equation 1-1 Ohm's law, in which R, V and I represent resistance, voltage and current, respectively

The first generation of QTC materials gave electric storage, as shown in Figure 1.12. The solid and dashed lines represent increasing and decreasing voltage. This phenomenon was undesirable due to the inconsistency of behaviour between uses [24, 97].

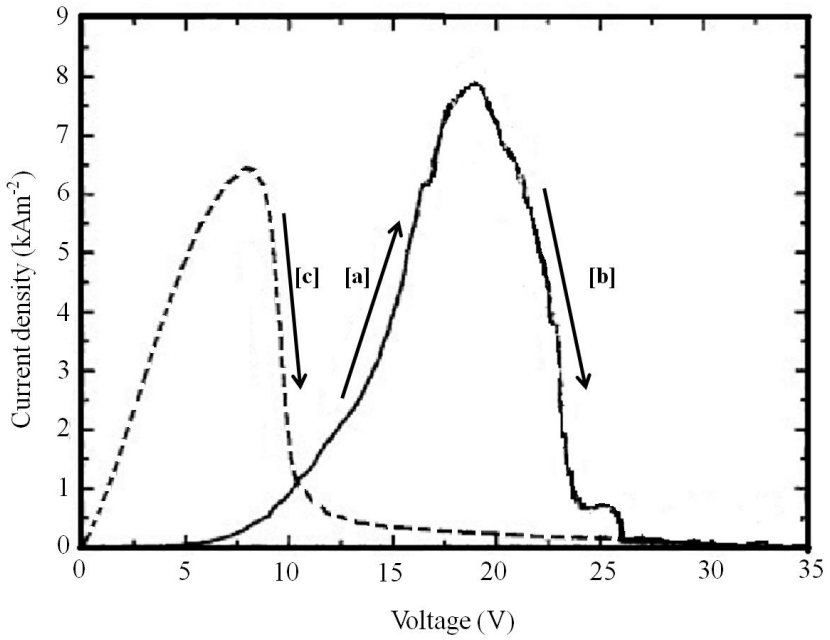

Figure 1.12 Current-voltage characteristics of a sample of a QTC when it is compressed uniaxially [7]

Figure 1.12 illustrates the electrical charge storage behaviour of a first generation QTC material. The performance can be explained by the generation of conduction paths throughout the material. Figure 1.13 [a] demonstrates that the electrical charge passes from one nickel particle to another, in close proximity. Consequently, this generates a current through the material, Figure 1.12 [a] area. However, some of the nickel particles are not close enough to pass the electrical charge to any other neighbouring particles. As a result, a dead end is created, to which the charge can flow but is not able to pass on (Figure 1.13 [b]). The current is shown on the area [b] of Figure 1.12. This leads to a charge being stored at the tips until the current decreases. After reducing the current, the charge can flow back along the path it followed before. Eventually, a new conduction path will be discovered (Figure 1.13 [c]) and an increase in the current will be created, as shown in area [c] of Figure 1.12. This charge storage situation is undesirable because of inconsistencies between uses. The second generation of QTC materials was designed to solve this problem (Figure 1.15).

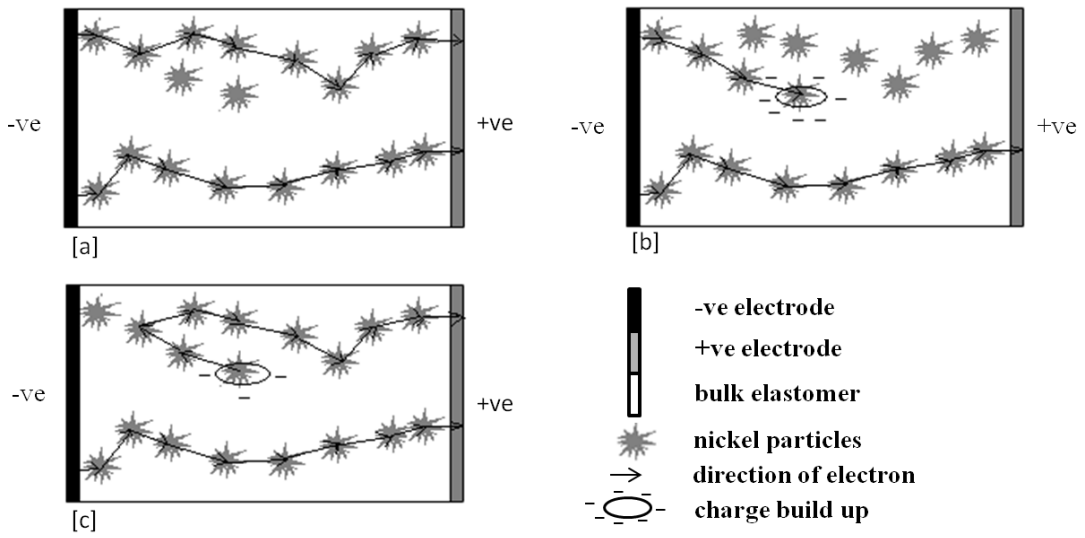

Figure 1.13 [a] Initial conduction paths developed with increasing voltage; [b] Charge storage on the spike tips as the voltage is increased; [c] Removal of stored charge as the voltage decreases

Acicular TiO_2 is introduced into the formulations of second generation QTC materials to solve the charge storage problem. The morphology of the acicular TiO_2 is shown in Figure 1.14. These types of TiO_2 cannot build up as many electrical field sites as can the nickel particles, as the number of TiO_2 tips per particle is essentially reduced to two. In this case, the acicular TiO_2 in the bulk material creates extra conduction paths. Figure 1.15 illustrates the generation of conduction paths in such QTCs.

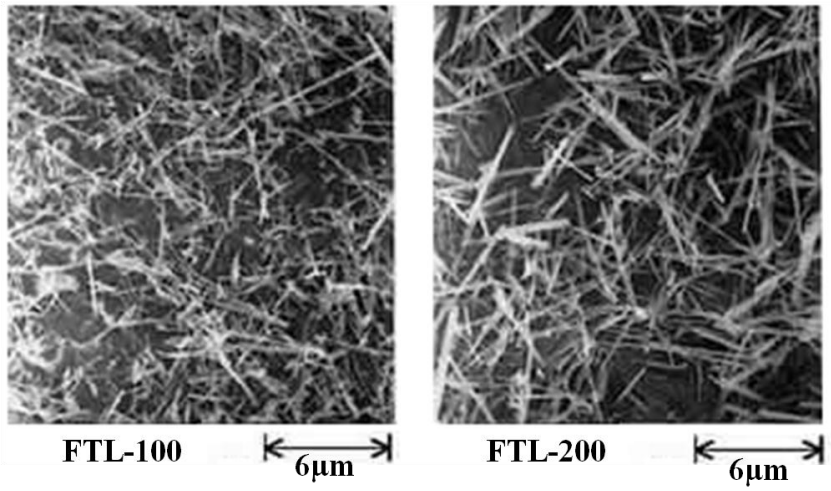

Figure 1.14 Morphology of acicular TiO_2 as used in second generation QTC materials

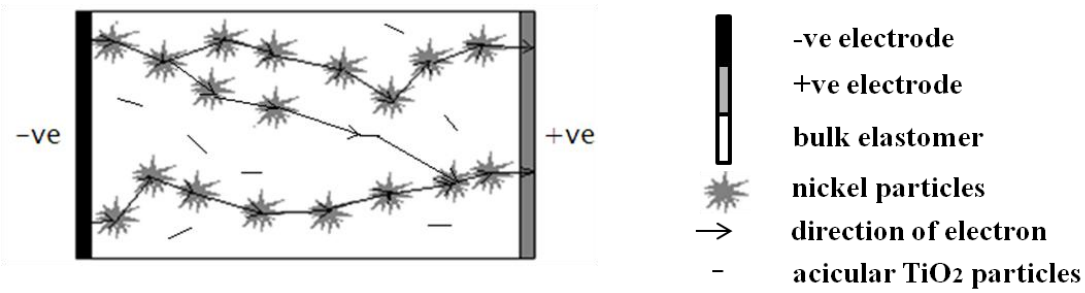

Figure 1.15 Introducing acicular TiO_2 filler particles, aiding conduction paths in QTC materials

Current QTC inks contain not only acicular TiO_2 as filler, but also contain pre-milled, spherical TiO_2. These TiO_2 particles are not used to enhance the opacity or whiteness of the ink films, but as a synergist to the electrical conductivity of the ink film. TiO_2 is a semiconductor. The role of spherical TiO_2 fillers is similar to that of acicular TiO_2 filler, which is to reduce the electrical sensitivity of the QTC film. However, the spherical TiO_2 can also deflect the electric charge, as demonstrated in Figure 1.16.

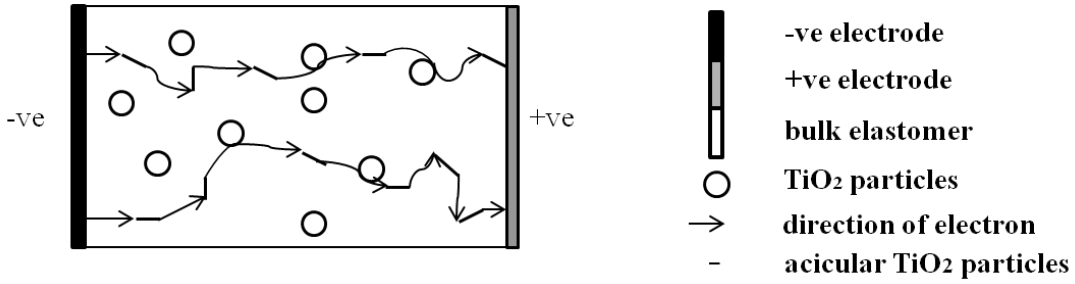

Figure 1.16 Proposed conduction paths in a Peratech QTC ink film

1.4.4 Theory and models of conduction mechanism of QTC materials

1.4.4.1 Quantum tunnelling theory

Quantum tunnelling theory in this section will be carried out in QTC materials, which is based on the theories of thermionic emission and electric field effects. They are used to illustrate the models of the transport mechanisms of electrons between metal fillers and the polymer matrix.

Quantum tunnelling phenomenon is dominant by quantum mechanics, which is different from classical mechanics. Classical mechanic describes the particle would be certain to be reflected off the potential barrier as it has insufficient energy to surmount. However, quantum mechanics illustrates the particle acts as a wave giving a wave function, Figure 1.17, which has sufficient energy to transmit through the barrier rather than just reflected [97, 157, 158].

Quantum mechanics describe a matter have properties of particles and waves. A particle with mass, m, and energy, E, is modelled in a one-dimensional rectangular potential barrier of height V_0>E. The particle will be more likely tunnel through the barrier from the left, as shown in Figure 1.17. Due to this model, regions 1 and 3 could represent two adjacent nickel particles in the QTC composite and region 2 could represent the insulating polymer matrix. As a result, expressions of the transmission coefficient, T, and the reflection coefficient, R, can be achieved by the wave function in those three regions [97, 157, 158], as shown in Equation 1-2 and Equation 1-3.

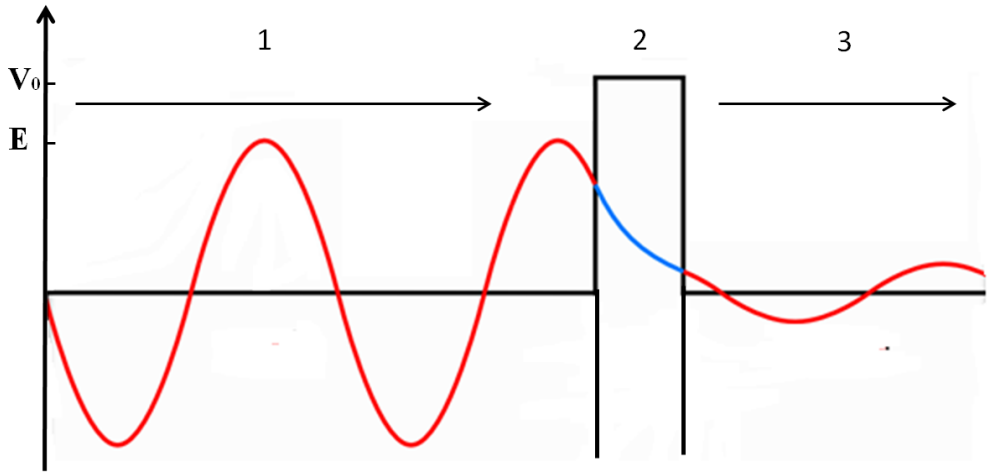

Figure 1.17 Quantum tunnelling through a one-dimensional potential barrier [157,158]

$$T = \frac{probabliy\ flux\ of\ transmitted\ wave\ in\ region\ 3}{probablity\ flux\ of\ inident\ wave\ in\ region\ 1}$$

Equation 1-2 Expression of the transmission coefficient, T, in quantum mechanics

$$R = \frac{|probability\ flux\ of\ reflected\ wave\ in\ region\ 1|}{probablity\ flux\ of\ incident\ wave\ in\ region\ 1}$$

Equation 1-3 Expression of the reflection coefficient, R, in quantum mechanics

1.4.4.2 Percolation theory

Percolation theory, introduced in 1957 by Broadbent and Hammersley, is widely used to describe the physical properties of composite materials, such as electrical resistivity, permeabilities of diphasic materials and thermal conductivity. The percolation threshold is the filler particle at minimum volume fraction value which can achieve the electrical behaviour with rapidly varying conductivity [100]. The electrical conductivity increases rapidly within a limited range of metal filler content; this metal filler content is the percolation threshold of the material. The concentration of the metal filler at the percolation threshold is associated with the shape of the filler particles.

When the metal filler fraction is high, as shown in Figure 1.18 [b], there are many possible conduction pathways. When the metal filler fraction is very low, as shown in Figure 1.18 [a], there is nearly no such conduction pathway as the metal clusters are small compared to the whole square lattice.

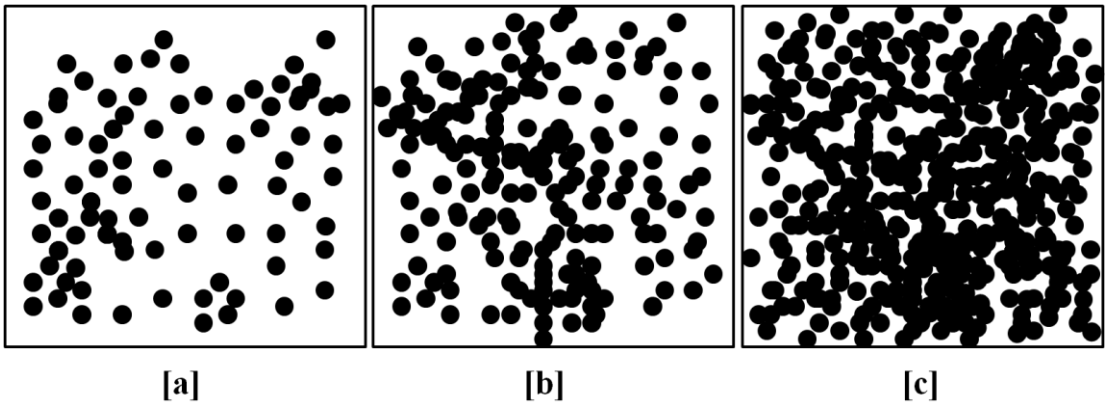

Figure 1.18 Schematic diagrams of square lattices representing the three stages of metal filler fraction. [a], [b] and [c] show the metal filler fraction below, at and above the critical fraction, respectively. Black dots represent filler particles

Percolation theory explains the conductor and insulator phase transition as the concentration of metal filler is increased through a metal-polymer composite. This unusual property requires the metal filler particles have tendency to randomly arranged into clusters throughout the insulating host polymer [111]. The conductivity through the composite is a factor of the number of percolation

pathways through the materials. Equation 1-4 shows the resistivity of a composite is a function of the volume fraction of conductive filler particles.

$$R \propto (\frac{1-\emptyset}{\emptyset_c})^t$$

Equation 1-4 Equation for the resistivity, R, of a composite material. Ø represents the volume fraction of conductive filler particles. $Ø_c$ represents the percolation threshold that is the critical volume fraction of conductive filler particles when a conducting pathway is formed through the insulating polymer. t represents an exponent for the percolation equation that usually ranges from 1 to 6.27 for 3D systems [111-113]

Figure 1.19 demonstrates the relationship between the volume fraction of metal filler and the electrical conductivity of a composite. It reveals that the conductivity increases very slowly when the metal filler volume fraction is below the percolation threshold, due to no direct electron contact from one to the other, as displayed in Figure 1.18 [b]. Once the volume fraction of metal filler reaches the percolation threshold, a conductive pathway will be formed. A further increase of volume fraction will cause the conductivity to increase dramatically; then an Ohmic law will be followed. Percolation theory can only explain the performance when the composite's filler is above the percolation threshold (Ø > Øc) accurately [113]. The reason of this is because when the volume fraction of metal filler is at the percolation threshold, Ø = Øc, even a slight deviation in filler volume fraction can influence the conductivity of the system [113, 114]. Percolation theory can be used to explain the behaviour of QTC materials as it assumes that the metal fillers are randomly diffused throughout the material.

Figure 1.19 shows the relationship between filler volume fraction and the electrical conductivity of a composite material that obeys percolation mechanism [113].

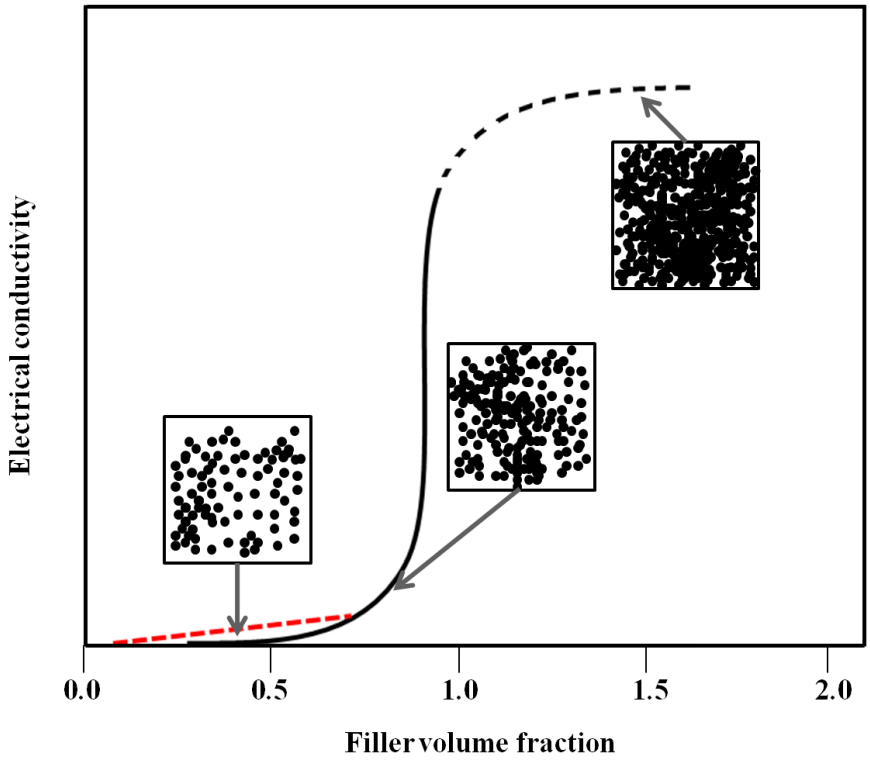

Figure 1.19 Relationship between filler volume fraction and the electrical conductivity of a composite material. The red and black dashed lines represent the ohmic region and maximum conductivity, respectively [113]

For systems on or close to the percolation threshold, percolation theory cannot be used to predict such sharp transitions. In this case, a slight variation in the filler volume fraction will have a relatively large effect on the conductivity [114]. In order to employ percolation theory to systems accurately, it is necessary to apply it when the filler volume fraction is above the percolation threshold. Also, the metal fillers are smooth spheres that do not have too much aggregation. Because of this, an improved theory will be described in the next sections.

1.4.4.3 McLachlan's general effective medium theory

The purpose of effective medium theory (EMT) is to describe the performance of QTC material is in proximity to the percolation threshold that cannot be explained successfully, as mentioned in Section 1.4.4.2 [113]. The EMT builds on the basic percolation theory. This means that each metal particle in the composite is represented as a single site on the three dimensional array. Therefore, the resistance between each pair of nearest neighbour particles will be associated. Thus the array

represents a network of randomly positioned particles with a random distribution of resistance between them all. EMT then replaces all of the resistance with one average resistance value. This EMT uses a homogeneous medium instead of a heterogeneous material to solve the complexity of analysis [115]. The theory removes the sharp transition from insulator to conductor at the percolation threshold, which can more illustrate accurately the behaviour of the conductivity of a composite. McLachlan raised the equation for the general effective medium (GEM) theory, as shown in Equation 1-5. This model simplifies the EMT model with quantitative accuracy when the filler volume fraction is at/near the percolation threshold. It was confirmed by Brosseau [115] that the GEM model fitted the experimental data for the dielectric response of a wide range of different carbon-black concentrations in polymers.

$$\frac{(1-V)(\varepsilon_m^{\frac{1}{s}}-\varepsilon^{\frac{1}{s}})}{\varepsilon_m^{\frac{1}{s}}+[\frac{1-V_c}{V_c}]\varepsilon^{1/s}}+\frac{V(\varepsilon_f^{\frac{1}{t}}-\varepsilon^{\frac{1}{t}})}{\varepsilon_m^{\frac{1}{t}}+[\frac{1-V_c}{V_c}]\varepsilon^{1/t}}=0$$

Equation 1-5 GEM theory, where V and V_c are the volume fraction of metal filler and the critical filler volume fraction, ε_m and ε_f are the relative complex permittivities of the matrix and filler, s and t are the exponent values.

1.4.4.4 Links-Nodes-Blobs model for conductive polymer composites

A Links-Nodes-Blobs (LNB) model was firstly derived by Lin and Lee to explain the Payne effect of rubbers with metal fillers [116, 117]. At the beginning, Payne and Medalia had found that the mechanical properties of filler-rubber composite did not behave the same as those of neat rubber [118]. The LNB model successfully demonstrated the macroscopic properties of a metal filler composite system with respect to the microscopic properties of metal fillers and polymeric matrix, at which the filler volume fraction is above the percolation threshold.

The model describes three main components, as it name suggested. The blobs are the filler particle aggregates, the links are chains of primary particles connecting blobs in a network and the nodes are connected joints among the

splitting links. The average distance between two nearest nodes is defined as ξ_p. Figure 1.20 exhibits the schematic image of [a] conductive chains in a percolative composite above threshold and [b] the links-nodes-blobs model [116].

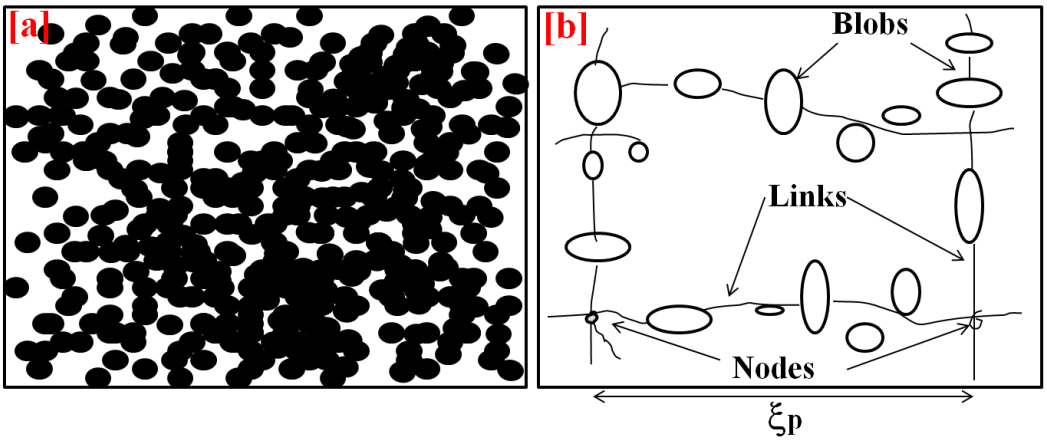

Figure 1.20 Schematic images of [a] conductive chains in a percolative composite above threshold and [b] the links-nodes-blobs model [116]

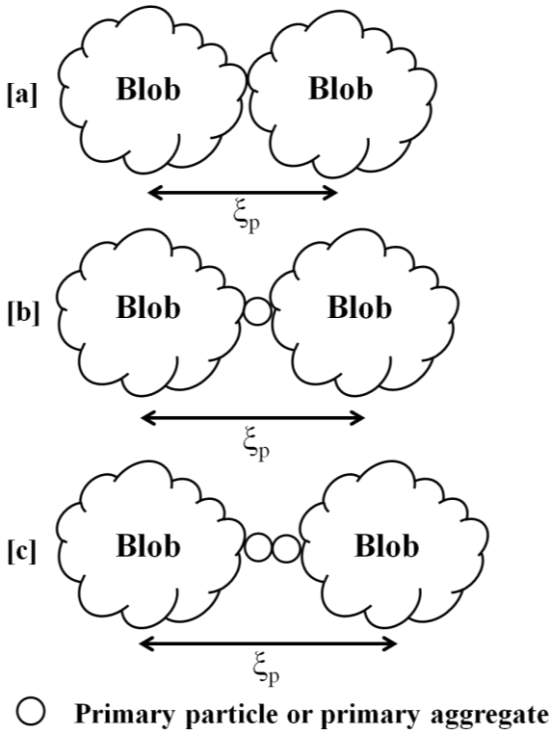

Figure 1.21 Schematic images of the LNB chain, where [a] formed by direct contact of two blobs, [b] with the L_1 number of singly connected bonds equal to one and [c] with the L_1 number of singly connected bonds equal to two [116]

In the LNB model, the links between the blobs include a continuous chain of primary particles, developing a network of interconnected blobs. Figure 1.21 shows the presence of the possible LNB chain, in which the smallest link length correlates to the direct contact of two blobs (Figure 1.21 [a]). The LNB model assumes that the blobs are completely rigid and only the polymer matrix deform along with the filler network, under compressions of the metal-rubber composite system [116].

$$\xi_p = \beta(\varphi - \varphi_c)^{-v}$$

Equation 1-6 The relationship between the critical length, ξ_p, and the difference of the filler volume fraction, (φ-φ_c), where β represents a proportional constant and v represents the fractional dimension

$$R_\xi(n) = R_1(n+1)$$

Equation 1-7 The resistance of a link made of n single bonds between (n+1) primary particles, where R_1 is contact resistance of a single connected bond

$$R_1 = \rho_1\left(\frac{t}{A_c}\right)$$

Equation 1-8 The contact resistance of a single connected bond, where ρ_1 is the resistivity across the contact region, t is the shortest distance between two contact points and A_c is the average contact area

$$\rho(n) = R_\xi(n)\left(\xi_p a\right)^2/(\xi a)$$

Equation 1-9 The resistivity of a repeated unit cell ρ(n), where a is the average diameter of a primary filler particle

The conductivity of a metal-polymer composite is determined by the loading of metal filler and the conductivity of the metal filler. It is assumed that the lowest resistivity is achieved from one side to the opposite side through a number of parallel pathways across blobs. In contrast, the links that made up of an electrically insulating polymer matrix results a much greater resistivity. Hence, the resistivity of the whole composite system is determined by the integral of the number of the links

and the number of blobs throughout the material. The macroscopic resistivity of a composite can therefore be expressed as above.

The macroscopic resistivity of a metal-rubber composite can be calculated by Equation 1-9.

1.4.5 Benefits of QTC materials

One of the major benefits of QTC materials is that when in a state of rest, the electrons will not be activated. In this state, the materials do not consume any energy until some pressure is applied. This, in turn, means that QTCs have a longer lifetime when acting as conductors. Furthermore, QTCs are cheap and easy to source (less than €1 per sensor), major factors when considering manufacturing [119]. Additionally, as mentioned above, QTCs can be used in a large variety of applications. They are commonly used in sensors and in switches [97].

1.5 Printing technologies relevant to QTC applications

In the later twentieth century, dramatic changes occurred in printing technology through the introduction printing into the electronics industry. The various printing technologies can be classified simply as direct printing (contact) and indirect printing (non-contact). Direct printing technologies include flexography, letterpress, gravure and various kinds of screen printing. Indirect printing technologies make the image firstly transfer from the image carrier to blanket cylinder and then to the substrate, such as offset lithography and digital printing. In direct printing, the image on the substrate is directly conveyed from the image carrier. However, in indirect printing, the image is conveyed from the image carrier to an intermediate rubber-covered blanket cylinder and then transferred to the substrate [120]

1.5.1 Screen printing technology of relevance to QTC applications

Screen printing is a relatively versatile printing process, due to its ability to provide printability on a large range of surface types, from textiles to ceramics [121]. Nowadays, the screen is composed of a finely woven mesh that stretches onto an ink-blocking stencil. The stencil uses the open areas on the mesh to transport ink onto the substrate. Inks are forced or pumped onto the open areas of the woven

mesh surface using a roller or squeegee, as shown in Figure 1.22 [25]. The squeegee with a stiff backing and a blade edge has a number of different hardness to choose. Shore A is the measurement of the hardness of a squeegee. During the screen printing process, initially a light sensitive emulsion is wiped across the mesh, (fabricated from nylon, polyester, steel or silk), in the dark. Then the unnecessary emulsion is burnt away leaving behind a clean area in the mesh, which results in an identical reproduction of the desired image during printing. The ink is then transferred onto the substrate with the movement of the squeegee. The screen and substrate are then separated and a drying procedure follows [121, 122].

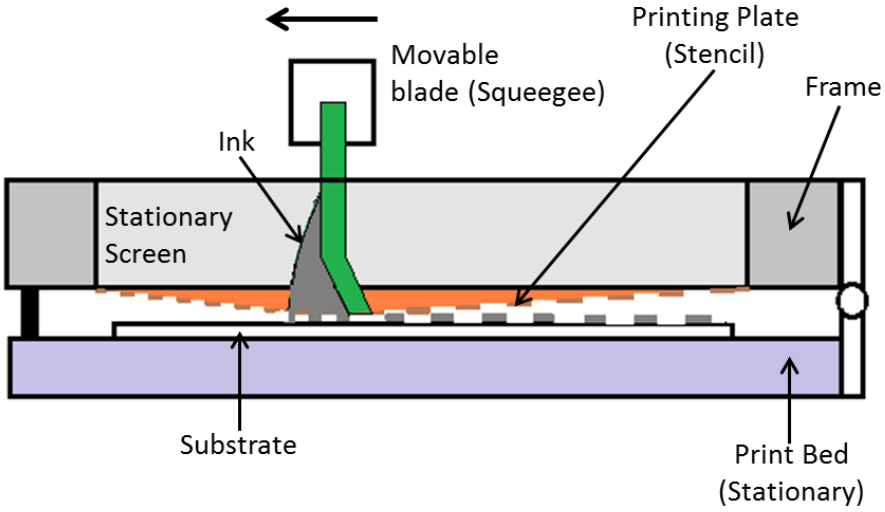

Figure 1.22 Diagram for a typical screen printing setup [25]

1.6 Inks relevant to QTC applications

An ink is a somewhat complex mixture that contains pigments or dyes. Printing inks were initially used to provide colour(s) in an organised way onto the surface of products. Nowadays, inks are not only used for visual effect, but also for the provision of novel functional properties, as deposition on materials, such as thin films, photovoltaics, OLED and *etc*.

1.6.1 Composition of inks

The composition of an ink can vary enormously, but it is commonly composed of colorants, the polymeric vehicle (binder), carrier (fluid medium) and additives. The

amount of colorant(s), binders and carriers are important variables of an ink formulation. However, the additives are usually present in very small amounts. The composition of inks can be classified as being either volatile or non-volatile. The volatile ingredients include organic solvents, water and coalescing agents. The non-volatile components include polymeric binders, pigments, extenders, dyes, resin precursors and additives [123].

1.6.1.1 Pigments

The distinction between a pigment and a dye is dependent on the solubility of the colorant in the vehicle system. A pigment is present in the ink as a solid. However, a dye is either itself is a liquid or is soluble in its vehicle [124-127]. Pigments can be simply classified as being either inorganic or organic in type. Generally, inorganic pigments are able to provide high resistance to the surrounding environment, such as heat, light, weathering, solvents and chemicals. Inorganic pigments are generally characterised as being relatively opaque due to their high refractive index. Organic pigments usually give high intensity and brightness of colour because the particles have a high refractive index and high transparency. The performance of a dye usually is influenced by the structure of the dye molecule. By contrast, the colour and the technical performance of a pigment is affected not only by the molecular structure, but also by the arrangement of crystal structure and the nature of the pigment particles (*e.g.* size, size distribution, shape, shape distribution, surface area and surface area distribution and the means by which the pigment might aggregate in the medium) [127].

1.6.1.1.1 Titanium dioxide

For many coatings and paints, TiO_2 is the most widely used pigment. Its properties include high refractive index and great opacity. The physical and chemical properties of TiO_2, such as various size ranges, determine its ultimate utilisation. TiO_2 exists in natural minerals as three forms, rutile, anatase and brookite, of which, the anatase form and the rutile form are the most common forms. Table 1-1 illustrates the differences of TiO_2 in rutile and anatase forms [128]. Figure 1.23 demonstrates the crystal structures of TiO_2 in rutile and anatase forms [128, 129]. TiO_2 can be used to control the resistance of the QTC printed films.

The two major production methods for TiO_2 are the sulphate process and the chloride process. The production of anatase form TiO_2 is dependent on the sulphate process, according to the schemes as illustrated below [130]:

$$FeTiO_3 + 2H_2SO_4 \longrightarrow TiOSO_4 + FeSO_4 + 2H_2O$$

$$TiOSO_4 \xrightarrow{OH^-} TiO_2n(H_2O) + H_2SO_4$$

$$TiO_2n(H_2O) \xrightarrow{\Delta} TiO_2n(H_2O) + nH_2O$$

The production of rutile form TiO_2 is dependent on the chloride process, according to the schemes below [130]:

$$TiO_2 \text{ (impure)} + 2Cl_2 + C \longrightarrow TiCl_4 + CO_2$$

$$TiCl_4 + O_2 \longrightarrow TiO_2 \text{ (pure)} + 2Cl_2$$

Table 1-1 Differences of TiO_2 in rutile and anatase forms [128]

	Rutile form	***Anatase form***
Crystal structure	**Tetragonal**	**Tetragonal**
Production	**Commercial**	**Commercial**
Density (g/cm^3)	**4.0**	**3.8**
Particle size (μm)	**0.17 – 0.25**	**0.14 – 0.18**
Dielectric constant	**114**	**48**
Hardness (Mohs)	**6 – 6.5 (brittle)**	**5.5 – 6.0 (brittle)**

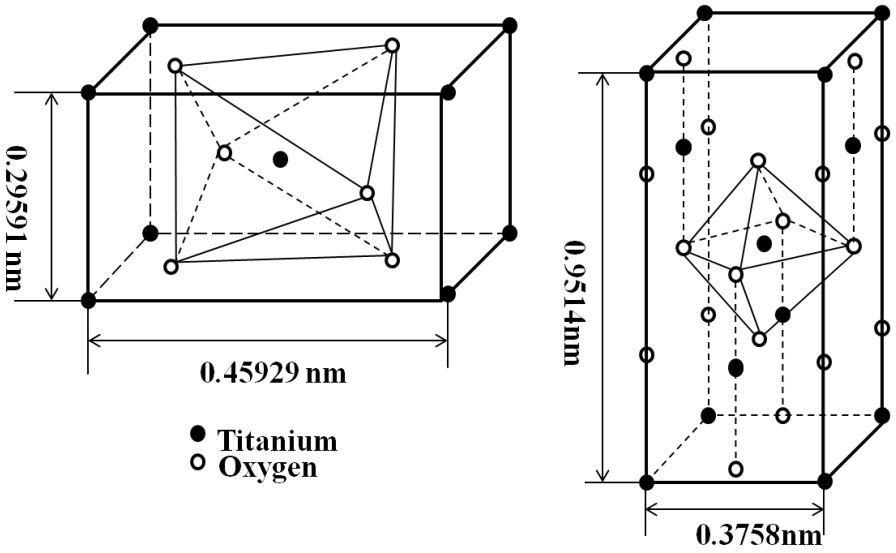

Figure 1.23 The crystal structures of rutile and anatase TiO_2 [128]

1.6.1.2 Carriers

Carriers act as a vehicle for the pigments and binders in the ink formulation and should control the viscosity so as to provide a basis for uniform ink application. Although the presence of the carrier is temporary, it influences not only the application characteristics of an ink, but also its performance, physical properties and the durability of the coating. Carriers can be organic solvents, water or combinations of monomers. Indeed, in some instances, each of these might be used. The major factors to consider when selecting a carrier of an ink formulation are dependent on solvency and evaporation rate requirements [131]. The solvents that are used should not be very volatile because of loss of excessive solvent during screen printing processes [132]. For viscosity/flow characteristic of a screen printable ink, there is no specific viscosity range for screen printing. The average viscosity could be in the range of 1.5 Pa s to 50.0 Pa s, or might be much higher [132, 133].

The objective of this research is to use a water-based binder to produce QTC ink formulations; hence the carrier will be water.

1.6.1.3 Binders

Binders are the most significant component in an ink formulation and determine the drying method, adhesion to the substrate, resistance and mechanical properties of the ink. A binding agent is used to bond pigments, the liquid vehicle, the additives and the substrate [127]. Binders are commonly macromolecules that have molecular masses ranging from 20,000 $gmol^{-1}$ to 1×10^{6} $gmol^{-1}$. The binder acts as a part of vehicle that also provides interaction capability for the ink, and during transfer of the pigmented ink onto the surface of the substrate [121]. In order to achieve an acceptable ink film, the binder must be adsorbed onto the surface of the pigment particles and to the substrate, allowing both of them to be solidified on the substrate forming a coherent macromolecular film of high molecular mass [121, 123, 134]. With the increasing molecular mass of the binder, the properties of the ink film can be altered. Such properties include the elasticity, hardness, adhesion, viscosity and deformation effects [24].

Binders used for printing QTC inks are mixed with the metallic pigment to form printed composites with novel properties. The metal particles are usually encapsulated into the polymer shell [135], which gives a host of composites. There are usually no chemical bonds formed between polymer chains and the particles. Thus, the printed composites maintain of some of the physical and chemical properties of the polymeric binders and the pigments combined. With such unique properties, a wide application potential is employed in diverse areas.

Poly(vinyl pyrrolidone) (PVP) has been widely used in a vast range of applications due to its non-toxicity, excellent biocompatibility and water solubility; such as fabrication of polymer membranes, additives to paints and coatings and as a medium for pharmaceutical tablets [136-140]. Apart from these benefits, PVP also has high dynamic elasticity [141] and is usually used to prevent the agglomeration of nanoparticles [142].

Poly(1-vinyl pyrrolidone-*co*-styrene) or, (PVP-S), is a copolymer that is commonly used in the fabrication of ultrafiltration membranes because of its hydrophilic units, 1-vinylpyrrolidone, and its hydrophobic unit, styrene.

In 1936, acrylic polymer was first commercially used in laminated safety glass as an adhesive interlayer [143]. Since then, acrylic polymers became highly used due to their excellent optical and thermoplastic properties. Acrylic emulsions or polymers are becoming widely popular in the coating industry because of their amazing colour stability and transparency, resistance to aging and to weathering. These acrylic polymers are commonly added into paint formulations as thickeners that increase the shear viscosity to achieve perfect pseudoplastic and thixotropic behaviour and prevent pigment settlement [144]. Acrylic polymers are usually prepared by solution polymerisation of copolymers of acrylate and methacrylate esters [143]. The solubility can be controlled and neutralised of un-ionised carboxylic acid groups by adding bases. The high solid content with low viscosity and low manufacturing cost are also acrylic polymers' advantages [145] along with its high resistance to heat and solvent and its remarkable gloss [146]. Therefore, acrylic copolymers are usually used in the printing and coating industries.

1.6.1.4 Additives

Additives are used to change the physical properties of the ink to and to adapt it to different situations in which it may be applied [147]. Printed films can experience problems during application and in storage. Factors of relevance include slow drying procedures; stiff and brittle ink surfaces, agglomerated pigment particles and improper viscosity *etc.* Therefore, understanding the relationships between additives and the ink system is vital when choosing the best route to ink formulation [131]. The most common additives used by ink manufactures include [127, 148] :

- Rheology modifiers: Used to modifying the rheology of an ink (*e.g.* viscosity, elasticity and rigidity) and also of the print.
- Waxes:Improve the rub resistance of an ink film.
- Driers/Initiators: Used to give acceleration of the curing process between the ink's components.
- Non-reactive binders: Used to provide print stability through their solid state, film forming properties (*e.g.* cellulose nitrate).

- Wetting agents: Used to reduce the vehicle's surface tension and assisting the ink vehicle with respect to penetration of the air pockets (gravure plates, anilox rollers *etc*).
- Defoamers: These prevent the formation of surface foam (usually in inks that contain an aqueous component) and the entrapment of air in an ink film.
- Plasticisers: These are used to improve the flexibility of the solid print film, to aid the rheological responsiveness and to improve the gloss of an ink film. They may also prevent the ink film from being brittle at low temperature.

1.6.2 Wet ink characteristics

Understanding the characteristics of a wet ink film is vital to the effective modelling and optimisation of a QTC ink, especially one that will be delivered by a screen printing process. The study of key characteristics of the fluid ink can help in building up a series of necessary operable parameters for a QTC ink. The key characteristics of such wet inks can be considered to be the flow properties (rheology/viscosity), the surface tension and the quality of the pigment dispersion.

1.6.2.1 Rheology and viscosity

The rheology of a fluid or melt describes the flow behaviour. Rheology is recognised as an important field of scientific study. In general, there are four categories of an ink that need to be recognised. These are elasticity, plasticity, rigidity and viscosity.

The viscosity of a fluid is one of the most significant characteristics of the flow properties of all liquids. Viscosity is the resistance to flow. The viscosity, η, whose unit is Pas, is the ratio of shear stress, σ, to shear rate, γ (Equation 1-10, Equation 1-11 and Equation 1-12). For instance, water has a low viscosity (1 mPas) while screen printing inks are more viscous than water, having a viscosity range from 1,000 mPas to 10,000 mPas for graphics and may reach up to 50,000 mPas for some highly loaded inks and adhesives. A Newtonian fluid, *e.g.* water, demonstrates a constant viscosity when changing the amount of shear force. The

viscosity of most inks decreases as the shear rate increases or as the shear stress decreases. This effect is termed the 'shear thining' or 'pseduoplasticity' phenomenon [149].

$$\eta = \frac{\sigma}{\gamma}$$

Equation 1-10 Shear viscosity, where η, σ and γ represent the viscosity, the applied shear stress and the shear rate respectively

$$\sigma = \frac{F}{A}$$

Equation 1-11 Shear stress, here, F is the force applied over an area A of the ink

$$\gamma = \frac{du}{dz}$$

Equation 1-12 Shear strain rate, where γ represents the change of velocity, u, formed by continuous layers of the ink in the z axis, when shear is applied

'Thixotropy is defined as the property of a liquid's pseudoplasticity, being time dependent flow [126].' Screen printing inks are thixotropic, as shown in Figure 1.24. They give pseudoplasticity with a hysteresis loop. The viscosity decreases when high shear forces are used. Screen printing inks thin during shearing, even though the shear stress is constant. When the inks stop flowing, the viscosity returns back to a value that is close, but not equal to the initial value, slowly or quickly. Thixotropy, which can be identified by the hysteresis loop, helps to define how an ink will behave when it is composed of varying viscosity generating phenomena. Rheopexy is the opposite of thixotropy. In rheopexy, there is an increase in the viscosity as shear forces are applied, as the dashed lines represent (Figure 1.24) [150].

The minimum shear stress that is required to cause a fluid to begin to flow is the 'yield point'. As long as the shear stress exceeds the yield point, the fluid will

flow. The usefulness of the yield point can be explained using non-drip paints as an example. After the removal of the applied force on the substrate and the flow has stopped, the paint's viscosity increases. The dripping of paints can be avoided because the yield point surpasses the force of gravity. Additionally, a high yield point can enable an ink to resist bleeding, but reduces its ability to flow. Inks with a low yield point can flow easily, but bleeding is more likely to occur. Therefore, determining whether or not the flow of an ink is dependent on the yield point is important to controlling any flow and levelling without excessive dripping [149, 150].

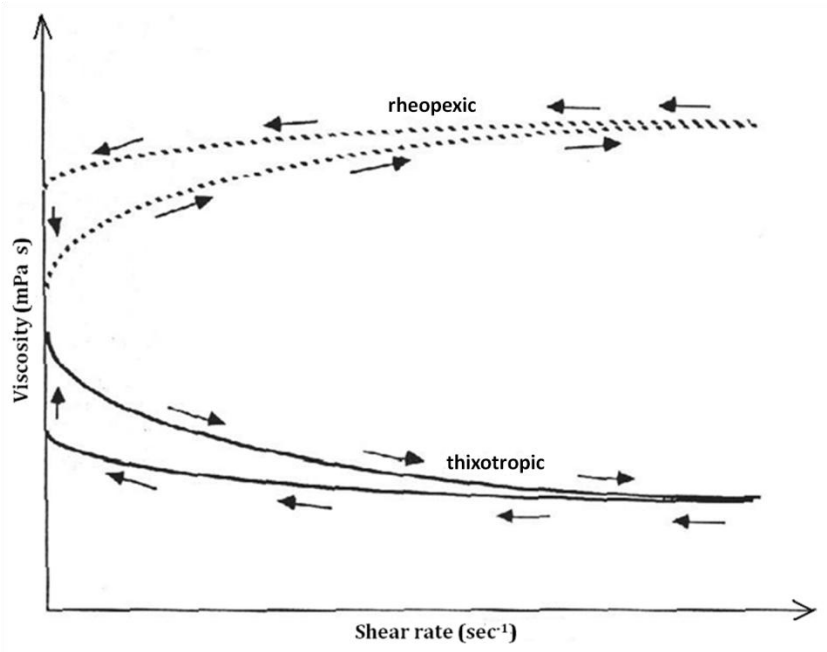

Figure 1.24 Viscosity vs. rate curves with time dependency [133]

Viscosity is dependent on the initial stress used and on the duration of the application of the shear force that is applied. In practice the time taken to return to the initial viscosity fluctuates due to the different ink properties [133, 149].

The applied temperature, solvent composition and the presence of thickeners can vary the viscosity of an ink significantly. The viscosity of most inks decreases as temperature increases. The temperature of the inks must be constant during the printing procedure. Increasing the temperature induces the thinning of most inks, which is due to the increasingly frequent molecular motions that occur with

increasing thermal energy. The viscosity of an ink decreases when a solvent is added. A thickener is a form of additive, such as one of the silicas or other fillers that allow the ink to increase in its viscosity. If inks are known to bleed excessively, thickeners are used to increase the viscosity and the yield point [149, 150].

1.6.2.2 Surface tension

Surface tension plays an important role during liquid flow and after the liquids has stopped flowing. The surface tension of the fluid and the critical surface tension of the substrate influence dramatically the printability of a fluid ink. Wetting phenomena are caused by the attraction forces between ink molecules and the intermolecular forces between ink molecules and the substrate surface. The ink attempts to form spherical droplets to diminish the surface area. The greater the liquid molecule's attraction force, the greater is the surface tension. Consequently, it is difficult for liquids with a high surface tension to wet and adhere onto a solid surface that has a low critical surface tension due to small intramolecular forces between the molecules of the liquid and the molecules of the solid. Solid surface substances can be wetted by lowering their surface tension. One can avoid wetting problems either by decreasing the surface tension of the ink molecules, increasing the surface energy of the substrate or both. One also needs to reduce any contamination. Surfactants will decrease the surface tension of the ink. However, surfactants can result in de-wetting if there is great affinity between the surfactant and the substrate. The surface tension of screen printing inks is usually less than 36 mN/m. That of the substrate is usually significantly greater than 40 mN/m [133].

1.6.2.3 Zeta potential

Zeta potential is a measurement of the magnitude of the charge attraction and repulsion between nanoparticles in solution (colloids). It is one of the parameters used to evaluate the stability of the QTC inks. When the zeta potential values are greater than +25 mV or less than -25 mV, the inks generally have high degrees of stability [151]. Because of van der Waal interactions, the particles with low zeta potential value will aggregate eventually [152].

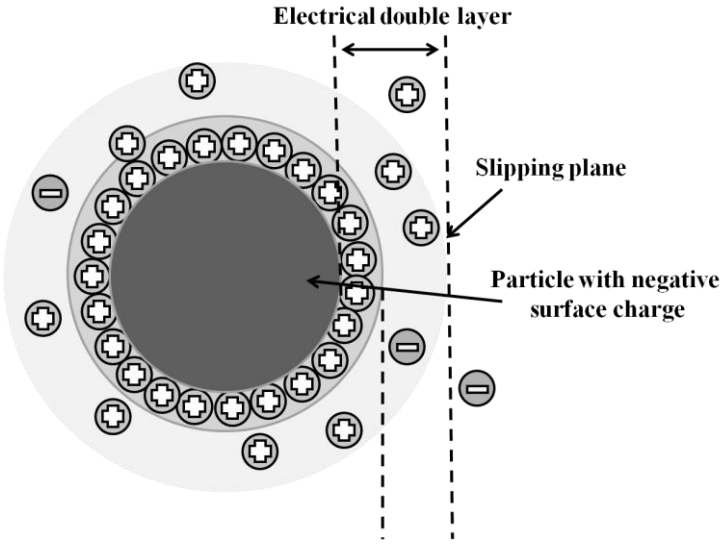

Figure 1.25 A thin layer of opposite charge is attracted by the surface charge from nanoparticles. An electrical double layer is formed around the nanoparticles, which results in an electrical potential that is known as zeta potential [152]

1.6.2.4 Pigment dispersion

Poor dispersion or inadequate milling may result in agglomeration of the pigment particles, the ink then being non-uniform. Aggregates of pigment particles influence not only the ink quality but also the printing operation [148]. As a result, there is a need to understand the mechanism of dispersion and stabilisation of pigment particles during the manufacture of an ink and in its processing. The major factors that can influence the formation of aggregates of pigment particles are the size and shape of the particles, the viscosity of the medium, the surface tension and the interfacial tension, the type of milling equipment used and the temperature of the dispersion [153, 154]. There are a number of methods for reducing the particle size while forming a dispersion, such as ballmills, and/bead mills, centrilmills, rollmills and heavy-duty pugs [155]. The dispersibility of an ink can be increased by adding surface active agents, *i.e.* wetting or dispersing agents, to reduce the surface tension of the vehicle.

There is an increasing use of nickel powders in coatings on dielectric substrates, designed to form a conductive film. The major requirement of the nickel

particles in a QTC ink is that the particles mix with water-based binders to form a stable QTC ink. Therefore, the effective dispersion of such nickel particles in different binders is an important factor. Propylene glycol is an effective dispersant stabiliser of nickel particles in various media, due to the glycol presenting a steric hindrance effect for emulsion in water formulations. In addition, oligomer polyester surfactants have been examined. These diminish the flow resistance given by the nickel particles, thus enhancing the creation of dispersions [85].

1.7 Strategies for the development of the screen printable ink formulations

Understanding strategies for the development of ink formulations is important. It is necessary and significant to consider the properties of ink formulations first. For example, the conductivity, the flexibility and adhesion of ink films on the substrate need to be taken into consideration [156]. Strategies for the development of QTC ink formulations need to be built on understanding of the nature of ink formulation, experimenting with the design of the mixture and modelling and optimising mixture formulations.

1.7.1 Nature of screen printable ink formulations

Before designing an ink formulation, the nature and characteristics of each different component need to be understood. For instance, a study of the morphology of the particles, the rheological properties of the fluids, the mechanical properties and the solid content of the binders should be rationalised, as should the various types of interaction that can (will) be used.

1.7.2 Experimental design of ink formulations

When designing an ink formulation that contains several different components, the factorial design method is an easy statistical method to use. The benefits of factorial design offer simple and precise methods for analysis, fewer experimental runs and fewer needs for independent observations on each factor.

In factorial designs, there are k factors with m levels in n observations. These indicate k variables in an ink formulation giving n experimental results. In

general, m is usually assigned as 2, in order to screen the results at the beginning of a R&D project. Therefore, the number of required experimental runs is shown as Equation 1-13 [156].

$$n = 2^k$$

Equation 1-13 Required experimental runs at two levels; k represents the number of variables

The construction of the design matrix is formalised by Yates Order, which describes a special structure that generates the least squares estimates for factor effects and all relative interactions. When a matrix is established, columns and rows are defined as variables and experimental runs. The formula for 'Sign Change' is illustrated by Equation 1-14 [156].

$$\textit{The number of sign changes} = 2^{n-1}$$

Equation 1-14 Formula for sign changes, where n represents the column number

1.7.3 Modelling and optimisation of ink formulations

When modelling and optimising the formulations, one problem that might occur is the use of a large number of multiple components and multiple performances. In order to simplify this problem, Equation 1-15, which expresses the performance of an ink as a function of the ink components, can be used.

$$Y = f(X_i)$$

Equation 1-15 Generic mathematical model for mixed system. Here, Y is the performance of the mixture, f represents a functional relationship and X_i is the composition of component i

For instance, the property of two component mixtures, using this generic mathematical model, can be extended as shown in Equation 1-16:

$$Y=f(X_1, X_2)=a_1X_1+a_2X_2+a_{12}X_1X_2$$

Equation 1-16 (a_1, a_2 are indications of the influences of components 1, 2. a_{12} is an indication of the influence of the interaction between components 1 and 2)

From experimental data, each individual ink system has a corresponding performance Y, as well as three unknown coefficients. Therefore, three equations with three unknown coefficients are established. As a result, each of the unknown coefficients can be calculated.

1.8 Aims of research

Owing to the fact that the development of QTC inks is a relatively new technology, the precise influence of each QTC ink component and the effect of any interactions between the ink's ingredients, on the performance of the QTC inks are not well understood. Thus, a study of the formulation procedures associated with QTC inks was an effective starting point towards helping to understand more thoroughly how the QTC system works.

The aim of this research was to develop water-based screen printable QTC inks that have/had similar electrical and mechanical properties to those of the QTC materials. Also, it is significant to produce repeatable and reliable electrical properties as QTC materials. Meanwhile, the thicknesses of the ink films would be thin enough to embed them into the flexible displays, *e.g.* electronics, textiles, pulse control, printable memory, computer, credit card, e-paper, mobile and tablets. Also, it was significant to interpret and to understand the mechanism of the electrical performance of the QTC inks under compression.

One of the most significant potential benefits of the proposed QTC inks is their large number of applications, as mentioned in last paragraph. Also, the printed

films will be low power consumption, as the electrons will not be activated until pressure is applied. This, in turn, means that QTC ink films have a longer lifetime when acting as conductors compared to other conventional ones. Furthermore, the proposed QTC ink film will display a large dynamic range, as the electrical resistance range covering over 12 orders of magnitude. Moreover, the printed films will be reliable, sensitive, intrinsically safe and rugged. Also, the proposed QTC inks will be environmental friendly as the binder used is water-based.

The primary aim of this research was to develop QTC inks that could be printed using printing techniques. These inks must display pressure-responsive electrical conductivity. Developing an ink formulation was the main challenge of the research, as various conditions of the printing process had to be satisfied in terms of wetting, adhesion and drying after deposition of liquid layers. Meanwhile, pressure-responsive electrical properties have to be achieved to allow the printed films to perform as QTC materials. In order to accomplish these electrical properties, an extremely high loading of metal content had to be applied to the ink, which also had to be screen printable.

Through the study of QTC material, it would be possible to establish an understanding of relevant mechanisms of operation. Such a study should covers mixture experimental design, modelling the electrical-mechanical properties and the composition relationships of the QTC inks and the optimisation of the QTC inks, in order to achieve similar electrical properties as those possessed by the QTC materials and characterisation of the QTC inks. In the process of the formulation development, various aspects would be addressed. Interpretation of data obtained to establish and understand the conductivity profile-structure/composition relationship would be an important part.

References

1. Lee, K.J., B.H. Jun, T.H. Kim, and J. Joung, *Direct synthesis and inkjetting of silver nanocrystals toward printed electronics.* Nanotechnology, 2006. **17**(9): p. 2424.
2. Kantola, V., J. Kulovesi, L. Lahti, R. Lin, M. Zavodchikova, and E. Coatanéa, *1.3 Printed Electronics, Now and Future.* Bit Bang, 2009: p. 63.

3. World, P.E. *Thinfilm memory EU certified* (online). Accessed 15 Dec 2014. Available from: http://www.printedelectronicsworld.com/articles/thinfilm-memory-eu-certified-00002368.asp?sessionid=1.
4. Leenen, M.A., V. Arning, H. Thiem, J. Steiger, and R. Anselmann, *Printable electronics: flexibility for the future.* physica status solidi (a), 2009. **206**(4): p. 588-597.
5. IDTechEx. *Printed electronics equipment market: profitable but subsidized* (online). Accessed 20/05/2015. Available from: http://www.idtechex.com/research/articles/printed-electronics-equipment-market-profitable-but-subsidized-00007044.asp?donotredirect=true.
6. Anderson, G. *A 3D Printing Stock with a PE of 40: Meet MGI* (online). Accessed 21/05/2015. Available from: http://3dprintingindustry.com/2014/02/19/3d-printing-stock-pe-40-meet-mgi/.
7. Bloor, D., A. Graham, E. Williams, P. Laughlin, and D. Lussey, *Metal–polymer composite with nanostructured filler particles and amplified physical properties.* Applied Physics Letters, 2006. **88**(10): p. 102103.
8. Lussey, D., *Conductive structures*, 2003, WO 2000079546A1.
9. PeratechLtd.com. *Peratech's QTC™ Material sensor technology licensed to Samsung Electro-mechanics* (online). Accessed 03 June 2013. Available from: http://www.peratech.com/pr_samsung.php.
10. PeratechLtd.com. *RFID & Card Security Applications* (online). Accessed 03 June 2013. Available from: http://www.peratech.com/rfid-and-card-security.html.
11. Nadeau, J., V. White, D. Dougherty, and J. Maurer, *Improved Ion-Channel Biosensors.* 2004. p: 7-8.
12. Martin, T.B., D. Lussy, F. Gaudiano, A. Hulse, M.A. Diftler, D. Rodriguez, P. Bielski, and M. Butzer, *Compact Tactile Sensors for Robot Fingers.* 2004. **9**(2) p: 1182-203.
13. Zhang, T., L. Jiang, X. Wu, W. Feng, D. Zhou, and H. Liu, *Fingertip Three-Axis Tactile Sensor for Multifingered Grasping.* 2014. **20**(4) p:1875 - 1885.
14. Cannata, G. and M. Maggiali, *Design of a tactile sensor for robot hands.* Sensors: Focus on Tactile Force and Stress Sensors, 2008: p. 271-288.
15. Clemens, W., W. Fix, J. Ficker, A. Knobloch, and A. Ullmann, *From polymer transistors toward printed electronics.* Journal of Materials Research, 2004. **19**(07): p. 1963-1973.
16. Li, Y., Y. Wu, and B.S. Ong, *Facile synthesis of silver nanoparticles useful for fabrication of high-conductivity elements for printed electronics.* Journal of the American Chemical Society, 2005. **127**(10): p. 3266-3267.
17. Cho, J.H., J. Lee, Y. Xia, B. Kim, Y. He, M.J. Renn, T.P. Lodge, and C.D. Frisbie, *Printable ion-gel gate dielectrics for low-voltage polymer thin-film transistors on plastic.* Nature materials, 2008. **7**(11): p. 900-906.
18. Li, X.-C.C., *Luminescent ink for printing of organic luminescent devices*, 2002, US6372154 B1.
19. Ishizaki, M., K. Kanaizuka, M. Abe, Y. Hoshi, M. Sakamoto, T. Kawamoto, H. Tanaka, and M. Kurihara, *Preparation of electrochromic Prussian blue nanoparticles dispersible into various solvents for realisation of printed electronics.* Green Chemistry, 2012. **14**(5): p. 1537-1544.

20. Rogers, J.A., Z. Bao, K. Baldwin, A. Dodabalapur, B. Crone, V. Raju, V. Kuck, H. Katz, K. Amundson, and J. Ewing, *Paper-like electronic displays: Large-area rubber-stamped plastic sheets of electronics and microencapsulated electrophoretic inks.* Proceedings of the National Academy of Sciences, 2001. **98**(9): p. 4835-4840.
21. Lee, Y., J.-r. Choi, K.J. Lee, N.E. Stott, and D. Kim, *Large-scale synthesis of copper nanoparticles by chemically controlled reduction for applications of inkjet-printed electronics.* Nanotechnology, 2008. **19**(41): p. 415604.
22. Technology, N. *Plastic Electronics: How they could change consumer technology* (online). Accessed 16 Dec 2014. Available from: http://www.bbc.co.uk/news/technology-20417384.
23. News. *Future directions in computing* (online). Accessed 16 Dec 2014. Available from: http://news.bbc.co.uk/1/hi/technology/7085166.stm.
24. Bloor, D., K. Donnelly, P.J. Hands, P. Laughlin, and D. Lussey, *A metal polymer composite with unusual properties.* Journal of physics D : applied physics., 2005. **38**(16): p. 2851-2860.
25. Ko, S.H., H. Pan, C.P. Grigoropoulos, C.K. Luscombe, J.M. Fréchet, and D. Poulikakos, *All-inkjet-printed flexible electronics fabrication on a polymer substrate by low-temperature high-resolution selective laser sintering of metal nanoparticles.* Nanotechnology, 2007. **18**(34): p. 345202.
26. Rogers, J.A. and Z. Bao, *Printed plastic electronics and paperlike displays.* Journal of polymer science part A: Polymer Chemistry, 2002. **40**(20): p. 3327-3334.
27. Wu, Y., Y. Li, and B.S. Ong, *A simple and efficient approach to a printable silver conductor for printed electronics.* Journal of the American Chemical Society, 2007. **129**(7): p. 1862-1863.
28. IDTechEx. *Printed, Flexible and Organic Electronics Forecasts, Players and Opportunities 2011-2021* (online). Accessed 21/05/2015. Available from: http://www.idtechex.com/research/reports/printed-organic-and-flexible-electronics-forecasts-players-and-opportunities-2011-2021-000264.asp.
29. IDTechEx. *Printed, Organic & Flexible Electronics Forecasts, Players & Opportunities 2015 - 2025* (online). Accessed 20/07/2015. Available from: http://www.idtechex.com/research/reports/printed-organic-and-flexible-electronics-forecasts-players-and-opportunities-2015-2025-000425.asp.
30. Mohanty, A.K., M. Misra, and L.T. Drzal, *Application of polyurethane prepolymer to preparation of wood powder/polrvinyl chloride composite material,* 2012, CN102433009 A.
31. Song, Q., J. Li, and X. Zeng, *Minimizing the increasing solid waste through zero waste strategy.* Journal of Cleaner Production, 2015, **104**, p: 199 – 210.
32. Kuo, Y., *Thin Film Transistor Technology--Past Present and Future.* Electrochemical Society Interface, 2013. **22**(1): p. 55-61.
33. Nie, X., H. Wang, and J. Zou, *Inkjet printing of silver citrate conductive ink on PET substrate.* Applied Surface Science, 2012. **261**, p: 554-560.
34. Lee, S.-W. and S.-K. Joo, *Low temperature poly-Si thin-film transistor fabrication by metal-induced lateral crystallization.* Electron Device Letters, IEEE, 1996. **17**(4): p. 160-162.
35. Kagan, C.R. and P. Andry, *Thin-film transistors*. 2003, **1**, p: 1-33.

36. Klauk, H., *Organic electronics: materials, manufacturing, and applications*. 2006: **1**, p: 3 - 29.
37. Madhavan, N., *Small-molecule organic semiconductors*, 2002, p: 49 – 56.
38. Yamazaki, S. and Y. Takemura, *Electric device, matrix device, electro-optical display device, and semiconductor memory having thin-film transistors*, 1998, US5349366 A.
39. Chotas, H.G., J.T. Dobbins III, and C.E. Ravin, *Principles of digital radiography with large-area, electronically readable detectors: a review of the basics.* Radiology, 1999. **210**(3): p. 595-599.
40. Bushberg, J.T. and J.M. Boone, *The essential physics of medical imaging*. 2011, **12**(1), p: 33 – 65.
41. Chen, C.-W., T.-C. Chang, P.-T. Liu, H.-Y. Lu, K.-C. Wang, C.-S. Huang, C.-C. Ling, and T.-Y. Tseng, *High-performance hydrogenated amorphous-Si TFT for AMLCD and AMOLED applications.* Electron Device Letters, IEEE, 2005. **26**(10): p. 731-733.
42. Comiskey, B., J. Albert, H. Yoshizawa, and J. Jacobson, *An electrophoretic ink for all-printed reflective electronic displays.* nature, 1998. **394**(6690): p. 253-255.
43. Chen, Y., J. Au, P. Kazlas, A. Ritenour, H. Gates, and M. McCreary, *Electronic paper: Flexible active-matrix electronic ink display.* nature, 2003. **423**(6936): p. 136-136.
44. Times, L.A. *The Business and Culture of Our Digital Lives* (online). Accessed 03/06/2015. Available from: http://latimesblogs.latimes.com/technology/2009/08/epaper-market-expands.html.
45. Computerworld. *E-paper display gives payment cards a changing security code* (online). Accessed 22/05/2015. Available from: http://www.computerworld.com/article/2924994/security0/e-paper-display-gives-payment-cards-a-changing-security-code.html.
46. TeleRead. *Amazon, Sony market percentages published: Are they meaningful? Probably not* (online). Accessed 20/07/2015. Available from: http://www.teleread.com/sony-reader/amazon-sony-market-percentages-published-are-they-meaningful-probably-not/.
47. Coleman, J.P., A.T. Lynch, P. Madhukar, and J.H. Wagenknecht, *Printed, flexible electrochromic displays using interdigitated electrodes.* Solar energy materials and solar cells, 1999. **56**(3): p. 395-418.
48. Liu, J. and J.P. Coleman, *Nanostructured metal oxides for printed electrochromic displays.* Materials Science and Engineering: A, 2000. **286**(1): p. 144-148.
49. Tehrani, P., L.-O. Hennerdal, A.L. Dyer, J.R. Reynolds, and M. Berggren, *Improving the contrast of all-printed electrochromic polymer on paper displays.* Journal of Materials Chemistry, 2009. **19**(13): p. 1799-1802.
50. Alexander J Webb, M.S., David Bloor, Del Atkinson, Adam Graham, Paul Laughlin and David Lussey, *A multi-component nanocomposite screen-printed ink with non-linear touch sensitive electrical conductivity.* Nanotechnology, 2013. **24**(166501): p. 1-9.
51. Park, K., D. Seo, and J. Lee, *Conductivity of silver paste prepared from nanoparticles.* Colloids and Surfaces A: Physicochemical and Engineering Aspects, 2008. **313**: p. 351-354.

52. Jain, A., D.B. Bhargava, and A. Rajput, *TOUCH-SCREEN TECHNOLOGY*. International Journal of Advanced Research in Computer Science and Electronics Engineering (IJARCSEE), 2013. **2**(1): p. pp: 074-078.
53. Kim, H.-K., S. Lee, and K.-S. Yun, *Capacitive tactile sensor array for touch screen application.* Sensors and Actuators A: Physical, 2011. **165**(1): p. 2-7.
54. Drafts, B., *Acoustic wave technology sensors*. IEEE Transactions on Microwave Theory and Techniques, 2001. **49**(4): p. 795-802.
55. Vellekoop, M.J., *Acoustic wave sensors and their technology.* Ultrasonics, 1998. **36**(1): p. 7-14.
56. Science, N. *How Do Photovoltaics Work?* (online). Accessed 27/05/2015. Available from: http://science.nasa.gov/science-news/science-at-nasa/2002/solarcells/.
57. Atwater, H.A. and A. Polman, *Plasmonics for improved photovoltaic devices.* Nature materials, 2010. **9**(3): p. 205-213.
58. Coakley, K.M. and M.D. McGehee, *Conjugated polymer photovoltaic cells.* Chemistry of Materials, 2004. **16**(23): p. 4533-4542.
59. Käfer, D., M. He, J. Li, M.S. Pambianchi, J. Feng, J.C. Mauro, and Z. Bao, *Ultra-Smooth and Ultra-Strong Ion-Exchanged Glass as Substrates for Organic Electronics.* Advanced Functional Materials, 2013. **23**(25): p. 3233-3238.
60. Sirringhaus, H., *25th Anniversary Article: Organic Field-Effect Transistors: The Path Beyond Amorphous Silicon.* Advanced Materials, 2014. **26**(9): p. 1319-1335.
61. Garbuzov, D.Z., S.R. Forrest, and P. Burrows, *Organic light emitting devices using phosphor layers; used for flat panel displays in television and computer screens*, 1999, US5721160 A.
62. Baude, P.F., D.A. Ender, T.W. Kelley, M.A. Haase, D.V. Muyres, and S.D. Theiss. *Organic semiconductor RFID transponders*. in *Electron Devices Meeting, 2003*, **14**(2) p: 12-56.
63. Dodabalapur, A., L. Rothberg, and T. Miller, *Color variation with electroluminescent organic semiconductors in multimode resonant cavities.* Applied Physics Letters, 1994. **65**(18): p. 2308-2310.
64. Gangwar, A. and B. Mazhari, *An Organic Device with Thin Film Transistor Merged with Light Emitting Diode through Use of an Accumulation Layer in TFT As an Electrode.* ECS Transactions, 2015. **67**(1): p. 199-204.
65. Holliday, S., J.E. Donaghey, and I. McCulloch, *Advances in charge carrier mobilities of semiconducting polymers used in organic transistors.* Chemistry of Materials, 2013. **26**(1): p. 647-663.
66. Katz, H.E., *Recent advances in semiconductor performance and printing processes for organic transistor-based electronics.* Chemistry of Materials, 2004. **16**(23): p. 4748-4756.
67. Sun, Y. and J.A. Rogers, *Inorganic semiconductors for flexible electronics.* Advanced Materials, 2007. **19**(15): p. 1897-1916.
68. Kim, D.-H., N. Lu, R. Ghaffari, and J.A. Rogers, *Inorganic semiconductor nanomaterials for flexible and stretchable bio-integrated electronics.* NPG Asia Materials, 2012. **4**(4): p. e15.
69. Kim, H., C. Gilmore, A. Pique, J. Horwitz, H. Mattoussi, H. Murata, Z. Kafafi, and D. Chrisey, *Electrical, optical, and structural properties of*

indium–tin–oxide thin films for organic light-emitting devices. Journal of Applied Physics, 1999. **86**(11): p. 6451-6461.

70. Wu, C., C. Wu, J. Sturm, and A. Kahn, *Surface modification of indium tin oxide by plasma treatment: An effective method to improve the efficiency, brightness, and reliability of organic light emitting devices.* Applied Physics Letters, 1997. **70**(11): p. 1348-1350.
71. De Jong, M., L. Van Ijzendoorn, and M. De Voigt, *Stability of the interface between indium-tin-oxide and poly (3, 4-ethylenedioxythiophene)/poly (styrenesulfonate) in polymer light-emitting diodes.* Applied Physics Letters, 2000. **77**(14): p. 2255-2257.
72. Berggren, M., D. Nilsson, and N.D. Robinson, *Organic materials for printed electronics.* Nature materials, 2007. **6**(1): p. 3-5.
73. Cook, B.S., J.R. Cooper, and M.M. Tentzeris, *Multi-layer RF capacitors on flexible substrates utilizing inkjet printed dielectric polymers.* Microwave and Wireless Components Letters, IEEE, 2013. **23**(7): p. 353-355.
74. Inui, T., H. Koga, M. Nogi, N. Komoda, and K. Suganuma, *A Miniaturized Flexible Antenna Printed on a High Dielectric Constant Nanopaper Composite.* Advanced Materials, 2014, **27**(6), p: 1112 – 1116.
75. Ng, T.N., P. Mei, G.L. Whiting, D.E. Schwartz, B. Abraham, Y. Wu, and J. Veres. *Comparison of conductor and dielectric inks in printed organic complementary transistors*. in *SPIE Organic Photonics+ Electronics*. 2014, **9185**(4), p: 223 – 532.
76. Feller, J., I. Linossier, and G. Levesque, *Conductive polymer composites (CPCs): comparison of electrical properties of poly (ethylene-co-ethyl acrylate)-carbon black with poly (butylene terephthalate)/poly (ethylene-co-ethyl acrylate)-carbon black.* Polymers for advanced technologies, 2002. **13**(10-12): p. 714-724.
77. Pang, H., L. Xu, D.-X. Yan, and Z.-M. Li, *Conductive polymer composites with segregated structures.* Progress in Polymer Science, 2014. **39**(11): p. 1908-1933.
78. Narkis, M., M. Zilberman, and A. Siegmann, *On the" curiosity" of electrically conductive melt processed doped-polyaniline/polymer blends versus carbon-black/polymer compounds.* Polymers for advanced technologies, 1997. **8**(8): p. 525-528.
79. Norman, R.H., *Conductive rubbers and plastics: their production, application and test methods*. 1970, **287**(1), p: 267 – 287.
80. Iijima, S., *Helical microtubules of graphitic carbon.* nature, 1991. **354**(6348): p. 56-58.
81. Piggott, M.R., *Load bearing fibre composites*. 2002: **9**(3), p: 155 -186.
82. Huang, Y., B. Xiang, X. Ming, X. Fu, and Y. Ge. *Conductive mechanism research based on pressure-sensitive conductive composite material for flexible tactile sensing*. in *Information and Automation, 2008.* **53**(3), p: 1614 – 1619.
83. Harris, P., *Carbon nanotube composites.* International Materials Reviews, 2004. **49**(1): p. 31-43.
84. Jia, Z., Z. Wang, C. Xu, J. Liang, B. Wei, D. Wu, and S. Zhu, *Study on poly (methyl methacrylate)/carbon nanotube composites.* Materials Science and Engineering: A, 1999. **271**(1): p. 395-400.

85. Tseng, W.J. and C.-N. Chen, *Dispersion and rheology of nickel nanoparticle inks.* Journal of Materials Science, 2006. **41**(4): p. 1213-1219.
86. Tokushige, M., T. Nishikiori, and Y. Ito, *Synthesis of Ni nanoparticles by plasma-induced cathodic discharge electrolysis.* Journal of applied electrochemistry, 2009. **39**(10): p. 1665-1670.
87. Chen, Y., D.-L. Peng, D. Lin, and X. Luo, *Preparation and magnetic properties of nickel nanoparticles via the thermal decomposition of nickel organometallic precursor in alkylamines.* Nanotechnology, 2007. **18**(50): p. 505703.
88. Yoshinaga, M., K. Yamamoto, N. Sato, K. Aoki, T. Morikawa, and A. Muramatsu, *Remarkably enhanced photocatalytic activity by nickel nanoparticle deposition on sulfur-doped titanium dioxide thin film.* Applied Catalysis B: Environmental, 2009. **87**(3): p. 239-244.
89. Kumar, R.V., Y. Koltypin, O. Palchik, and A. Gedanken, *Preparation and characterization of nickel–polystyrene nanocomposite by ultrasound irradiation.* Journal of applied polymer science, 2002. **86**(1): p. 160-165.
90. Zach, M.P. and R.M. Penner, *Nanocrystalline nickel nanoparticles.* Advanced Materials, 2000. **12**(12): p. 878-883.
91. Yao, Y., Y. Chen, M. Tai, D. Wang, and H. Lin, *Magnetic anisotropy effects in nano-cluster nickel particles.* Materials Science and Engineering: A, 1996. **217**: p. 281-285.
92. Chen, D.-H. and S.-H. Wu, *Synthesis of nickel nanoparticles in water-in-oil microemulsions.* Chemistry of Materials, 2000. **12**(5): p. 1354-1360.
93. Carroll, K.J., J.U. Reveles, M.D. Shultz, S.N. Khanna, and E.E. Carpenter, *Preparation of elemental Cu and Ni nanoparticles by the polyol method: an experimental and theoretical approach.* The Journal of Physical Chemistry C, 2011. **115**(6): p. 2656-2664.
94. Wang, W.-N., Y. Itoh, I.W. Lenggoro, and K. Okuyama, *Nickel and nickel oxide nanoparticles prepared from nickel nitrate hexahydrate by a low pressure spray pyrolysis.* Materials Science and Engineering: B, 2004. **111**(1): p. 69-76.
95. Cushing, B.L., V.L. Kolesnichenko, and C.J. O'Connor, *Recent advances in the liquid-phase syntheses of inorganic nanoparticles.* Chemical Reviews, 2004. **104**(9): p. 3893-3946.
96. Singh, M., M. Kumar, F. Štěpánek, P. Ulbrich, P. Svoboda, E. Santava, and M. Singla, *Liquid-Phase Synthesis of Nickel Nanoparticles stabilized by PVP and study of their structural and magnetic properties.* Advanced Materials Letters, 2011. **2**(6): p. 409-414.
97. Lantada, A.D., P. Lafont, J.L.M. Sanz, J.M. Munoz-Guijosa, and J.E. Otero, *Quantum tunnelling composites: Characterisation and modelling to promote their applications as sensors.* Sensors and Actuators A: Physical, 2010. **164**(1): p. 46-57.
98. News, E.I. *Quantum trick for pressure-sensitive mobile devices* (online). Accessed 07/08/2015. Available from: http://einewz.blogspot.co.uk/2010/02/quantum-trick-for-pressure-sensitive.html.
99. Lussey, D., *Polymer composition*, 2001, WO2008135787A1.

100. McLachlan, D.S., M. Blaszkiewicz, and R.E. Newnham, *Electrical resistivity of composites.* Journal of the American Ceramic Society, 1990. **73**(8): p. 2187-2203.
101. Nauman, S., I. Cristian, and V. Koncar, *Simultaneous application of fibrous piezoresistive sensors for compression and traction detection in glass laminate composites.* Sensors, 2011. **11**(10): p. 9478-9498.
102. Wang, Y. and C. Anderson, *Formation of thin transparent conductive composite films from aqueous colloidal dispersions.* Macromolecules, 1999. **32**(19): p. 6172-6179.
103. Fukada, E. and I. Yasuda, *On the piezoelectric effect of bone.* Journal of the Physical Society of Japan, 1957. **12**(10): p. 1158-1162.
104. Liu, W. and X. Ren, *Large piezoelectric effect in Pb-free ceramics.* Physical Review Letters, 2009. **103**(25): p. 257602.
105. design, E. *What's The Difference Between Piezoelectric And Piezoresistive Components* (online). Accessed 20/07/2015. Available from: http://electronicdesign.com/components/what-s-difference-between-piezoelectric-and-piezoresistive-components.
106. Lundberg, B. and B. Sundqvist, *Resistivity of a composite conducting polymer as a function of temperature, pressure, and environment: Applications as a pressure and gas concentration transducer.* Journal of Applied Physics, 1986. **60**(3): p. 1074-1079.
107. Hartmann, B., *Pressure and Temperature Dependence of Electrical Conduction in Polymers.* Journal of Rheology (1978-present), 1986. **30**(4): p. 843-852.
108. Gargaud, M., *Encyclopedia of astrobiology*, 2011: **465**(1), p: 57-79.
109. Graham, A., *Electrcial Properties and Vapour Sensing Characteristics of a Novel-Metal Polymer Composite*, 2008, University of Durham.
110. Sarid, D., *Fowler–Nordheim Tunneling.* Exploring Scanning Probe Microscopy with MATHEMATICA, Second Edition: 2007, **11**(10), p. 160-169.
111. Youngs, I.J., *Exploring the universal nature of electrical percolation exponents by genetic algorithm fitting with general effective medium theory.* Journal of Physics D: Applied Physics, 2002. **35**(23): p. 3127.
112. Feng, S. and P.N. Sen, *Percolation on elastic networks: new exponent and threshold.* Physical Review Letters, 1984. **52**(3): p. 216.
113. Clerc, J., V. Podolskiy, and A. Sarychev, *Precise determination of the conductivity exponent of 3D percolation using exact numerical renormalization.* The European Physical Journal B-Condensed Matter and Complex Systems, 2000. **15**(3): p. 507-516.
114. Krupa, I. and I. Chodák, *Physical properties of thermoplastic/graphite composites.* European Polymer Journal, 2001. **37**(11): p. 2159-2168.
115. Brosseau, C., *Generalized effective medium theory and dielectric relaxation in particle-filled polymeric resins.* Journal of Applied Physics, 2002. **91**(5): p. 3197-3204.
116. Lin, C.R., Y.C. Chen, and C.Y. Chang, *A Links-Nodes-Blobs Model for Conductive Polymer Composites.* Macromolecular theory and simulations, 2001. **10**(4): p. 219-224.

117. Lin, C.R. and Y.D. Lee, *Strain-dependent dynamic properties of filled rubber network systems.* Macromolecular theory and simulations, 1996. **5**(6): p. 1075-1104.
118. Medalia, A., *Effect of carbon black on dynamic properties of rubber vulcanizates.* Rubber chemistry and Technology, 1978. **51**(3): p. 437-523.
119. Connolly, C., *Switches and pressure sensors benefit from novel composite material.* Sensor Review, 2004. **24**(3): p. 261-264.
120. Taggi, A.J. and P. Walker, *Printing processes.* Kirk-Othmer Encyclopedia of Chemical Technology, 1996, **27**(4), p: 456 – 524.
121. Stephens, J., *Screen process printing: a practical guide*. 1987, **46**(3), p: 23 – 34.
122. Kipphan, H., *Handbook of Print Media.* ISBN-10: 3540669418, 2008, **464**(4), p: 345 -543.
123. Stoye, D. and W. Freitag, *Paints, Coatings and Solvents*, 1997 , **35**(1), p: 2 – 10.
124. Christie, R., *Colour chemistry*. 2014: Royal Society of Chemistry.
125. Christie, R.M., *Pigments: structures and synthetic procedures*. 1994: Oil & Colour Chemists' Association.
126. Finley, C., *Printing paper and inks*. 1997: Delmar.
127. Lin, J.T.G.a.L., *Colour and Image Creation: Inks, paints and packaging materials*. Vol. 4. 1999, The Department of Colour Chemistry, The University of Leeds.
128. Buxbaum, G., *Industrial inorganic pigments*. 2008: John Wiley & Sons.
129. Yang, H.G., C.H. Sun, S.Z. Qiao, J. Zou, G. Liu, S.C. Smith, H.M. Cheng, and G.Q. Lu, *Anatase TiO2 single crystals with a large percentage of reactive facets.* nature, 2008. **453**(7195): p. 638-641.
130. Reck, E. and M. Richards, *Titanium Dioxide- Manufacture, Environment and Life Cycle Analysis: The Tioxide Experience.* Surface Coatings International, 1997. **80**(12): p. 568-572.
131. Koleske, J.V., *Paint and coating testing manual: of the Gardner-Sward handbook*, 1995, **17**(5), p: 57-63.
132. Leach, R.H., *The printing ink manual*. 1993: **68**(3), p: 575 – 624.
133. Gilleo, K., *Rheology and Surface Chemistry for Screen Printing.* Screen Printing Magazine, 1989, **54**(3), p: 321 – 338.
134. Řeháček, K., *Pigment-Binder Interaction in Paints.* Industrial & Engineering Chemistry Product Research and Development, 1976. **15**(1): p. 75-81.
135. Tang, E., G. Cheng, and X. Ma, *Preparation of nano-ZnO/PMMA composite particles via grafting of the copolymer onto the surface of zinc oxide nanoparticles.* Powder Technology, 2006. **161**(3): p. 209-214.
136. Sun, M., Y. Su, C. Mu, and Z. Jiang, *Improved antifouling property of PES ultrafiltration membranes using additive of silica− PVP nanocomposite.* Industrial & Engineering Chemistry Research, 2009. **49**(2): p. 790-796.
137. Qin, J.-J., Y.-M. Cao, Y.-Q. Li, Y. Li, M.-H. Oo, and H. Lee, *Hollow fiber ultrafiltration membranes made from blends of PAN and PVP*. Separation and purification technology, 2004. **36**(2): p. 149-155.
138. Marchese, J., M. Ponce, N. Ochoa, P. Prádanos, L. Palacio, and A. Hernández, *Fouling behaviour of polyethersulfone UF membranes made with different PVP.* Journal of Membrane Science, 2003. **211**(1): p. 1-11.

139. Lafreniere, L.Y., F.D. Talbot, T. Matsuura, and S. Sourirajan, *Effect of poly (vinylpyrrolidone) additive on the performance of poly (ether sulfone) ultrafiltration membranes.* Industrial & Engineering Chemistry Research, 1987. **26**(11): p. 2385-2389.
140. Wan, L.-S., X.-J. Huang, and Z.-K. Xu, *Diffusion and structure of water in polymers containing N-vinyl-2-pyrrolidone.* The Journal of Physical Chemistry B, 2007. **111**(5): p. 922-928.
141. Noskov, B., A. Akentiev, and R. Miller, *Dynamic surface properties of poly (vinylpyrrolidone) solutions.* Journal of colloid and interface science, 2002. **255**(2): p. 417-424.
142. Naseri, M.G., E. Saion, and N.K. Zadeh, *The amazing effects and role of PVP on the crystallinity, phase composition and morphology of nickel ferrite nanoparticles prepared by thermal treatment method.* International Nano Letters, 2013. **3**(1): p. 19.
143. Brase, I.E., *Acrylic acid-alkali metal vinyl sulfonate copolymer water solubility enhancer*, 1990, US4898677 A.
144. Lee, D.Y. and J.H. Kim, *Preparation of small-sized carboxylated latexes by emulsion polymerization using alkali-soluble random copolymer.* Journal of applied polymer science, 1998. **69**(3): p. 543-550.
145. Kuo, P.L. and C.J. Chen, *Functional polymers for colloidal applications. V. Novel behavior of polymeric emulsifiers in emulsion polymerization.* Journal of polymer science part A: Polymer Chemistry, 1993. **31**(1): p. 99-111.
146. Astafieva, I., X.F. Zhong, and A. Eisenberg, *Critical micellization phenomena in block polyelectrolyte solutions.* Macromolecules, 1993. **26**(26): p. 7339-7352.
147. Andrew, H. and L. Long, *Challenges of UV curable ink-jet printing inks - a formulators perspective.* Pigment & Resin Technology, 2004. **33**(5): p. 280-286.
148. Finley, C., *Printing paper & inks*. 1997, **37**(4), p: 23 – 36.
149. Zettlemoyer, A. and G. Lower, *The rheology of printing inks. III. Studies of simple dispersions.* Journal of Colloid Science, 1955. **10**(1): p. 29-45.
150. Gilleo, K., *Rheology and surface chemistry for screen printing.* Screen Print Magaz, 1989, **313**(5), p. 128-132.
151. nanoComposix. *Zeta Potential Analysis of Nanoparticles* (online). Accessed 03/08/2015. Available from: http://50.87.149.212/sites/default/files/nanoComposix%20Guidelines%20for%20Zeta%20Potential%20Analysis%20of%20Nanoparticles.pdf.
152. Hunter, R.J., *Zeta potential in colloid science: principles and applications*. 2013, **2**(5), p: 13 – 19.
153. Walker, N.A. and P.E. Rose, *Pigmented ink jet inks*, 2003, US20140099643 A1.
154. Williams, P.A., *Handbook of industrial water soluble polymers*. 2008, **32**(4), p: 46 – 53.
155. Lambourne, R. and T. Strivens, *Paint and surface coatings: theory and practice*. 1999, **63**(3), p: 23 – 32.
156. Lin, L., J.T. Guthrie, and W. He, *Computer-aided modelling of anti-corrosion coatings formulations.* Journal of Materials Science, 2003. **38**(5): p. 1097-1104.

157 Thomas, L., F. Lionti, R. Ballou, D. Gatteschi, R. Sessoli, and B. Barbara, *Macroscopic quantum tunnelling of magnetization in a single crystal of nanomagnets.* 1996. **383**(2), p:145 – 147.

158 Lantada, A.D., P.L. Morgado, J.E. Otero, J.M. Munoz-Guijosa, and J.L.M. Sanz, *Neural network approach to modelling the behaviour of quantum tunnelling composites as multifunctional sensors.* Smart Materials and Structures, 2010. **19**(12): p. 125007.

Chapter 2. Experimental

It is crucial to follow established and repeatable procedures in the preparation and use of ink components. In the preparation of QTC inks, experimental methods can vary in terms of the nature of the raw materials to be used, their loadings, their shapes and sizes. In the laboratory work, safety precautions, such as the use of fume cupboards, safety glasses, gloves and care in the use of chemicals were taken based on Material Safety Data Sheets (MSDS).

In the study described in this chapter, the characteristics of materials including substrate for printing and ink components are introduced. Knowledge that is obtained from the characterisation of a sample material helps one to understand its interaction with other components and with itself when it is used in complex formulations. For the characterisation of pigments, electron microscopy, particle size analysis and zeta potential are useful techniques. For polymeric binders, thermal analysis, spectroscopy, rheology and microscopy are effective techniques to characterise polymers' nature. Furthermore, the methods of preparation and printing for QTC inks are detailed with regard to the nature and role of the ink components.

2.1 Materials

Materials used to prepare, characterise and apply the QTC inks are detailed into two sections, *i.e.* Substrates for Printing and Ink Components.

2.1.1 Substrates for printing

In printing technology, the term substrate is used to describe the base material that a printing ink or coating can be applied onto [1]. Substrates for screen printing cover a wide range of types, such as paper, carton-board, card, plastics, glass, metal, textiles and so on [2]. In this study, two different substrates were typically used for testing and investigating the electrical properties and the mechanical properties of QTC inks. The two different substrates are described below.

2.1.1.1 Carton-board/paperboard for rapid ink testing

Carton-board (see Figure 2.1) is often the preferred substrate that is used when there is a need to relate the printability of an ink with the ink's dispersion characteristics, flow properties, strength, hue and gloss [3]. The fibrous carton-board used was supplied by Incada Exel, Proctor Paper & Board Ltd., Westland Square, Leeds. This carton-board had a gammage of 240 g/m^2, a thickness of 400 μm and good smoothness for ink coverage and uniform ink adsorption characteristics.

Ink flow testing is one of the important criteria that can be used to test an ink's property. The carton-board was used as a base substrate for a quick assessment of the suitability of the ink. A high viscosity ink, which would be hard to achieve a smooth and uniform film, would not be suitable for printing process. If the ink had too low a viscosity, it would also not be used as it would bleed and not remain on the substrate.

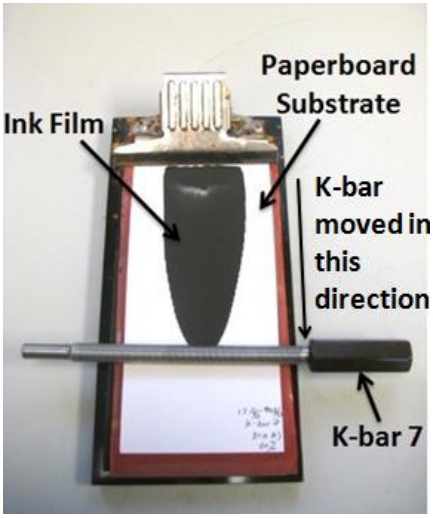

Figure 2.1 Carton-board used in a check of the ink's deposition characteristics, hue and gloss in ink printability testing

2.1.1.2 The poly(ethylene terephthalate)-based inter-digitated electrodes

The susbtrate on which the QTC inks were printed onto (Figure 2.2) was supplied by Peratech Ltd., Old Repeater Station, Richmond, UK and is comprised of poly(ethylene terephthalate) (PET) sheet that had been pre-printed with carbon containing inks and with silver inks to give electrodes. These were used to make contact with the ink films to establish an electrical circuit. The carbon-based

electrodes (according to the Technical Data Sheet the thickness of each was about 7–8 µm) were produced from a screen printing ink (supplied by Henkel Ltd.) that was very compatible with the polyester film. The thickness of the dried carbon electrode was approximately 8 µm and the resistivity of that was 170 Ω sq^{-1}. The electrodes used to test the electrical resistance of the printed film are shown in Figure 2.2.

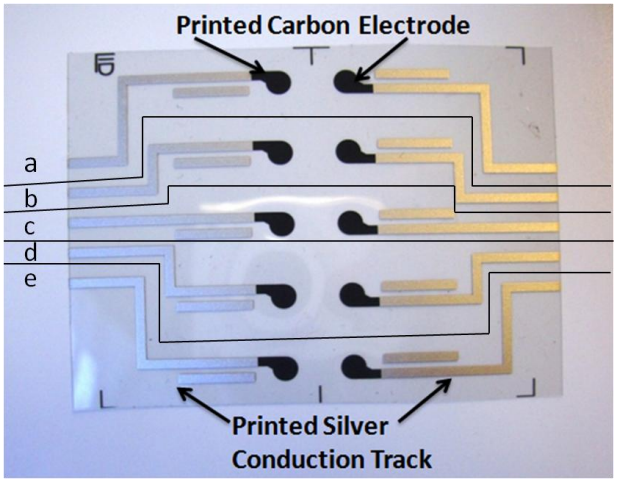

Figure 2.2 PET substrate pre-printed with 5 arrays (*i.e.* a, b, c, d and e) of silver conduction tracks and carbon electrodes

2.1.2 Ink components

Inks are commonly composed of colorant(s) (*i.e.* pigment or dye), binder(s), carrier (*i.e.* organic solvent or water) and additive(s), as shown in Figure 2.3. One objective of this project was to formulate water-based inks, due to their ease of application and their environmental friendliness.

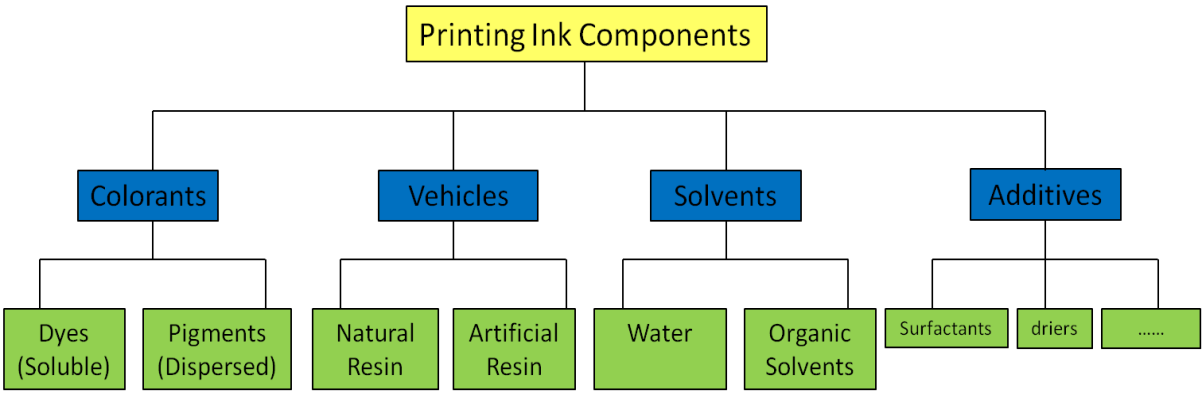

Figure 2.3 Diagram showing the printing ink components

2.1.2.1 Pigments of relevance to QTC inks

There are four metal powders and one alloy powder used in formulating the composite inks, as shown in Table 2-1.

Table 2-1 Metallic powders used in this study

Powder	*Supplier*	*Nature and characteristic*
Ni	*Vale Inco Europe Ltd, Swansea, West Glamorgan*	*This has a fine, spiky characteristic, which has electrical conductivity value of 14.3 Siemens/m. The particle size distribution ranges from 1 to 100 µm. Such nickel powders rarely become surface oxidised [4].*
Fe	*Sigma Aldrich Ltd, Gillingham, Dorset, UK*	*This iron powder has a fine characteristic and light grey colour, which has electrical conductivity value of 10.1 Siemens/m.*
Cu	*Echart UK Ltd, Unit C The Sidings Station Road Ampthill, Bedforeshirem, UK*	*This is a flaky material that was developed to be resistant to oxidation. This has electrical conductivity value of 58.5 Siemens/m.*
Bronze	*Echart UK Ltd, Unit C The Sidings Station Road Ampthill, Bedforeshirem, UK*	*This is a flaky powder, oxidation resistant which is heat treated. This has electrical conductivity value of 7.4 Siemens/m.*
Zn	*Sigma Aldrich Ltd, Gillingham, Dorset, UK*	*This has non-flaky, non-spiky powder that is coarse in nature. This has electrical conductivity value of 16.6 Siemens/m.*

2.1.2.2 Water-based polymeric binders

The properties of the binders have a significant influence on the performance of coatings or inks. Polymeric binders provide the basis for ink mobility and flow properties. The water-based binders that were used in this research are listed in Table 2-2, in which the details of the supplier and chemical nature of each of the chemicals are given. All the binders used in this research were mixtures of at least one polymer and water, but owing to commercial confidentiality, the formulation of each polymeric binder was not available.

Doubly-distilled, deionised water, discharged from an Elga, 18 Ω, Purelab-flex-Velolia distiller, was used where relevant in the preparation of the wet ink samples and in adjusting the solids contents of the various ink formulations.

Table 2-2 Binders used in the study

Binder Name	*Supplier*	*Chemical Nature*
PVP	*Sigma Aldrich Ltd, Gillingham, Dorset, UK*	*The product name is poly(vinyl pyrrolidone) and average molecular weight is 360,000 g/mol.*
PVP-S	*Sigma Aldrich Ltd, Gillingham, Dorset, UK*	*The product name is poly (1-vinyl pyrrolidone-co-styrene) copolymer. It is composed of 2-Pyrrolidone, 1-ethenyl-, polymer with ethenyl benzene and the loading for these components is ≥38 to ≤42 wt%. The water loading in this binder is ≥58 to ≤ 62 wt%. The styrene loading is 64 wt% in the solid content. The average molecular weight is 645.87 g/mol.*
Polymeric emulsion (PE1)	*Hi–Tech Products Ltd., Derbyshire DE11 9DH*	*This is a colloidal stabilised emulsion that gives a hard polymer based system. It is supplied as approximately 40–44 wt% solids in an emulsion which mainly contains a alkali soluble acrylic copolymer. The product is modified with a PTFE (poly(tetrafluoroethylene)) wax, IPA (isopropyl alcohol), some soft polymer and around 15 wt%*

		binder solution.
Polymeric emulsion (PE2)	*Hi–Tech Products Ltd., Derbyshire DE11 9DH*	*This is an alkali soluble acrylic copolymer emulsion, which is neutralised in MEA (monoethanolamine). The product is also modified with PTFE, IPA and antifoam.*
Printofix 83 (PE3)	*Clariant Products Ltd., Marc Leyendecker, 6 rue Louise Michel, 94600 Choisy le Roi, France*	*This is an aqueous dispersion of a styrene-acrylic copolymer and the viscosity is approximately 100 mPa s (20 °C).*
PSE1	*Evonik Industries Ltd, Milton Keyne, UK, MK10 0AF*	*This is a hazy emulsion which included a silicone modified polyurethane dispersion. The solids content was approximately 33%. The solvent blend contained dipropyleneglycol dimethyl ether and water in the ratio of 5:60. The viscosity of this binder was approximately <200mPa s (20 °C).*
PSE2	*PennWhite Ltd. 6 Aston Way, Middlewich, UK CW10 0HS*	*This is a polydi(siloxane) emulsion with a solid content of approximately 35 wt%.*
PSE3	*Formulated Polymer Products Ltd. 8 Garden St, Bury, UK BL0 9BQ*	*This is a poly (isoprene) emulsion. The solid content of that is approximately 64 wt%.*

2.1.2.3 Titanium dioxides

Three different grades of TiO_2 were used to modify the electrical properties of QTC inks. Two different types of TiO_2 were used in this project (rutile and anatase) due

to their different physical properties, such as the specific surface area, the particle size and the surface treatment. TiO_2 can be used to control the resistance sensitivity of the printed films, as introduced in 1.4.3 . The three grades of TiO_2 that were used in this research are listed in Table 2-3, together with the supplier, surface treatment details, pigment types and TiO_2 contents [5-7].

Table 2-3 Three grades of TiO_2 used in the study [5-7]

Commercial Name	*Kronos TiO_2 [1080]*	*Kronos TiO_2 [2190]*	*Kronos TiO_2 [2300]*
Supplier	*Kronos Titan GmbH*	*Kronos Titan GmbH*	*Kronos Titan GmbH*
Production	*Anatase pigment produced by the chloride process*	*Rutile pigment produced by the sulphate process*	*Rutile pigment produced by the sulphate process*
Pigment Type	*Anatase Pigment*	*Rutile Pigment*	*Rutile Pigment*
Surface Treatment	*Sb (very small amount)*	*Al (1.55%)*	*Al (2.57%)*
TiO_2 Content	*> 98%*	*> 94%*	*> 94.5%*
Sample Identification Code	*TiO_2 a*	*TiO_2 b*	*TiO_2 c*

2.2 Equipment

Several pieces of the equipments were used to print the prepared QTC inks and to characterise the ink components, printed films and the inter-digitated electrodes. The equipment is classified into two major categories, *i.e.* equipment for ink preparation and testing and equipment for ink and ink film characterisation.

2.2.1 Equipment for ink preparation, ink application and electrical resistance testing

2.2.1.1 Draw-down of the QTC inks using K-bar, prepared on carbon board substrate, for rapid/initial ink testing

The draw-down K-bar is a wired rod that is used to deposit a defined region of "print" for ink assessment (see Figure 2.1). The electrical conductivity was tested after the inks or the coatings had been dried. In addition, the approximate thickness of each coating was controlled by the use of different sizes of K-bar. In Figure 2.1, the K-bar 7 is depicted. Consequently, wet ink with an approximate thickness of 75 µm was produced on the substrate. Details of carton board were given in Section 2.1.1.1. Each size K-bar can produce films of its corresponding wet film thickness, as shown in Table 2-4.

Table 2-4 Wet film thicknesses can be created by the different sizes of K-bars

K-bar Number	*Wet film thickness*
1	*6 µm*
2	*12 µm*
3	*24 µm*
4	*36 µm*
5	*50 µm*
6	*60 µm*
7	*75 µm*
8	*100 µm*

2.2.1.2 Screen printing equipment

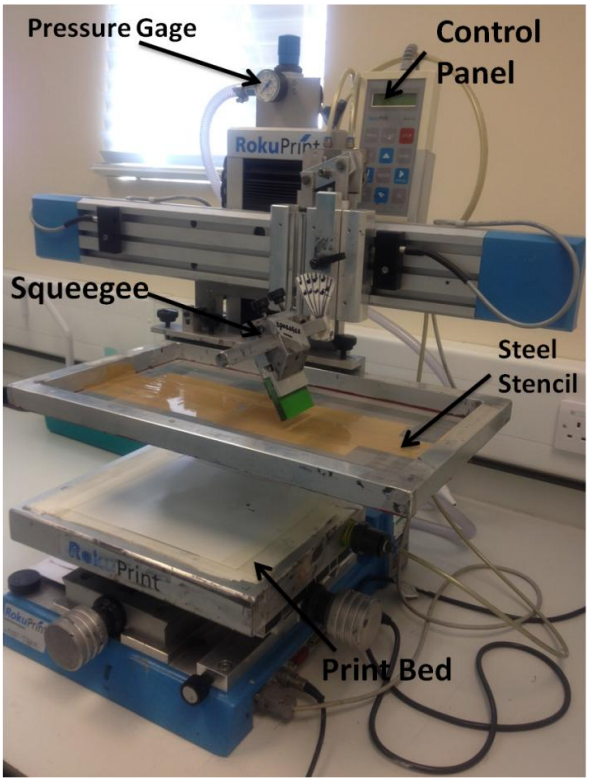

Figure 2.4 Roku Print SD05 semi-automatic screen printer used in this research

A Roku Print SD05 screen printing unit was used in screen printing, as shown in Figure 2.4. This is a piece of semi-automatic equipment, having pressure and speed controls. Figure 2.5 shows a schematic diagram of the screen printing technique. In operation, the ink was forced through the open areas of the coated stainless stencil mesh surface using a squeegee under a 4 bar pressure. The squeegee setup was mechanically adjustable. The print setup was controlled electronically via the control panel. The QTC ink was screen printed onto carbon–silver interdigitated electrode sheets that had been pre-printed onto the PET substrate (as shown in Figure 2.2). In this study, a squeegee of 80 shore A hardness (supplied by S. Wood Service, Unit 14 Centre Park, Marston Business Park, Rudgate Tockwith, York) was used, at an angle of 60° to the horizontal, in the print direction. The screen was locked into the holder. The off-contact gap between screen and print bed was set at 3 mm.

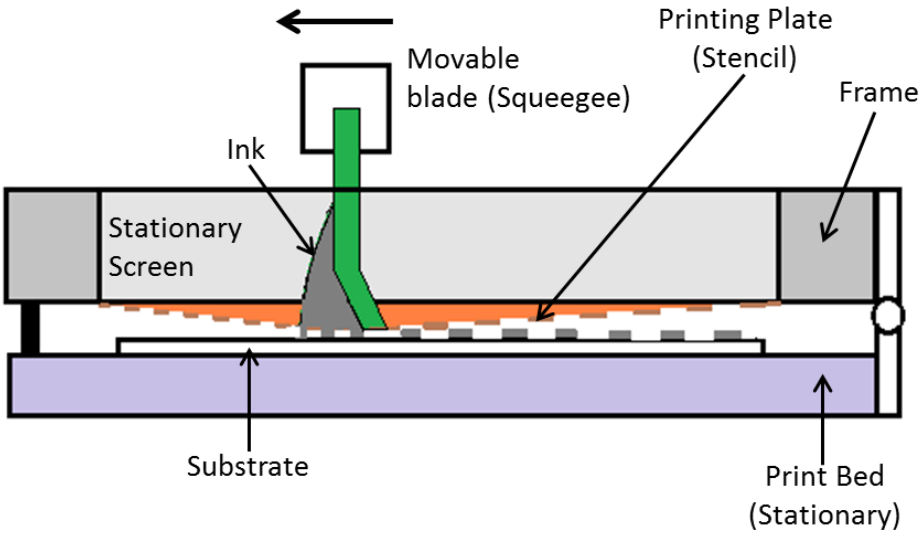

Figure 2.5 A schematic diagram of screen printing technique

The specifications of the woven mesh screen are given in Table 2-5 [9]. This specification of screen was chosen to provide a durable screen.

Table 2-5 Specification of the aluminium screen used in this study [9]

Frame	*Mesh-stated parameters*	*Emulsion-Stated parameters*
Aluminium 20 mm x 20 mm box section, 400 mm x 210 mm print area	*Stainless steel, 32 µm thread thickness, 56 µm opening, stretched to 18 N tension*	*38 % solids UV-curing emulsion, 2 coats per side*

2.2.1.3 Overhead stirrer

The mixing equipment used for preparing QTC inks was an IKA–Werke Eurostar digital overhead stirrer, as shown in Figure 2.6. Figure 2.6 displays the overhead stirrer with a double blade impeller head fitted. The rotation speed ranged from 50 rpm to 2000 rpm. The speed control dial was able to ensure a constant speed that could be provided even with changes in viscosities of the sample. Double blade impeller was chosen to ensure that the mechanical agitation would not damage the

spikes of the nickel particles within the QTC inks. It was experimented that the pressure sensitive properties of ink films have disappeared, as the ink films became completely conductive. This meant that triple blade impeller could remove the spike tips of nickel particles during mixing.

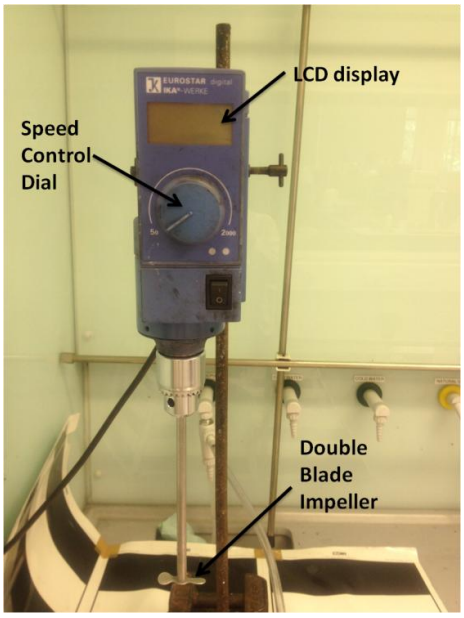

Figure 2.6 IKA-Werke Eurostar overhead stirrer and double blade impeller used in the research

2.2.1.4 Keithley-Picoscope instrument

A customised setup was used in Peratch Ltd for measuring the Current-Voltage characteristics of the print samples. The setup (as shown in Figure 2.7) consisted of the following units:

- Lloyd LR 5K Instron 5543 universal testing machine (UTM) with Merlin software
- 500 N load cell for the Instron UTM
- Keithley 2100 6 ½ digit multimeter (DMM)
- Base platform to support samples
- Rubber dome tipped truncated aluminium probe that has same size of the carbon contact on the inter-digitated electrodes
- Gold plated crimp female contacts to ensure the connections with the inter-digitated electrodes

- Two jacketed copper wire cable assemblies – 4 mm jack to crocodile clip to gold plated male pin contact
- Glass bar magnet

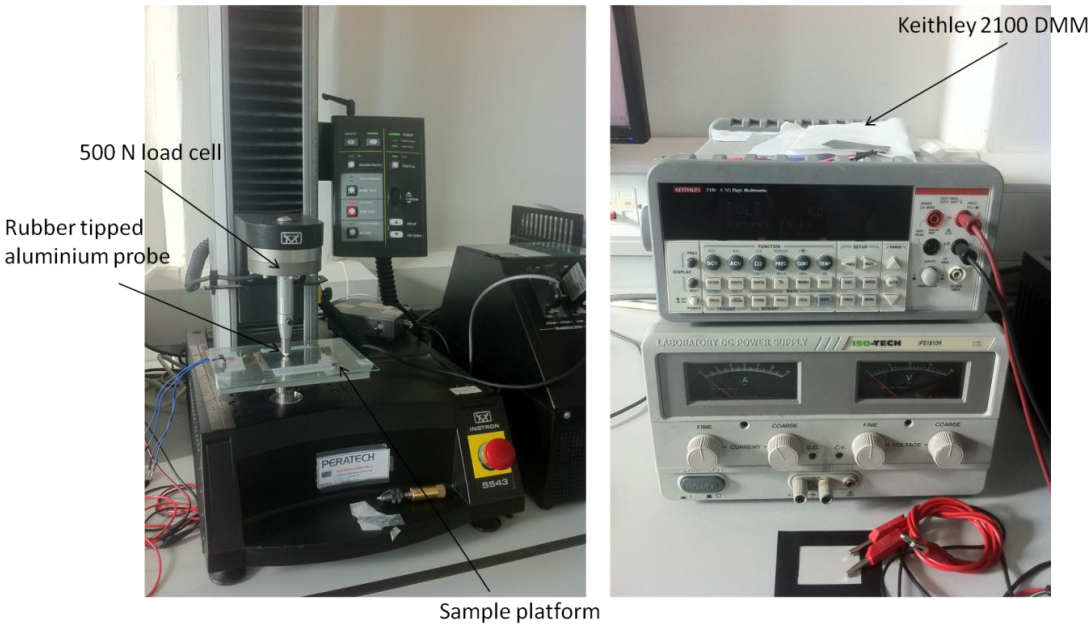

Figure 2.7 Customised UTM setup used for Force vs. Resistance testing

The aluminium probe was attached to the load cell on the UTM. The UTM was used able to apply a controlled force to the sample sensors. The ends of the cable assemblies were plugged into the sockets on the DMM. The gold plated male contact pins were plugged into the gold plated female contacts of the sensors at the other end. The sensors were kept level on the base plate by the use of a bar magnet. The DMM supplied a constant current to the attached sensors and measured the voltage across the sensors. The DMM was connected to the UTM. The UTM was connected to a PC running the Merlin software. The voltage measurements from the DMM were recorded via the UTM in the Merlin software.

2.2.1.5 Lloyd LR 5K Plus digital material tester

The Lloyd LR 5 K testing instrument combines high performance, flexibility and ease of use. It was used to measure the elastic modulus of each polymeric binder

and each printed film. Figure 2.8 shows the instrumental setup for the measurement of the stress-strain behaviour of the binder films and the printed films.

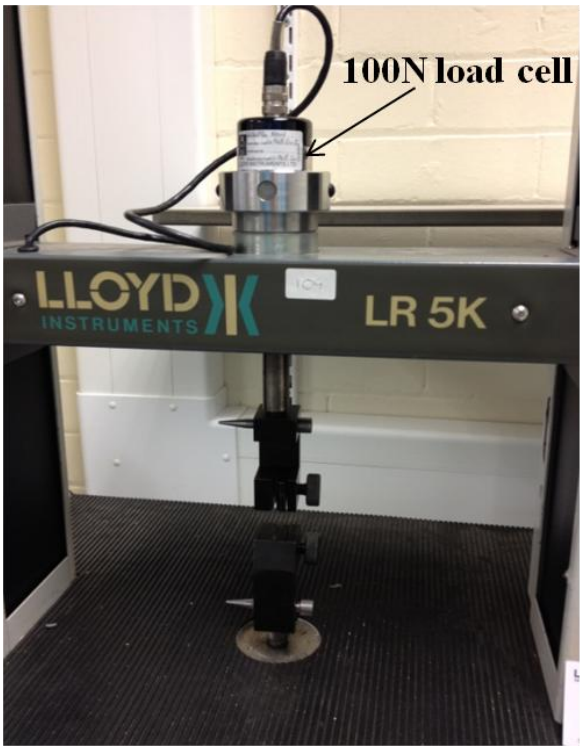

Figure 2.8 Instrumental setup for the measurement of the stress-strain behaviour of the binder films and the printed films

2.3 Selective characterisation of raw materials

2.3.1 Selective characterisation of pigments

The pigments used in this research were the nickel powder and three different grades of TiO_2.

2.3.1.1 Scanning electron microscopic (SEM) evaluation of pigments

Scanning electron microscopy is a widely used technique, where a focused beam of electrons is scanned across the surface of an electrically conductive specimen. A deposited conductive layer on the surface of the specimen is therefore necessary to avoid charging.

Figure 2.9 shows a schematic diagram of a basic SEM instrument. The electrons are produced and accelerated using a field emission gun (FEG) or

thermionic source in a high vacuum column. The electrons are then focused on the sample by passing through two or three condenser lenses which demagnify the spot size down to 0.4 nm to 5 nm in diameter. The electron spot is then rastered by deflection coils. The electrons interact with the surface of the specimen with a resolution down to 1 nm, generating other electrons from the material surface and then subsequently forming the image. Different interactions between the electron beam and the surface of the specimen occur, with secondary electrons and back scattered electrons being the most common. The secondary electrons emitted by the sample were collected by an Everhart-Thomley (E-T) detector and are represented on the screen by a brightness which corresponds to the measured intensity.

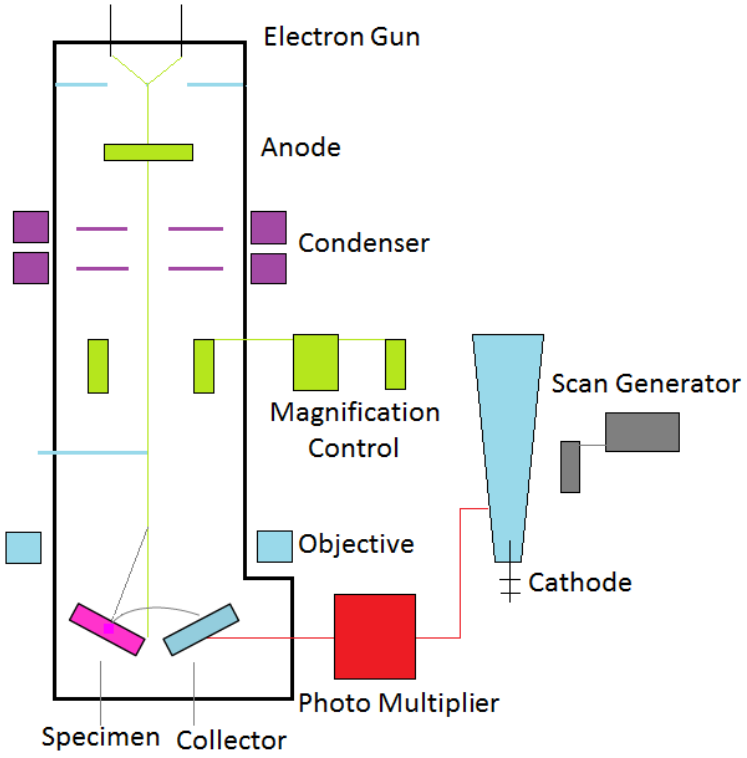

Figure 2.9 Schematic diagram showing the components of an SEM column. A beam of electrons is produced at the top of the microscope by an electron gun. The electron beam follows a vertical path through the microscope, which is held within a vacuum. The beam travels through electromagnetic fields and lenses, which focus the beam down towards the sample. Once the beam hits the sample, electrons and X-rays are ejected from the sample

The instrument used for the scanning electron microscopy was a Jeol JSM-6610LV model. The sample preparation involved the deposition of a representative

amount of the sample powder, onto a standard SEM stub using carbon-conductive tape. The sample was then gold-coated using a Bio-Rad SC500 diode sputter coating unit. The sample was examined under the electron microscope over the magnification range of x 200 to x 15000, using an accelerating voltage range from 5 kV through to 30 kV.

2.3.1.2 Estimation of metal contents

Scanning electron microscopy with energy dispersive X-ray spectroscopy is a widely used surface analytical technique. Energy-dispersive X-ray spectroscopy (EDX) is used to map the elemental distribution of a sample. A highly-focused scanning primary electron beam is used to generate high resolution images that have excellent depth. The primary electrons use 0.5 kV–30 kV energy to strike the surface of a sample. As a consequence, secondary electrons with low energy can be produced. The major surface topography of the sample is mostly dependent on the intensity of these generated secondary electrons. As a result, by scanning the electron beam across the sample, the metal atom content and the metal atom ratio in the pigment sample can be achieved [10].

The EDX component of the JOEL JSM-6610LV, Oxford SEM Instrument was mainly used to detect the location of TiO_2, which has small particle size. 100 frames of data were collected using an accelerating voltage of 15 kV under the aperture 3 mode of operation for each sample. In each case, an elemental distribution for a selected microscopic area of a specimen was monitored.

2.3.1.3 Particle size analysis of pigments

Particle size analysis data for the relevant samples was obtained using a Malvern Mastersizer 2000. This instrumental uses is a laser diffraction technique, covering the particle size range between 20 nm and 2000 μm. Preparation of the sample involved pasting a small amount of the sample (20 mg) in a 50 mL glass beaker with a few drops of Air Products Surfynol CT – 324, a dispersing additive specific for the dispersion of the inorganic pigments. 50mL of distilled water were then added to the beaker and the mix was then treated in an ultrasound bath for 5 minutes. Each sample was then run on the Malvern Mastersizer, following a standard operating procedure.

2.3.1.4 Zeta potential measurements

The sample preparation procedure used for the zeta potential measurement was the same as that used in analysing the particle size (as demonstrated in Section 2.4.1.3). The prepared sample was then transferred into a zeta capillary cell for zeta potential measurement, using the Malvern Mastersizer Instrument. The measurement was recorded using Phase Analysis Light Scattering mode at 25 °C The prepared samples included nickel powder; three grades of TiO_2 and both nickel powder and TiO_2 dispersing in different binders.

2.3.2 Characterisation of polymeric binders

2.3.2.1 Fourier Transform Infrared Spectrophotometric (FTIR) characterisation

The polymeric binders that were later used to bind the pigments in the ink were characterised by FTIR spectrometry. Each polymeric binder was dried overnight in a 60 °C oven until a constant weight was achieved. This was used to evaporate the water molecules from the binder and also avoid the water band showing in the FTIR spectrometry. Spectra were recorded for each binder sample using a Bruker Platinum-ATR spectrophotometric scanning in the range of 400 to 4000 cm^{-1}. The unit was operated in an attenuated total reflectance mode, at room temperature. Small amounts of each sample were applied on the crystal area of the platinum-ATR.

2.3.2.2 Rheological studies

A TA Instruments AR 1500ex cone and plate rheometer was used to carry out the rheometric analyses of the polymeric binders. The competition of the samples varied according to different water-based polymers. The instrument was fitted with a Peltier plate for temperature control giving a temperature range of -20 to 200 °C + 0.1 °C. The maximum heating rate used was 20 °C/minute. A solvent trap was available to prevent the ink from evaporating. The torque range was 0.1 µN.m to 150 mN.m + 1nN.m. The cone used had the following dimensions:

- Diameter – 40 mm
- Angle – 3 deg 59 min 49 sec
- Truncation – 98 µm

At the start of each session, the instrument was zeroed and the bearing mapped. The gap distance between the tip of the cone and the plate was set to 33 µm. The temperature of the plate was set at 25 °C. Polymeric binders were deposited onto the centre of the plate and the cone lowered to the gap distance. Any excess ink around the edge of the cone was carefully removed whilst the bearing was locked. The bearing was then unlocked and the solvent trap fitted to prevent any involuntary loss of mass through evaporation.

The samples were conditioned at a shear rate of 10 s^{-1} for 30 s and then allowed to equilibrate without shear for 120 s. A shear stress ramp procedure was used. The shear rate was increased from 0.1 s^{-1} to 1000 s^{-1} over a 300 s time period. The shear rate was then decreased from 1000 s^{-1} to 0.1 s^{-1} over a further 300 s. The shear strain response of the sample was taken throughout the procedure. This operation was repeated for all of the samples in the range of different polymeric binders.

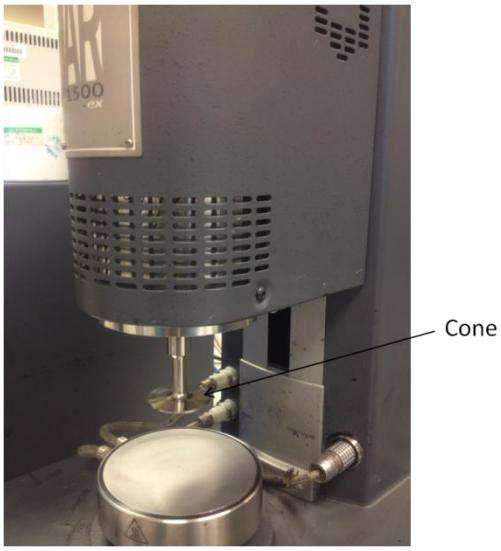

Figure 2.10 TA instrument used for measuring the viscosity vs. shear rate of the binder-based formulations (without of pigment) and the QTC inks

2.3.2.3 Thermogravimetric (TGA) analysis

Aspects of the thermal integrity (stability) of products can be determined by thermogravimetric analysis (TGA). This technique is used to measure the mass loss and the rate of weight change of a material as a function of temperature. Thus, the studies have thermodynamic and kinetic significance of temperature and time. TGA can be used to assess the composition of multi-component systems, aspects of thermal stability and oxidative stability, decomposition kinetics and the determination of the volatile content of materials. Each binder-based sample was heated for 50 min from 0 to 500°C. The heating rate for each binder sample was 10°C/min and the amount of the binder sample ranged from 20 mg to 60 mg. The N_2 gas balance purge flow rate was 40 mL/min and the sample purge flow rate was 60 mL/min.

2.3.2.4 Estimation of solid content

The binder formulations used in this research were mixtures of at least one polymer and water. The understanding of solid content of each binder is of importance. This is because polymer content in each water-based binder will significantly affect the correlation between polymers and nickel particles. Measurement of the latter was achieved by weighing an arbitrary amount of the binder composition accurately to 4 decimal places before and after evaporation of any solvent from the composition. A small amount of each binder was separately placed on to a watch glass (W_1) and the total weight recorded (W_2). The binder sample was then dried in the oven at 100 °C overnight. Then the weight of the sample on the watch glass was recorded (W_3). The solid content for the water - based binder was calculated using Equation 2-1. Each evaluation was repeated three times and an average value with standard deviation was taken.

$$\text{Solid Content (\%)} = \frac{W3-W1}{W2-W1} * 100\%$$

Equation 2-1 Calculation of the solid content for the screen printable binders

2.4 Methods of preparation and printing for QTC inks

Several ink formulations were prepared to be applied on the electrodes to create the circuit of the working area. Several methods, each of which depended on the order of the addition of each ink component were devised and employed. The order of addition of ink components was determined by the role of the component in the ink and by the resulting efficiency of the incorporation of the subsequent components. These methods evolved with the incorporation of new components and the final ink properties.

2.4.1 Formulation of ink 1

Inks prepared during the initial stage of the study were mixtures containing only polymeric binder and the nickel powder. The ink that only contained nickel powder and polymeric binder behaved very much like QTC commercial materials. However, TiO_2 was needed to be added into the ink to achieve an easier manipulated printed ink with respect to solve the electron storage problem in composites, as mentioned in Section 1.4.4. The sequence of preparation for such inks is illustrated in Figure 2.11.

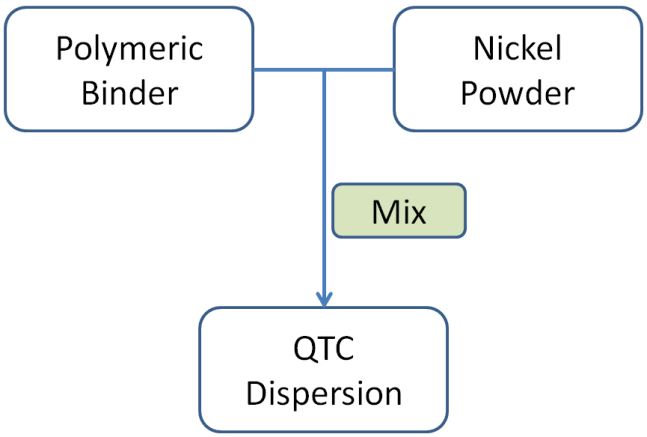

Figure 2.11 Flow diagram relevant to ink formulation 1

2.4.2 Formulation of ink 2

The creation of ink formulation 2 followed from ink formulation 1. Here, TiO_2 was used and added into ink formulation 1. The sequence of inclusion of such an ink preparation is illustrated in Figure 2.12. Three grades of TiO_2 were used in this

project, due to their different physical properties. It was thought that the species TiO_2 could be used to control the resistance sensitivity of the printed films.

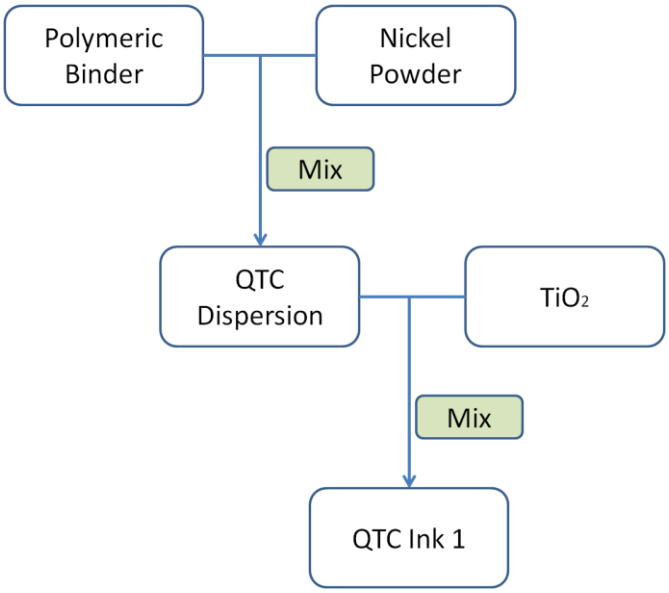

Figure 2.12 Flow diagram relevant to ink formulation 2

2.4.3 Formulation of ink 3

Ink formulation 3 was similar to Ink formulation 2. The only difference between them is in the sequence of the addition of the pigments, *i.e.* nickel powder and TiO_2. The method of preparation is schematically illustrated in Figure 2.13.

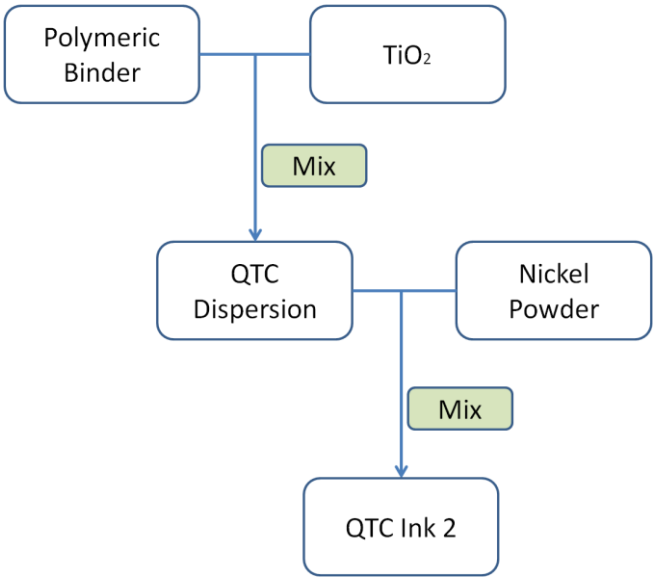

Figure 2.13 Flow diagram relevant to ink formulation 3

2.4.4 Preparation of QTC Inks

As mentioned previously, in the initial stages of the preparation of the QTC inks, only small amounts of ink formulated. The mixing of the ink formulations was carried out using the IKA-Werke Eurostar overhead stirrer (as shown in Figure 2.6). The binder and "TiO_2" were mixed by the stirrer at the greatest speed (2000 rpm) for 10 min. Then the mixture was mixed with nickel powder at 800 rpm for 10 min. This lower speed was used in cases where the shape and texture of nickel particles could be destroyed, thus losing the unusual electrical properties. The procedure of ink preparation was carried out by weighing separately the different quantities of the binder and the TiO_2 and then mixing both of these components together with the nickel powder.

2.4.5 Preparation of the printed substrates for electrical property testing

2.4.5.1 Procedure for the screen printing of QTC inks

Before testing their electrical properties the QTC inks needed to be printed onto the measurable circuit. The following sequence was used, preparation of the QTC ink then screen printing of the QTC ink onto the pre-printed carbon and silver inter-digitated electrodes of the PET substrate.

Section 2.2.1.2 demonstrates the instruction of screen printing technique. The substrate (as shown in Section 2.1.1.2) was held in position on the stationary print bed with masking tape around the edges. In screen printing, the ink was applied to the print area of the screen and manually coated across the appropriate print area. A squeegee pressure of 4 bars and a speed setting equivalent of 10% on the basis of the screen printer operation profile were used. Triplicate printed samples of each QTC ink were prepared. Printed samples were removed and allowed to dry on a clean petri-dish in a 30 °C oven overnight until a constant weight was achieved. The dried ink layer was 0.6 cm in diameter, which was consistent with the size of the open area on the woven mesh.

2.4.6 Characterisation of ink and printed films

Most of the characterisation methods that mentioned in Section 2.3 can be used to characterise QTC inks and their printed films, including SEM, particle size analysis,

zeta potential measurements, metal content estimations, FTIR, TGA analysis and rheological studies.

2.4.6.1 Estimation of nickel content in the printed film

The major aim of this research is to fabricate the pressure sensitive ink and its printed film behaves as QTC material does. In this case, the nickel filler content is significant to determine the conductivity of the printed film. Therefore, the estimation of nickel content in the printed sample is of importance. The estimation of nickel content in the printed film can be calculated by weight according to Equation 2-2.

$$\%\ \text{Ni Content} = \frac{x}{x+y+(1-x-y)*S} * 100\%$$

Equation 2-2 represents the estimation of nickel content in the ink print. Here, x and y are the concentrations of nickel powder and TiO_2 added in the ink respectively. S represents the solid content of the polymeric binder in the ink formulation which can be found from the TGA analysis.

2.4.6.2 Contact angle measurements

Contact angle studies were carried out to investigate the wetting behaviour of ink-substrate combination. This allows one to investigate aspects of work of adhesion and wettability properties of the ink on the substrate. One drop of the ink was applied from a 5mL syringe onto the surface of the PET substrate that was then transferred onto the platform of the contact angle measuring machine. The viewing tube was used to view the extinction of the light spot and record the contact angle reading of the ink.

2.4.6.3 Hardness testing

The hardness testing of the ink prints was measured using a type 7262 Sheen Instrument's hardness rocker tester. A coated panel of 100 cm^2 area was used and then mounted on the base which was attached to the cross bar. The counter was set to zero and the rocket was released. The hardness of the surface was measured in regard of the number of times the light beam was broken by a projecting plate that was allowed to swing. With each completed rock, a value was recorded. During

this procedure, the shield door was closed in order to protect the measurement system from interference. Each time the final reading was taken when the counter had finally stopped. Each test was carried out in triplicate and the mean hardness value was calculated.

2.4.7 Experimental setup for the force-sensitive electrical resistance measurements on the printed formulations

2.4.7.1 Preparation of the printed substrates for the force sensitive electrical resistance measurements

Printed inter-digitated electrodes were cut in half and overlaid so that the printed experimental ink was sandwiched between two carbon contacts. These carbon contacts and silver tracks were fabricated by screen printing onto the flexible poly(ethylene terephthalate) (PET) substrates. A silver conducting track and a carbon contact were firstly printed. Then the QTC ink was printed on the carbon contact using the semi-automatic screen printing machine, as shown in Figure 2.4. This design means that any electric current passes through the pressure sensitive ink layer. It was ensured that the electrodes and conductive silver tracks from each half were aligned to form a test structure before each group of electrodes was crimped using the gold-plated contacts, (as shown in Figure 2.15).

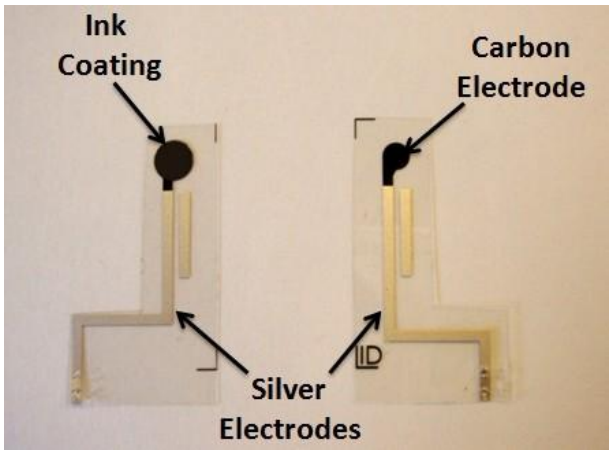

Figure 2.14 Images of QTC printed film (left) on the pre-printed inter-digitated electrodes and pre-printed inter-digitated electrodes

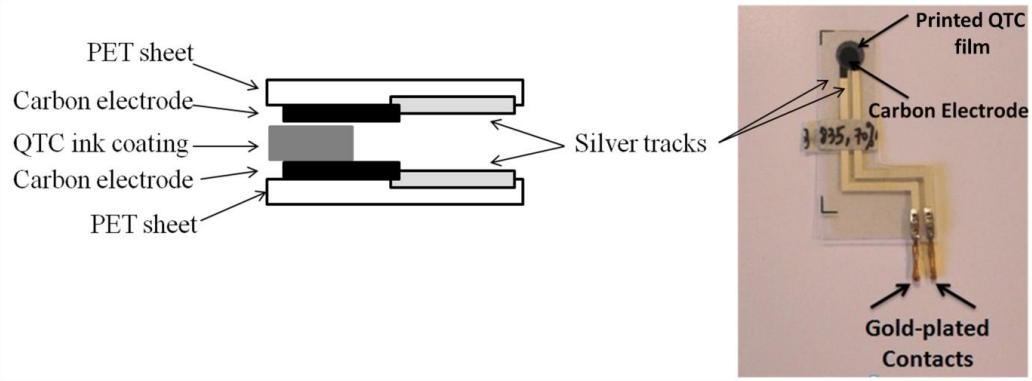

Figure 2.15 Schematic cross-section of printed composition (left) for the pressure sensitive testing. Two pre-printed electrodes were overlaid and aligned before each group of electrodes were crimped. The printed QTC film was sandwiched between the two carbon electrodes

An electrical circuit was established to assess the relationship between the electrical properties of each printed film at a known applied force. Each dried printed sample was placed on a hard flat table, while a block with mass 0.2035 g and diameter 0.8 cm, was used as a base for mounting the other known weights on, when measuring the electrical resistance of the printed ink film as a function of known applied force, as shown in Figure 2.17. An attempt was made to establish a constant contact area when the different loads were applied. The resistance measurements were taken using a Caltek Instrument AG 1021 digital multimeter, (supplied by Caltek Industrial Ltd, Kwai Change, N. T., Hong Kong). The electrode area was compressed using a set of cylindrical weights, in the range 5 g, 10 g, 20 g, 50 g, 100 g, 200 g and 500 g. The multimeter's electrodes were placed in contact with the two gold-plated contacts (Figure 2.15) and the resistivity readings were recorded.

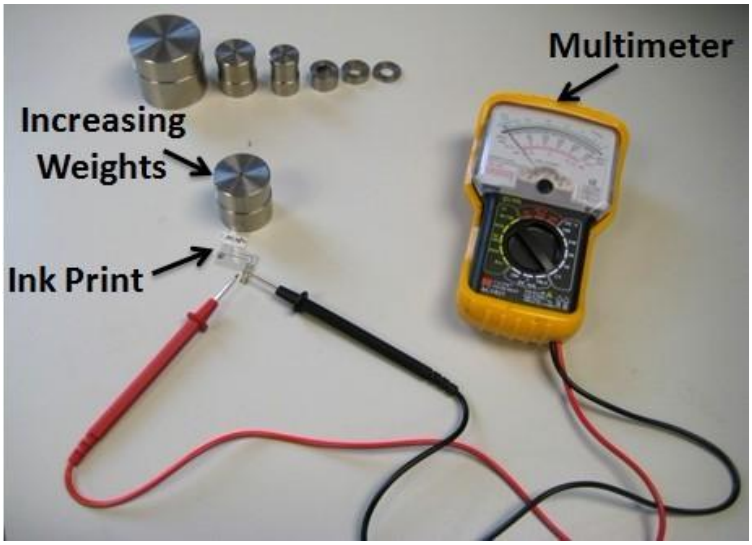

Figure 2.16 Setup for measuring the electrical resistance of a printed QTC film

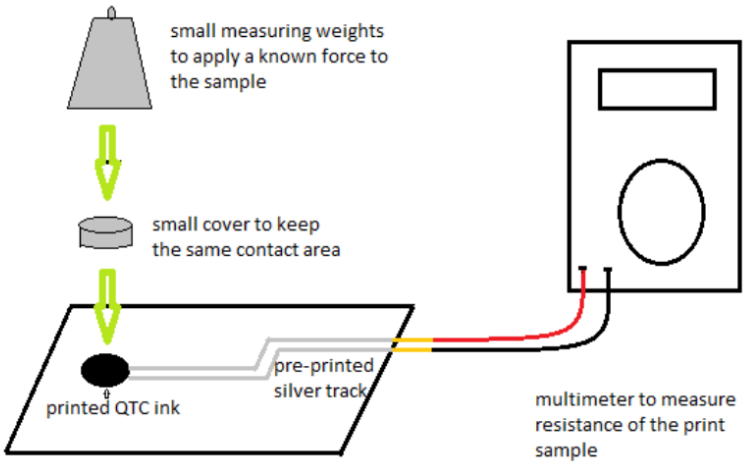

Figure 2.17 A schematic diagram of the setup used for measuring the electrical resistance of printed QTC samples

2.5 QTC ink preparation

2.5.1 Sequence of addition of mixed ink components

Before characterising the QTC inks and QTC printed films, several methods, each of which depended on the order of the addition of each ink component were proposed and experimented, as mentioned from Section 2.4.1 to Section 2.4.3. The order of addition of mixing ink was determined by the role of the ink component in the printed sample.

Differences between the formulation of ink 2 and ink 3 mentioned in Section 2.4.2 and in Section 2.4.3, respectively, is the order of addition of the pigment, *i.e.* nickel powder and TiO_2. Formulation of ink 2 was nickel powder firstly mixed with each binder and subsequently TiO_2 was added into the nickel mixture. Formulation of ink 3 was TiO_2 firstly mixed with each binder and subsequently nickel powder was added into the TiO_2 mixture, of which TiO_2 was apparently mixed longer time than that of in formulation of 2. Figure 2.18 is one of the specific examples to show the result of resistance-force plots for the printed films with and without TiO_2. The electrical resistance vs. force profiles of the PVP3 film (70 wt% of nickel powder and 30 wt% of PVP-based binder) and of the PVP8a film (70 wt% of nickel powder, 5 wt% of TiO_2 and 25 wt% of PVP-based binder) are shown in Figure 2.18. It was observed that the electrical resistance of the PVP3 film was more sensitivity with applied compression than that of the PVP8a film. This is because the particle size of TiO_2 was nearly 100 times smaller than that of nickel particle, which resulted in inadequate mixing and aggregates of TiO_2. Furthermore, the particle size distribution graphs of TiO_2 dispersed in different water-based binders also confirmed that TiO_2 were hardly to achieve well dispersed emulsions. Therefore, the conductive fillers easily contacted to each other to form a completely conductive film when the mixing of the ink was inadequate, so the electrical resistivity varied with applying compression quickly. As a result, formulation of ink 3 was accepted and used for the further preparation of QTC inks, as the electrical property of the printed sample from ink formulation 2 did not behave as that of the QTC commercial material.

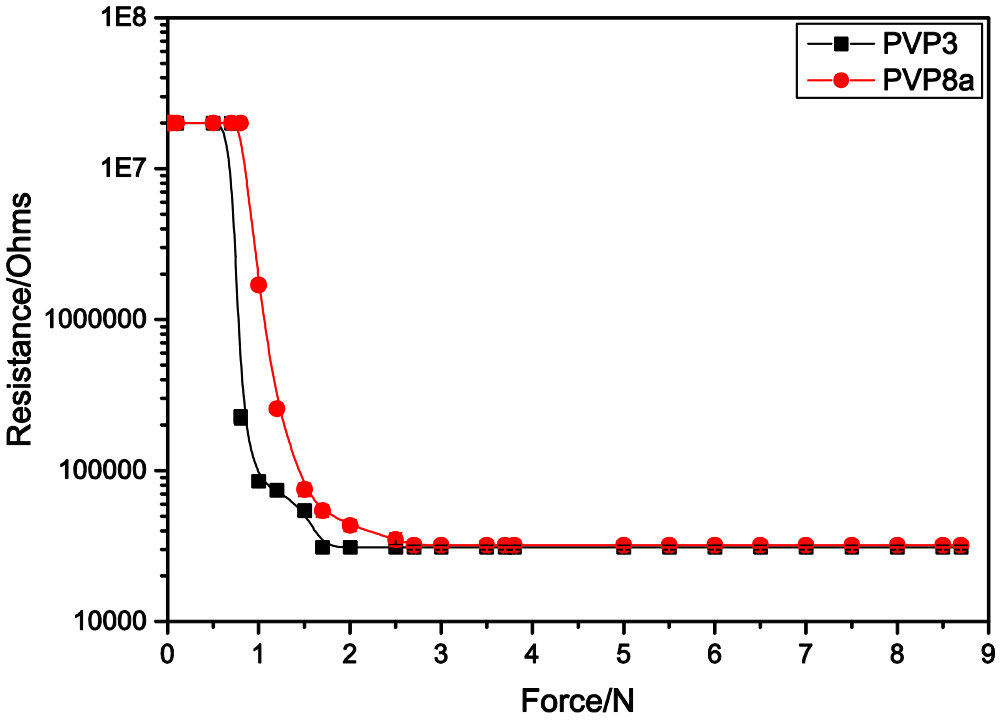

Figure 2.18 Variation of electrical resistance under applied compression for PVP-based print with (red) and without TiO_2a (black)

2.5.2 Experimental design of ink formulations

Experimental design of ink formulations was dependent on the statistical factorial design, which was introduced in Section 1.7.2. The number of required experimental runs can be calculated by Equation 2-3.

$$n = 2^k$$

Equation 2-3 Required experimental runs at two levels n. k represents the number of variables.

Figure 2.19 demonstrates the factorial design (top) for the ink formulations, which resulted in the surface designs (bottom) that contain the full designed formulations. Before starting the preparation of QTC ink, the ink formulations were picked up as integrals.

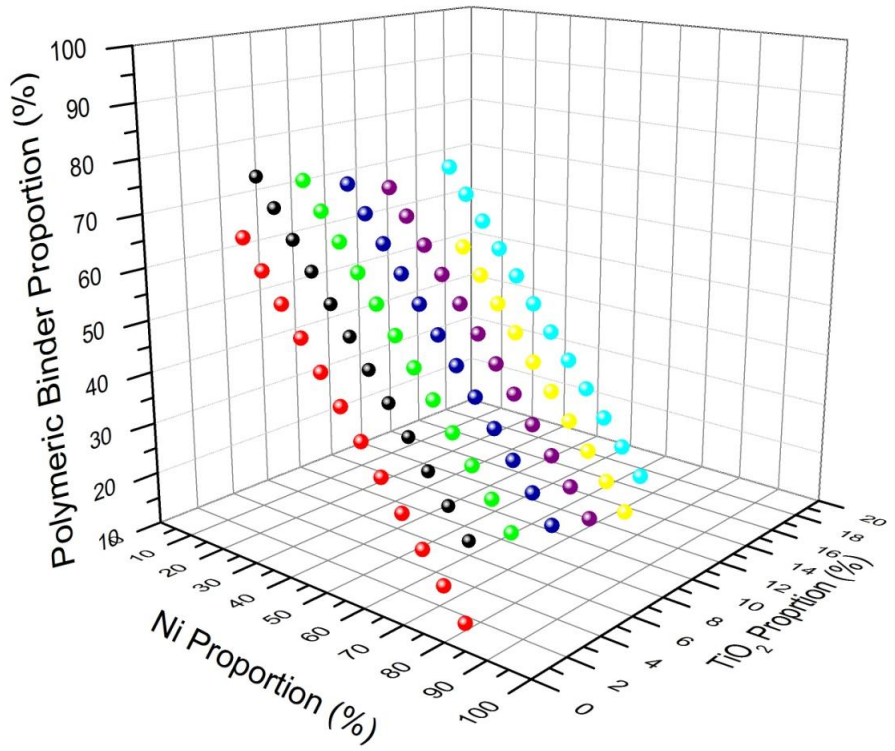

Figure 2.19 Ink formulations processed in the research

References

1. Finley, C., *Printing paper and inks*. 1997: **34**(3), p: 37-48.
2. Kipphan, H., *Handbook of Print Media.* 2008, **634**(3), p: 65 – 85.
3. Leach, R.H., *The printing ink manual*. 1993: **32**(5), p: 42 – 51.
4. Fang-Gao, C., et al., *Enhanced piezoresistivity in Ni–silicone rubber composites.* Chinese physics B, 2009. **18**(2): p. 652.
5. Kronos. *KRONOS 1080* (online). Accessed 23/07/2015. Available from: http://polymer-additives.specialchem.com/product/a-kronos-kronos-1080.
6. KRONOS. *KRONOS 2190* (online). Accessed 23/07/2015. Available from: http://kronostio2.com/en/component/jdownloads/finish/121/12.
7. KRONOS. *KRONOS 2300* (online). Accessed 23/07/2015. Available from: http://kronostio2.com/en/component/jdownloads/finish/122/276.
8. Stephens, J., *Screen process printing: a practical guide*. 1987, **87**(2), p: 123-145.
9. Ltd, S.W.S. *Mesh Treatment & Stencil Production* (online). Accessed 07/08/2015. Available from: http://www.steve-wood.co.uk/mesh-treatments-stencil-production/.
10. *Scanning Electron Microscopy coupled with Energy Dispersive X-ray (SEM/EDX) Spectroscopy* (online). Accessed 10/03. Available from: http://www.surfacesciencewestern.com/analytical-services/scanning-electron-microscopy-coupled-with-energy-dispersive-x-ray-semedx-spectroscopy/.

Chapter 3. Preparation, characterisation, optimisation and application of water-based PVP, PVP-S, PE1, PE2 and PE3-based QTC inks

In order to evaluate whether or not a printing process is successful, controlled and uniform, ways of ink deposition are needed when the inks are applied to substrates. It is important to use consistent inks, printing processes and substrates that are well defined and well controlled [1, 2]. Prior to the preparation of QTC inks, the ink components need to be analysed and characterised. Whether or not an ink can be used to produce images and print qualities consistently is dependent on the substrate properties and the ink properties. Printing quality is a combination of visual perception and the functional characteristics of the printed films. For this research, the functional characteristics of printed films were considered to be of importance. One characteristic is the need to formulate pressure-sensitive inks that behave in a similar manner to those providing the electrical properties of a QTC switching material.

In the study described in this chapter, nickel powder, three grades of TiO_2 and five water-based polymeric binders for use in composite inks were investigated on the basis of the contribution by each binder to the formulation, printability, electrical conductivity, rheology, thermal stability and the mechanical properties of the inks. The pigments (*i.e.* nickel powder and TiO_2) were characterised by their morphologies and sizes. Five different binders were used individually to form composite inks based on homo-polymeric and co-polymeric binder options. The effects of the binder chemistry, the composition of the inks and the application conditions on the rheological, electrical and thermal properties of the inks were investigated.

Materials and methods that are relevant to the work described in this chapter have been detailed in Chapter 2.

3.1 Preparation and characterisation of the raw materials used in the formulation of QTC inks

It is essential to characterise effectively raw materials before using them in experimental procedures because the information acquired relates to the material's properties, structure and composition. This characterisation assists in establishing the experiments, in understanding the complex formulations and in modelling the QTC inks. In the characterisation of the pigments, scanning electron microscopy, particle size analysis, zeta potential analysis and spectroscopy were effective tools. For the characterisation of the polymeric binders, Fourier Transform Infrared Spectrometry, rheological studies and thermogravimetric analyse were useful analytical/characterisation techniques.

3.1.1 Characteristics of the major pigment, nickel powder (Type 123, Inco Ltd.), in the QTC ink formulations

The pigments used in these ink formulations were considered to be the highly essential component because they convey functional identity to the ink, (*i.e.* the conductivity of printed films). Scanning electron microscopy (SEM) is useful tool for providing information relating to the topography of the surface and also for investigation of pigment distribution in printed film. Therefore, SEM was widely used in this study to represent the morphology of the pigment particles.

3.1.1.1 SEM evaluations of the nickel powder and the QTC material

SEM, particle size analysis and zeta potential analysis were used to characterise the nickel powder (supplied by Inco Ltd.) that was used in all investigations. Nickel powder was used as a major pigment in the QTC ink formulations and was also included in the QTC materials, as shown in Figure 3.2 and Figure 3.3. Representative electron micrographs were recorded at magnifications from × 200 to × 8000. This technique was applied to the nickel powders, as shown in Figure 3.1.

The SEM electron micrographs of the powders indicated that the primary particles were irregularly sized and tended to exist as distorted, irregular and pseudo-spherical fused aggregates, ranging from around 1 to 10 μm in size. These aggregates have an essential contribution through quantum tunnelling phenomena.

Thus, the size distribution of nickel particles in the printed film is of importance. The nickel particles are shown as spiky with porous surface features that effectively enhance the surface area. Their large surface area can therefore be expected to affect significantly the flow characteristics, particle size distribution and stability of both the fluid QTC inks and of the electrical properties of the dried printed film.

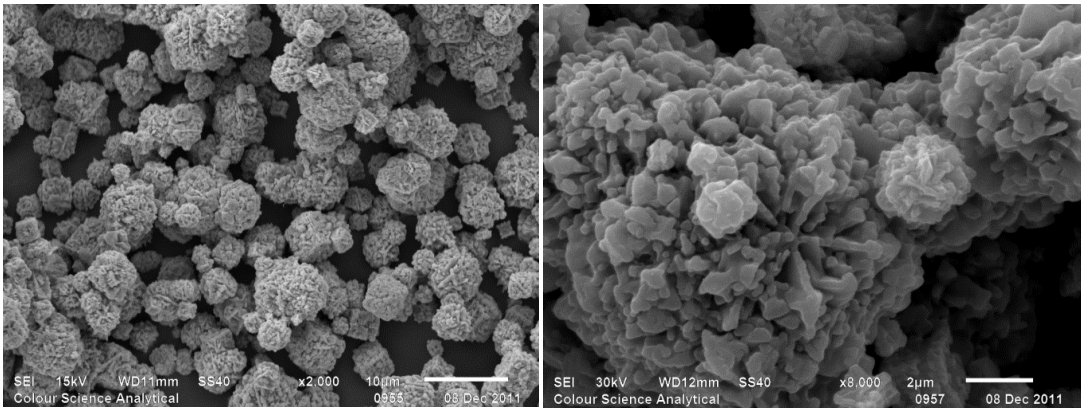

Figure 3.1 SEM images of nickel powder at × 2000 (left) and × 8000 (right) magnifications

Figure 3.2 and Figure 3.3 demonstrate the morphologies of surfaces and cross-sections of QTC commercial materials, respectively. The distribution of nickel particles in the QTC material was used as a guidance criterion to characterising and formulating the QTC inks that have similar pressure-responsive electrical properties as commercial QTC materials.

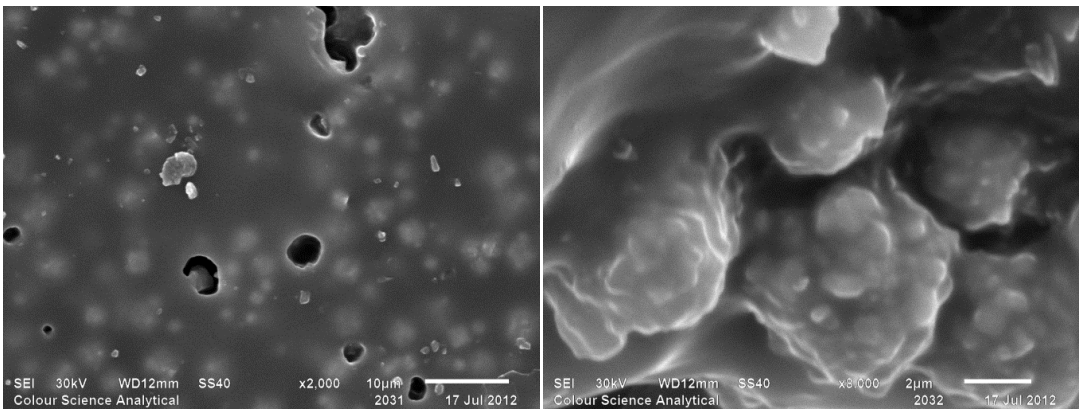

Figure 3.2 SEM images of a QTC material's surface at × 2000 (top) and × 8000 (bottom) magnifications

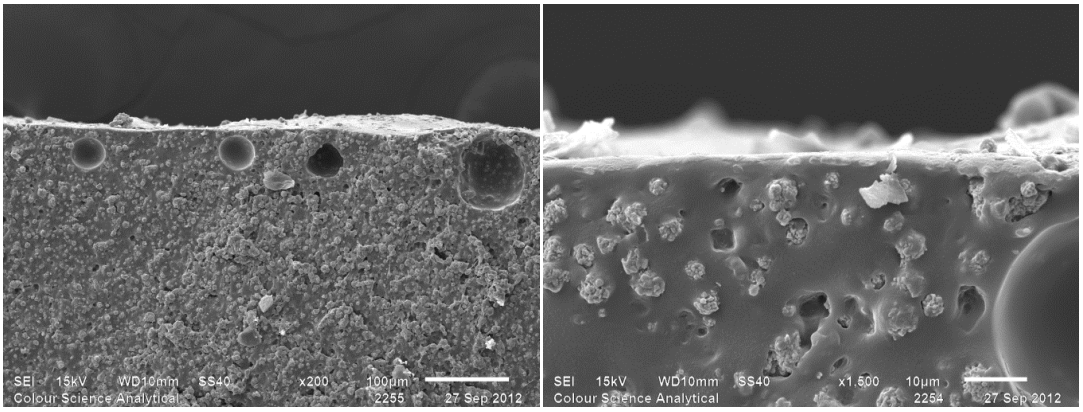

Figure 3.3 SEM images of a QTC material's cross-section at × 200 (left) and × 1500 (right) magnifications

The irregular shape and size of the nickel clusters (as shown in Figure 3.1) does not match those of the particles that are present at the surface of the conductive filler material that is present in QTC materials, Figure 3.2. The quantum tunnelling performance is due to the irregular, spiked surface structure of the nickel powder which builds up a higher concentration of electron charges at their spiky tips. From the cross-section images of the QTC material, it is seen that a high load of spiky spherical nickel particles are binding into the continuous polymeric matrix. The nickel particles vary in size and in their distribution in the polymeric matrix is anomalous. Some areas had a large concentration of nickel particles, but others had a low concentration in the QTC material. The Links-Nodes-Blobs model can be used to describe this heterogeneous distribution, as mentioned in Section 1.4.4.3. The aggregates of nickel particles are blobs that link with other aggregates through a Fowler-Nordheim tunnelling pathway. This tunnelling process is the result of the maintained spiky surface, thus a gentle mixing process is important. Long mixing processes can even the distribution of nickel particles, but it might also remove the spikes from the nickel surfaces [3]. Therefore, a suitable mixing process for QTC inks was considered and tested.

The morphologies of the QTC material reveal that variation between different samples is common. It is crucial to focus on the electrical resistance at a specific applied force.

The presence of several voids within the cross-section of the QTC material is the result of air bubbles. This is probably because when the QTC was moulded in the manufacturing process, the Ni-silicone composite at the bottom was squeezed to make the inside air bubbles flow to the top, which then met to produce big air bubbles at the upper layer of the composite.

3.1.1.2 Particle size analysis of the nickel powder

The particle size analysis data for the nickel powder, obtained using the Malvern Mastersizer 2000, indicates that the bulk of the near-spherical fused particle aggregates lie in a size range between 2 and 50 µm, with aggregates also being present (around 200 µm) (see Figure 3.4). This particle size range distribution matches that obtained for the sample observed under the scanning electron microscope. Such a broad distribution and the presence of large aggregates suggest that printing problems might be encountered when using a range of printing processes. This suggests that screen printing (using suitable mesh diameters) might be the main viable printing option. The mean particle size of nickel particles is 10 µm.

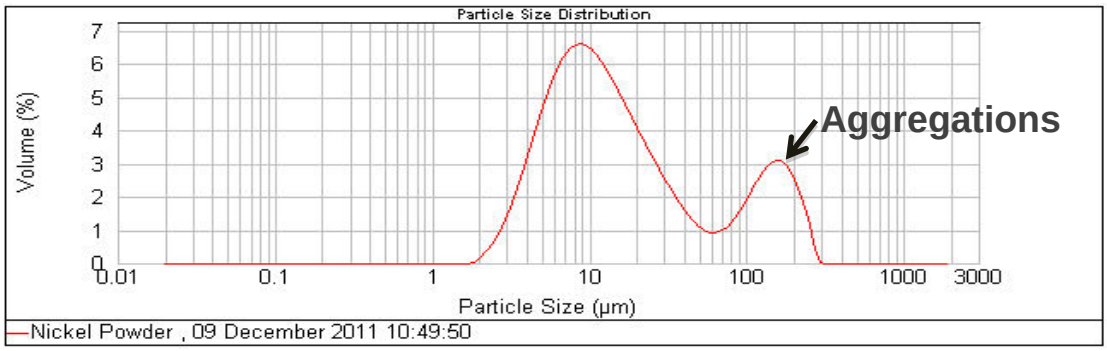

Figure 3.4 Particle size distributions of nickel particles from the Mastersizer 2000

3.1.2 Characteristics of water-based binders, PVP, PVP-S, PE1, PE2 and PE3, in screen printing

In the printing processes, it is ideal to have inks with maximum strength and desirable minimum viscosity. As a result of these criteria, the selection of particular

polymeric binders can be significant as they are used to adjust the adhesion to the substrates and fast press speeds [4].

In the evaluation of screen printable inks, rheology and surface chemistry are useful and critical tools, by which to screen the binders. The use of rheometry illustrates the properties of fluids which include viscosity *vs.* shear rate. The viscosity, indicated in mPas, is the main characteristic of interest [5].

3.1.2.1 Viscosity characteristics of PVP, PVP-S, PE1, PE2 and PE3 polymeric binders

Ideal viscosity values and good rheological characteristics are required by the inks. Thus, it is important to monitor the flow patterns of the QTC inks under the highly controlled conditions relating to the applied shear stress and shear strain rate at constant temperature. Figure 3.5 shows that the various polymeric binders that were studied exhibited shear thinning characteristics at 25°C. The viscosities of the inks decreased with an increase in the shear rate. The shear thinning behaviour of the inks was more pronounced between shear rate values of 1 s^{-1} and 1000 s^{-1}, which is relevant to the screen printing equivalent shear thinning rate [6].

In order to produce screen printable QTC inks, the polymeric binders must be thixotropic. This means that the inks usually have a higher viscosity under normal conditions, but become lower in viscosity when a constant force or a stress is applied. In addition to the thixotropy, the viscosity ranges for screen printing inks are usually in the range from 1 Pa s to 50 Pa s [6]. Figure 3.5 gives the viscosity *vs.* shear rate plots for the water-based binders, PVP, PVP-S, PE1, PE2 and PE3. These binders are thixotropic in their nature, as seen in their shear time dependent, thinning behaviour. The PVP binder had the greatest viscosity of 48.6 Pa s compared with the other four binders. PVP-S gave an approximate viscosity of 0.78 Pa s. PVP and PVP-S can be used in screen printing inks. The flexographic printing ink binders, PE1 and PE2, gave similar viscosities, around 0.25 Pa s, with an increase in the applied shear stress. The lowest in viscosity amongst these five binders was the PE3, which gave a viscosity value of 0.025 Pa s. The values of the viscosities for PVP and PVP-S at any particular value of shear rate are greater than those for PE1,

PE2 and PE3 binders because of the differences in the molecular weights, structures, chain length and flexibility of the polymers.

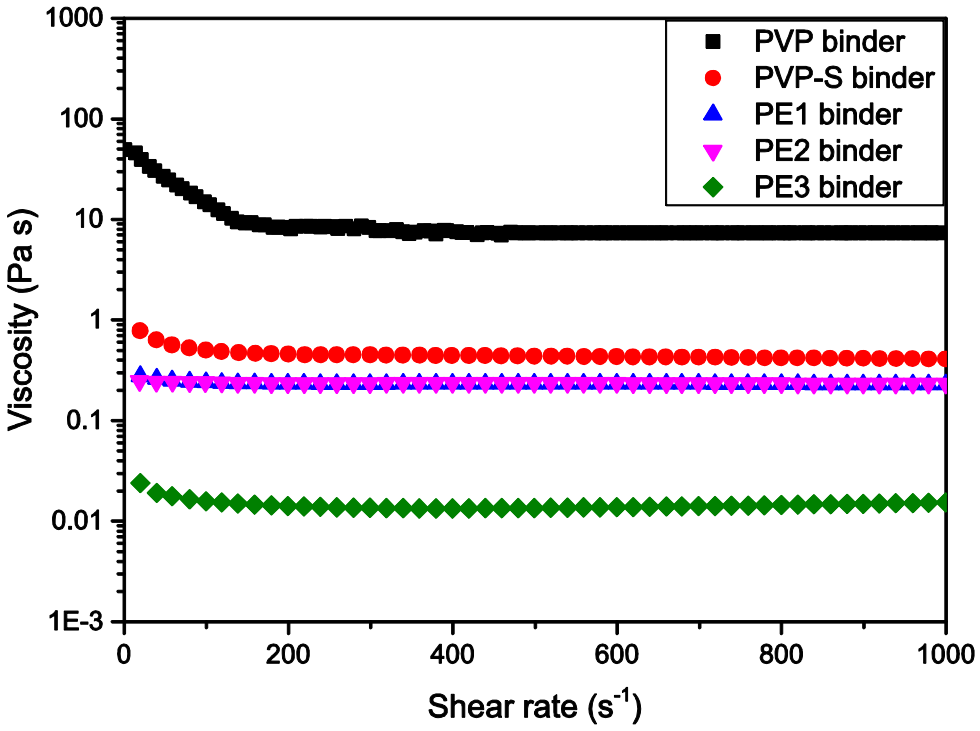

Figure 3.5 The relationship between viscosity and shear rate for each individual polymeric binder at 25 °C

Five water-based polymeric binders, PVP, PVP-S, PE1, PE2 and PE3 were applied onto a carton board substrate using a K-bar coater (Number 3), to check some of the ink's dispersion characteristics, flow and strength for an initial ink property testing. It was observed that the PE3 emulsion kept bleeding into the substrate due to its hydrophilicity, low viscosity and yield point. For this reason, the PE3-based binder was not suitable and thus was discarded for screen printing evaluations. The other emulsions did not flow on the surface but remained on the substrate after the K-bar coater was applied, indicating suitable adhesion.

3.1.2.2 Solid content estimations of polymeric binders, PVP, PVP-S, PE1, PE2 and PE3

The binders used in this project were mixtures of at least one polymer and water. Knowledge of the solid content of each binder is therefore of importance.

The measurement of the solid content can be achieved by weighing an arbitrary amount of the binder composition accurately before and after evaporation of any solvent from the composition. The binder sample was dried overnight in an oven, until a constant weight was achieved, at 100 °C. The solid content for each binder was calculated, (as illustrated in Section 2.4.2.4). Each evaluation was repeated three times then the average value and the standard deviations were taken. The solid content of each water-based binder is shown in Table 3-1, which indicates that PE2 has the highest volume of water in its composition. The water content in each water-based binder is of significance and is related to the ultimate loading of nickel content, thus affecting the conductivity of the printed film(s).

Table 3-1 Solid content calculations of each polymeric binder by drying the binders overnight at 100 °C in an oven

	PVP	*PVP-S*	*PE1*	*PE2*	*PE3*
Solid content	(38.2 +2.1)%	(45.1+1.7)%	(45.5+0.9)%	(23.9+1.3)%	(38.7+2.4)%

3.1.2.3 Thermogravimetric analysis of water-based binder compositions, PVP, PVP-S, PE1, PE2 and PE3

Thermal stability or decomposition information, regarding commercial polymeric binders, can be determined by thermogravimetric analysis (TGA). TGA is an effective technique that provides information concerning the physical properties and the chemical properties of materials when increasing the temperature of the study. This technique is used to measure the amount of mass loss and the rate of weight change of a material as a function of temperature and/or time. Therefore, the extent of water loss form the polymer binder is determined by the gradient of the TGA thermogram. TGA can be used to assess the composition of multi-component systems, aspects of thermal stability and oxidative stability, decomposition kinetics and the determination of the volatile content of materials. The TGA analysis of the five polymeric emulsions, under an inert atmosphere is demonstrated in Figure 3.6. Table 3-2 shows the solid contents of the binders that were used in the research,

achieved from the TGA analyse. Each binder sample was progressively heated over 50 minutes, from 0 °C to 500 °C.

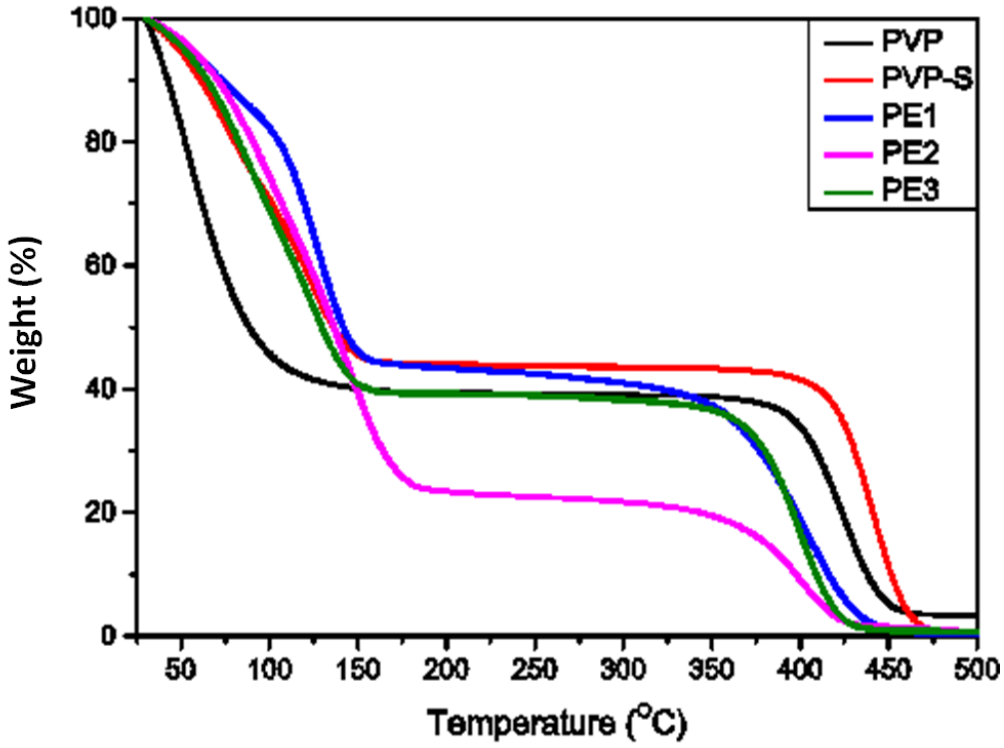

Figure 3.6 TGA analysis of PVP, PVP-S, PE1, PE2 and PE3 polymeric binders, in which each binder sample was heated at 10 °C/min, from 0 to 500 °C

Figure 3.6 gives the differences in thermal stability for each of the five binders, as the temperature was increased. Decomposition arises during the TGA-induced breakdown of the polymeric binders. In the TGA profile, each thermogram indicates a curve which can be correlated to loss of water as the heating temperature was increased to 123.67°C, 165.54 °C, 169.88 °C 192.36 °C and 178.26 °C for PVP, PVP-S, PE1, PE2 and PE3 binders, respectively. Therefore, solid content for each individual binder, PVP, PVP-S, PE1, PE2 and PE3 is 39.84%, 43.85%, 43.57%, 23.57% and 38.95%, respectively, as represented in Table 3-2. The extent to which the PE1 binder holds onto water was greater than that shown by the other polymeric binders. PVP, PVP-S, PE2 and PE3 had a similar ability to hold onto water. The overall thermal stability/reactivity of the five binders is similar.

The horizontal line sections of each profile indicate no weight loss over the temperature range. This is then followed by further mass loss that take place up to

410°C, 429 °C, 376 °C, 375 °C and 379 °C for PVP, PVP-S, PE1, PE2 and PE3 binders, respectively. Then, what remained of the polymers from each binder became thermally decomposed, from 375 °C to 450 °C.

The fact that the PE2 polymeric binder has shown greatest affinity to the solvent components, allows for a greater extent of structure formations in the QTC inks that are contained in the PE2 binder, in comparison to those containing the PVP, PVP-S, PE1 and PE3 binders.

Table 3-2 Solid content for each individual binder dispersion, PVP, PVP-S, PE1, PE2 and PE3 from TGA analysis

	PVP-based binder dispersion	*PVP-S-based binder dispersion*	*PE1-based binder dispersion*	*PE2-based binder dispersion*	*PE3-based binder dispersion*
Solid content (the first turning point)	**39.84% at 160 °C**	**43.85% at 166 °C**	**43.57% at 170 °C**	**23.57% at 192 °C**	**38.95% at 178 °C**

Comparing Table 3-1 with Table 3-2, the difference in the results between the two different measuring methods is less than 2%. As a result, the solid content given by evaporating the solvent is credible.

3.2 Screening the ink formulations of PVP, PVP-S, PE1 and PE2-based QTC inks

The purpose of the study described in this section was to investigate the ink property and electrical properties of each printed film to screen the candidates. It was intended that from this preliminary trial, any ink that gave poor results would be discarded.

3.2.1 The effect of water-based binders on inks and on printed films properties

The results of the study of the viscosity *vs.* shear rate relationships, Section 3.1.2.1, indicate that the viscosity of the PE3-based binder was too low for screen printing application. Therefore, the PE3-based binder was discarded and excluded from further investigation.

The ink formulations of the water-based polymeric QTC inks are shown in Table 3-3. The sample codes for each ink formulation were related to the polymeric binder used in formulation.

Table 3-3 Ink formulations for initial screening of available water-based inks for further research. The percentage quoted (%) is by weight.

Aqueous ink formulations	***85% Ni 15% Binder***	***80% Ni 20% Binder***	***75% Ni 25% Binder***	***70% Ni 30% Binder***	***60% Ni 40% Binder***	***50% Ni 50% Binder***	***40% Ni 60% Binder***	***30% Ni 70% Binder***
PVP-based ink sample code	**PVP0**	**PVP1**	**PVP2**	**PVP3**	**PVP4**	**PVP5**	**PVP6**	**PVP7**
PVP-S-based ink sample code	**PVP-S0**	**PVP-S1**	**PVP-S2**	**PVP-S3**	**PVP-S4**	**PVP-S5**	**PVP-S6**	**PVP-S7**
PE1-based ink sample code	**PE1-0**	**PE1-1**	**PE1-2**	**PE1-3**	**PE1-4**	**PE1-5**	**PE1-6**	**PE1-7**
PE2-based ink sample code	**PE2-0**	**PE2-1**	**PE2-2**	**PE2-3**	**PE2-4**	**PE2-5**	**PE2-6**	**PE2-7**

3.3 Results and discussion

3.3.1 Printability

Each ink, (Table 3-3) was mixed following the same process of ink preparation, at room temperature, as described in Section 2.5. Adequate amounts of ink were transferred to the carton board substrates. The printability of each ink was followed

and examined. The printability of screen printing ink was affected by the smoothness, the surface chemistry and the structure of the surface coating layer.

It was found that the inks could not form smooth films on the carton board substrate, when the inks containing nickel powder were more than 85 wt% or the water-based binder was less than 15 wt%. These inks formed coarse pastes on the substrates because of the high loading of nickel powder, resulting in large aggregation of nickel particles. Although the solid content of the PE2-based binder was the lowest (23.9 wt%), the ink containing nickel powder (85 wt%) and the PE2-based binder (15 wt%) still could not mix and be applied effectively.

Additionally, PVP-based inks consisting of nickel powder with more than 75 wt% in the formulations were not able to develop, owing to the high molecular weight (*i.e.* $\bar{M}_n$ 360,000 g/mol) of the PVP binder. This large molecular weight gives high viscosity and mechanical strength to the PVP polymer [7]. Apart from Ni-PVP-based ink, the maximum loading of nickel powder was 80 wt% and the specific polymeric binder (PVP-S, PE1 or PE2) was 20 wt%. When the ink was mixed with nickel powder (30 wt%) and a polymeric binder (70 wt%) it was transferred onto the carton board substrate for the printability tests. It was found that the viscosity of this ink was too low so it bled on the carton board. Inks containing nickel powder (35 wt%) and options of each individual polymeric binder (65 wt%) were created, but the ink film still could not be fabricated due to its low viscosity. Through experiments it was found that the minimum loading of nickel powder in order to fabricate a uniform and continuous ink film was 40 wt%. This observation indicated that the nickel loading lower than 40 wt% within ink formulation was not sufficient as printing of the ink formulation was unsuccessful.

From the printability test results discussed above, it was shown that inks with nickel powder and polymeric binder ranges from 40 wt% to 80 wt% and 60 wt% to 20 wt%, respectively, were applied on a PET substrate through a stencil mesh using a screen printing technique. Each of the printed films was dried overnight to obtain a constant weight in a clean petri-dish. Table 3-4 summarises the availability of ink formulations that can be produced by screen printing equipment.

Table 3-4 Ink formulations for the availability of screen printable inks. Red crosses (X) denotes the inks that failed to be produced and/or applied onto the carton substrates

Aqueous ink formulations	*85% Ni 15% Binder*	*80% Ni 20% Binder*	*75% Ni 25% Binder*	*70% Ni 30% Binder*	*60% Ni 40% Binder*	*50% Ni 50% Binder*	*40% Ni 60% Binder*	*30% Ni 70% Binder*
PVP-based ink sample code	**PVP0**	**PVP1**	**PVP2**	**PVP3**	**PVP4**	**PVP5**	**PVP6**	**PVP7**
	×	×	×					
PVP-S based ink sample code	**PVP-S0**	**PVP-S1**	**PVP-S2**	**PVP-S3**	**PVP-S4**	**PVP-S5**	**PVP-S6**	**PVP-S7**
	×							×
PE1-based ink sample code	**PE1-0**	**PE1-1**	**PE1-2**	**PE1-3**	**PE1-4**	**PE1-5**	**PE1-6**	**PE1-7**
	×							×
PE2-based ink sample code	**PE2-0**	**PE2-1**	**PE2-2**	**PE2-3**	**PE2-4**	**PE2-5**	**PE2-6**	**PE2-7**
	×							×

3.3.2 Electrical properties responding to external forces for a commercial QTC bulk material

The objective of the research was to investigate the electrical properties of the inks' responses to external forces, thus establishing a basis for creating printed films, in accordance with viable QTC commercial materials. Thus, it was considered to be necessary to demonstrate the variation in resistance as a function of compression for a QTC bulk material, as shown in Figure 3.7.

A commercial QTC material comprises a mixture of spiky nickel particles, of approximately 1-100 μm diameter, and an elastomeric poly(siloxane) matrix. These fulfil different roles [8], of which the nickel particles and the polysiloxane contribute electrically as conductive fillers and insulating matrix, respectively. The nickel particles are coated with a polymer matrix, as shown in Figure 3.2 and Figure 3.3 that have sharp projections on the surface [3, 9]. As a result, the particles themselves do not "communicate" to form chains with each other directly. QTC contains a nickel Type 123 and Type 287 (supplied by Inco Ltd.), dispersed in a blend of liquid monomers. These nickel-monomer combinations are polymerised to

give a flexible and elastic sheet with a thickness of 1-2 mm [3, 8]. The particle size distributions of nickel type 123 and nickel type 287 are in the range of 3.5 to 4.5 μm and 2.6 to 3.3 μm,a respectively. A silicone based monomer or urethane based monomer is used. Siloxane-based monomers, include Alphasil 2000 (Alphas Industries Ltd.), Silicoset 153 (Ambersil Ltd.), Silastic T4 (Dow Corning) and RTV6166 (GE Silicones). The urethane-based monomer includes F42 (supplied by Techsil Ltd.) [3, 10]. In order to establish a material that reaches or exceeds the percolation threshold, the ratio of conductive filler to polymer matrix, within the solid state formulation should be in the range of 4:1 to 6:1 [11].

At approximately 10^{12} Ω, when the QTC materials are in an unstressed state, they exhibit electrically insulating characteristics, in which the filler particles are above the percolation threshold. The resistance of the QTC material becomes extremely sensitive and decreases with an increase in external forces, if the filler particles are close to the percolation threshold. When a high compression is applied, it results in the filler particles coming into close physical contact. In this case, the resistance of the QTC material should become consistently lower (less than 10 Ω).

Commercial QTC materials have been employed in a vast range of applications as switches or sensors due to their unusual property arising from the deformation of the particles. However, the composition of the commercial QTC material could not be used for any printing techniques because of its high viscosity and high loading of nickel powder in the QTC material. Therefore, developing ink formulations that are printable, with their printed films behaving similarly to the electrical properties in the commercial QTC material under external applied compression will be a major target to focus on.

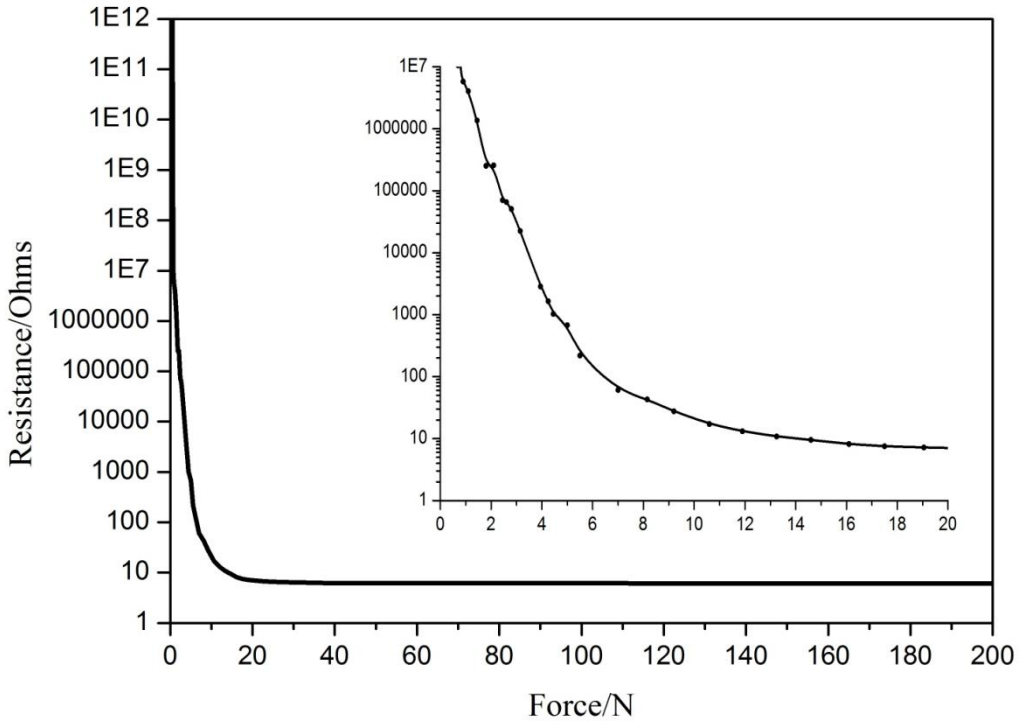

Figure 3.7 Variation in resistance as a function of external compression for a commercial Ni-silicone QTC material [5]

3.3.3 Comparisons of the effects of conductive fillers on the electrical-mechanical properties of PVP, PVP-S, PE1 and PE2-based printed films

3.3.3.1 The effect of conductive fillers on the electrical-mechanical properties of PVP-based printed films

Figure 3.8 displays the variation in electrical resistance as a function of compression for different formulations of PVP-based printed films. It was found that the electrical resistance of all the PVP-based printed films possessed electrically insulating behaviour when the compression applied on top was less than 0.7 N. After an increasing pressure was applied, the PVP-based printed films changed from insulating behaviour to conductive characteristics. The initial electrical resistance was too large to measure, the instrumental limit of the digital meter being $2 \times 10^7\ \Omega$. Therefore, in order to report the electrical resistance of each printed film, the off-limit value of the resistance was set as $2 \times 10^7\ \Omega$. The lowest applied force on the

printed film was recorded at 0.01 N. Each plotted data point has its corresponding standard deviation, as calculated from five replicate tests.

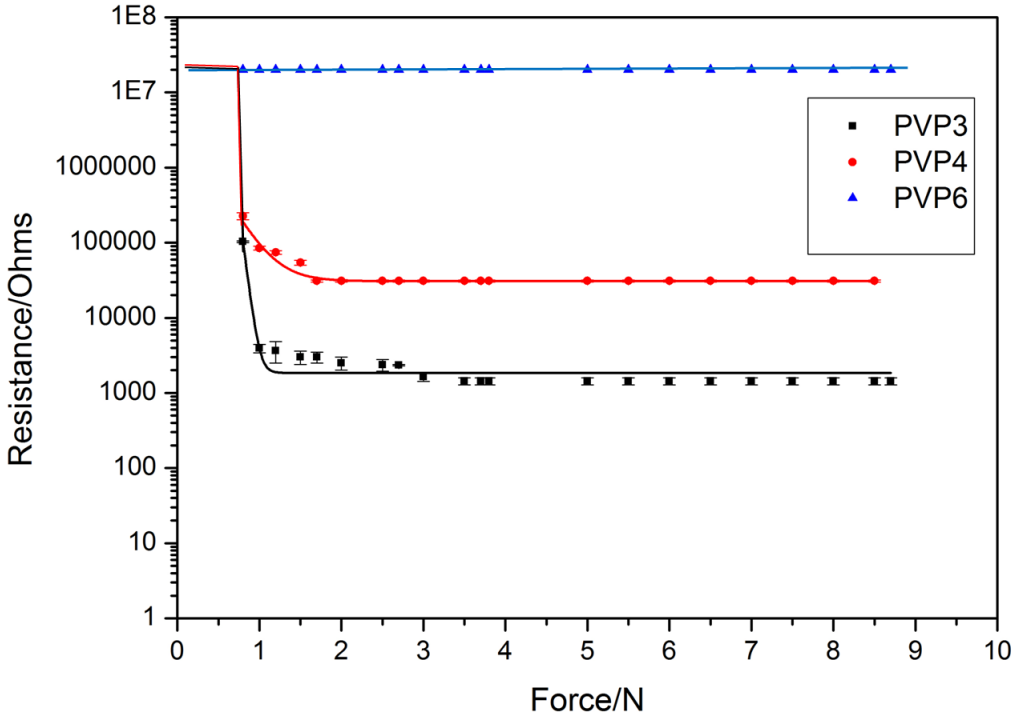

Figure 3.8 Data showing the dependence of electrical resistance on the applied force over five tests for different nickel amounts of PVP-based pressure-sensitive printed films

Within the error range, printed films that were made from PVP3 and PVP4 formulations exhibited pressure-sensitive electrical properties, as shown in Figure 3.8. The resistance of PVP3 and PVP4 printed films were reduced to the lowest values when the compressions were approximately 3 N and 1.5 N, respectively, beyond which different resistances were observed. PVP3 showed controlled electrical switching behaviour and PVP4 behaved more like electrical sensing materials. Electrical switching behaviour means that the resistance rapidly changed with increasing force. Electrical sensing behaviour means that the resistance gradually changes with increasing force. The two contrasting behaviours shown by the printed films (PVP3 and PVP4) arise because of the loading of the conductive filler that both inks contain, being more likely to form aggregations in the printed film as the conductive filler content increases. In this case, the conductive pathways are effectively increased which results in a change in electrical resistance. The

influence of the particle size distribution of the nickel particles in the PVP-based binder on the electrical properties as mentioned in Section 3.3.3.2 could also prove the aggregations of conductive filler. In summary, the resistance of PVP3 and PVP4 printed films fell quickly with increasing applied force up to a point that was dependent on the nickel filler loading, and then changed at a slower extent.

From the plots for the PVP3 and PVP4 printed films, it is found that the sensitivity was dependent on the filler loading. Therefore, the resistance of PVP3 formulation becomes more sensitive to external compression than that of PVP4 formulation. The resistances of printed films from PVP3 and PVP4 changed by four and three orders of magnitude, respectively, at a force of 2 N. At this point, the electrical resistances of PVP3 and PVP4 become constant with increasing applied compression. During the whole compression procedure for the PVP-based printed films, both the percolation and quantum tunnelling procedures were represented at low applied forces, resulting in a sharp reduction in resistance. Consequently, the conduction mechanism at low applied force might not be the same as that at large applied force in a composite system [12]. As the Poisson ratio of a PVP polymer is normally less than 0.5, it means that the volume of the polymer decreases under applied compression [12], *i.e.* uniaxial stress. As a result, the nickel filler volume fraction, (as calculated by Equation 3-1), would initially increase with an increase in the uniaxial pressure [13]. When the volume fraction of nickel powder was near the percolation threshold, the resistance of the printed film was extremely sensitive to applied pressure. When the nickel volume fraction was far from the percolation threshold, the printed film should not behave very sensitively. If a further external force is applied to the printed film, the volume fraction of nickel content will be above the percolation threshold. In this case, the resistance of the printed film will be saturated and constant. It has been reported that the percolation threshold value is very difficult to determine in a composite [14]. In the meantime, the current of this printed film displays linearly proportional to the voltage, displaying an Ohmic behaviour. Due to the external uniaxial stress, the distance between nickel particles and nickel aggregates is reduced. As a result, the composite system becomes the same as that of a metallic feature owing to the physical contact of nickel particles [12, 14-18].

$$\text{PVF} = \frac{V_p}{V_p + V_b} \times 100 = \frac{W_p/\rho_p}{\left(W_p/\rho_p\right) + (1 - W_p)/\rho_b} \times 100$$

Equation 3-1 PVF represents for pigment volume fraction, in which V, W and ρ present the pigment's volume, weight and density, respectively. The subscripts of p and b correspond to the pigment and binder, respectively [19]

The electrical resistance values fluctuated with changing the applied force, for PVP5. The printed film was less sensitive to the external force because the volume fraction of nickel content was low and well below the percolation threshold. Apparently, the Ni-PVP composite sample was heterogeneous, which means the nickel particles were randomly distributed in the printed film. Therefore, the conduction pathways for each external compression were not the same, especially regarding printed film with a low nickel content which results in a fluctuated electrical resistance under an external uniaxial force.

For PVP-based inks with even lower nickel loadings, *e.g.* PVP6 (40 wt% nickel powder and 60 wt% PVP binder) and PVP7 (30 wt% nickel powder and 70 wt% PVP binder), it was observed that their corresponding printed films behaved as complete electrical insulators even when the external uniaxial compression was 500 N. This is because of the low nickel filler loading, so the electrical properties were similar to those of a film that contained only the host polymer matrix. As a consequence, the resistance of the printed film was constantly high.

The electrical-mechanical properties of Ni-PVP-based printed films (Figure 3.8), PVP3 and PVP4, behaves similarly to the commercial QTC materials (Figure 3.7). The PVP3 film behaves more as an electrical switch and the PVP4 film behaves more as an electrical sensor. Both the PVP3 and PVP4 are electrically insulating under a low compression. However, the lowest resistance value of the PVP3 printed film (~2000 Ω) and the PVP4 printed film (~4000 Ω) is much greater than that of a commercial QTC material (~10 Ω). This achieved greater resistance of Ni-PVP-based composites is not acceptable in accordance with the objective of the research; that the printed film changes from an electrical insulator to an electrical conductor under an external compression. The possible reasons of the impact on the electrical properties of the PVP-based films caused this are discussed as follows.

3.3.3.2 Size distributions of the nickel particles in PVP-based inks

Figure 3.9 shows the size distribution graphs for different Ni-PVP-based inks, based on the nickel content, *i.e.* PVP3 (70 wt% of nickel powder and 30 wt% of binder) and PVP6 (40 wt% of nickel powder and 60 wt% of binder). It can be seen that the larger nickel powders tended to agglomerate, (ranging from 100 µm to 300 µm), for the PVP3 printed film, which made an essential contribution to the quantum and percolation tunnelling. This is because of the intermolecular forces between nickel particles, *i.e.* van der Waals attractive force and magnetic dipole-dipole attractions [20]. This led to the PVP3 printed film having an electrical switching behaviour. However, the low loading of nickel powder in the PVP6 printed films leads to an electrical insulating behaviour.

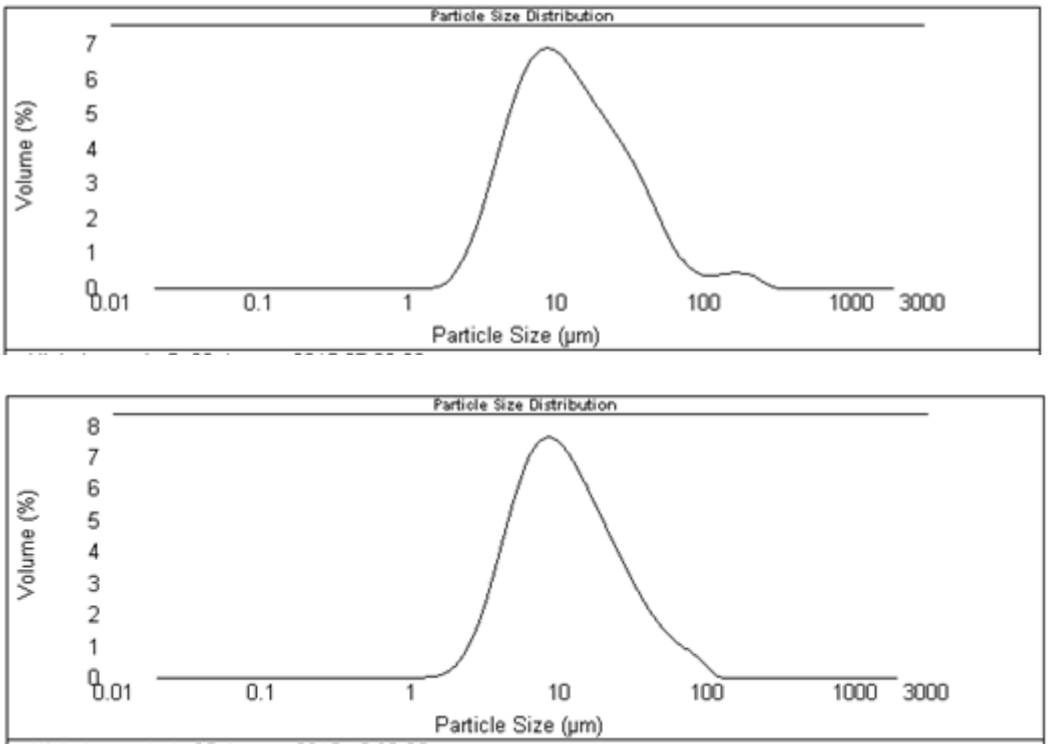

Figure 3.9 Size distribution graphs of PVP3 (top) and PVP6 (bottom) pigmented inks

3.3.3.3 Thermal stability of the PVP-based ink

Decomposition arising during the TGA-induced breakdown of the PVP-based binder and a PVP-based printed film is shown in Figure 3.10. Two different regions for each sample can be observed at the same temperature, which reveals that only the

polymeric binder changed when the samples were heated. The nickel particles that were bound in the PVP-based polymer did not alter at all, despite heating from 30 °C to 500 °C. The loss in mass can be attributed to the evaporation of water from the polymeric binder and ink from 30 °C to 150 °C. The weight losses of water in the PVP polymeric binder and PVP3 ink are 61.8% and 14.2% respectively. The water loss (17.2%) in the PVP3 ink, through TGA analysis is close to the theoretical water percentage (18.5%) that can be calculated from 30% (polymeric binder concentration) multiplying by 61.8% (water content of the PVP-based binder). The pattern shows that the estimation of nickel content in the ink film, Section 2.4.7.8, is correct. It is assumed that the second weight loss (~ 12.3%), of PVP3 ink, from 400 °C to 450 °C corresponds to the decomposition of PVP polymer. Apart from that, the degradation of PVP polymer is 11.5% and this can be calculated theoretically from 30% (polymeric binder concentration) multiplied by 38.2% (solid content of PVP-based binder). This proves the assumption that the second weight loss is the decomposition of PVP polymer. The remaining weight of the PVP3 ink is approximately 70% (as shown in Figure 3.10), which corresponds with the initial addition of nickel powder in the ink. It is also evident that the second weight loss relates to the degradation of PVP polymer. This reveals the nickel particles are merely physically present and have no chemical bonding reaction with the PVP polymers in the Ni-PVP composite.

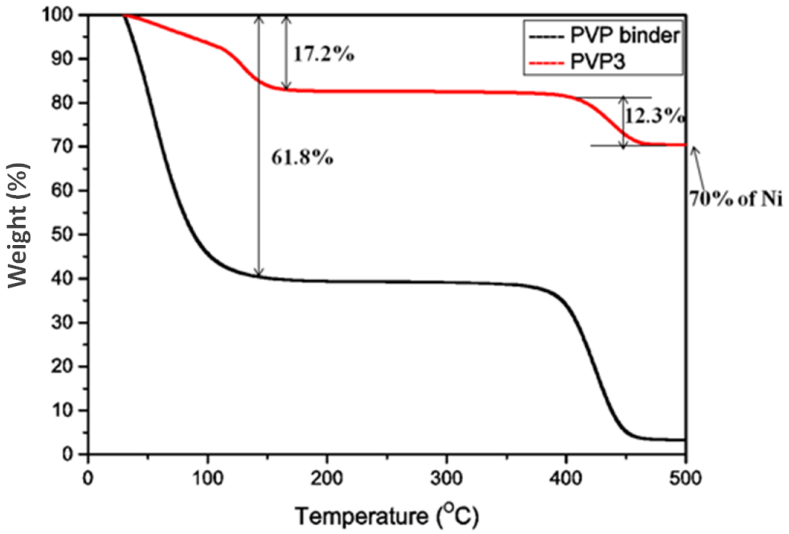

Figure 3.10 TGA mass loss profile for PVP polymeric binder and PVP3 ink, in which each sample was heated for 50 minutes from 0 to 500 °C, at 10 °C/minute

3.3.3.4 The effect of conductive fillers on the electrical-mechanical properties of PVP-S-based printed films

Figure 3.11 shows the dependence of the electrical resistance on the applied force for different nickel contents in the PVP-S-based pressure-sensitive printed films. In general, PVP-S-based printed films follow a similar pattern in their electrical properties, as PVP-based printed films. The PVP-S1 and the PVP-S2 printed films showed classical electrical switching behaviour and the other PVP-S-based printed films showed controlled electrical sensing behaviour. The differences between the various PVP-S-based printed films involved the nickel content. As the nickel content of the ink was increased, the printed film became more sensitive with a typical electrically switching behaviour. It is reported that a high proportion of conductive filler can reduce the percolation value [21]. As a result, high loading of nickel powder would be expected to improve the electrical sensitivity of the printed films.

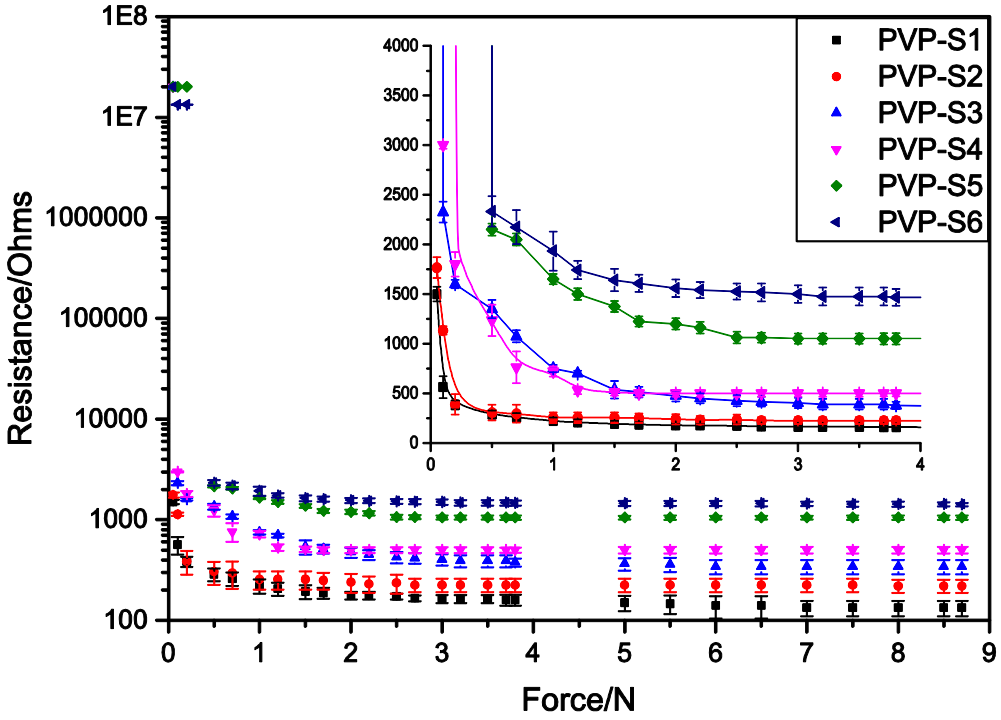

Figure 3.11 Data showing the dependence of electrical resistance on applied force over five tests for different nickel amounts of PVP-S-based pressure-sensitive printed films

When the volume fraction of the nickel loading is far below the percolation threshold, the resistance of the composite reduces gradually with an increasing external uniaxial force. This behaviour occurs due to quantum tunnelling. It has been reported that the coating film is more continuous when the volume fraction of the nickel particles is below the percolation threshold, *i.e.* critical pigment volume fraction [19]. Consequently, the conductive nickel fillers are physically separated from each other preventing aggregation, causing electrical resistance of the printed film to be high. When the volume fraction of the nickel was close to the percolation threshold, the resistance of the printed films became very sensitive to the external uniaxial force resulting in a sharp reduction in the resistance. In this case, both the percolation and the quantum tunnelling processes were presented by the composites. When the volume fraction of nickel content was above the percolation threshold, the resistance of the printed films became saturated and constant, because of the physical contact of nickel particles, resulting in a metallic conduction. Furthermore, the film is discontinuous when the volume fraction of the nickel particles is above the percolation threshold because the pigment particles are surrounded by the presence of air pockets that replace the binder [19].

The lowest resistance value was achieved by the PVP-S1 printed film under more than 1 N uniaxial compression, which was approximately 100 Ω. Furthermore, the lowest resistance value increases with decreasing nickel filler content as expected. However, the difference in the lowest resistance values between two printed samples is not proportional to the difference of their nickel content, as shown in Figure 3.12. For instance, the difference in resistance values between PVP-S1 and PVP-S2 is around 70 Ω. This value difference is not equal to that between PVP-S2 and PVP-S3 printed films, which is around 150 Ω. This is because of the printed samples were clearly not homogeneous, as shown in the morphologies of the printed films, in Section 3.3.4.2, as the resistivity, current density and electric field would not be constant throughout the samples [3].

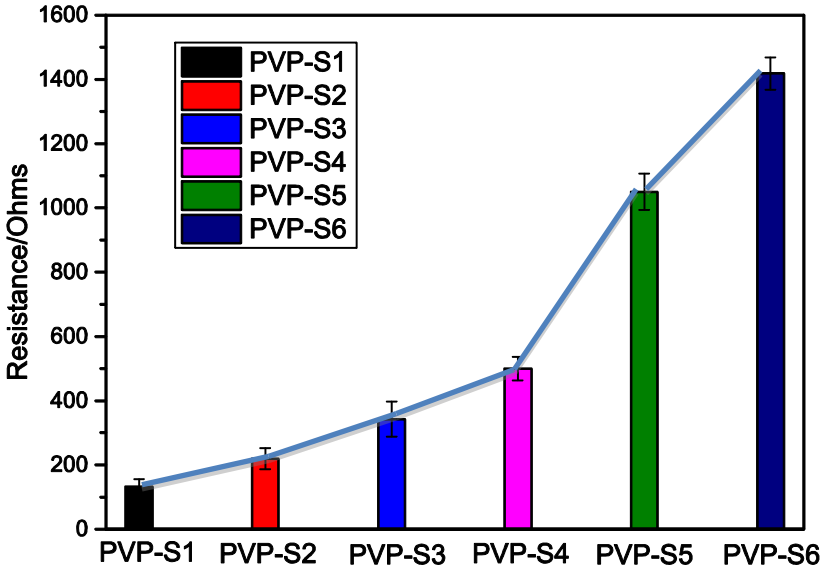

Figure 3.12 Data showing the lowest resistance values for each PVP-S-based printed film that contains different nickel contents

In summary, a range of screen printable Ni-PVP-S-based films with pressure-sensitive performance has been developed. The electrical sensitivity of the printed films could be varied by the nickel contents. The printed films, PVP-S1 and PVP-S2, behaved more electrical switching behaviour and the other PVP-S-based printed films that contained lower nickel amounts behaved more electrical sensors. The R-F plot of PVP-S-based films (see Figure 3.11) showed similar trend as that of the QTC commercial material (see Figure 3.7). However, the high loading of nickel powder in the PVP-S1 and the PVP-S2 printed films yielded lower resistance (~ 1700 Ω) in comparison to the other PVP-S-based printed films under no applied external compression. This electrical conductive behaviour did not follow the objective of the research.

The PVP-S3 and the PVP-S4 printed films did not show the electrical insulating behaviour when no compression was applied, but the initial resistance values were greater than those of the PVP-S1 and the PVP-S2 films, ~ 2300 Ω and ~ 3000 Ω, respectively. Also, the electrical resistance of the PVP-S3 film reduced very quickly with increasing applied force, which means it was too sensitive. The optimisation of this electrically sensitive printed film is discussed in Section 3.4, in order to develop an acceptable sensing film as the QTC commercial material. The lowest resistance value of the PVP-S4 film was slighter greater than that of the PVP-

S3 film due to the lower loading of nickel powder in the PVP-S4. However, it is difficult to modify the conductivity of the film, which was determined by the nickel amounts. Therefore, the electrical-mechanical properties of the PVP-S3 printed film contained 70 wt% of nickel powder and 30 wt% of the PVP-S-based binder dispersion would be focussed to optimise with the further electrical properties according to those of the QTC commercial material.

For the rest of the PVP-S-based printed films, PVP-S5 and PVP-S6, the PVP-S5 and the PVP-S6 with lower nickel loading was not perform conductive enough, even under a greater external compression, (over 1000 Ω), as shown in Figure 3.12. Thus, these printed films would not be further investigated.

3.3.3.5 Thermal stability of the PVP-S-based inks

Figure 3.13 displays the TGA analysis for the PVP-S polymeric binder and the PVP-S3 (70 wt% Ni and 30 wt% of polymeric binder) ink. The results and discussion concerning Figure 3.13 are similar to those given by the PVP polymeric binder and the PVP3 ink, in Section 3.3.3.3. It reveals that the nickel particles are physically present but have no chemical reaction with PVP-S polymer in the Ni-PVP-S composite.

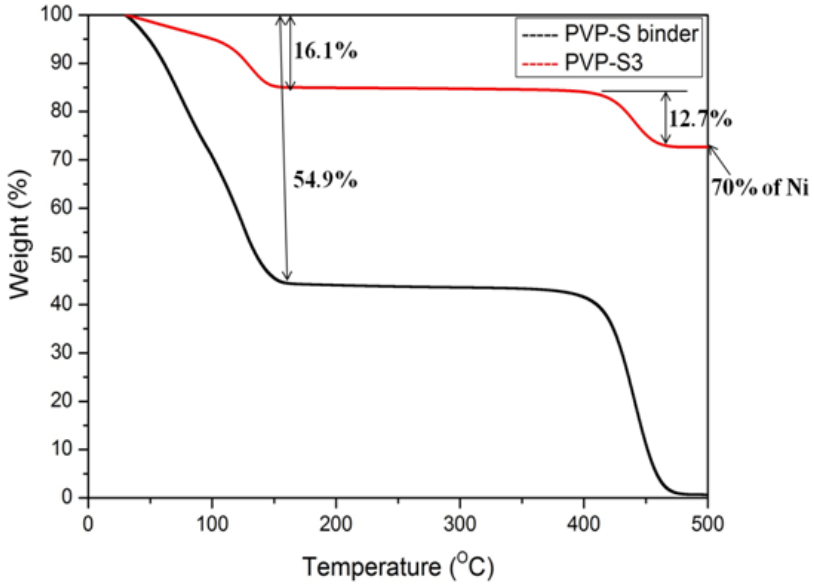

Figure 3.13 TGA mass loss profile for PVP-S polymeric binder and PVP-S3 ink, in which each sample was heated for 50 minutes from 0 °C to 500 °C, at 10 °C/min

3.3.3.6 The effect of conductive fillers on the electrical-mechanical properties of PE1-based and PE2-based printed films

Figure 3.14 and Figure 3.15 show the dependence of electrical resistance on the applied force for different nickel contents of PE1-based and PE2-based pressure-sensitive printed films that follow a similar trend to the PVP-based and PVP-S-based printed films. It can be seen that the electrical resistance of the PE1-based and the PE2-based composite is strongly determined by the nickel powder content under a constant applied force. PE1-1, PE1-2 and PE1-3 printed films showed electrically switching behaviour and the other PE1-based printed films showed controlled electrical sensing behaviour. For PE2-based printed films, the PE2-1 printed film showed typically electrical switching behaviour and the other PE2-based printed films showed controlled electrical sensing behaviour. The reason for this behaviour is the increase in conductive filler content which reduces the percolation value, which resulted in an improvement in the electrical sensitivity.

When the nickel powder content was well below the percolation threshold, the resistance of the composite diminished exponentially with increasing external uniaxial force. This performance follows the quantum tunnelling mechanism. When the volume fraction of nickel loading was close to the percolation threshold, the resistance of the prints became very sensitive to the external uniaxial force, due to both percolation and the quantum tunnelling processes being present in the composite system. When the volume fraction of nickel content was above the percolation threshold, the conductivity of the printed films became maximal and constant. This is because of physical contact between the nickel particles, resulting in a metallic conductive feature.

The lowest resistance values were achieved with the PE2-based printed films under more than 1N uniaxial compression. The lowest resistance value for PE2-based printed film was achieved by the PE2-1 film under more than 1.5 N of uniaxial force, at approximately 70 Ω. Furthermore, a reduction in nickel content resulted in an increase in the lowest resistance value, as expected. However, the difference in the lowest resistance value between two film samples is not proportional to the difference in their nickel content. For instance, the difference in resistance values between PE1-1 and PE1-2 is around 70 Ω. This difference value is

not as twice as much as between PE1-3 and PE1-4 printed films, which is around 450 Ω. The difference in resistance values between PE2-1 and PE2-2 is around 50 Ω. This difference in value is not equal to that between PE2-2 and PE2-3 printed films, which is around 150 Ω. This is because the printed samples are clearly not homogeneous, as shown in the printed films' morphologies, in Section 3.3.5.2. Thus, the resistivity, current density and electric field are not constant throughout the samples [3]. For each individual plot, it can be seen that sensitivity increases as the filler content of the printed film increases. This has been interpreted in the last section.

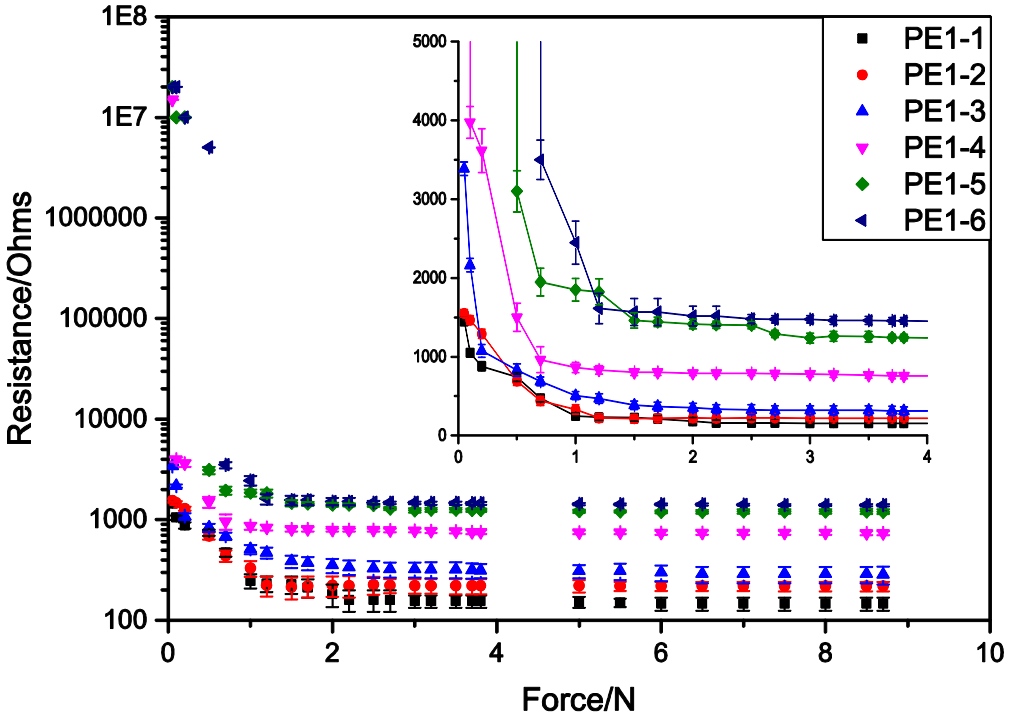

Figure 3.14 Data showing the dependence of electrical resistance on the applied force over five tests for different nickel amounts of PE1-based pressure-sensitive printed films

In summary, it has been shown that the pressure sensitivity of electrical resistance for a water-based printed film is a function of compressive force. The electrical resistance for each printed film generally exceeds 1 kΩ when the lowest applied force of 0.01 N, contacts the printed film. Then the resistance displays a large reduction, even in response to a force as low as 0.1 N. That is to say, the conductivity of the printed film shows a significant increase from 0.01 N to 0.1 N of

applied force. This is, however, different from other high-loading composites that show a slight resistance change with applied force below 5 N [22-25]. For QTC printed films, the significant increase in resistance is owing to the progressively intimate contact between the upper carbon electrode on PET substrate and the lower ink film. At greater applied forces, *i.e.* > 0.1 N, the conduction pathways are established through the printed film because of the compression used [25].

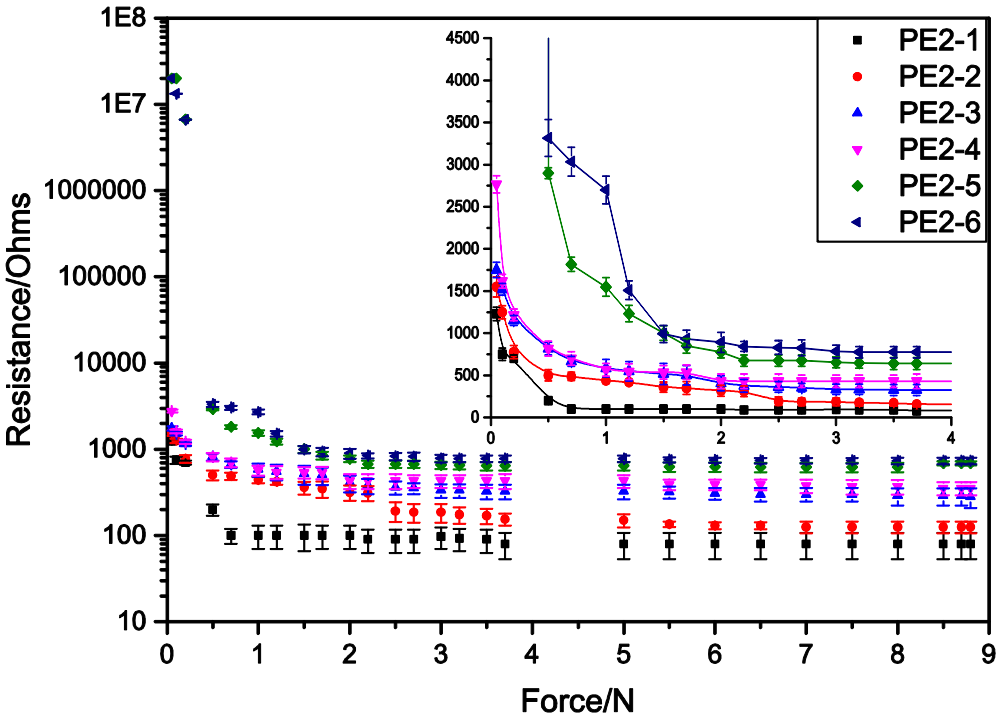

Figure 3.15 Data showing the dependence of electrical resistance on the applied force over five tests for different nickel amounts of PE2-based pressure-sensitive printed films

The printed films produced were flexible and black in colour. The flexibilities of these printed films were dependent on the grade of polymer that was used as a matrix, the nickel powder loading and the thickness of the sheets. The most flexible films had a low nickel powder loading. The flexibility of each water-based printed film is further discussed in Section 3.3.4.5. It has been reported that an increase in metallic filler content (*i.e.* nickel powder) can result in a reduction of sensitivity to external compression [12].

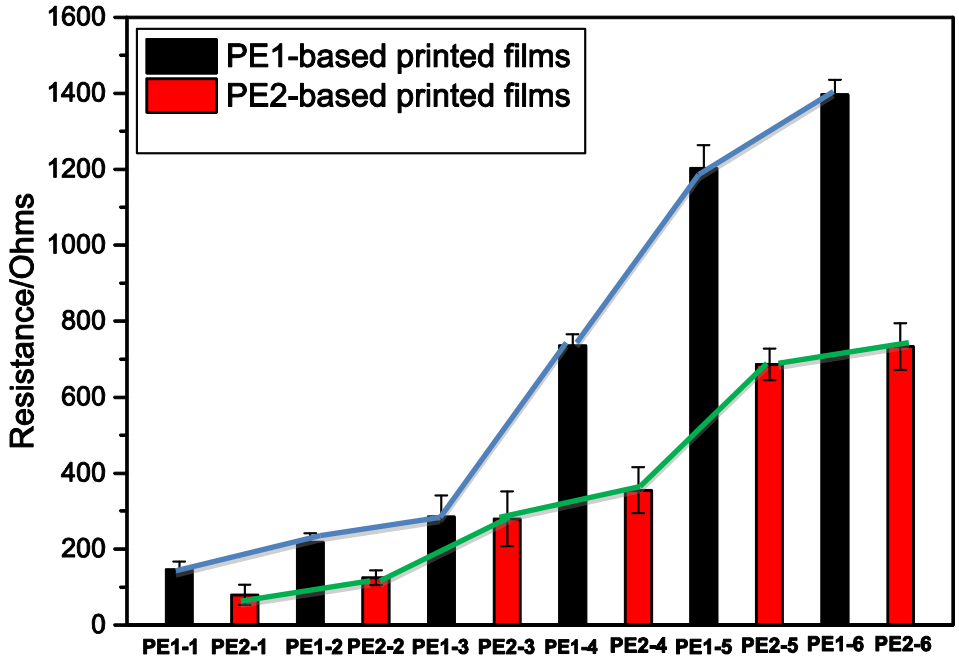

Figure 3.16 Relationship showing the lowest resistance values for each PE1-based and PE2-based printed film that contain different nickel contents

In conclusions, several screen printable Ni-PE1-based films with pressure-sensitive behaviour have been successfully developed. The electrical sensitivity of the PE1-based printed films could be varied by the nickel amounts. The printed films, PE1-1, PE1-2 and PE1-3, showed more electrical switching behaviour and the other PE1-based printed films that contained lower nickel amounts showed more electrical sensing behaviour. The R-F plot of the PE1-based films (see Figure 3.14) exhibited similar trend as that of the QTC commercial material (see Figure 3.7). However, the PE1-1, the PE1-2 and the PE1-3 printed films with high loading of nickel powder did not show electrical insulating behaviour under no external compression was applied. This electrical conductive behaviour did not follow the objective of the research. For the PE1-1 and the PE1-2 printed films, it was difficult to further optimise the electrical properties as the high loading of nickel powder, which would not allow any allocation of the TiO_2 pigment. Even though the PE1-3 printed film was conductive initially, this electrical performance could be modified and optimised by the introduction of the different grades of TiO_2 (as discussed in Section 3.4). Therefore, the PE1-3 film was the ink formulation that would be further investigated and discussed.

For the other PE1-based printed films, PE1-4, PE1-5 and PE1-6, they behaved electrical insulating behaviour under no pressure was applied. However, they did not perform conductive enough under large compressions, because of the low nickel contents in the films. Thus, these printed films would not be further investigated or optimised.

For the PE2-based printed films, the PE2-3 film was chosen to further investigate and optimise because of the same reason for screening the PE1-based films.

3.3.3.7 Thermal stability of the PE1-based and the PE2-based inks

Figure 3.17 displays the TGA analysis data for the PE1 polymeric binder and PE1-3 (70 wt% Ni and 30 wt% of polymeric binder) ink. The results and discussion arising from Figure 3.17 are similar to those relating to the PVP polymeric binder and the PVP3 ink (see Section 3.3.3.3).

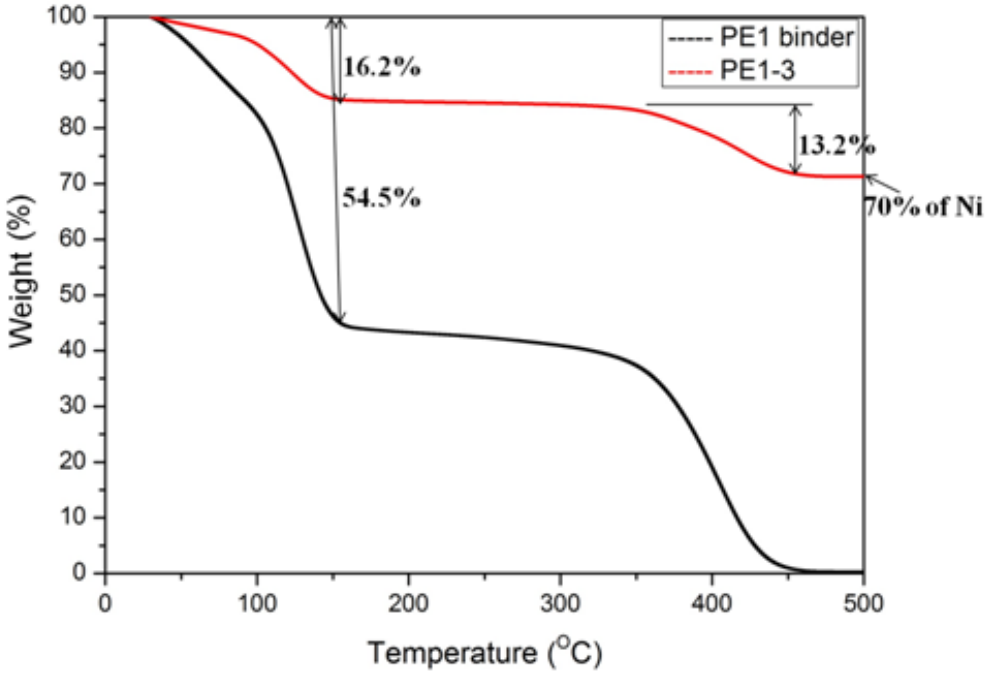

Figure 3.17 TGA analysis profile for the PE1 polymeric binder and the PE1-3 ink, in which each sample was heated for 50 minutes from 0 °C to 500 °C at 10 °C/minute

Two different mass loss regions in each sample can be observed at the same temperature, which reveals that only the polymeric binder changed when the samples were heated. The first mass loss rate can be attributed to evaporation of water from the polymeric binder and ink at 30 °C to 150 °C. The weight loss of water in the PE1 polymeric binder and PE1-3 ink is 54.5% and 16.2%, respectively. It is revealed that the water loss (16.2%) in PE1-3 ink, through TGA analysis, is close to the water percentage (16.4%) that can be calculated by 30% (polymeric binder concentration) multiplying by 54.5% (water content of the PE1-based binder). It shows that the estimation of the nickel content in the printed film in Section 2.4.7.8 was correct. It can be assumed that the second weight loss (~ 13.2%) of PE1-3 ink from 350 °C to 450 °C corresponds to the decomposition of PE1 polymer. The mass loss from the PE1 polymer was 13.6% calculated by 30% (the polymeric binder concentration) multiplying by 45.5% (the solid content of the PE1-based binder). This supports the assumption that the second weight loss concerns the decomposition of PE1 polymer. The remaining mass (%) of the PE1-3 ink is approximately 70% (as shown in Figure 3.17), which equals the initial addition of nickel powder in the ink. It is also evident that the assumption of the second weight loss is the degradation of PE1 polymer. This reveals that the nickel particles are physically binding and have no chemical reaction with the PE1 polymer in the Ni-PE1 composite.

Figure 3.18 displays the TGA mass loss profile for PE2 polymeric binder and PE2-3 (70 wt% Ni and 30 wt% of polymeric binder) ink. The results and discussion from Figure 3.18 are similar to those for the PVP polymeric binder and the PVP3 ink, considered above.

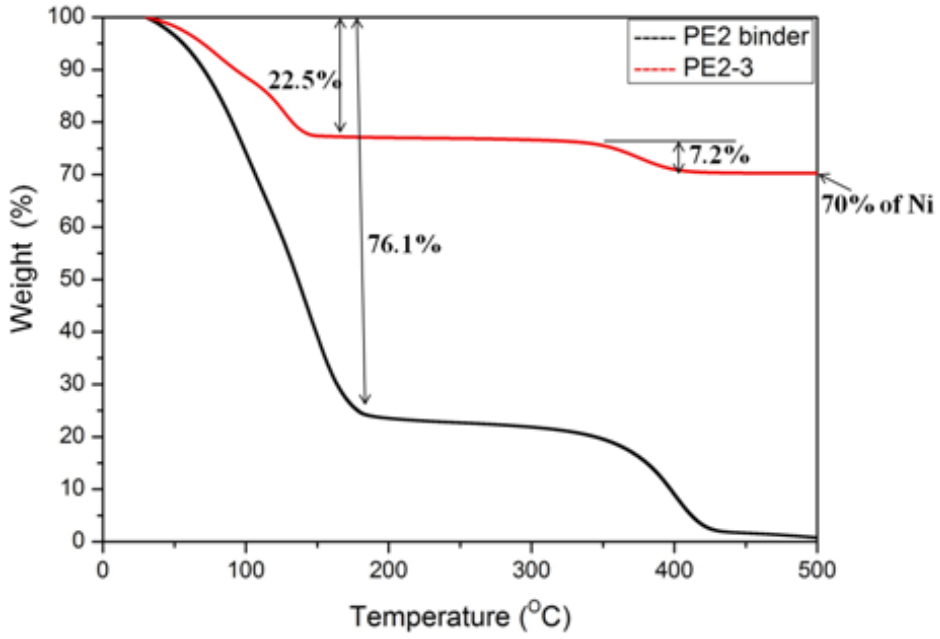

Figure 3.18 TGA analysis profile for the PE2 polymeric binder and the PE2-3 ink, in which each sample was heated for 50 minutes from 0 °C to 500 °C at 10 °C/minute

Two different mass loss regions for each sample can be observed at the same temperature, which indicates that only the polymeric binder changed when the samples were heated. This is because the nickel particles bound in PE2 polymer did not change during heating from 30 °C to 500 °C. The first mass loss rate can be attributed to the evaporation of water from the polymeric binder and ink at 30 °C to 180 °C. The weight loss of water from the PE2 polymeric binder and the PE2-3 ink are 76.1% and 22.5% respectively. It is revealed that the water loss (22.5%) in the PE2-3 ink, through TGA analysis, is close to the water percentage (22.8%) that can be calculated by the 30% (polymeric binder concentration) multiplying by 76.1% (water content of PE2-based binder). It is assumed that the second weight loss (~ 7.2%) of the PE1-3 ink, from 360 °C to 420 °C, corresponds to the decomposition of PE2 polymer. Apart from this, the degradation of the PE2 polymer is 7.2% that can be calculated by 30% (polymeric binder concentration) multiplying by 23.9% (solid content of PE2-based binder). This indicates that the second weight loss relates to the decomposition of PE2 polymer. The remaining weight of the PE2-3 ink is approximately 70% (as shown in Figure 3.17), which equals the initial addition of nickel powder in the ink. It is also evident that the assumption of the second weight

loss is the degradation of PE2 polymer. This reveals that the nickel particles are physically binding and have no chemical reaction with PE2 polymer in the Ni-PE2 composite.

3.3.4 Characterisation of PVP and PVP-S-based printed films

3.3.4.1 Comparisons of the effects of PVP and PVP-S-based binders on the electrical-mechanical properties of their corresponding printed films

Poly(vinyl pyrrolidone) (PVP) has been widely used in a vast range of application due to its non-toxicity, excellent biocompatibility and water solubility, such as fabrication of polymer membranes, additives to paints and coatings and medium for pharmaceutical tablets [26-30]. Apart from these benefits, PVP also has high dynamic elasticity [31] and is usually used to prevent the agglomeration of nanoparticles [32].

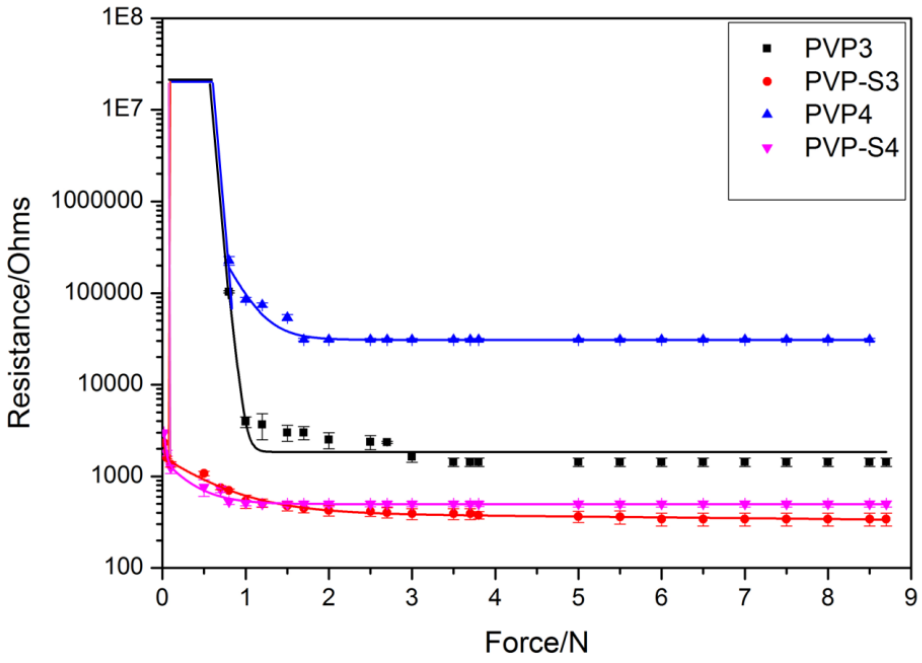

Figure 3.19 Comparison of changing electrical resistance with change in the applied external uniaxial force for printed samples having different binder (PVP and PVP-S) contents

Figure 3.19 gives a comparison of the effect of the PVP and the PVP-S-based binders on the electrical-mechanical properties. Each individual plot shows that the resistance of PVP-based printed films is much greater than those with the

same nickel content in the PVP-S-based printed samples, under the same applied compression. The nickel contents of each PVP and PVP-S-based printed film have been calculated and are displayed in Table 3-5. The ink formulations of the PVP and the PVP-S-based printed films contain similar amounts of nickel. However, this nickel content did not influence the same electrical properties in PVP and PVP-S-based printed films. This is because of the differences in the chemical structures of the polymeric binders that the two inks contain, *i.e.* PVP and PVP-S. The characteristics of the two different polymeric binders (PVP and PVP-S) were discussed in Section 3.1.2.

PVP is easily adsorbed onto a large number of materials, such as metals, metal oxides [33], graphite [34], silica [35] and poly(styrene) [36]. The chemical structure of PVP is given in

Figure 3.21a. A schematic representation of the Ni-PVP composite is shown in Figure 3.20, the strong hydrogen bonds that form between the carbonyl groups of PVP and the hydroxyls on the nickel particle surfaces [26, 37]. PVP was easily adsorbed onto the nickel particle surfaces [26, 37, 38]. Thus, Ni-PVP core-shell structures were formed. Therefore, a PVP matrix could essentially prevent the aggregation between nickel particles because of the steric hindrance that is usually present at larger molar mass values (> 10,000 g/mol) [20, 32, 39]. In this case, the poly(vinyl) sections have repulsive forces between each other [20, 32, 39]. Consequently, nickel particles could be well separated from each other in PVP-based printed films, resulting in the high resistance. The "hairy" Ni-PVP composites were brought closer when a large external force was applied, which led to a reduction in the resistance of the PVP-based printed film.

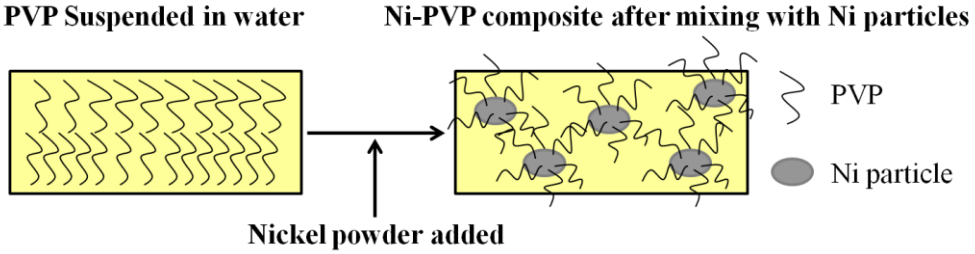

Figure 3.20 Schematic diagram illustrates the formation of PVP-coated nickel particles

Poly(1-vinyl pyrrolidone-*co*-styrene) or, (PVP-S), is a copolymer that is commonly used in the fabrication of ultrafiltration membranes because of its hydrophilic units, 1-vinylpyrrolidone, and its hydrophobic unit, styrene, as shown in

Figure 3.21. Hence, the introduction of PVP-S should significantly improve the miscibility of hydrophobic polymer blends in aqueous solution.

Table 3-5 Solid content of the PVP and the PVP-S-based samples with different nickel contents

	PVP-based	*PVP-S-based*
Solid content of polymeric binder itself	*38.2%*	*45.1%*
Solid content of ink sample with 70% Ni and 30% binder	*86% (PVP3)*	*84% (PVP-S3)*
Solid content of ink sample with 60% Ni and 40% binder	*80% (PVP4)*	*77% (PVP-S4)*

The content of the PVP-S emulsion contains 64 wt% of the hydrophobic component, styrene. Therefore, the amount of the hydrophilic component, 1-vinylpyrrolidone, is considerably less than that in the PVP emulsion. The nickel particles were influenced by the hydrophilic units, as shown in Figure 3.20. As a result, there were more free nickel aggregates that were not physically adsorbed on the substrates when the nickel loadings in the PVP and PVP-S-based inks were the same. This is why the resistance values of PVP-S-based printed films were much lower than those of the PVP-base printed films.

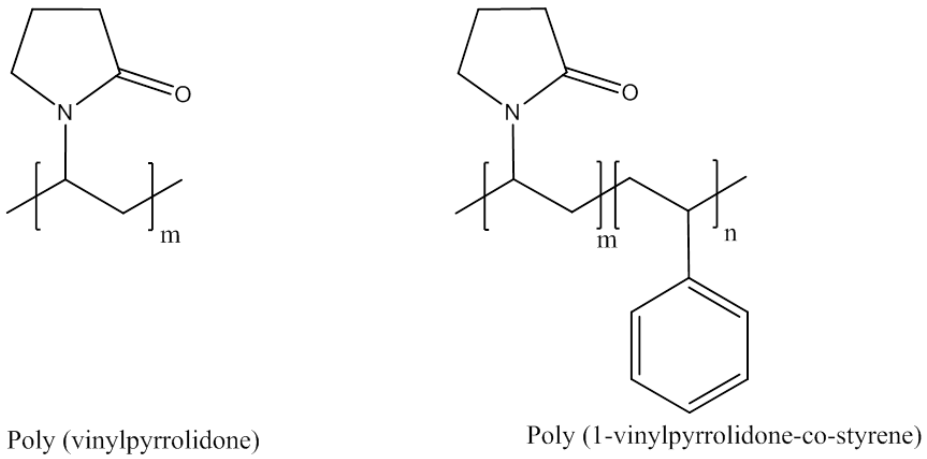

Poly (vinylpyrrolidone)

Poly (1-vinylpyrrolidone-co-styrene)

Figure 3.21 Chemical structures of (left) poly (vinyl pyrrolidone) and (right) poly (1-vinyl pyrrolidone-*co*-styrene)

3.3.4.2 SEM aspects of PVP films and of PVP-S-based printed films

The nature of the ink surface and associated cross-sections were achieved by high resolution SEM. SEM images could use to clearly characterise the nickel particles in the polymer matrices. Figure 3.22 and Figure 3.23 demonstrate the morphologies of the surfaces and the cross-sections of the PVP and the PVP-S-based printed films, respectively, which consist of nickel powder (70 wt%) and each specific polymeric binder (30 wt%). Representative electron micrographs were recorded at magnifications from × 500 to × 2500.

It is reported that PVP is an excellent dispersant, used to prevent the agglomeration of metal nanoparticles [40]. The distribution of the nickel particles in the PVP matrix, in Figure 3.22, confirms this point, whereby the nickel particles are well dispersed and separated individually from each other. These near-spherical particles are identified as nickel particles by the EDX analysis and by the morphology of the pure nickel powder (see Figure 3.1). As seen in the surface and cross-sections of the PVP3 printed film, only a small number of nickel particles aggregate in a self-assembled flower-like structure, probably due to dipole attraction and surfactant coating [20, 26]. Furthermore, near-spherical nickel particles are in a PVP matrix. This good dispersion of the nickel particles supports the long lasting time for electrical insulating behaviour under no pressure was applied for the PVP-based printed film. This printed film became less sensitive to external forces compared to the PVP-S-based printed films, since the nickel particles are further

away from each other. As a result, the lowest resistance value under a high external force was greater than that for the other printed films. Moreover, the volume fraction of nickel particles was further away from the percolation threshold, which leads to changes in the resistance when a high external force is applied.

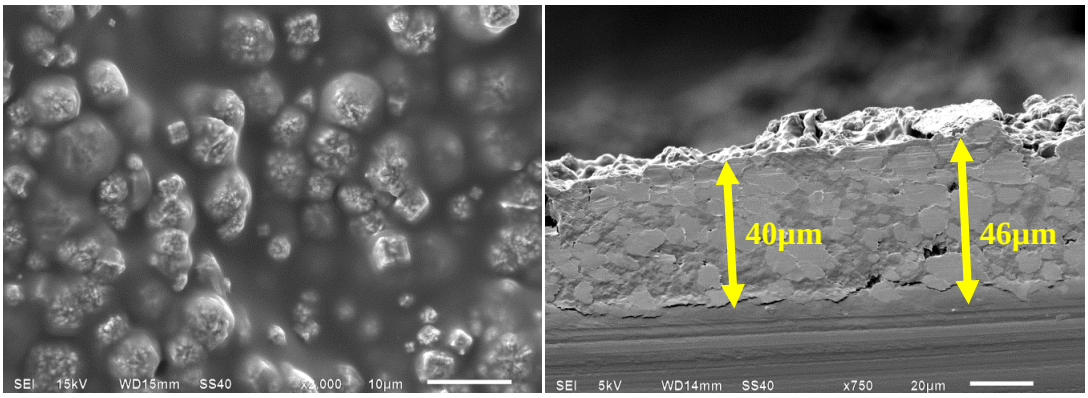

Figure 3.22 SEM images of PVP3 film's surface at × 2000 (left) and cross-section (right) at × 750 magnifications

Figure 3.23 demonstrates the morphologies of the surface and the cross-section of a PVP-S3 printed film. The PVP-S3 printed film was more brittle than the PVP3 printed film as seen in the presence of cracks. Poly(styrene) is a rigid and brittle thermoplastic polymer, often employed in plastic, packaging materials and container industries [41]. Measurement of the modulus of elasticity for each solid stated binder and each printed film is discussed in Section 3.3.4.5. The morphologies of PVP-S-based printed films were different from those of the PVP-based printed films because the repeating styryl unit in the PVP-S polymer are not as hydrophilic and miscible as the PVP polymer. The cross-section of PVP-S3 printed film shows that the nickel particles are binding in a continuous PVP-S polymer matrix. The thickness of the PVP-S3 printed film (~ 43 µm) is nearly as twice thick as the PVP3 printed film (~ 24 µm).

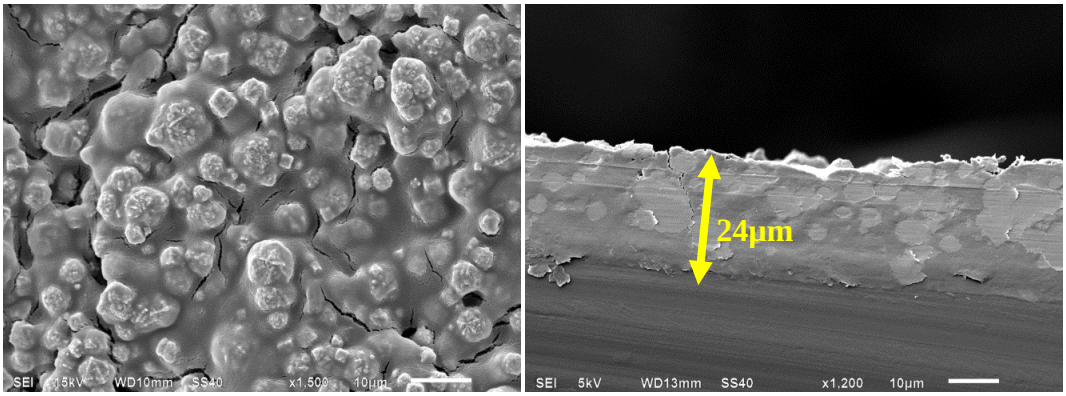

Figure 3.23 SEM images of PVP-S3 film's surface at × 2000 (left) and cross-section (right) at × 1200 magnifications

3.3.4.3 Particle size distribution of nickel particles in the PVP and the PVP-S-based binders

Figure 3.24 displays the particle size distributions of nickel particles dispersed in the PVP3-based ink and the PVP-S3-based ink, which contained 70 wt% of nickel powder and 30 wt% of each individual polymeric binder. This indicates that the nickel particles are dispersed in the PVP-based binder, sizes ranging from 1 µm to 100 µm in size. Nickel particles dispersed in the PVP-S-based binder formed a broad distribution of large aggregates from 2 µm to 300 µm. These size distribution profiles, of nickel particles in the PVP-based and PVP-S-based binders, support the morphologies obtained from the PVP-based and the PVP-S-based printed samples. Such broader particle size distribution graph obtained by the PVP-S3 film caused the more electrical switching behaviour and more conductive property with the comparison of the PVP3 film. Also this broader particle size distribution graph indicates that the nickel particles in the PVP-S-based binder formed worse dispersion than those in the PVP-based binder.

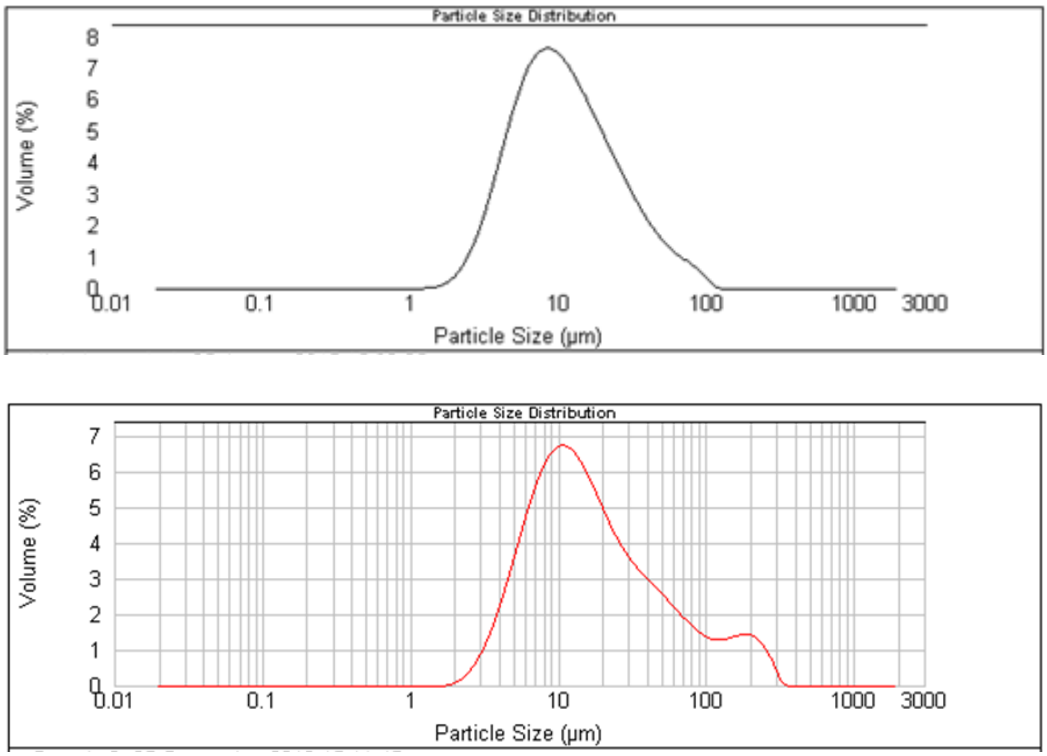

Figure 3.24 Size distributions of nickel particles in the PVP-based ink (top) and the PVP-S-based ink (bottom)

3.3.4.4 Thermal stability of the PVP-based ink and the PVP-S-based ink

Figure 3.25 shows the differences in the thermal stability of the two inks with different polymeric binders, *i.e.* PVP-based and PVP-S-based binders. It can be seen that the extent to which the PVP-S-based binder holds onto water was greater than that shown by the PVP-based binder. This better affinity to water of the PVP-S-binder could help its printed film to have electrical switching behaviour and better conductivity, compared to that of the PVP-based printed film. Additionally, the PVP-based binder has a greater affinity for water (see the temperature at the first turning point in Figure 3.25), and it made the film with PVP swell to a greater extent than the PVP-S-based film [42]. "The water molecules are able to penetrate in the free space of the polymer chains [43]". It was reported that the water molecules in a polymer could significantly reduce the breakdown of the electric field [44]. This explains the better conductivity of PVP-S-based films compared to PVP-based films.

The overall thermal stability of the two binders is similar. In the TGA profiles of each ink, each thermogram indicates a profile that can be correlated to a loss of water as the heating temperature was increased up to 125 °C and 150 °C for the PVP3 ink and for the PVP-S3 ink, respectively. This is then followed by decomposition reactions that take place up to 400 °C.

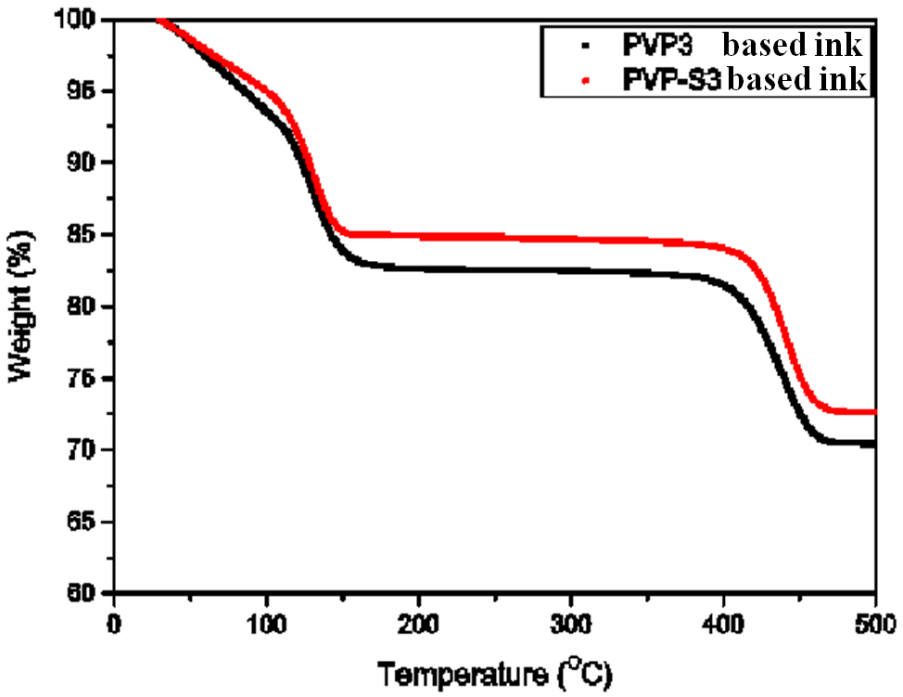

Figure 3.25 TGA, 10°C/min plots of the PVP3 ink and the PVP-S3 ink

3.3.4.5 Mechanical properties of the PVP3 printed film and the PVP-S3 printed film

The modulus of elasticity is a significant parameter to investigate the compression of a printed film. The protocol for the measurement of the elastic modulus was detailed in Chapter 2. The elastic modulus of the PVP3 printed film and the PVP-S3 printed film is shown in Figure 3.26. The elastic modulus of the unfilled PVP and the unfilled PVP-S films is demonstrated in Figure 3.27. It is seen that the addition of nickel particles increases the elastic modulus in both the PVP and the PVP-S films. The metallic nickel particles, 190 - 220 GPa, are rigid that have higher elastic modulus than the polymers generally [72]. Two dramatic elastic modulus values arise for the PVP3 and the PVP-S3 films. The nickel content of each printed film was similar, thus any significant difference in elastic modulus would be due to the differences between the binding polymers. The PVP polymer has a dramatically

lower elastic modulus value than the PVP-S polymer. This is because of the larger molecular weight of the PVP polymer, *i.e.* 360,000 g/mol [45], with a comparison with that of the PVP-S polymer, *i.e.* 645.87 g/mol. The PVP-S polymer exhibits a much greater elastic modulus. Such a low elastic modulus of the PVP3 film prevented nickel aggregation and electrical conductive behaviour (see Figure 3.19).

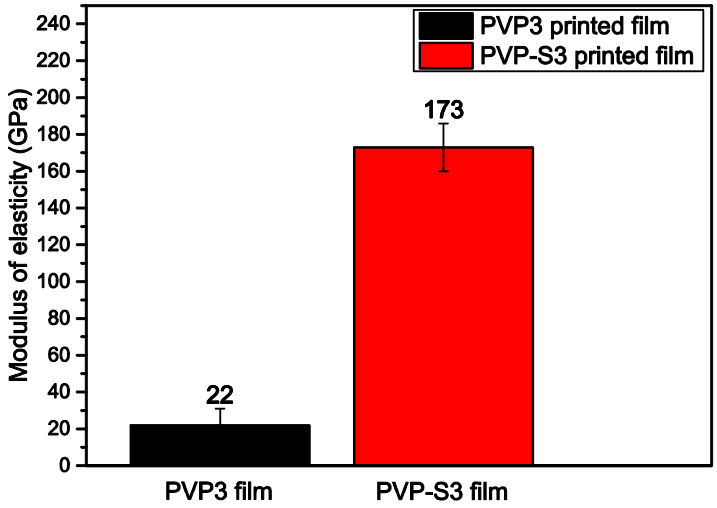

Figure 3.26 Modulus of elasticity for the PVP3 printed film and the PVP-S3 printed film

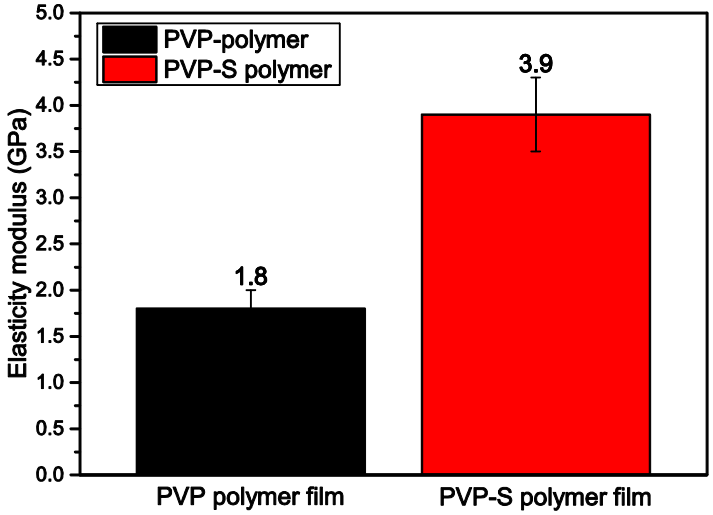

Figure 3.27 Modulus of elasticity for the PVP binder film and the PVP-S binder film

3.3.5 Characterisation of PE1-based printed film and PE2-based printed film

3.3.5.1 Comparison of the effects of PE1-based binder and of PE2-based binders on the electrical-mechanical properties

It is very difficult for many of the polymers, used in inks or coatings to disperse well into water because of the differences of surface tension and polarity. The well-controlled and precise viscosity and pH value of inks can be used to help the polymer dispersion. Figure 3.28 gives a schematic image of the neutralisation of a polymer by base solubilisation. As shown, the acid is formed before the solubilisation, at low pH. The polymers are water-insoluble emulsion polymers owing to the formation of a hydrophobic network. On the addition of a base to neutralise the dispersion, *i.e.* pH > 7, these particles become water-soluble because of the repulsive force between carboxylate poly anions. As a consequence, this efficiently results in an increase of viscosity and thickening properties, as shown in the salt form, Figure 3.28. These linear polymers can use in film application, similar to those concerned in this study. Besides, a thixotropic and pseudoplastic flow of emulsion will be achieved. The hydrophobic groups build up associations with other hydrophobic polymers in the formulation, such as those present in surfactants and dyes. However, when the pH > 9.5, the emulsion viscosity will be reduced and the drying rate will be low. Therefore, the pH applications for acrylic copolymers range from 8 to 9 [47-51].

The detailed composition of the two water-based polymeric emulsions, PE1 and PE2, is not known. Both are used in the manufacture of high quality water-based inks and coatings and are mainly comprised of an alkali-soluble acrylic copolymer. The solubility of many carboxylated polymers in aqueous alkaline solution has been made [46, 47, 51, 52]. Several publications have reported that alkali soluble acrylic copolymers containing a large number of carboxyl groups usually form aggregations of micelles [53], similar to those of polymeric surfactants, due to the intermolecular and/or intramolecular hydrophobic interactions [54-57]. Figure 3.29 represents the schematic diagram of a micelle structure of acrylic copolymer adsorbing on the nickel particle.

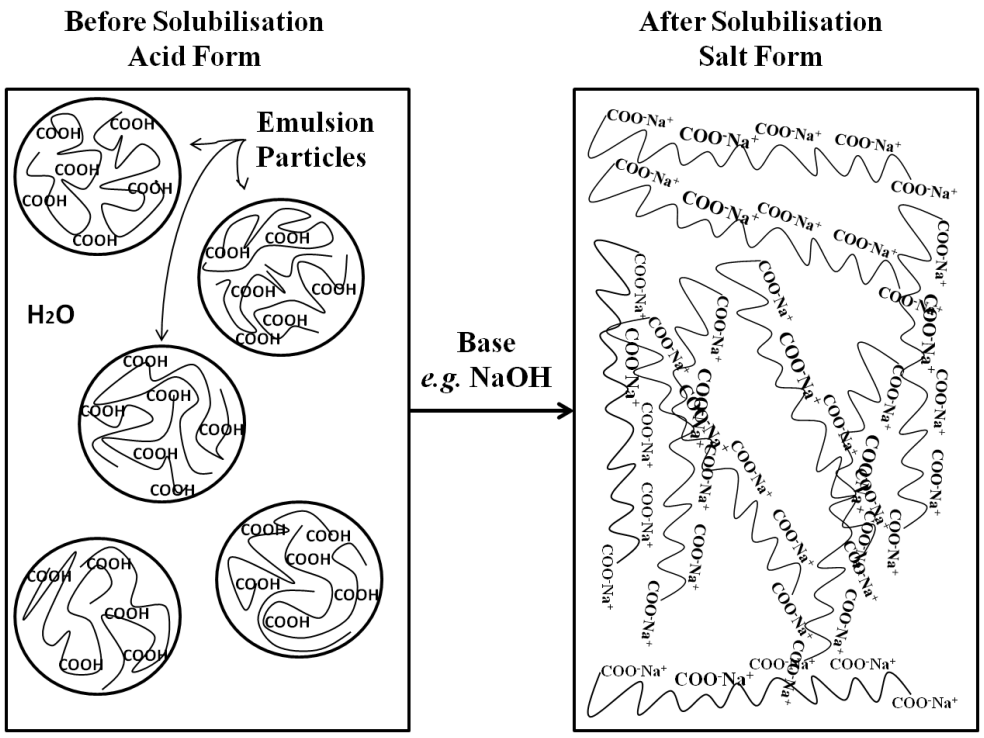

Figure 3.28 Schematic image of polymer neutralisation by base solubilisation [48]

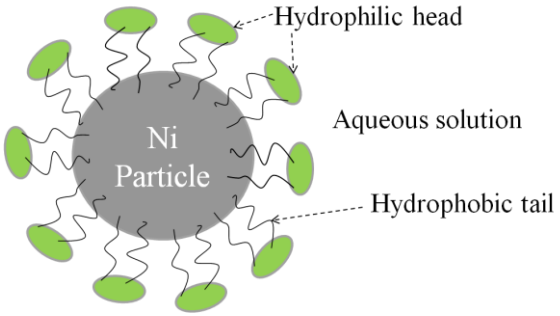

Figure 3.29 Schematic representation of a nickel particle surrounded by an adsorbed alkali soluble acrylic copolymer [54-57]Table 3-6 gives the nickel content of the PE1-based printed film and the PE2-based printed film at different ink formulations. The PE1-1 and PE2-3 printed films have similar nickel contents, *i.e.* 90 wt%. Therefore, the results arising from the use of similar nickel contents, of PE1 and PE2-based printed films (*i.e.* PE1-1 and PE2-3, PE1-2 and PE2-4 and PE1-4 and PE2-6) has been plotted in the same graph, as shown in Figure 3.30.

Table 3-6 Solid content of PE1 and PE2-based samples at different nickel loadings

	PE1-based	*PE2-based*
Solid content of binder itself	*45.5%*	*23.9%*
Solid content of ink with 80 wt% Ni and 20 wt% binder	*90% (PE1-1)*	*94% (PE2-1)*
Solid content of ink with 75 wt% Ni and 25 wt% binder	*87% (PE1-2)*	*93% (PE2-2)*
Solid content of ink with 70 wt% Ni and 30 wt% binder	*84% (PE1-3)*	*91% (PE2-3)*
Solid content of ink with 60 wt% Ni and 40 wt% binder	*77% (PE1-4)*	*86% (PE2-4)*
Solid content of ink with 50 wt% Ni and 50 wt% binder	*69% (PE1-5)*	*81% (PE2-5)*
Solid content of ink with 40 wt% Ni and 60 wt% binder	*60% (PE1-6)*	*74% (PE2-6)*

As expected, the low resistance values of the printed films decrease with an increase in nickel content. These printed films are also very sensitive to external forces in their response. When the applied external compression was over 1 N, the resistances of all of the printed films decreased slowly to their lowest value. The rapid reduction in the resistance at stress values that were less than 1 N, gave quantum tunnelling mechanism and percolation tunnelling mechanism [12].

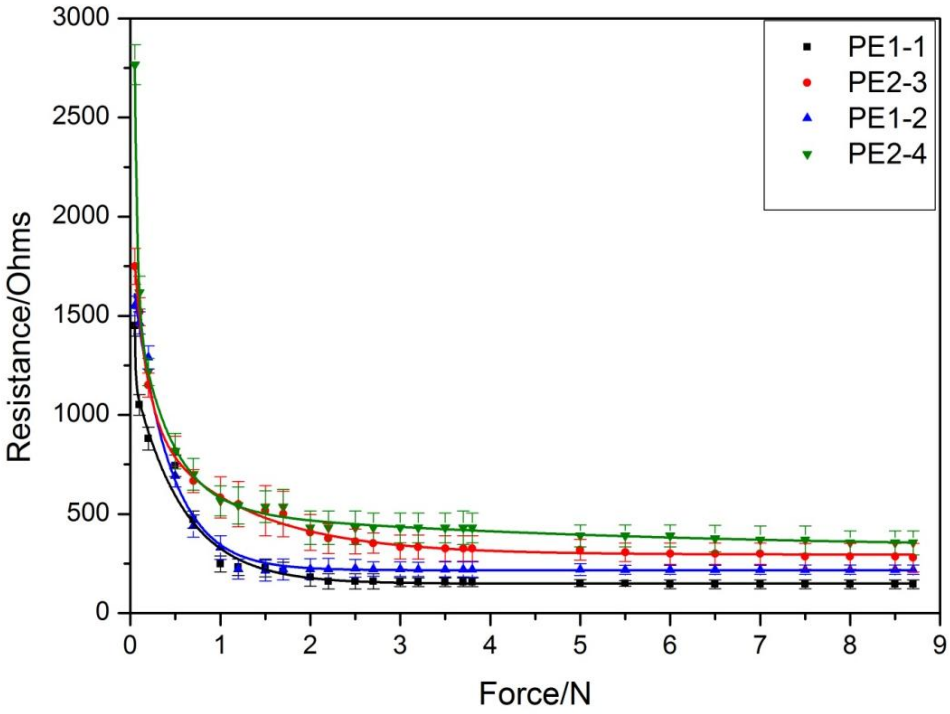

Figure 3.30 Comparison of the electrical resistance on the external uniaxial force for PE1 and PE2-based printed samples with nickel content ranges from 70 wt% to 80 wt%

The reason that samples with the same nickel content of PE1-based printed film and PE2-based printed film gives differently in resistance values (horizontal lines of Figure 3.30) is because of the chain lengths of PE1 and PE2-based alkali acrylic copolymers. Alkali soluble acrylic copolymers and nickel particles form a micellar structure, as displayed in Figure 3.29. The chain lengths of PE2 acrylic copolymer are longer than those of PE1 copolymer, which results in keeping each Ni-PE2 micelle further apart. Similarly, nickel particles in each Ni-PE1 micelle were much closer to each other, as demonstrated in Figure 3.31. As a consequence, a greater electric field of nickel particles in PE1-based printed films can be built up, so a lower resistance value of PE1-based printed film is achieved, when the same external force is applied.

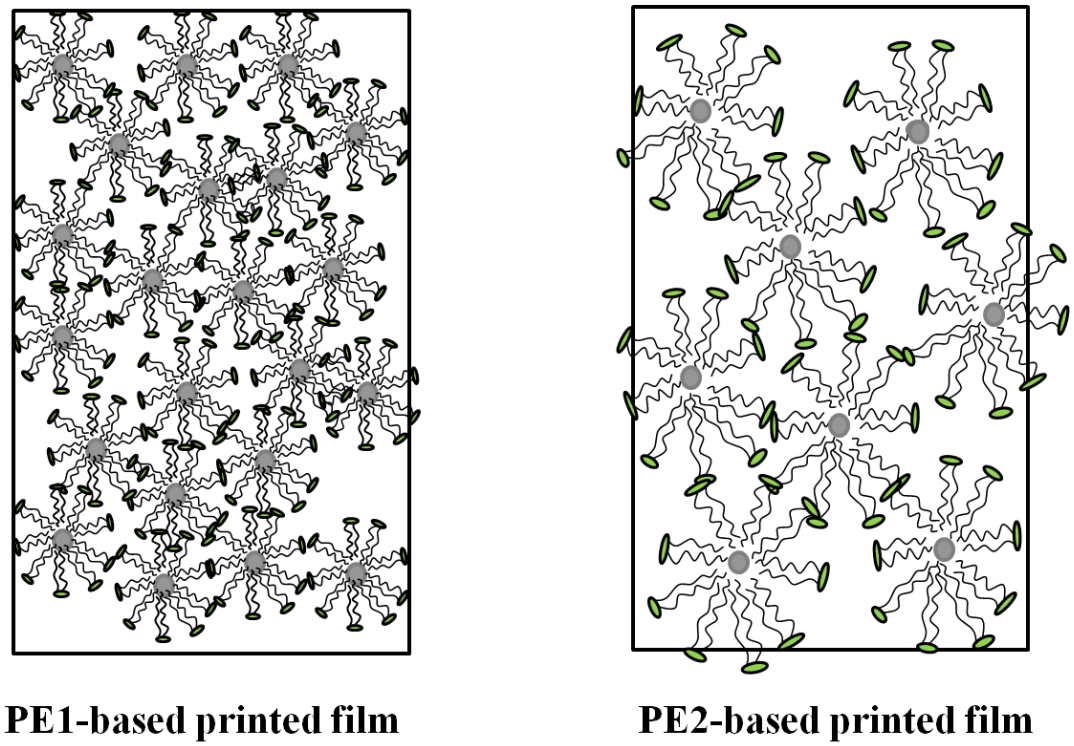

Figure 3.31 Schematic diagrams of micellar Ni-polymeric assemblies of the PE1-based printed film and the PE2-based printed film [53]

3.3.5.2 Morphologies of the PE1-based printed film and the PE2-based printed film

Figure 3.32 and Figure 3.33 demonstrate the morphologies of the respective surfaces at ×2000 and cross-sections at ×750 magnifications of the PE1-based and the PE2-based alkali soluble acrylic copolymer printed films. These films displayed a high density of nickel particles. These near-spherical particles can be identified as nickel as they correspond with the SEM image of pure nickel powder, as shown in Figure 3.1. The near-spherical nickel particles are widely dispersed across the surfaces in the Ni-PE1-3 printed films and Ni-PE2-4 printed films, which have similar nickel proportions of approximately 85 w% in their solid states. In both of the acrylic copolymer based printed films, the polymer is designed to coat the nickel particles, preventing them from coming into direct physical contact. As a consequence, a high resistance of composites should be achieved when the volume fraction of nickel particles is below the percolation threshold. Some nickel particles tend to form clusters, especially in the PE1-based printed film, as shown in Figure 3.32. This is

because the chain lengths of PE1-based polymer are shorter than those of PE2-based polymers, as demonstrated in schematic image in Figure 3.31. Therefore, the nickel particles are better dispersed and separated in a continuous PE2-based polymer compared to the PE1-based printed film in which there are a number of voids. These voids could effectively bring the nickel particles closer to each other under an external compression, which resulted in more electrical switching and more conductive PE1-based printed film (see Figure 3.29). However, the continuous PE2-based polymer matrix could prevent the nickel particles from contacting each other due to the presence of less voids of the PE2-3 printed film. Also, there is a larger number of spiky tips on the nickel particles exposing to the surface of the PE1-3 film than that of the PE2-3 film, which led to higher electrical field was generated in the PE1-3 film. This is another reason to explain the electrical switching behaviour of the PE1-based films and the electrical sensing behaviour of the PE2-based films. The PE2-4 printed film shown in Figure 3.33 only has a few cracks across the surface. The nickel particles in the PE1-based binder were barely able to form a continuous and smooth film surface. Some of the direct physical contact of nickel particles results in lower resistance or better conductivity of the PE1-based printed film under external forces when the volume fraction of nickel particles is above the percolation threshold. This is why the electrical sensitivity of the PE1-based printed films has been shown to be greater than that of the PE2-based printed films at similar nickel loading, as demonstrated in Figure 3.30. The thicknesses of the PE1-3 and the PE2-4 printed films are similar in the range of 40 µm to 50 µm.

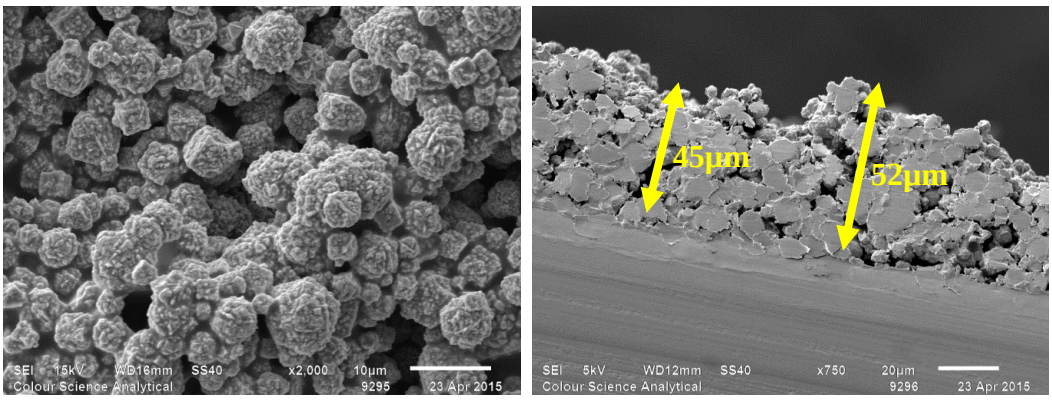

Figure 3.32 SEM images of PE1-3 film's surface at × 2000 (left) and cross-section (right) at × 750 magnifications

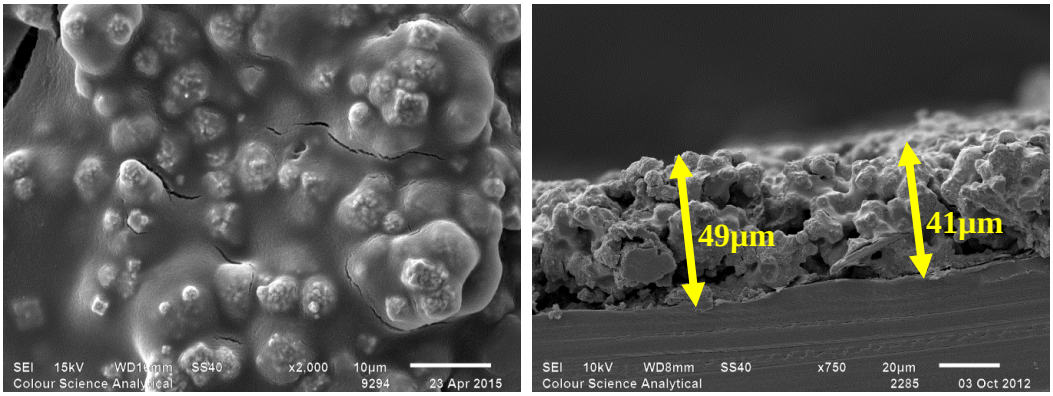

Figure 3.33 SEM images of PE2-4 film's surface at × 2000 (left) and cross-section (right) at × 750 magnifications

3.3.5.3 Particle size distribution of the PE1-based and the PE2-based ink

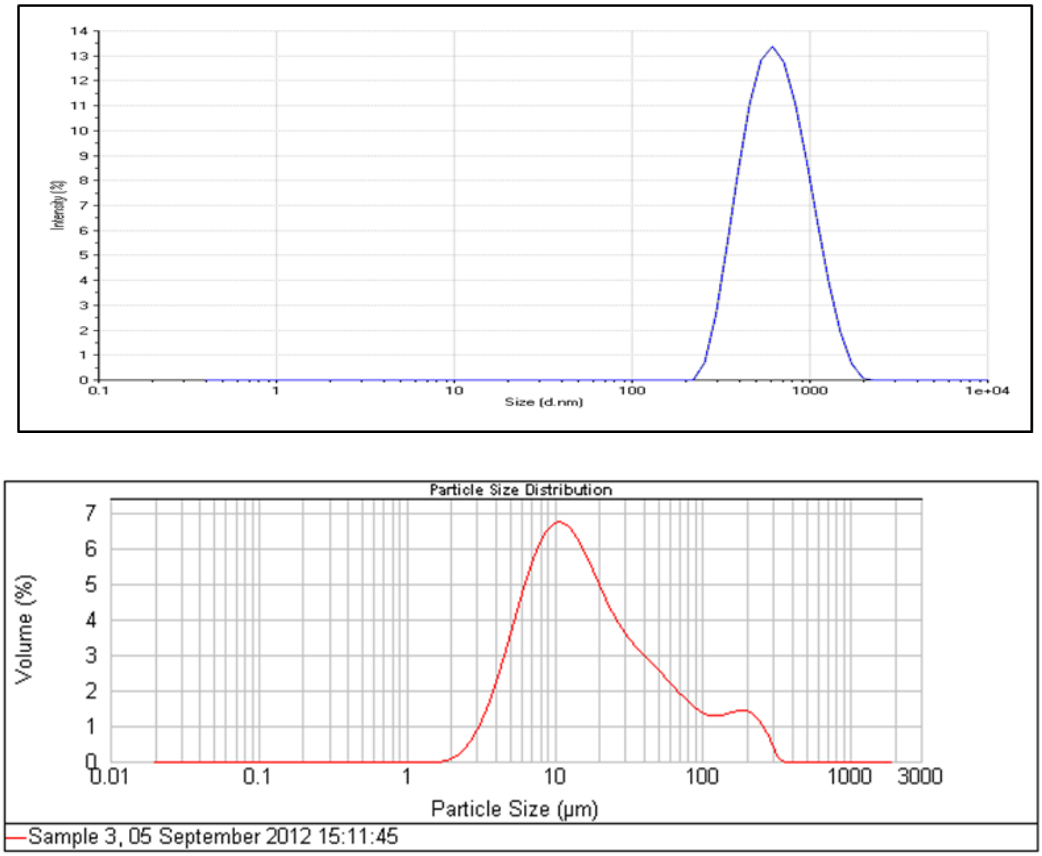

Figure 3.34 Size distribution graphs of nickel particles dispersed in the PE1-based binder (top) and the PE2-based binder (bottom)

Figure 3.34 displays particle size distributions of nickel particles dispersing in the PE1-3 ink and the PE2-4-based ink. It is indicated that nickel particles aggregate to form larger sizes and a greater number of irregular particle clusters in the PE1-based binder than those in the PE2-based binder. The average size of the nickel aggregates is approximately 600 μm in the PE1-based binder, which is around 60 times greater than that of the pure nickel particles (see Figure 3.4). Nickel particles dispersed in the PE2-based binder formed a small distribution of large aggregates from 100 μm to 300 μm. These size distribution graphs of the nickel particles in the PE1-based binder and the PE2-based binder match those obtained for morphologies of the PE-based printed samples (see Figure 3.32 and Figure 3.33).

3.3.5.4 Thermal stability of the PE1-based and the PE2-based inks

Figure 3.35 shows the differences in thermal stability between two inks with different polymeric binders, *i.e.* PE1-based and PE2-based binders. It can be seen that the extent to which the PE1-based binder holds onto water was slightly greater than that shown by the PE2-based binder. This better affinity to water of the PE1-binder could help its printed film to have electrical switching behaviour and better conductivity compared to that of the PE2-based printed film. Additionally, the greater affinity for water for the PE1-based binder could make the film swell to a greater extent than PE2-based film [42]. "The water molecules are able to penetrate in the free space of the polymer chains" [43]. It was reported that the water molecules in a polymer could significantly reduce the breakdown of the electric field [44]. This explains the better conductivity of PE1-based films.

The overall thermal stability of the two binders is similar, in the TGA profiles of each ink, and each thermogram indicates a curve which can be correlated to loss of water as the heating temperature was increased to 140 °C and 150 °C for the PE1-3 ink and for the PE2-3 ink, respectively. This is then followed by any decomposition reactions that take place around 350 °C.

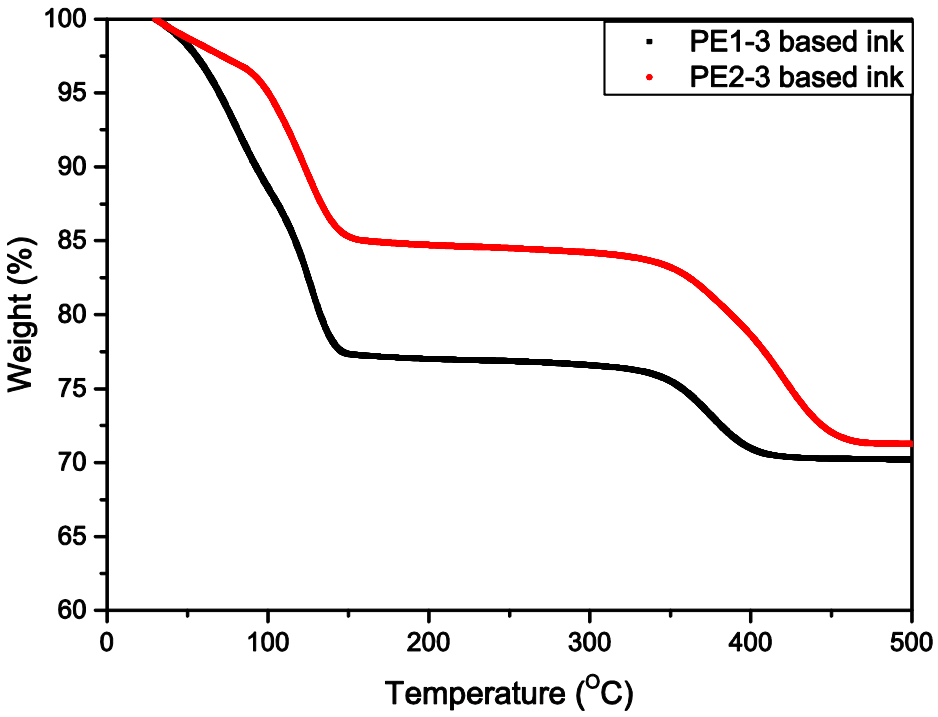

Figure 3.35 TGA plots of the PE1-3 ink and the PE2-3 ink with heating rate of 10 °C/min

3.3.5.5 Mechanical properties for the PE1-3 and the PE2-3 printed films

Modulus of elasticity is a significant parameter in investigating the compression of the PE1-based and the PE2-based printed film, as shown in Figure 3.36. Two dramatic elastic modulus values can be seen in the PE1-3 and the PE2-3 films. The nickel content in each printed film was similar, thus such significant difference in elastic modulus was due to the distinction of the binding polymers. It was known that the PE2-based polymer had a longer chain length than the PE1-based polymer. In general, longer polymer chains can get tangled and combined with each other which results in low elastic modulus, however, shorter polymer chains can lose the ductility which results in high stiffness. Therefore, the PE2-based printed film exhibited much lower elastic modulus than the PE1-based printed film. Such a low elastic modulus of PE2-based film prevented nickel aggregation and electrically conductive behaviour (see 3.3.5.1).

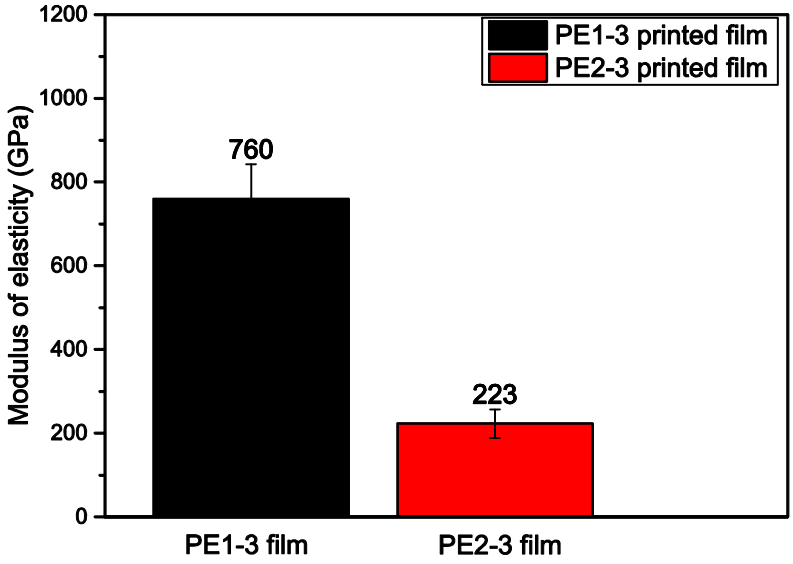

Figure 3.36 Elasticity modulus for the PE1-3 and PE2-3 printed films

3.3.6 Zeta potential measurements of nickel particles dispersed in a range of water-based binder components

It is important to examine the stability of nickel particles in different polymeric binders, which significantly affects the conductivity of the printed films. Zeta potential values can be used to evaluate the stability of nickel particles in different polymer-based binders. It is a measurement for the charge repulsion or attraction between particles [58]. The polymer coating does not only prevent the nickel particles from aggregation, but it can also affect the size and dispersity of the particles [20, 60]. Generally, it was reported that the greater the absolute zeta potential measurement, the higher stability of particles in the solution [59].

Table 3-7 shows the zeta potential analyses results and conductivity values for nickel particles (70 wt%) dispersed in each of the PVP, the PVP-S, the PE1 and the PE2-based binders (30 wt%). It is shown that the conductivity values for nickel particles dispersed in water-based binders are similar within the difference of 0.027 mS/cm. This is because of the fact that the carriers and pigments of the inks, water and nickel powder, respectively, made the majority contribution of electron movements and transportations.

Zeta potential measurements for nickel particles in the PE1-based binder and the PE2-based binder are -22.3+5.1 mV and -27.8+5.67 mV, respectively. It

indicates that the nickel particles in the PE2-based binder are more stable than those in the PE1-based binder as the more negative zeta potential value achieved by the Ni-PE2-based ink. These zeta potential results can therefore explain the more electrically sensing behaviour of the Ni-PE2-based printed film (Figure 3.44) and the more electrically switching behaviour of the Ni-PE1-based printed film (Figure 3.43).

Similarly, for the PVP-based ink and the PVP-S-based ink, the nickel particles in the PVP-based binder were slightly more stable with a comparison to those in the PVP-S-based binder. This explains the electrically sensing behaviour of the PVP-based printed films and the electrically switching behaviour of the PVP-S-based printed films (see Figure 3.11).

Table 3-7 Zeta potential and conductivity values for nickel particles dispersed in PVP, PVP-S, PE1 and PE2-based binders

Samples	*Zeta potential (mV)*	*Conductivity (mS/cm)*
Ni powder dispersed in PVP	*-3.35 + 3.73*	*0.357*
Ni powder dispersed in PVP-S	*-0.942 + 4.24*	*0.351*
Ni powder dispersed in PE1	*-22.3 + 5.1*	*0.378*
Ni powder dispersed in PE2	*-27.8 + 5.67*	*0.369*

3.3.7 Fourier Transform Infrared Spectrometer (FTIR) analysis for the water-based polymeric binders and ink in the solid state

Figure 3.37 is an FTIR spectra used to detect the possible interactions between the PVP and nickel particles in the solid state. The pure PVP and the Ni-PVP composites are characterised by a Bruker Platinum-ATR spectrometer in the range of 400 to 4000 cm^{-1}. Both FTIR samples of the pure PVP and the Ni-PVP composites are prepared and dried overnight, in order to evaporate the water from the inks. Then the ink films were ground prior to being employed on the crystal area of Platinum-ATR.

For the FTIR spectra of the PVP and the PVP3 films in Figure 3.37, characteristic bands can be seen at 2955 cm^{-1} (C-H stretch) and 1654 cm^{-1} (C=O). In

addition, there is a broad band displayed at 3435 cm^{-1}, which was in similar literature a study is reported as the presence of water [61-63]. Due to no obvious differences and the same pattern of band appearance in the FTIR spectra of the PVP film and the PVP3 film, it can be concluded that there was no new bond forming between the PVP polymer and the nickel particle [40, 61, 64]. This result suggests no chemical interaction between the PVP polymer and the nickel particles. The PVP polymer was acting as a polymer matrix physically binding with nickel particles. If any interaction or cross-linking occurs, the functional groups in the FTIR spectra would then demonstrate band shifts or broadening in terms of the FTIR spectrum of the pure PVP polymer.

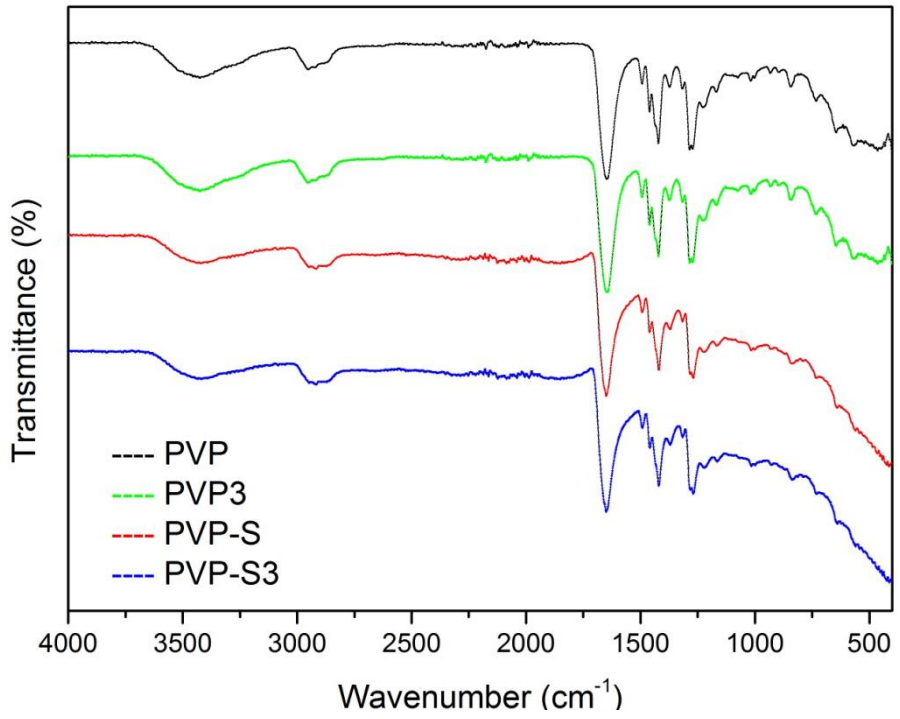

Figure 3.37 FTIR analysis for PVP and PVP-S-based polymers and prints

Figure 3.21 shows structures of the PVP and the PVP-S polymers, and the difference between them is the styrene moiety in PVP-S. Figure 3.37 demonstrates the FTIR spectra of the PVP-S and the Ni-PVP-S composites [65-67]. The FTIR spectra of the PVP-S and the Ni-PVP-S composites do not have any differences in band signals; this denotes that there is no new bond forming between the PVP-S polymer and the nickel particles, suggesting no chemical interaction between them.

The function of the PVP-S polymer is to work as a polymer matrix physically binding with nickel particles. If any interaction or cross-linking occurs, the functional groups in the FTIR spectra would then show band shifts or broadening in terms of the FTIR spectrum of the pure PVP-S polymer.

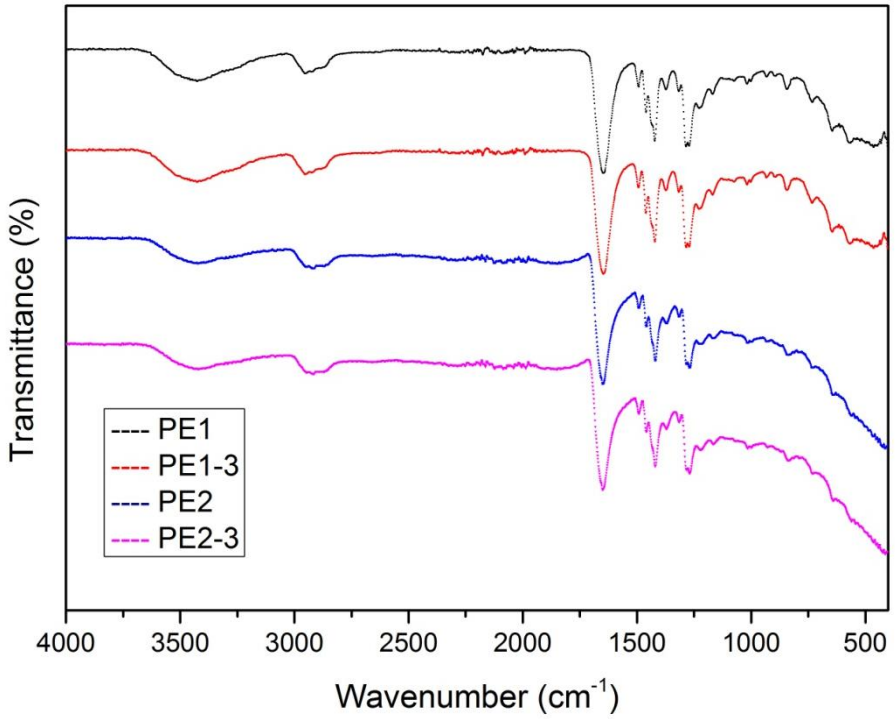

Figure 3.38 FTIR analysis for PE1 and PE2-based polymers and prints

The FTIR spectra in Figure 3.38 are used to detect possible interaction between the PE1/PE2 and the nickel particles in the solid state. There were no obvious differences and as there is also the same bands appeared in the FTIR spectra of the PE1 polymer and the PE1-3 printed film. This denotes that there is no new bond forming between the PE1 polymer and the nickel particles [61-63].

The FTIR spectra of the pure PE2 polymer and the PE2-3 printed film in Figure 3.38 have shown the same relationship as the PE1 polymer and the nickel particles. There is no new bond forming or interaction between the PE2 polymer and the nickel particles. The PE2 polymer is behaving as a polymer matrix binding with nickel particles physically [38-40].

3.3.8 Contact angle measurements

Contact angle studies were carried out to investigate the adhesion and wettability properties of the PVP, PVP-S, PE1 and PE2 based inks on the carbon contacts of PET substrates. The compositions of inks are the same, *i.e.* 70 wt% of nickel power and 30 wt% of polymeric emulsions. Due to the stated large molecular weight of PVP, *i.e.* 360,000 g/mol, the polymeric binder was too viscous to allow for the measurement of the contact angle. Therefore, all of the four water-based binders were diluted to 50 wt%. Then one drop of each binder was applied in a non-sessile manner, from a 5mL syringe onto the PET sheet, mounted on a Contact-θ-meter. Figure 3.39 demonstrates the contact angle values for each water-based binder. The alkali soluble acrylic copolymer based binders, PE1 and PE2, immediately displayed the contact angle values of 64 ° and 50 ° respectively. However, the PVP and the PVP-S gave contact angle values > 90 °, the limit of the instrument. The PVP-S-based ink showed, a contact angle value of 75 ° after 10 minutes, which means that the ink was spread, adsorbed and wetted the substrate over time. The PVP-based ink did not spread at all. The PVP-based inks did not wet onto nor adhere to the PET sheet. It is already an established fact that the wetting of the acrylic copolymers is better than those of the PVP-based ink and the PVP-S-based ink on PET sheets [68].

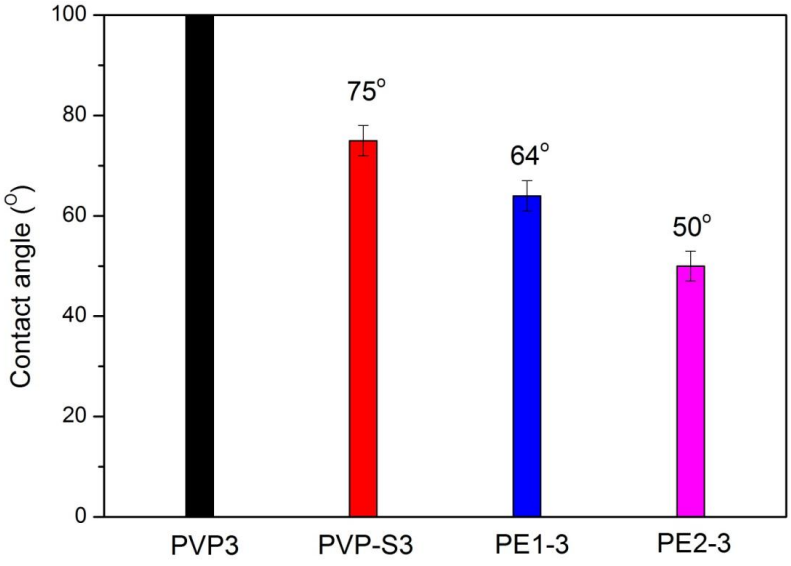

Figure 3.39 The contact angles of the PVP, the PVP-S, the PE1 and the PE2-based inks on carbon contacts of PET sheets

3.3.9 Conclusion

In summary, a series of potential screen printable inks and possibly functional pressure-sensitive switches and sensors, consisting of electrical insulating water-based binder and electrical conductive nickel particles, has been developed.

The electrical resistance of the printed films changed exponentially with increasing applied force. With an increase in external uniaxial force, it is shown that the resistance decreased rapidly when increasing the amount of nickel powder, due to the fact that the volume fraction of nickel content being close to the percolation threshold. In this case, printed films with a high loading of the nickel powder could be used as electrical switches. When the volume fraction of the nickel was above the percolation threshold, the resistance of the printed films became electrically conductive and constant, following the Ohmic law. The lowest resistance values of the printed films under high external compression decreased with increase in the nickel loading in the ink.

As seen from the morphologies of surfaces and cross-sections of printed films, it can be concluded that the use of a polymeric matrix based on a large molecular weight and a high viscosity was able to produce continuous and uniform printed film which was devoid of cracks. However, this binding polymer would not be suitable for the fabrication of QTC inks, since their use would result in higher resistivity values, *i.e.* PVP-based printed films. The nickel aggregates aided the conductivity of the printed films. The polymeric binders had a significant effect on the rheological properties and the electrical properties of the inks. The thermal stability studies of each of the water-based inks showed the affinity of the water molecules. This played an important role on the electrical properties of the films. The mechanical properties also influenced the electrical properties of the various printed films.

The TGA analysis between the polymeric binder and the ink has confirmed that the nickel particles are physically binding and have no chemical reaction with the polymer in the Ni-polymer composite. FTIR spectra of the polymeric binder and ink in the solid state have also confirmed that there is no new chemical bond forming between core particle (nickel) and the coating polymer. Nickel particles are

physically binding with the polymer matrix. The polymer therefore is acting as an insulating binding matrix for the spherically irregular nickel particles.

The electrical resistance of PVP-based printed films were much greater than that of other films. Furthermore, the PVP-based ink did not adhere nor wet, the PET sheet well.

3.4 Optimising the response of the electrical properties to the external forces for printed films with adding TiO_2

TiO_2 is one of the more widely used pigments in the coatings and paints industries due to its high refractive index (*i.e.* brightness and opacity). The physical properties of TiO_2 determine its use in the different applications, such as in fibres, in textiles, in architectural paints, in coatings, in plasters and in packagings. TiO_2 exists in natural minerals as three forms, *i.e*. rutile, anatase and brookite. TiO_2 has been employed in a vast range of applications, such as toothpaste, paints, plastics, coatings, fillers, papers, inks, solar cell [69, 70], photocatalysis [71], food and medicines.

3.4.1 Characteristics of the introduction of the three different grades of TiO_2 in the QTC ink formulations

Three different grades of TiO_2 were used in this research in an investigation of the charge storage phenomena, as illustrated in Section1.4.3. This is because these grades of TiO_2 cannot build up as many electrical field sites as can the nickel particles, as the number of TiO_2 tips per particle is essentially reduced to none. In such a circumstance, the TiO_2 in the bulk material creates extra conduction paths and deflect the electric charge (Section 1.4.3). Therefore, these TiO_2 could be used to control the electrical sensitivity of the printed films.

The three grades of TiO_2 that were used in this study were chosen on the basis of differences in the specific surface areas that influenced printed films on the electrical properties. The appropriate differences in the surface treatments, TiO_2 contents, densities, specific surface areas and refractive index of the three grades of TiO_2 are given in Table 3-8. The specific surface area values of the three grades of TiO_2 were measured by the laser diffraction particle sizing technique.

Table 3-8 Three grades of TiO_2 used in the research

Commercial Name	*Kronos TiO_2 [1080]*	*Kronos TiO_2 [2190]*	*Kronos TiO_2 [2300]*
Supplier	Kronos Titan GmbH	Kronos Titan GmbH	Kronos Titan GmbH
Pigment Type	Anatase Pigment	Rutile Pigment	Rutile Pigment
Surface Treatment	Sb (very low amount)	Al (1.55%)	Al (2.57%)
TiO_2 Content	> 98%	> 94%	> 94.5%
Density (g/cm^3)	3.8	4.1	4.1
Refractive Index	67	103	101
Specific Surface Area (m^2/g)	25.3	6.78	8.41
Average particle Size (nm)	146	128	134
Sample Name Code	a	b	c

3.4.1.1 Scanning electron microscopic evaluations of the three grades of TiO_2

SEM images of the TiO_2 species used are shown in Figure 3.40. The diameter of these species ranges from 170 nm to 300 nm. The particles in the three grades of TiO_2 were all roughly spherical in shape. Also, it can be seen that some anomalous aggregates of the TiO_2 are present on the surface. The diameters of the particles for the three grades of TiO_2 are similar, being approximately 0.2 μm. The average particle size of nickel powder was 10 μm in average (see Figure 3.4), which is nearly 50 times bigger than that of the individual species of TiO_2.

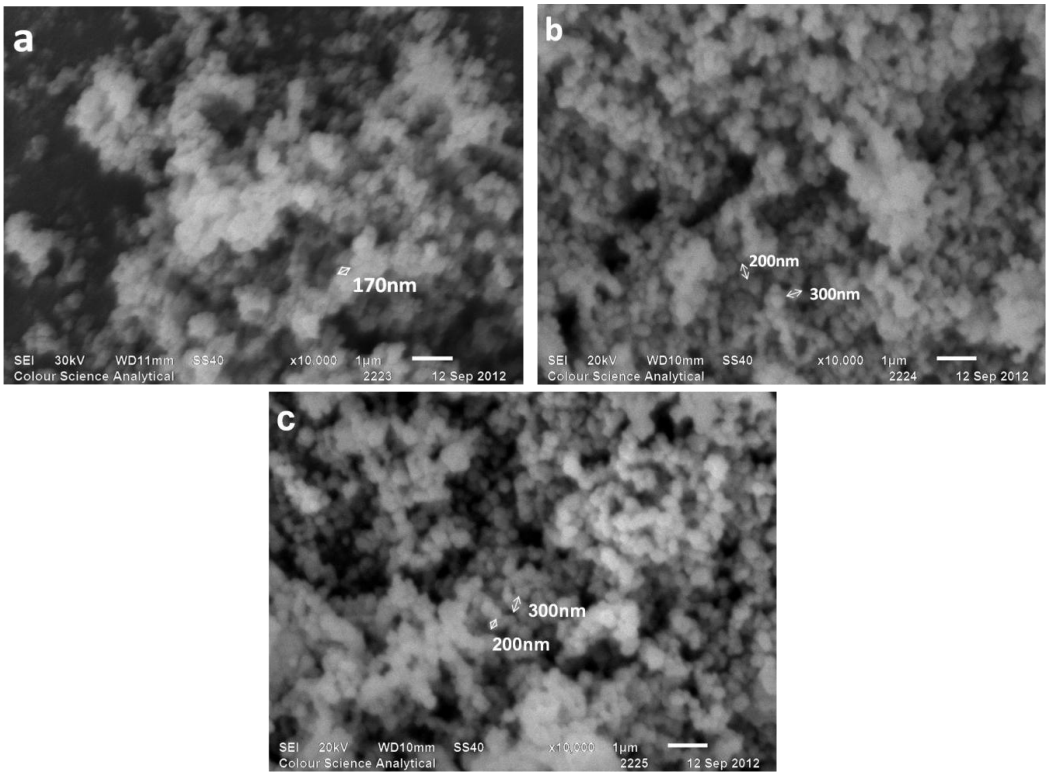

Figure 3.40 Scanning electron micrographs of the three commercial grades of TiO_2 powder, TiO_2(a), TiO_2(b) and TiO_2(c) (samples as supplied)

The specific surface area of the nickel particle is 0.872 m^2/g that measured by the laser diffraction particle sizing technique. This specific surface area is much smaller than that of the TiO_2 (see Table 3-8). This is because the specific surface area is increased as reducing the particle size [157]. The specific surface area will be also increased if the particles have pores. Specific surface area is usually used to evaluate the activity and adsorption capacity of a material.

3.4.1.2 FTIR spectra for the three different grades of TiO_2

FTIR spectra were obtained from the three different grades of TiO_2 and shown in Figure 3.41. The broad absorption peaks around 470 cm^{-1} for TiO_2b and TiO_2c arises from the stretching of Ti-O-Ti bonding of the rutile phase [72]. The FTIR spectrum for anatase phase TiO_2a did not show this significant absorption peak.

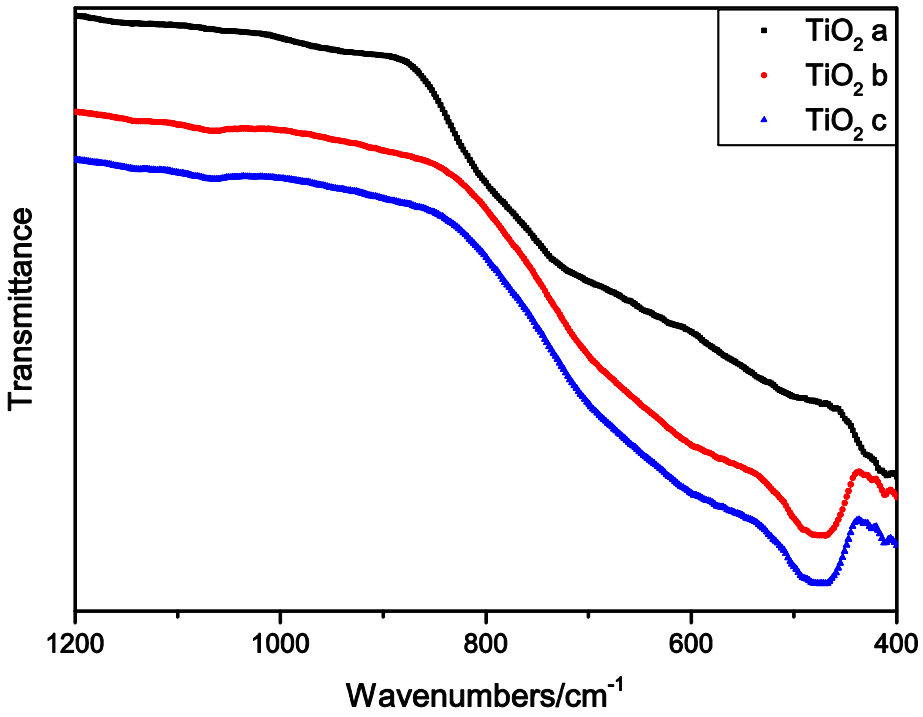

Figure 3.41 FTIR spectra for TiO_2a, TiO_2b and TiO_2c nanoparticles

3.4.2 Ink formulations for optimising the electrical properties response to the external forces for the printed films

In Section 3.3.3, response of the electrical properties to the external forces from the PVP-S, the PE1 and the PE2-based printed films was discussed, demonstrating that the lower resistances of printed films (with less than 70 wt% of the nickel powder), for the PVP-S, the PE1 and the PE2-based printed films, were greater than those of the printed films (with more than 70 wt% of nickel loading), under the external applied forces. The printed films with a high nickel powder loading (*i.e.* > 70 wt%) gave greater conductivity, but did not have the electrical insulating performances required of QTC materials. Consequently, focus was placed on those ink formulations with 70 wt% of the nickel loading to modify and optimise the sensitivity of the printed films. The addition of semiconducting TiO_2 particles into the ink formulations has been reported to have a significant influence on the sensitivity due to their small particle sizes and their large specific surface areas [25]. Table 3-9 gives a route to the composition of each ink formulation, which can be achieved by combination of Table 3-8 and Table 3-9.

Table 3-9 names each ink formulation. Ink sample codes for the inks consisting of nickel powder (70 wt%), water-based binders and TiO_2

	70% Ni 2.5% TiO_2 27.5% binder medium	*70% Ni 5% TiO_2 25% binder medium*	*70% Ni 7.5% TiO_2 27.5% binder medium*	*70% Ni 10% TiO_2 20% binder medium*	*70% Ni 12.5% TiO_2 17.5% binder medium*	*70% Ni 15% TiO_2 15% binder medium*
PVP-S-based	***PVP-S8***	***PVP-S9***	***PVP-S10***	***PVP-S11***	***PVP-S12***	***PVP-S13***
PE1-based	***PE1-8***	***PE1-9***	***PE1-10***	***PE1-11***	***PE1-12***	***PE1-13***
PE2-based	***PE2-8***	***PE2-9***	***PE2-10***	***PE2-11***	***PE2-12***	***PE2-13***

3.4.3 Results and discussion

3.4.3.1 Responses of electrical property to external forces of the printed films containing the anatase phase of TiO_2

Figure 3.42 displays the variation in electrical resistance as a function of the applied compression force for PVP-S-based printed films. These contain 70 wt% of nickel powder and different amounts of TiO_2a. Data relating to the printed film fabricating by the PVP-S3 formulation are also presented in the plot so that one can compare the electrical and mechanical properties of PVP-S-based films that contained TiO_2a. The responses of electrical property to external forces for the PVP-S-based printed film including the two rutile phases of TiO_2, TiO_2b and TiO_2c, is exhibited in the Section 3.4.3.6.

Figure 3.42 is given that the electrical-mechanical properties of PVP-S-based films containing TiO_2 display similar tendency in comparison to that of PVP-S-based films are exclusive with TiO_2. The initial resistance values of the each PVP-S-based printed film were improved by increasing the loading of TiO_2. When the amount of TiO_2a was more than 5 wt% were studied, the initial resistance values

increased towards electrical insulating. This is because as expected the greater of the presence of the semiconducting TiO_2 in the films, the greater ability of preventing the metal filler, the nickel particles, from having physical contacts with each other. This greater ability of TiO_2 could significantly increase the initial resistance of the film was owing to the much smaller particle size and the much larger specific surface area, compared to those of nickel particles.

When the applied compression was more than 0.01 N, the resistance of PVP-S-based printed films reduced gradually. The greater the amount of TiO_2 that was added, the lesser was the reduction of resistance (see the green dash line in Figure 3.42), under the same applied compression. That is to say, the greater the amount of TiO_2 that was added could reduce the electrical sensitivity of the printed films.

For the printed films based on PVP-S8a, PVP-S9a and PVP-S10a, the resistance decreased to the lowest values when the applied compression reached around 1 N. However, for the printed films PVP-S11a, PVP-S12a and PVP-S13a, the resistance was reduced to the lowest value when the applied compression reached around 1.5 N. This change in performance arises from the lesser the TiO_2 that was added into the ink, it was easier for the volume fraction of metal filler to reach to the percolation threshold. When the volume fraction of metal filler is above the percolation threshold, the resistance of PVP-S-based printed films would be expected to become constant with increasing applied compression. Also, the resistance of the printed films was minimal and constant. The current of the printed film was linearity in proportion to the voltage, showing Ohmic behaviour. The distance between each nickel particle becomes less, when the further external compression is applied. As a result, the composite system developed the same as would a metallic component, owing to the physical characteristics of nickel particles (horizontal sections of [a] and [b] in Figure 3.42), the films with TiO_2 had slightly lower resistance values than those without TiO_2. This performance arises probably because TiO_2 acts as a semiconducting synergist that has similar effect on the photocatalytic activity in a carbon nanotube [158] to assist the electrical conductivity of the printed film, as illustrated in 1.4.3. The TiO_2 improved the electron migration and created extra conduction pathway, when a highly external compression was applied.

Figure 3.43 shows the variations of resistance in increasing external applied forces for PE1-based printed films with different proportions of TiO_2a. As a result, the electrical resistance of the printed film changes exponentially with increasing applied force. After the increasing pressure was applied, the printed films changed from insulating behaviour to conductive characteristic. In Figure 3.43, it can be seen that the PE1-based films changed from electrically switching behaviour to more like electrically sensing behaviour with increasing the loading of TiO_2 in the inks.

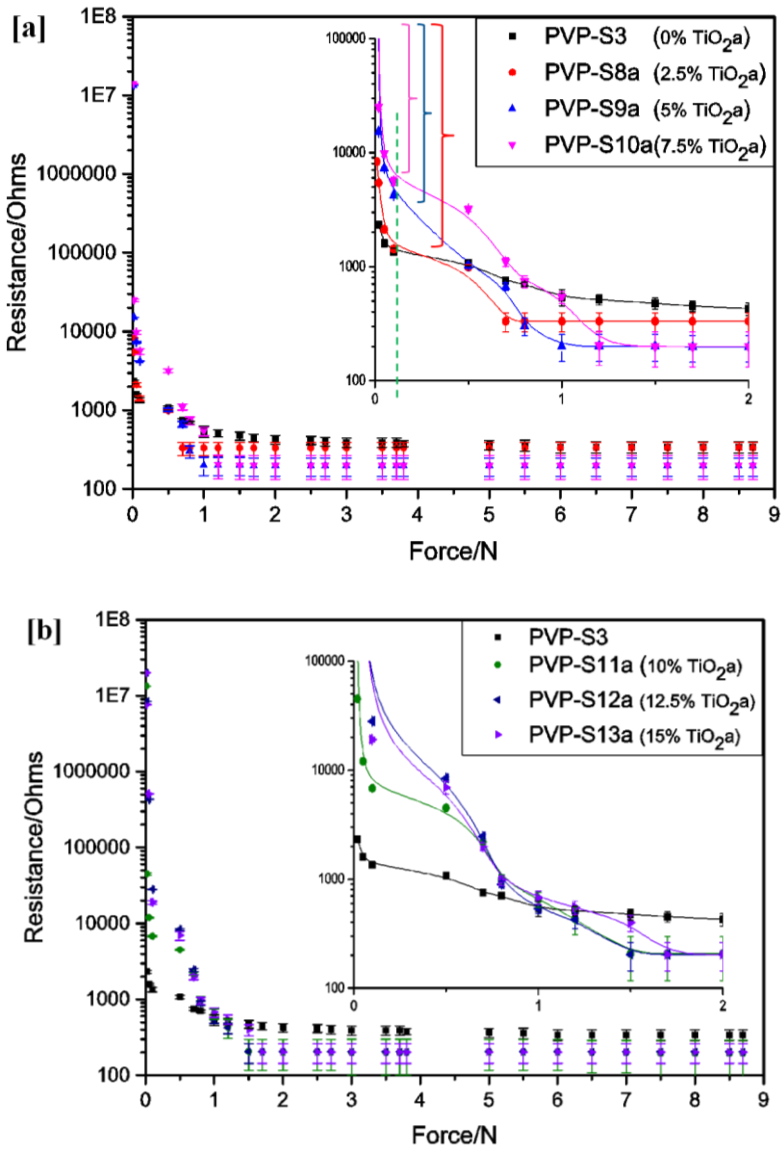

Figure 3.42 Variations of resistance on increasing the external applied force for PVP-S-based printed films, containing different amounts of TiO_2a. Plots [a] and [b] represent inks containing the nickel powder (70 wt%) that have TiO_2 loadings from 0 to 7.5 wt% and from 10 wt% to 15 wt%, respectively

The initial resistance values of the each PE1-based printed film could be greater by increasing the loading of TiO_2. When the PE1-based inks contained more than 10 wt% of TiO_2a, the initial resistance values increased to be electrically insulating. The presences of semiconducting TiO_2 in the printed films greatly assisted with separating the metal filler (nickel particles) from physical and positioned contacts. When more than 0.01 N compressions were applied, the resistances of PE1-based printed film reduced gradually. The more amount of TiO_2 was added, the slower the reduction of resistance was. For PE1-based printed films in Figure 3.43, their resistances decreased to the lowest values when the applied compressions reached around to 1.5 N. In this case, both of percolation and quantum tunnelling procedures were presented at low applied compression. When the volume fraction of nickel powder was in the vicinity of percolation threshold, the resistance of the print was going to be extremely sensitive to the applied compression. With the addition of TiO_2 in the ink formulation, the sensitivity could be reduced. When the volume fraction of metal filler was above the percolation threshold, the resistances of PE1-based printed films became constant and saturated as applied compressions were increased. The distance between each nickel particle was becoming closer, when the further external compression was applied. In a result, the composite system became same as a metallic feature, owing to the physical contacts of nickel particles. When behaving metallic features (horizontal sections Figure 3.43), the prints with TiO_2 have slightly lower resistance values than those without TiO_2. The reason of this performance was assumed that TiO_2 was used as a semiconducting synergist to assist the electrical conductivity of the film. TiO_2 improved electron migration and creates extra conduction paths, when a highly external compression was applied.

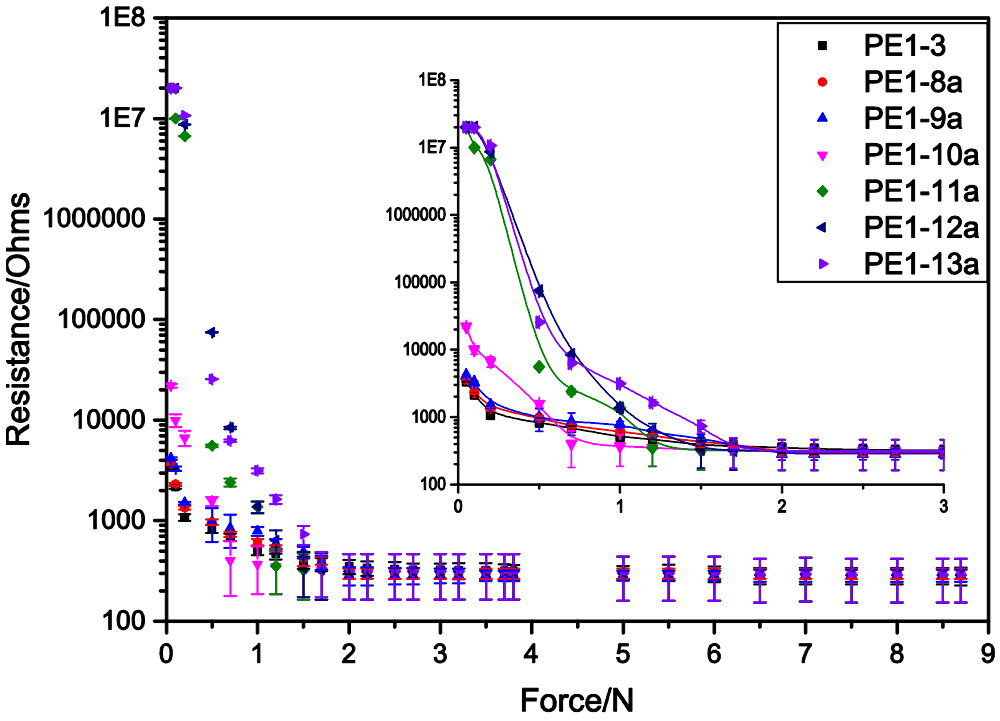

Figure 3.43 Variations of resistance in increasing external applied forces for the PE1-based printed films with different proportions of TiO_2a

Figure 3.44 shows the variations of resistance in increasing external applied forces for PE2-based prints with different proportions of TiO_2a. The electrical resistance of PE2-based printed films showed similar tendency as that of PE1-based films. The electrical resistance of the printed ink changed exponentially with increasing applied force. Increasing the loading of TiO_2 could be used to alter the sensitivity of PE2-based printed films. Generally, with an increase in the loading of TiO_2, PE2-based printed film could change from electrically switching behaviour to electrically sensing behaviour. Also, the use of TiO_2 could be used to optimise the initial resistivity of printed film from electrically conductive to electrically insulating.

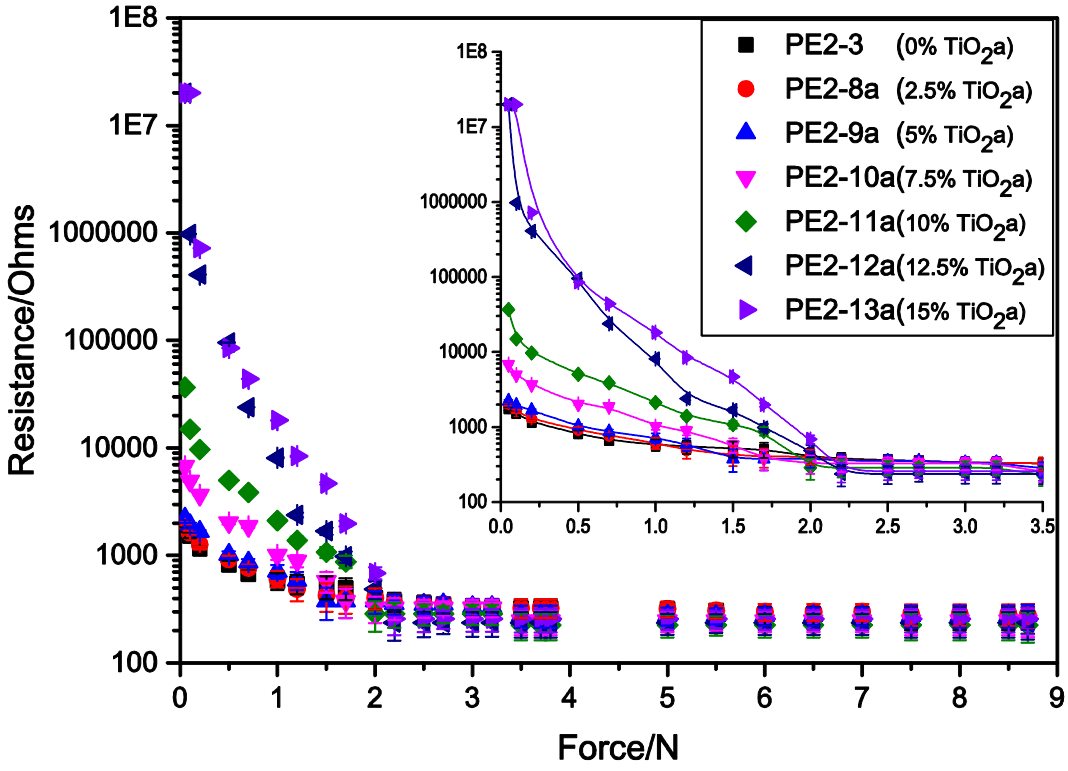

Figure 3.44 Variations of resistance with increasing external applied force for the PE2-based printed films containing different amounts of TiO_2a, but same amount of nickel powder

When the PE2-based inks have the amount of TiO_2a was more than 12.5 wt%, the initial resistance values increased to be electrically insulating. The presences of semiconducting TiO_2 in the printed films assisted with greatly separating the metal filler (nickel particles) from physical and positioned contacts. The more amount of TiO_2 was added, the slower the reduction of resistance was. For PE2-based printed films in Figure 3.44, their resistances decreased to the lowest values when the applied compressions reached around to 2 N. In this case, both of percolation and quantum tunnelling procedures were presented at low applied compression. When the volume fraction of nickel powder was in the vicinity of percolation threshold, the resistance of the printed film was extremely sensitive to the applied compression. With the addition of TiO_2 in the ink formulation, the sensitivity could be reduced. The more TiO_2 was added, the slower resistance was decreased. When the volume fraction of metal filler was above the percolation threshold, the resistances of PE2-based printed films became constant and saturated as applied compressions were increased. In the meantime, the current of the printed

film displayed linearly proportional to the voltage, which acted as Ohmic behaviour. The distance between each nickel particle was becoming closer, when the further external compression was applied. In a result, the composite system became the same as a metallic feature, owing to the physical contacts of nickel particles. When behaving metallic features (horizontal sections Figure 3.44), the printed films with TiO_2 had slightly lower resistance values than those without TiO_2. The reason of this performance was assumed that TiO_2 is used as a semiconducting synergist to assist the electrical conductivity of the printed film. TiO_2 improved the electron migrations and created the extra conduction paths, when a highly external compression was applied.

3.4.3.2 Comparisons of the effects of TiO_2 on the electrical-mechanical properties of the same nickel content of the PE1 and PE2 -based printed films

Table 3-10 gives the nickel contents of the PE1-based films and the PE2-based printed films, in which PE1-8a and PE2-11a, PE1-9a and PE2-13a had similar metal contents that were focussed to investigate the effects of TiO_2 on the electrical-mechanical property. Figure 3.45 shows the resistance-force profiles for the PE1-based films and the PE2-based printed films. Comparing the data with those relating to the PE1 and the PE2-based printed films, (without TiO_2 (see Figure 3.30)), there was no significant change in the resistance-force profiles of the films. As expected, the resistance decreased with increasing applied compressions. The lowest resistance was obtained from PE1 and PE2-based printed films (horizontal sections of plots) were similar. This arises because the materials contained similar nickel content. However, the resistance of PE2-based printed films was less than those of PE1-based printed films. This maybe because the alkali-soluble acrylic copolymer and nickel particles formed micellar structure, as displayed in Figure 3.29. In this regard, nickel particles in each PE2-based micelle were dissociated, due to the steric hindrance of the influence of the polymer chains comparing to the PE1-based polymer chains. Thus, a greater electric field in the PE1-based printed film than that in PE2-based film could be built, resulting in a lower resistance value of the PE1-based printed films than that of the PE2-based printed film, when the same external compression was applied. The TiO_2 in the PE1-based films and PE2-based films did

not make much difference to the conductivity. Their lowest resistivity values were very similar. This result implies that the addition of TiO_2 in the PE2-based binder made a greater influence on the electrical conductivity than that in the PE1-based binder (see Figure 3.30), because the lowest electrical resistance of the PE2-based films was much greater than that of the PE1-based films. This is probably because the synergistic effect of TiO_2 in the PE2-based acrylic copolymer made large contribution to the electrical conductivity [158].

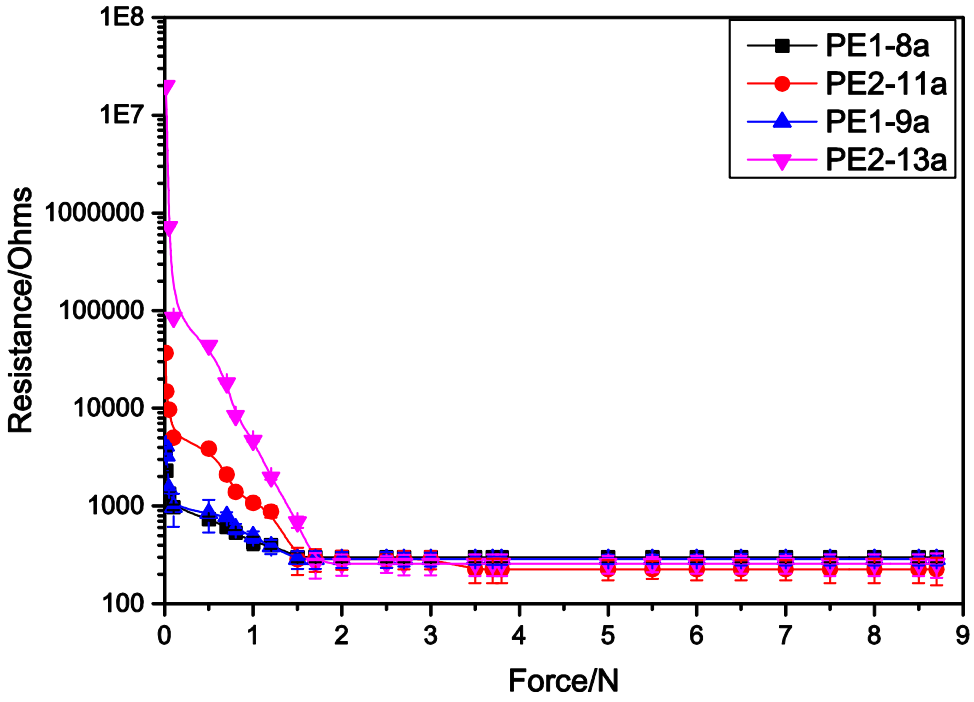

Figure 3.45 Comparisons of the electrical resistance on the external compression for printed samples with different binder, PE1 and PE2, contents (Table 3-10)

The PE1-based printed films behaved more like electrically switching materials and was also because of the good TiO_2 distribution in the PE2-based binder, a point that is further discussed in Section 3.4.3.4.

Table 3-10 Solid content of PE1 and PE2-based inks at different TiO_2 proportions

	PE1-based print	*PE2-based print*
Solid content of binder itself	***45.5%***	***23.9%***
Ni content of ink sample with Ni (70wt%), TiO_2 (2.5wt%) and binder (27.5wt%)	***82.3% (PE1-8a)***	***88.5% (PE2-8a)***
Ni content of ink sample with Ni (70wt%), TiO_2 (5wt%) and binder (25wt%)	***81.0% (PE1-9a)***	***86.4% (PE2-9a)***
Ni content of ink sample with Ni (70wt%), TiO_2 (7.5wt%) and binder (22.5wt%)	***79.8% (PE1-10a)***	***84.5% (PE2-10a)***
Ni content of ink sample with Ni (70wt%), TiO_2 (10wt%) and binder (20wt%)	***82.6% (PE1-11a)***	***82.6% (PE2-11a)***
Ni content of ink sample with Ni (70wt%), TiO_2 (12.5wt%) and binder (17.5wt%)	***77.4% (PE1-12a)***	***80.8% (PE2-12a)***
Ni content of ink sample with Ni (70wt%), TiO_2 (15wt%) and binder (15wt%)	***76.2% (PE1-13a)***	***79.0% (PE2-13a)***

3.4.3.3 SEM images of the PE1-based and the PE2-based printed films with TiO_2

The SEM images of the printed films, PE1-9a and PE2-9a, are shown in Figure 3.46. The large number of the nickel aggregates can be seen to have spherical clusters, (PE1-9a film). However, the nickel particles aggregated as can be seen in the PE2-9a film. The PE2 polymer correlated well with the particle, which would be discussed in TGA analyses (Section 3.4.3.5). As such the morphology of the PE2-

9a film, the overall interaction resulted in the electrical resistance decrease being less in comparison that given by the PE1-9a film under the same external force.

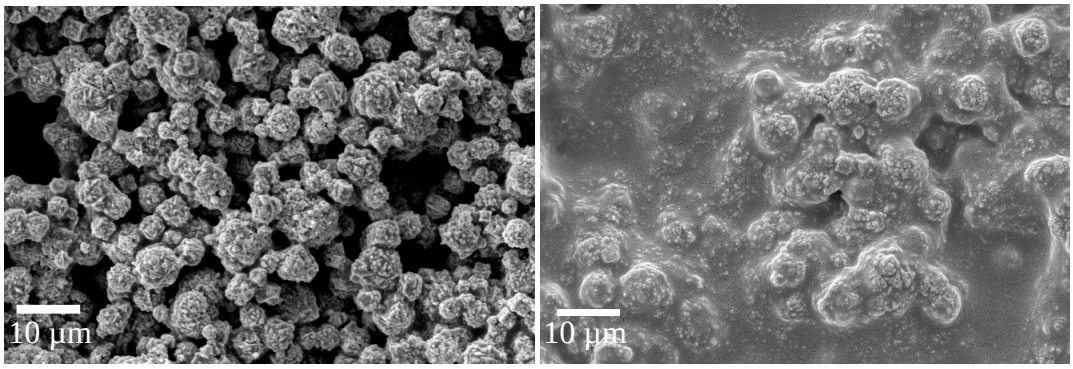

Figure 3.46 SEM images of surfaces of the PE1-9a (left) and the PE2-9a (right) printed films at ×1500 magnifications

3.4.3.4 Particle size distributions of the PE1-based and the PE2-based inks

Figure 3.47 shows the particle size distributions of particles in the PE1-9a ink and the PE2-9a ink. It indicates that the bulk of particle aggregates lie in the size range between 100 µm and 1000 µm for the PE1-9a ink. The average size of the detected particles is approximately 300 µm. Also the TiO_2 in the PE1-9a ink formed a broad distribution of large aggregates from 100 µm to 1000 µm. The average particle size of TiO_2a is around 0.2 µm (see Table 3-8) that is much smaller than that of TiO_2a in the PE2-based binder. Therefore, it can be assumed that the TiO_2a particles are adsorbed on the nickel aggregates, resulting in a very wide range of particle size distribution for the Ni-PE2-based ink. This particle size range distribution matches that obtained for the sample observed under scanning electron microscopy, as shown in Figure 3.46. This large particle aggregates in the PE1-based film could cause the more electrical conductive and more electrical sensitive behaviours of the PE1-based printed film with respect to those of the PE2-based film.

The particle size analysis data for the PE2-9a ink indicates that the bulk of Ni-PE2 composites lie in the size range between 1 µm and 40 µm, with composites also being present between 0.1 µm and 1 µm. The particle sizes ranging from 1 µm to 40 µm are nickel aggregates and those ranging from 0.1 µm to 1 µm are TiO_2 aggregates.

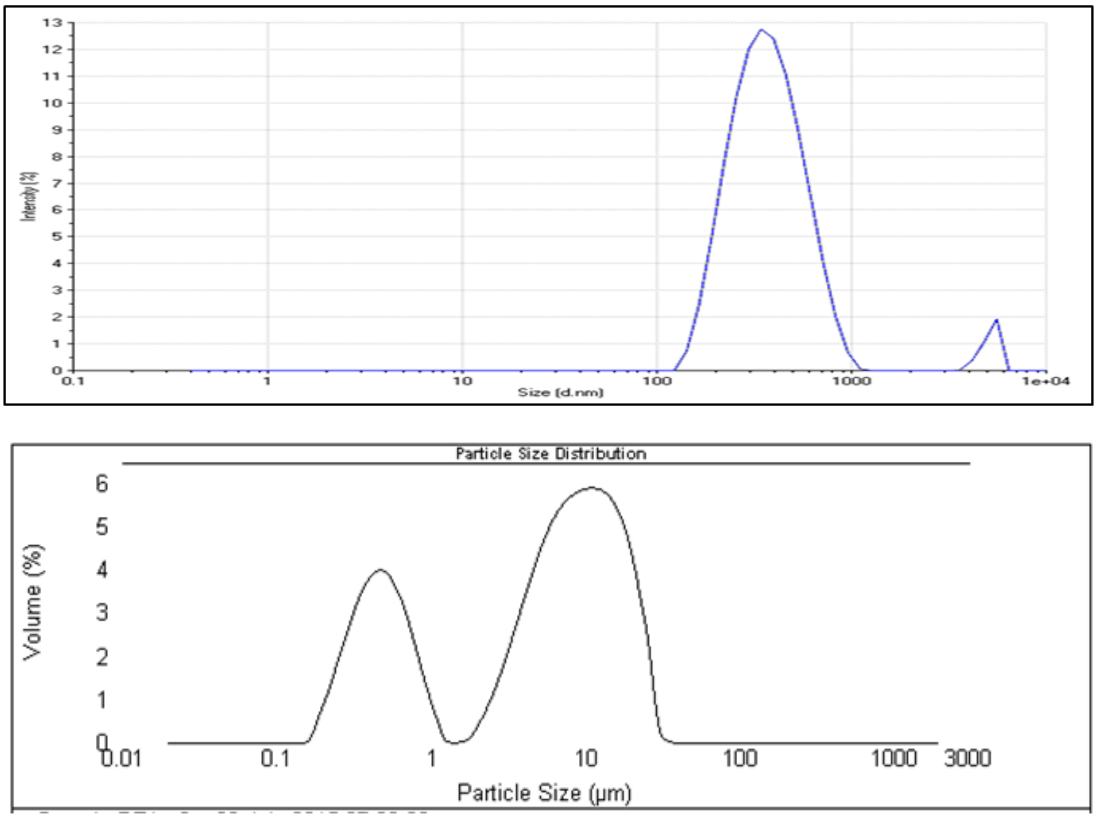

Figure 3.47 Particle size graphs of the PE1-9a ink (top) and the PE2-9a ink (bottom)

3.4.3.5 TGA analyses of the PE1-based and the PE2-based inks

Differences in the thermal stability of the nickel particles and the TiO_2 particles in the PE1-based binder and in the PE2-based binder can be seen in Figure 3.48. The extent to which the PE2-based binder holds onto water was slightly greater than that shown by the PE1-based binder. As a consequence, the PE1-based printed film showed more electrically switching behaviour and the PE2-based printed film showed more electrically sensing behaviour. The overall thermal stability of the two inks is similar. In the TGA profile of each ink, each thermogram indicates a curve that can be correlated to the loss of water as the heating temperature was increased up to around 140 ^{O}C and 150 ^{O}C, for the PE1-binder and the PE2-binder, respectively. This is then followed by any decomposition that takes place around 350 ^{O}C.

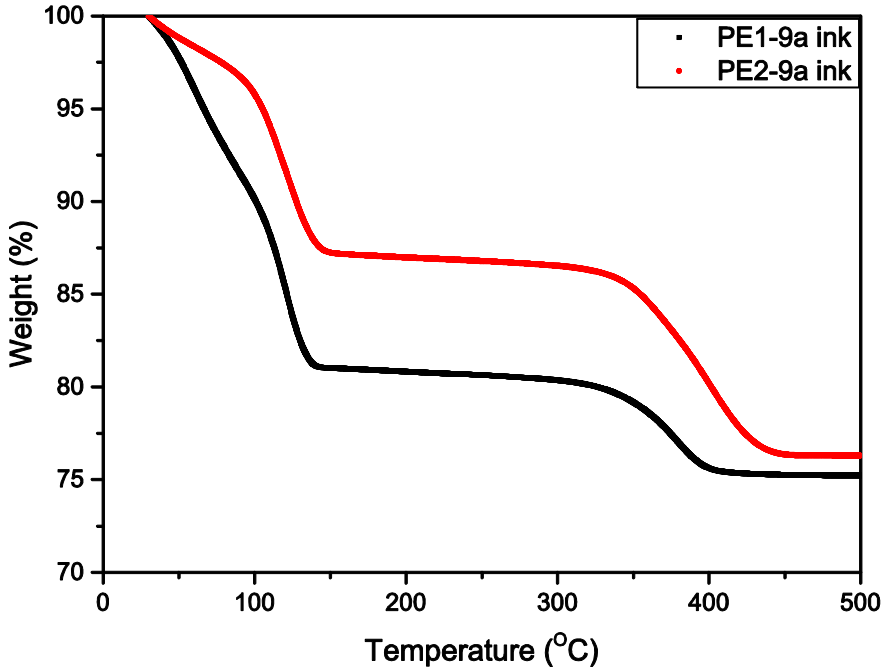

Figure 3.48 TGA evaluations of the PE1-9a ink and the PE2-9a ink, at heating rate 10 ^{O}C/min

3.4.3.6 The effect of the different grades of TiO_2 on the electrical-mechanical properties for selected water-based printed films

Figure 3.49 to Figure 3.51 represent the resistance-force profiles for the PVP-S, the PE1 and the PE2-based inks that contain nickel powder (70 wt%), water-based binder (25 wt%) and TiO_2 (5 wt%) in one of the three different grade options. The influence of these three grades of TiO_2 in different amounts on the electrical-mechanical property of printed films was also assessed. The results show the similar tendencies of resistance-force profiles for inks containing 5 wt% of each of the types of TiO_2. The resistance-force profiles for ink formulations with nickel powder (70 wt%), water-based binders (25 wt%) and one of the different grades of TiO_2 (5 wt%) are presented as representatives of the other different ink formulations that contained different amounts and different grades of TiO_2.

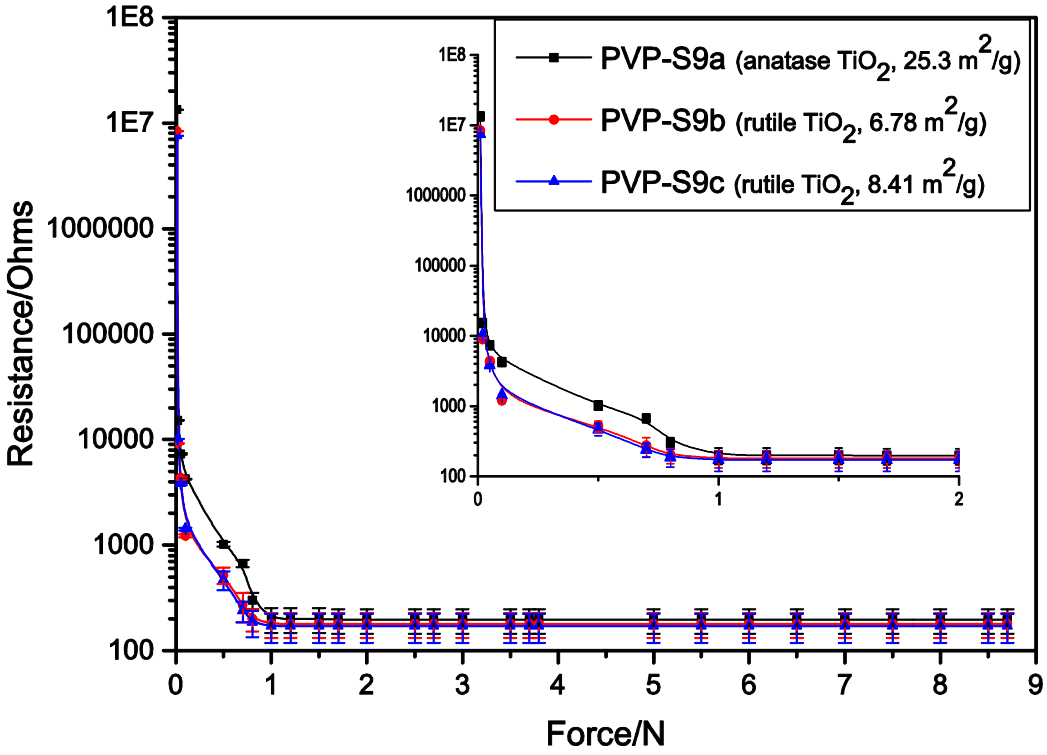

Figure 3.49 Resistance-force profiles for the same ink formulations for the PVP-S-based inks, containing one of the three different grades of TiO_2.

Figure 3.49 to Figure 3.51, indicate that TiO_2a, TiO_2b and TiO_2c played similar roles in the resistance-force profiles of the PVP-S, the PE1 and the PE2 printed films that are to reduce the electrical sensitivity. The effect of TiO_2a on the resistances under various compressions for the PVP-S, the PE1 and PE2-based printed films has been considered (Section 3.4.3.1). Films containing TiO_2b or TiO_2c were more sensitive to compression than those containing TiO_2a. The reason for this was mainly because the specific surface area of the three grades of TiO_2, *i.e.* TiO_2a (25.3 m^2/g), TiO_2b (6.78 m^2/g) and TiO_2c (8.41 m^2/g). The largest surface area of anatase pigment, TiO_2a, made the greatest contribution to reduce the electrical sensitivity of printed films and also significantly interacted with surrounding polymer and nickel particles in printed films. Also, the electrical performance differences could arise from the band gap differences between the anatase (TiO_2a) and the rutile TiO_2 structures (TiO_2b and TiO_2c), being 3.20eV and 3.03eV, respectively [73]. Thus, anatase TiO_2a needs greater external energy to excite the electrons from the valence band to the conduction band. Therefore, the reduction of the resistance of the anatase TiO_2a was less than that of the rutile TiO_2b

and TiO_2c. Furthermore, the resistance-force profile for TiO_2b was different from that for TiO_2c, which could be because the surface of Al content in TiO_2c (2.57 wt%) is greater than that in TiO_2b (1.55 wt%) (see the EDX mapping images for the printed films, Figure 3.56, Figure 3.57 and Figure 3.58). Thus, the resistances of the printed films containing TiO_2c were slightly lower than those containing TiO_2b. Also, the printed films containing TiO_2b or TiO_2c gave slightly lower resistance values than those containing TiO_2a, when the volume fractions of nickel powder were above the percolation threshold. The dielectric constants for anatase TiO_2 and rutile TiO_2 are 48 and 114, respectively [74, 75]. The dielectric constant is a measure of the ability to store electrical energy in an electric field. Therefore, TiO_2b and TiO_2c would be able to store more electric charge than TiO_2a. As a result, the printed films with TiO_2b and TiO_2c were slightly more conducive than those with TiO_2a, when large external compressions were applied.

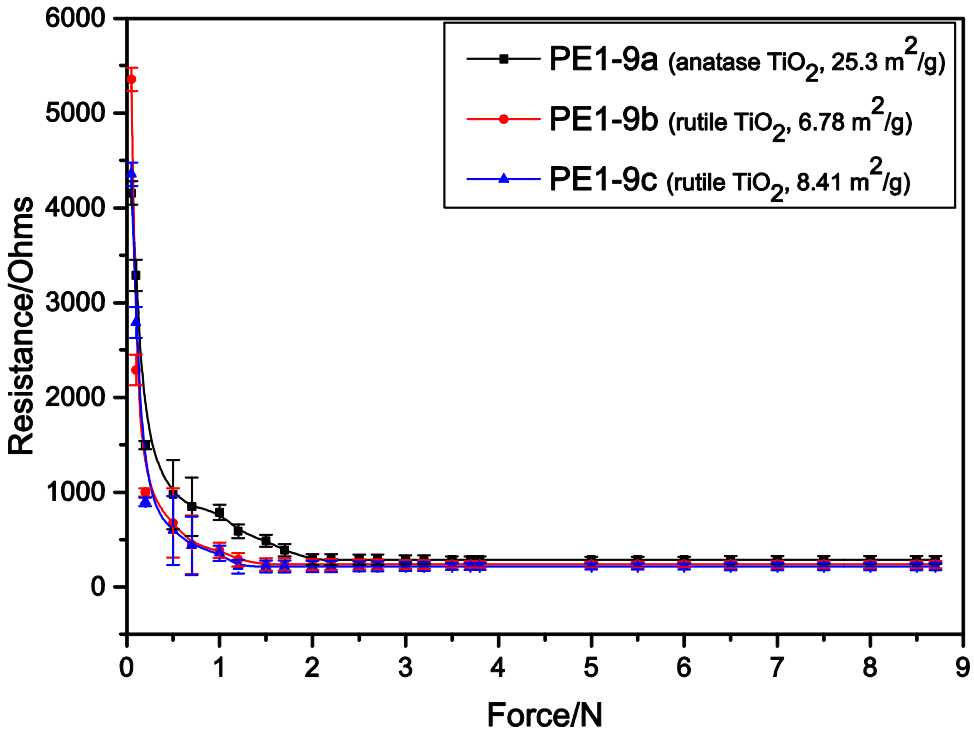

Figure 3.50 Resistance-force profiles for the same ink formulations for the PE1-based inks, containing one of the three different types of TiO_2

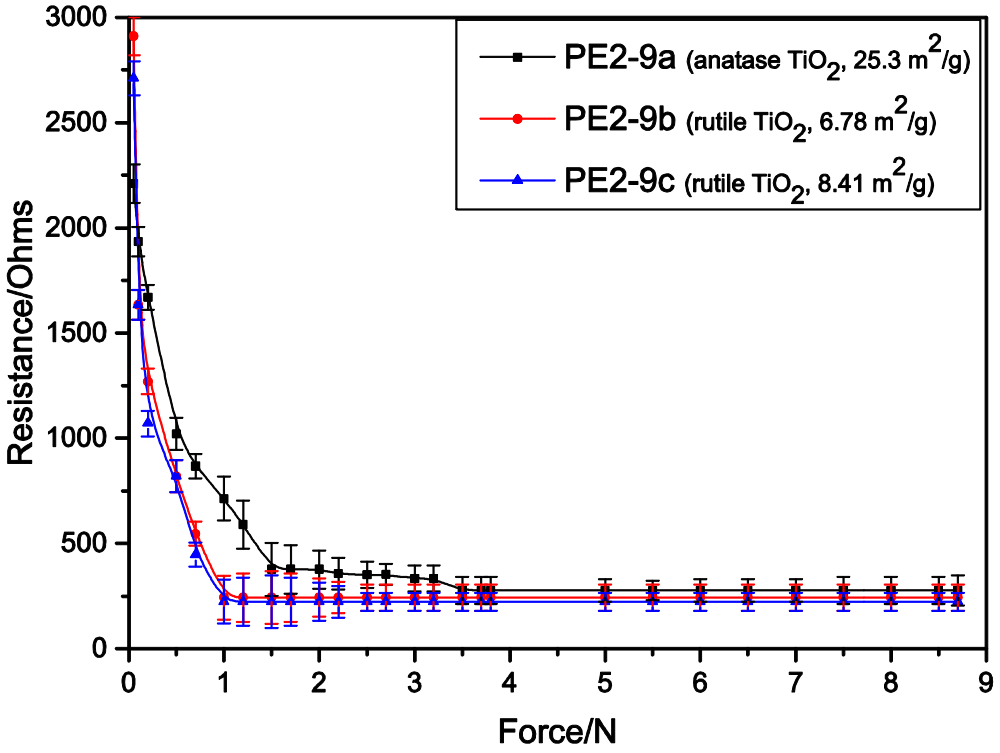

Figure 3.51 Resistance-force profiles for the same ink formulations for the PE2-based inks, containing one of the different types of TiO_2

3.4.3.7 SEM evaluations of the printed films containing TiO_2

The surfaces and cross-sections of the printed films were obtained from high resolution scanning electron microscopy. SEM images were conducted to establish the presence of the nickel and TiO_2 particles in the polymer matrices, clearly and intuitively. Also, Energy-dispersive X-ray spectroscopy (EDX) was used to identify particular elements, their relative proportions and distributions in the printed samples. In order to assess the distribution of TiO_2, Figure 4.36 shows the images of the three grades of TiO_2 (*i.e.* TiO_2a, TiO_2b and TiO_2c).

Figure 3.52 to Figure 3.54 show the morphologies of the surfaces, at 1500 and 10,000 magnifications, of PE1-9a, PE1-9b and PE1-9c, in which area displayed a number of near-spherical clusters. EDX shows these near-spherical particles to be nickel, which were presented as cores, covered by the PE1-based polymer and TiO_2. Those small spherical particles distributed on the nickel and dispersed in the polymer could be TiO_2, according to the shapes and sizes referred to Figure 3.40. There are many voids between the near-spherical clusters due to reduced amount of

the PE1-based acrylic copolymer. Figure 3.52 to Figure 3.54 shown that there is no significant difference between PE1-9 printed films that containing one of the three grades of TiO_2.

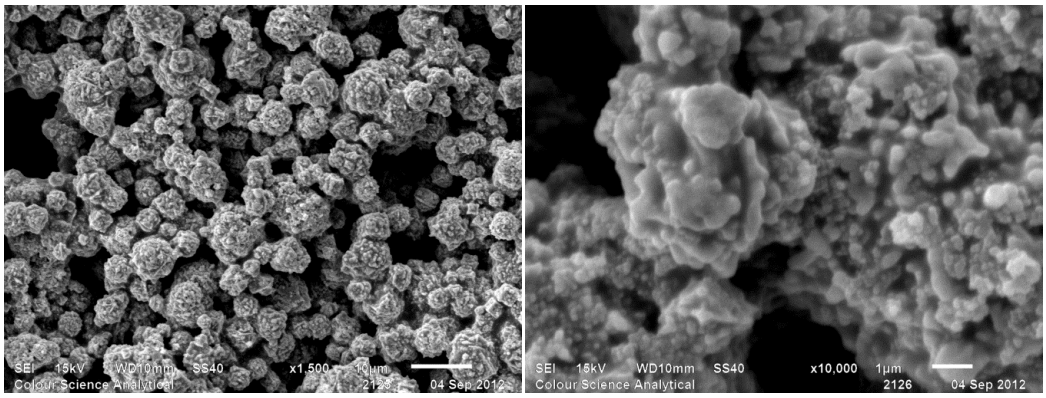

Figure 3.52 SEM images of PE1-9a printed film's surfaces at ×1500 and ×10,000 magnifications

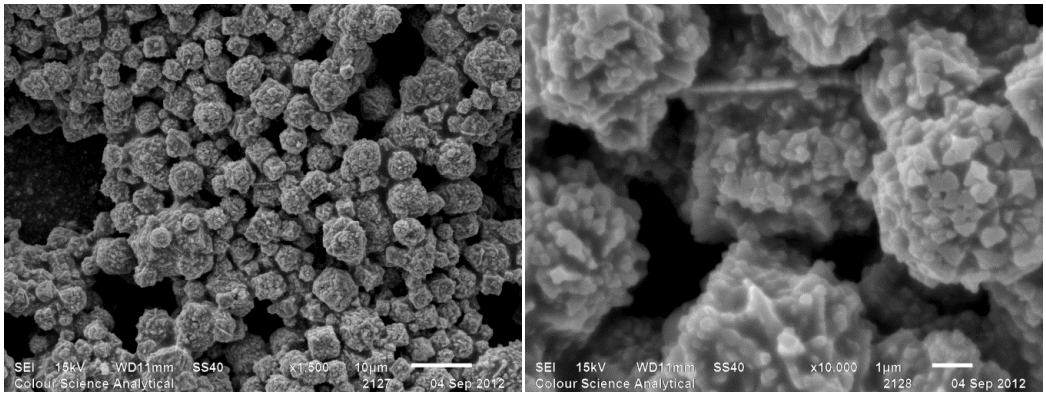

Figure 3.53 SEM images of PE1-9b printed film's surfaces, at ×1500 and ×10,000 magnifications

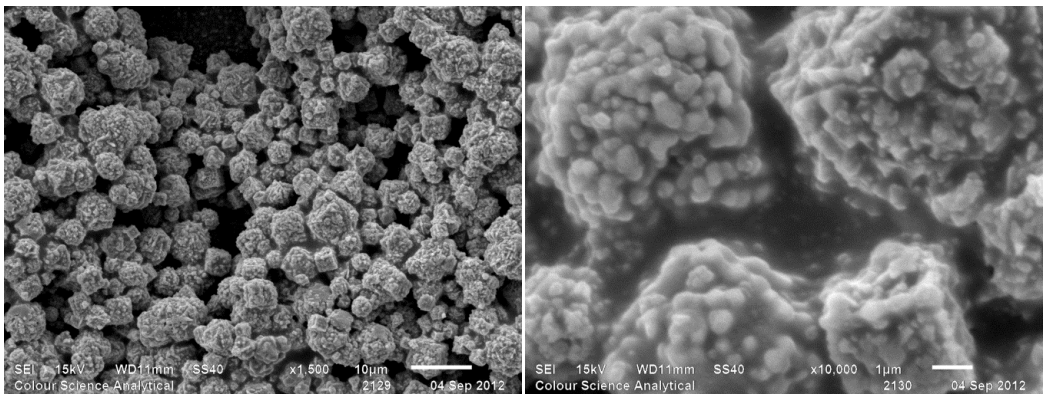

Figure 3.54 SEM images of PE1-9c printed film's surfaces at ×1500 and ×10,000 magnifications

Figure 3.55 represents the surface, at ×1500 and cross-section at ×750 magnifications, of the PE1-9a printed film. The thickness of this screen printing film was around 25 µm to 30 µm, as deduced from the SEM images.

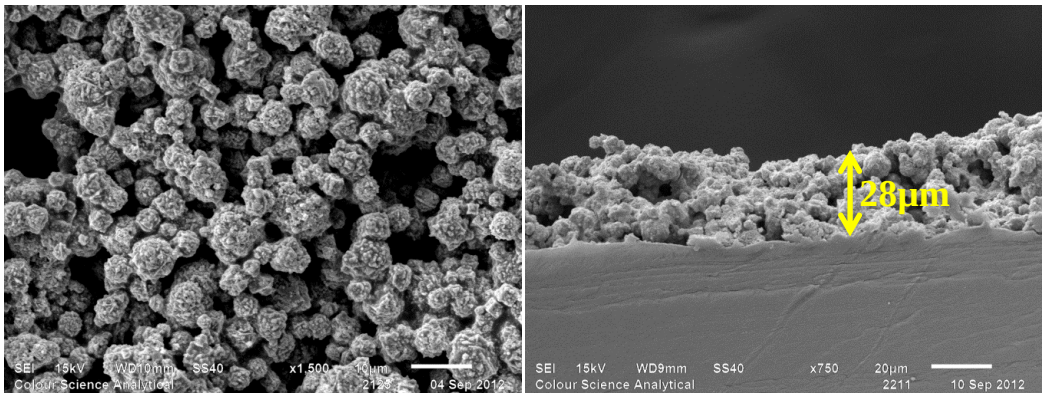

Figure 3.55 SEM images of surface and cross-section of PE1-9a printed films, at ×1500 and ×750 magnifications, respectively

Images of the surfaces and EDX analyse of the PE2-9 printed films, containing one of the three different grades of TiO_2, are shown in Figure 3.56 to Figure 3.58. There are a few cracks in the PE2-based printed films, which is different from PE1-based printed films that have some voids. PE2-based printed films are more continuous, because the PE2-based acrylic copolymer has longer polymer chain than the PE1-based polymer. The polymer with too short polymer chain such as the PE1-based polymer is no advantageous for gradually reducing resistance in resistance-force plot, when the external compression was applied. Also, the use of a polymer with a high molecular weight and a high polymer chain length would prevent the nickel particles from contacting each other.

EDX spectra (Figure 3.56, Figure 3.57 and Figure 3.58) display the distributions of relative elements, from which one can identify the TiO_2 and the nickel particles. The TiO_2 pigments were well dispersed in the printed films, as traced from the distribution of the element Ti. It can be seen that the element Ti is nearly homogeneously spread all over the film surfaces, particularly throughout the PE2-polymers. The chemical composition recorded with the EDX analysis is given in Table 3-11. The element of Ni from the nickel powder and the elements of C and O from the PE2-polymer are similar in Figure 3.56 to Figure 3.58, thus the atomic concentration and the weight concentration of the elements, Ti, O and Al, from three

different grades of TiO_2 but exclusive of C, O and Ni were recorded. The atomic concentration of the element Al in rutile TiO_2b and rutile TiO_2c is 1.55% and 2.28%, respectively. This matches the physical properties of TiO_2b and TiO_2c from MSDS sheets (Table 3-8).

Table 3-11 The normalised atomic concentration (top) and the normalised weight concentration (bottom) for the three different grades of TiO_2 in the PE2-based printed film with the same formulations, which was achieved by the EDX element analysis

Atomic conc. %	*Anatase TiO_2a*	*Rutile TiO_2b*	*Rutile TiO_2c*
Element Ti	**20.27**	**33.57**	**24.13**
Element O	**79.73**	**64.88**	**73.59**
Element Al	**0**	**1.55**	**2.28**

Weight conc. %	*Anatase TiO_2a*	*Rutile TiO_2b*	*Rutile TiO_2c*
Element Ti	**43.22+1.77**	**59.82+1.62**	**48.27+1.47**
Element O	**56.78+1.77**	**38.62+1.66**	**49.16+1.54**
Element Al	**0**	**1.56+0.23**	**2.57+0.29**

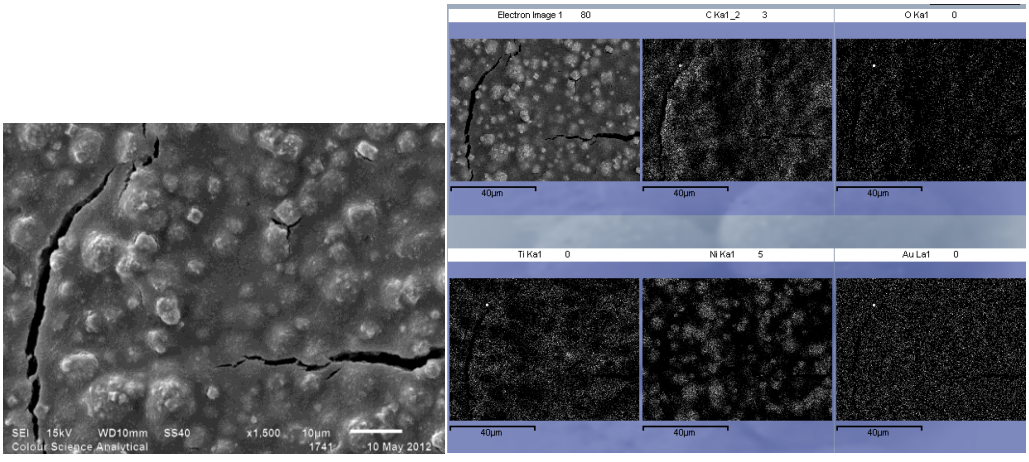

Figure 3.56 SEM image of PE2-9a printed film (left), which was mapped by EDX (right)

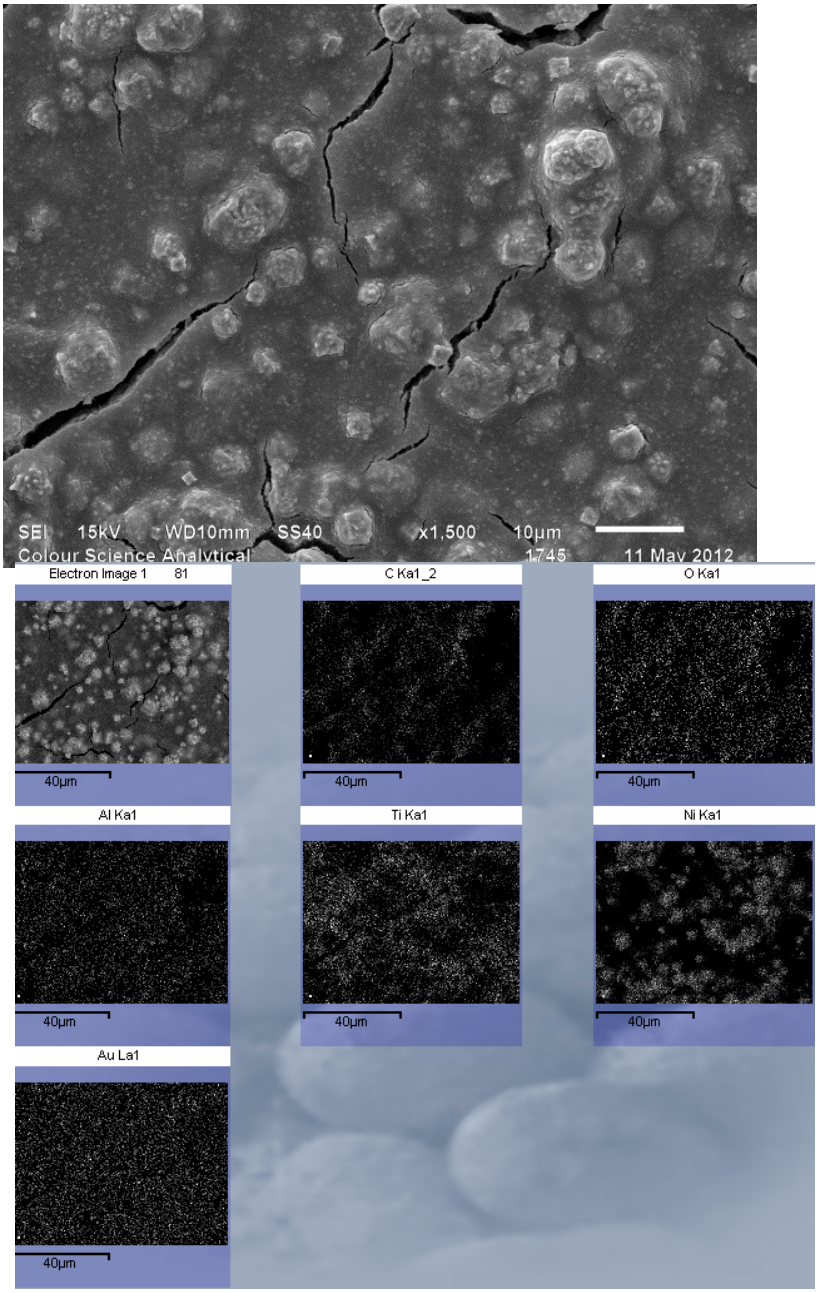

Figure 3.57 SEM image of PE2-9b printed film (left), which was mapped by EDX (right)

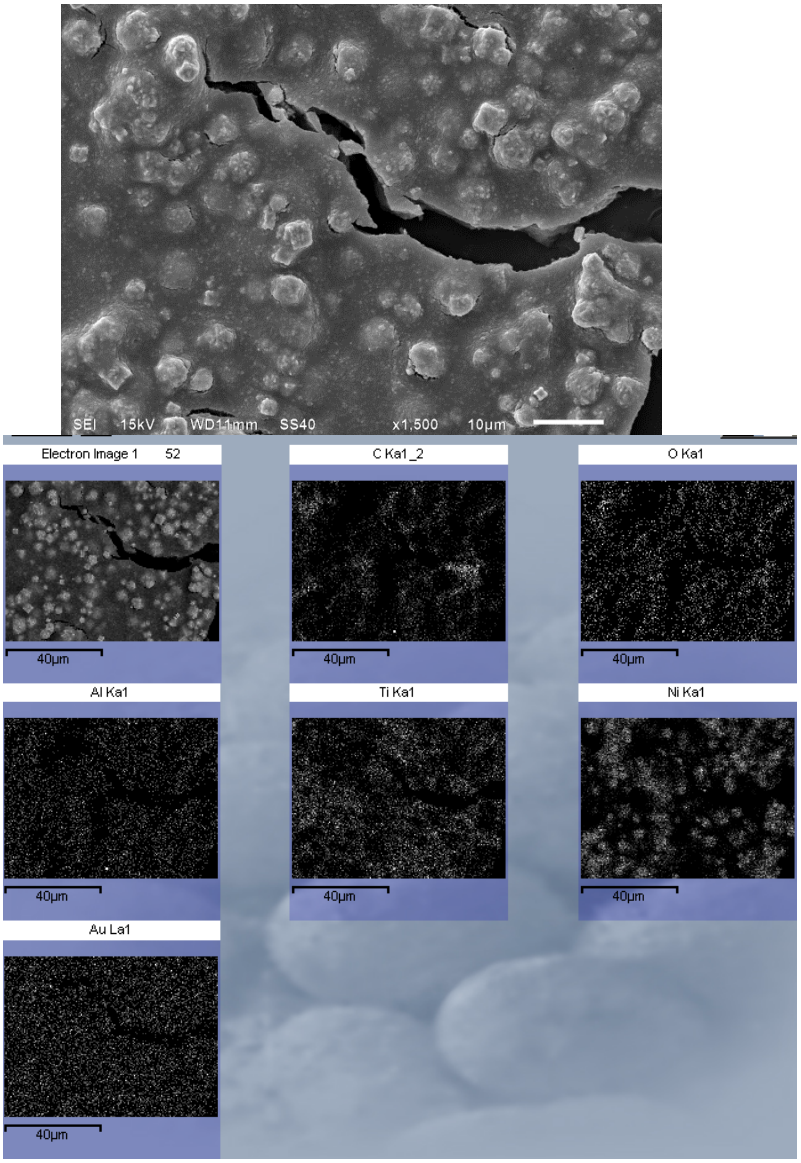

Figure 3.58 SEM image of PE2-9c printed film (left), which was mapped by EDX (right)

SEM images of surfaces and EDX spectra for the PE2-11 printed films containing one of the three grades of TiO_2 are presented in Figure 3.59, Figure 3.60 and Figure 3.61. The surfaces of the PE2-11 printed films (10% of TiO_2, 70% of Ni and 20% of PE2-binder) have slightly more cracks than those for PE2-9 printed films (5% of TiO_2, 70% of Ni and 25% of PE2-binder). This is because the greater TiO_2 pigment loading in the PE2-11 film could reinforce the tensile strength with regard to the PE2-9 film, resulting in more rigid film.

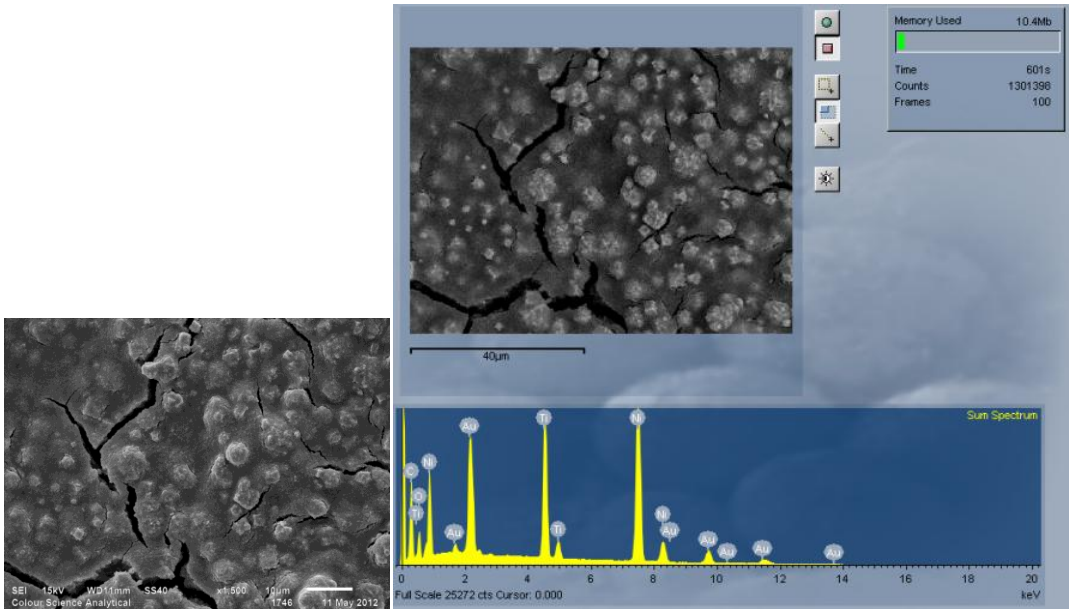

Figure 3.59 SEM image of PE2-11a printed film (left), which was mapped by EDX (right)

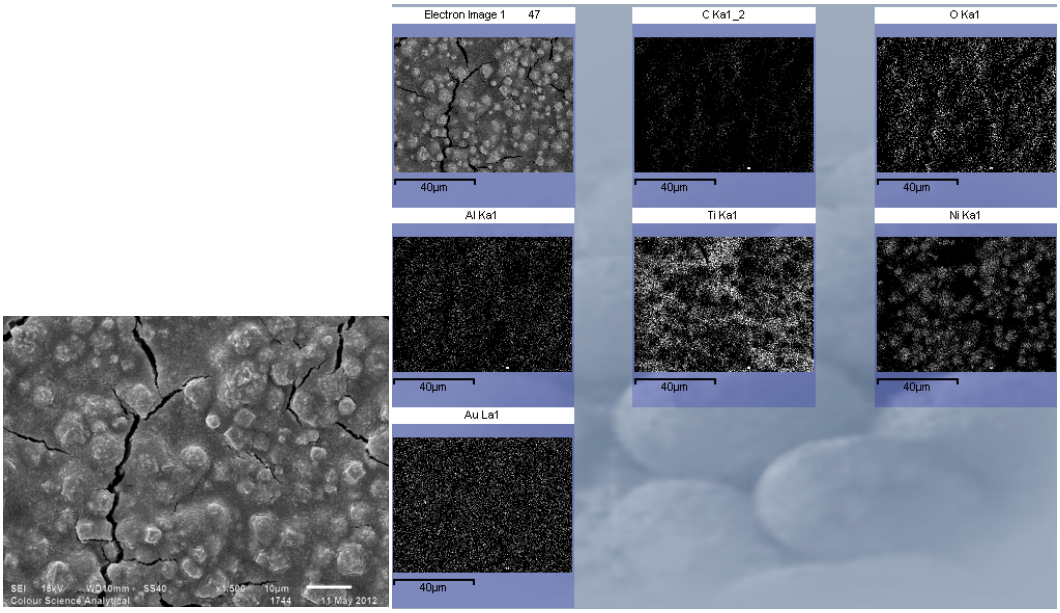

Figure 3.60 SEM image of PE2-11b printed film (left), which was mapped by EDX (right)

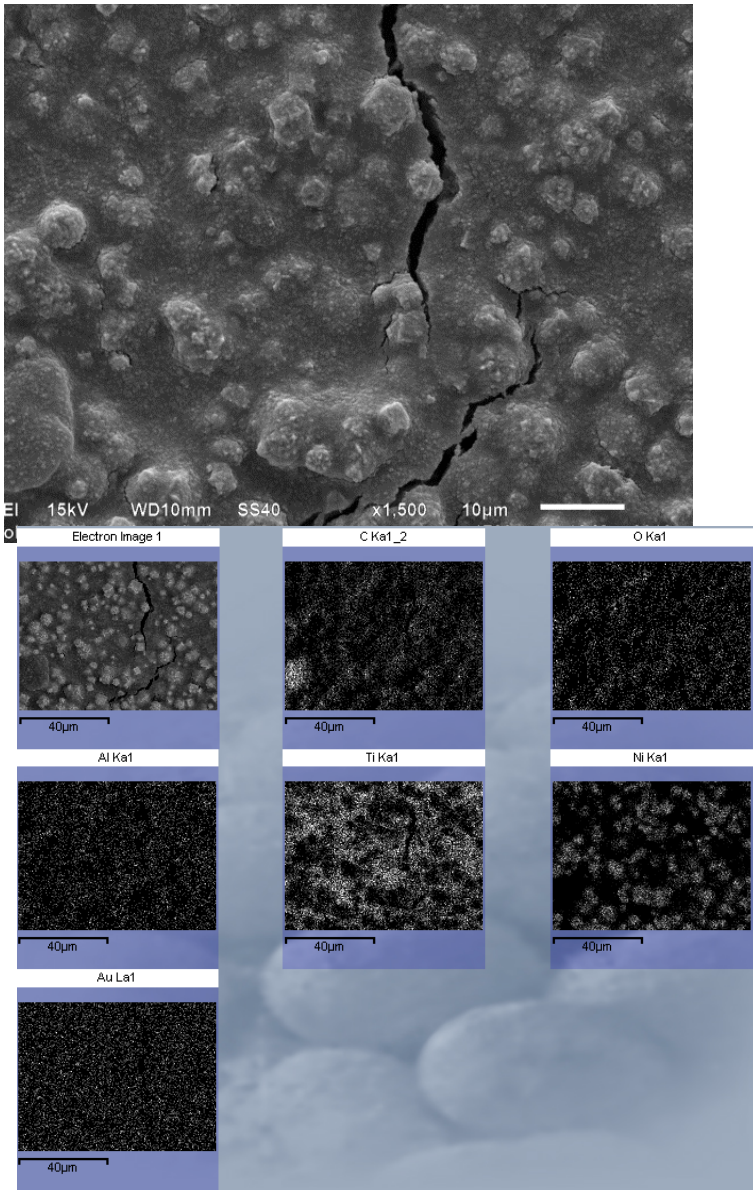

Figure 3.61 SEM image of PE2-11c printed film (left), which was mapped by EDX (right)

3.4.3.8 Particle size distribution graphs of particulates in the PE1-9a inks containing one of the three grades of TiO_2

The particle size distribution of the PE1-9a inks that contained one of the three grades of TiO_2 are shown in Figure 3.62. These indicates that the bulk of aggregates lie in the size range between 1 µm and 100 µm, with aggregates also being present between 0.1 µm and 1 µm. The particle sizes ranging from 1 µm to 100 µm are nickel aggregates and those ranging from 0.1 µm to 1 µm are TiO_2 aggregates. In

Figure 3.62, it can be seen that the three grades of TiO_2 were not significantly different in their particle size distribution.

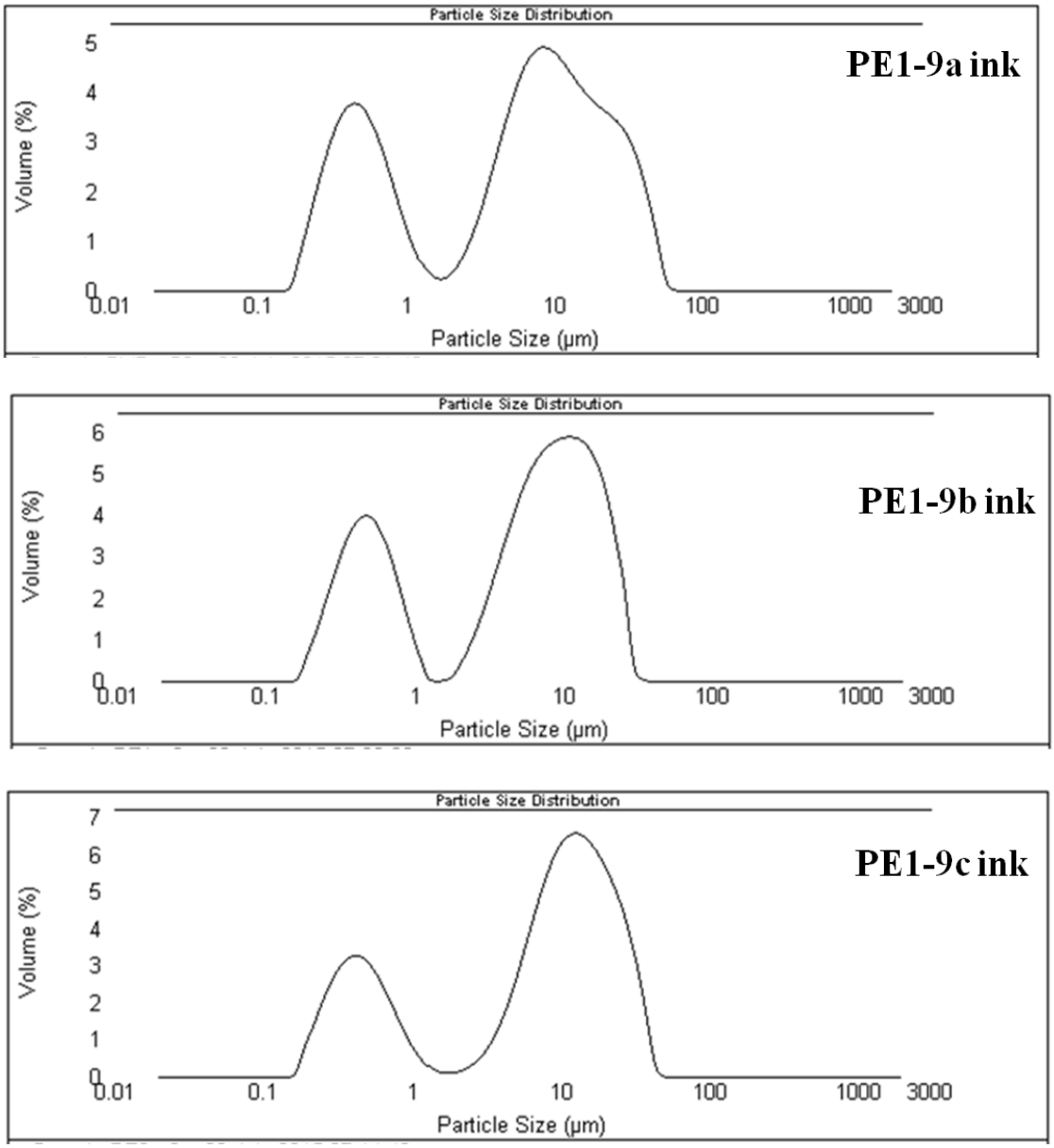

Figure 3.62 Particle size distributions of the particles in the PE1-9a ink, the PE1-9b ink and the PE1-9c ink

3.4.3.9 Zeta potential measurements on the three grades of TiO_2 dispersed in PE2-based binder

Across the three grades of TiO_2 dispersed in the same PE2-based binder that zeta potential values for TiO_2a, TiO_2b and TiO_2c were the same within experimental

errors, as shown in Figure 3.63. This would suggest that there was no significant difference in the emulsion stability for the three grades of TiO_2.

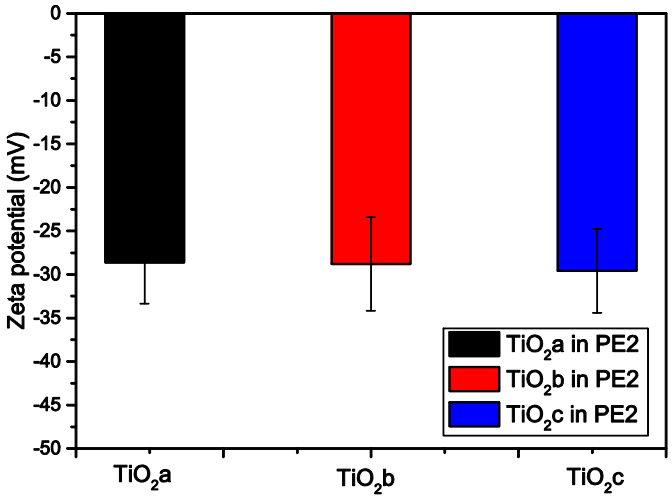

Figure 3.63 Bar graph shows the zeta potential measurements for three grades of TiO_2 dispersing in PE2-based binder

3.4.4 Conclusions

The electrical properties of screen printable printed films have been successfully altered by the addition of TiO_2. The loading of TiO_2 had a significant effect on modifying the printed films from being electrically switching to showing electrically sensing behaviour. This has also assisted the printed films to have electrically insulating property when no pressure was applied. It was found that the anatase form of TiO_2 had a significant effect on the electrical properties of the final printed films due to its large specific surface area.

References

1. Rentzhog, M., *Characterisation of water-based floxographic inks and their interacitons with polymer-coated board.* 2004, **23**(4), p: 34 – 45.
2. Thompson, B., *Printing materials: Science and technology*. 1998: **26**(3), p: 433 – 456.
3. Bloor, D., K. Donnelly, P.J. Hands, P. Laughlin, and D. Lussey, *A metal polymer composite with unusual properties.* Journal of physics D : applied physics., 2005. **38**(16): p. 2851-2860.
4. Leach, R.H., *The Printing Ink Manual*. 1993, **43**(6), p: 65 – 72.
5. Jang, D., D. Kim, and J. Moon, *Influence of fluid physical properties on ink-jet printability.* Langmuir, 2009. **25**(5): p. 2629-2635.
6. Gilleo, K., *Rheology and Surface Chemistry for Screen Printing.* Screen Printing Magazine, 1989, **63**(4), p: 143 – 165.

7. Fornes, T., et al., *Nylon 6 nanocomposites: the effect of matrix molecular weight.* Polymer, 2001. **42**(25): p. 09929-09940.
8. Lantada, A.D., et al., *Quantum tunnelling composites: Characterisation and modelling to promote their applications as sensors.* Sensors and Actuators A: Physical, 2010. **164**(1): p. 46-57.
9. News, E.I. *Quantum trick for pressure-sensitive mobile devices* (online). Accessed 07/08/2015. Available from: http://einewz.blogspot.co.uk/2010/02/quantum-trick-for-pressure-sensitive.html.
10. Lussey, D., *Conductive structures*, 2003, WO 2000079546A1.
11. Bloor, D., et al., *Metal–polymer composite with nanostructured filler particles and amplified physical properties.* Applied Physics Letters, 2006. **88**(10): p. 102103.
12. Fang-Gao, C., Y. Feng, W. Shao-Xiang, Z. Na, and S. Gui-Lin, *Enhanced piezoresistivity in Ni–silicone rubber composites.* Chinese physics B, 2009. **18**(2): p. 652.
13. Hollaway, L., *Polymers and polymer composites in construction*. 1990: **65**(5), p: 76 – 85.
14. Martin, J.E., R.A. Anderson, J. Odinek, D. Adolf, and J. Williamson, *Controlling percolation in field-structured particle composites: Observations of giant thermoresistance, piezoresistance, and chemiresistance.* Physical Review B, 2003. **67**(9): p. 94 - 207.
15. Li, W.W., L.H. Li, L.X. Mo, and J.L. Fu. *Effect of Polyvinylpyrrolidone Ratio on Synthesis of High Concentration Nano-Silver Colloid*. in *Advanced Materials Research*. 2012. **45**(3), p: 98 - 102.
16. Heaney, M.B., *Resistance-expansion-temperature behavior of a disordered conductor–insulator composite.* Applied Physics Letters, 1996. **69**(17): p. 2602-2604.
17. Heaney, M.B., *Electrical transport measurements of a carbon-black—polymer composite.* Physica A: Statistical Mechanics and its Applications, 1997. **241**(1): p. 296-300.
18. Ruschau, G. and R. Newnham, *Critical volume fractions in conductive composites.* Journal of composite materials, 1992. **26**(18): p. 2727-2735.
19. Perera, D.Y., *Effect of pigmentation on organic coating characteristics.* Progress in organic coatings, 2004. **50**(4): p. 247-262.
20. Singh, M., et al., *Liquid-Phase Synthesis of Nickel Nanoparticles stabilized by PVP and study of their structural and magnetic properties.* Advanced Materials Letters, 2011. **2**(6): p. 409-414.
21. Pang, H., L. Xu, D.-X. Yan, and Z.-M. Li, *Conductive polymer composites with segregated structures.* Progress in Polymer Science, 2014. **39**(11): p. 1908-1933.
22. Knite, M., et al., *Polyisoprene-carbon black nanocomposites as tensile strain and pressure sensor materials.* Sensors and Actuators A: Physical, 2004. **110**(1): p. 142-149.
23. Qu, S. and S.-C. Wong, *Piezoresistive behavior of polymer reinforced by expanded graphite.* Composites science and technology, 2007. **67**(2): p. 231-237.

24. Abyaneh, M.K. and S.K. Kulkarni, *Giant piezoresistive response in zinc–polydimethylsiloxane composites under uniaxial pressure.* Journal of Physics D: Applied Physics, 2008. **41**(13): p. 135405.
25. Alexander J Webb, M.S., David Bloor, Del Atkinson, Adam Graham, Paul Laughlin and David Lussey, *A multi-component nanocomposite screen-printed ink with non-linear touch sensitive electrical conductivity.* Nanotechnology, 2013. **24**(166501): p. 1-9.
26. Sun, M., Y. Su, C. Mu, and Z. Jiang, *Improved antifouling property of PES ultrafiltration membranes using additive of silica− PVP nanocomposite.* Industrial & Engineering Chemistry Research, 2009. **49**(2): p. 790-796.
27. Qin, J.-J., Y.-M. Cao, Y.-Q. Li, Y. Li, M.-H. Oo, and H. Lee, *Hollow fiber ultrafiltration membranes made from blends of PAN and PVP.* Separation and purification technology, 2004. **36**(2): p. 149-155.
28. Marchese, J., M. Ponce, N. Ochoa, P. Prádanos, L. Palacio, and A. Hernández, *Fouling behaviour of polyethersulfone UF membranes made with different PVP.* Journal of Membrane Science, 2003. **211**(1): p. 1-11.
29. Lafreniere, L.Y., F.D. Talbot, T. Matsuura, and S. Sourirajan, *Effect of poly (vinylpyrrolidone) additive on the performance of poly (ether sulfone) ultrafiltration membranes.* Industrial & Engineering Chemistry Research, 1987. **26**(11): p. 2385-2389.
30. Wan, L.-S., X.-J. Huang, and Z.-K. Xu, *Diffusion and structure of water in polymers containing N-vinyl-2-pyrrolidone.* The Journal of Physical Chemistry B, 2007. **111**(5): p. 922-928.
31. Noskov, B., A. Akentiev, and R. Miller, *Dynamic surface properties of poly (vinylpyrrolidone) solutions.* Journal of colloid and interface science, 2002. **255**(2): p. 417-424.
32. Naseri, M.G., E. Saion, and N.K. Zadeh, *The amazing effects and role of PVP on the crystallinity, phase composition and morphology of nickel ferrite nanoparticles prepared by thermal treatment method.* International Nano Letters, 2013. **3**(1): p. 19.
33. Pattanaik, M. and S.K. Bhaumik, *Adsorption behaviour of polyvinyl pyrrolidone on oxide surfaces.* Materials Letters, 2000. **44**(6): p. 352-360.
34. Bourlinos, A.B., et al., *Aqueous-phase exfoliation of graphite in the presence of polyvinylpyrrolidone for the production of water-soluble graphenes.* Solid State Communications, 2009. **149**(47): p. 2172-2176.
35. Graf, C., et al., *A general method to coat colloidal particles with silica.* Langmuir, 2003. **19**(17): p. 6693-6700.
36. Smith, J., J. Meadows, and P. Williams, *Adsorption of polyvinylpyrrolidone onto polystyrene latices and the effect on colloid stability.* Langmuir, 1996. **12**(16): p. 3773-3778.
37. Zhang, Q., T. Zhang, J. Ge, and Y. Yin, *Permeable silica shell through surface-protected etching.* Nano letters, 2008. **8**(9): p. 2867-2871.
38. Wang, J., T. Tsuzuki, B. Tang, P. Cizek, L. Sun, and X. Wang, *Synthesis of silica-coated ZnO nanocomposite: the resonance structure of polyvinyl pyrrolidone (PVP) as a coupling agent.* Colloid and polymer science, 2010. **288**(18): p. 1705-1711
39. Ghosh, G., et al., *Synthesis and characterization of PVP-encapsulated ZnS nanoparticles.* Optical Materials, 2006. **28**(8): p. 1047-1053.

40. Ghosh, G., M.K. Naskar, A. Patra, and M. Chatterjee, *Synthesis and characterization of PVP-encapsulated ZnS nanoparticles.* Optical Materials, 2006. **28**(8): p. 1047-1053.
41. Qian, D., E.C. Dickey, R. Andrews, and T. Rantell, *Load transfer and deformation mechanisms in carbon nanotube-polystyrene composites.* Applied Physics Letters, 2000. **76**(20): p. 2868-2870.
42. Lakouraj, M.M., M. Tajbakhsh, and M. Mokhtary, *Synthesis and swelling characterization of cross-linked PVP/PVA hydrogels.* Iranian Polymer Journal, 2005. **14**(12): p. 1022.
43. Bernal, A., I. Kuritka, and P. Saha, *Poly (vinyl alcohol)-poly (vinyl pyrrolidone) blends: Preparation and characterization for a prospective medical application.* Mathematical Methods and Techniques in Engineering and Environmental Science, 2014: **565**(3), p. 978-1.
44. Wang, Q., Z. Suo, and X. Zhao, *Bursting drops in solid dielectrics caused by high voltages.* Nature communications, 2012. **3**(5): p. 1157.
45. Nicholson, L.M., K.S. Whitley, T.S. Gates, and J.A. Hinkley. *How molecular structure affects mechanical properties of an advanced polymer*.
46. Frief, J.M., *Acrylic Polymers as Coatings Binders.* Paint and Coating Testing Manual, 1995: **45**(3), p. 39.
47. Tirtaatmadja, V., K. Tam, and R. Jenkins, *Rheological properties of model alkali-soluble associative (HASE) polymers: Effect of varying hydrophobe chain length.* Macromolecules, 1997. **30**(11): p. 3271-3282.
48. Fordyce, D., J. Dupré, and W. Toy, *Alkali-Soluble Acrylic Emulsions.* Industrial & Engineering Chemistry, 1959. **51**(2): p. 115-115.
49. Saravari, O., P. Phapant, and V. Pimpan, *Synthesis of water-reducible acrylic–alkyd resins based on modified palm oil.* Journal of applied polymer science, 2005. **96**(4): p. 1170-1175.
50. Jones, M.-C., M. Ranger, and J.-C. Leroux, *pH-sensitive unimolecular polymeric micelles: synthesis of a novel drug carrier.* Bioconjugate chemistry, 2003. **14**(4): p. 774-781.
51. Muroi, S., K. Hosoi, and T. Ishikawa, *Alkali solubility of carboxylated polymer emulsions.* Journal of applied polymer science, 1967. **11**(10): p. 1963-1978.
52. Brase, I.E., *Acrylic acid-alkali metal vinyl sulfonate copolymer water solubility enhancer*, 1990, US4898677 A.
53. Lee, D.Y. and J.H. Kim, *Preparation of small-sized carboxylated latexes by emulsion polymerization using alkali-soluble random copolymer.* Journal of applied polymer science, 1998. **69**(3): p. 543-550.
54. Kuo, P.L. and C.J. Chen, *Functional polymers for colloidal applications. V. Novel behavior of polymeric emulsifiers in emulsion polymerization.* Journal of polymer science part A: Polymer Chemistry, 1993. **31**(1): p. 99-111.
55. Astafieva, I., X.F. Zhong, and A. Eisenberg, *Critical micellization phenomena in block polyelectrolyte solutions.* Macromolecules, 1993. **26**(26): p. 7339-7352.
56. Wang, T., I. Iliopoulos, and R. Audebert, *Aqueous solution behavior of hydrophobically modified poly (acrylic acid).* Water Soluble Polymers. Synthesis, Solution Properties and Applications, 1991. **467**(3): p. 218-231.
57. Kawaguchi, S. and K. Ito, *Dispersion polymerization*, in *Polymer Particles*. 2005, **56**(3), p. 299-328.

58. Hunter, R.J., *Zeta potential in colloid science: principles and applications*. 2013: **34**(2), p: 67 – 86.
59. Zhang, Y., M. Yang, N.G. Portney, D. Cui, G. Budak, E. Ozbay, M. Ozkan, and C.S. Ozkan, *Zeta potential: a surface electrical characteristic to probe the interaction of nanoparticles with normal and cancer human breast epithelial cells.* Biomedical microdevices, 2008. **10**(2): p. 321-328.
60. Shen, L., P.E. Laibinis, and T.A. Hatton, *Bilayer surfactant stabilized magnetic fluids: synthesis and interactions at interfaces.* Langmuir, 1999. **15**(2): p. 447-453.
61. Sethia, S. and E. Squillante, *Solid dispersion of carbamazepine in PVP K30 by conventional solvent evaporation and supercritical methods.* International Journal of Pharmaceutics, 2004. **272**(1): p. 1-10.
62. Van den Mooter, G., P. Augustijns, N. Blaton, and R. Kinget, *Physico-chemical characterization of solid dispersions of temazepam with polyethylene glycol 6000 and PVP K30.* International Journal of Pharmaceutics, 1998. **164**(1): p. 67-80.
63. Van den Mooter, G., M. Wuyts, N. Blaton, R. Busson, P. Grobet, P. Augustijns, and R. Kinget, *Physical stabilisation of amorphous ketoconazole in solid dispersions with polyvinylpyrrolidone K25.* European journal of pharmaceutical sciences, 2001. **12**(3): p. 261-269.
64. Giri, N., R. Natarajan, S. Gunasekaran, and S. Shreemathi, *13C NMR and FTIR spectroscopic study of blend behavior of PVP and nano silver particles'.* Archives of Applied Science Research, 2011. **3**(5): p. 624-30.
65. Nagarajan, R., S. Tripathy, J. Kumar, F.F. Bruno, and L. Samuelson, *An enzymatically synthesized conducting molecular complex of polyaniline and poly (vinylphosphonic acid).* Macromolecules, 2000. **33**(26): p. 9542-9547.
66. Ishihara, N., T. Seimiya, M. Kuramoto, and M. Uoi, *Crystalline syndiotactic polystyrene.* Macromolecules, 1986. **19**(9): p. 2464-2465
67. Roy, D., J.T. Guthrie, and S. Perrier, *Graft polymerization: grafting poly (styrene) from cellulose via reversible addition-fragmentation chain transfer (RAFT) polymerization.* Macromolecules, 2005. **38**(25): p. 10363-10372.
68. Kim, J. and C. Kim, *Ultrafiltration membranes prepared from blends of polyethersulfone and poly (1-vinylpyrrolidone-co-styrene) copolymers.* Journal of Membrane Science, 2005. **262**(1): p. 60-68.
69. O'regan, B. and M. Grätzel, *A low-cost, high-efficiency solar cell based on dye-sensitized colloidal TiO2 films.* 1991, **867**(32), p: 435 – 476.
70. Ito, S., P. Chen, P. Comte, M.K. Nazeeruddin, P. Liska, P. Péchy, and M. Grätzel, *Fabrication of screen-printing pastes from TiO2 powders for dye-sensitised solar cells.* Progress in photovoltaics: research and applications, 2007. **15**(7): p. 603-612
71. Linsebigler, A.L., G. Lu, and J.T. Yates Jr, *Photocatalysis on TiO2 surfaces: principles, mechanisms, and selected results.* Chemical Reviews, 1995. **95**(3): p. 735-758.
72. Mali, S.S., C.A. Betty, P.N. Bhosale, and P. Patil, *Synthesis, characterization of hydrothermally grown MWCNT–TiO2 photoelectrodes and their visible light absorption properties.* ECS Journal of Solid State Science and Technology, 2012. **1**(2): p. M15-M23.
73. Scanlon, D.O., C.W. Dunnill, J. Buckeridge, S.A. Shevlin, A.J. Logsdail, S.M. Woodley, C.R.A. Catlow, M.J. Powell, R.G. Palgrave, and I.P. Parkin,

Band alignment of rutile and anatase TiO2. Nature materials, 2013. **12**(9): p. 798-801.

74. Buxbaum, G., *Industrial inorganic pigments*. 2008, **64**(7), p: 143 – 152.
75. Busani, T. and R. Devine, *Dielectric and infrared properties of TiO2 films containing anatase and rutile.* Semiconductor science and technology, 2005. **20**(8): p. 870.
76. Alloys, N. *Nickel - Properties, Fabrication and Applications of Commercially Pure Nickel* (online). Accessed 05/02/2016. Available from: http://www.nickel-alloys.net/commercially_pure_nickel.html.

Chapter 4. Preparation and characterisation of the polysiloxane-based and the polyisoprene-based inks and modelling of the electrical properties of printed films

In this section, nickel powder, anatase TiO_2 and three highly elastic polymeric binders for use in composite inks, were investigated on the basis of the contribution made by each binder to the formulation, electrical resistance, flow properties, thermal degradation change and mechanical properties of the inks. In particular, a model based on the variation of the electrical resistance under an applied force was built up.

4.1 Ink formulation of the PSE1, the PSE2 and the PIP-based inks

Three dispersions PSE1 (Evonik Ltd.), PSE2 (PennWhite Ltd.) and PIP (Formulated Polymer Products Ltd.) were used in the QTC ink formulations. The PSE1 binder is a siloxane-modified polyurethane dispersion, whose solvent contains dipropyleneglycol dimethyl ether and water in the ratio of 5:60. The PSE2 binder is a poly(disiloxane) emulsion. The PIP binder is a poly(isoprene) emulsion. Type 123 nickel powder was supplied by Inco Ltd. and the TiO_2 was supplied by Kronos Titan GmbH Ltd. and used in the ink formulations as pigments, to contribute the electrical properties. More relevant information on the different ink components was given in Section 2.1.2.

The poly(ethylene terephthalate) (PET) based interdigitated electrode substrate was supplied by Peratech Ltd. has been pre-printed with carbon-based inks and with silver-based inks to assemble circuit, as detailed in Section 2.4.5.

The ink formulations containing the nickel powder, the TiO_2 and one of the different polymeric binders are shown in Table 4-1. The different loadings of the nickel powder, the TiO_2 and the polymeric binder were chosen due to the different solid contents of each polymeric binder. This would cause the each ink component in the printed film to be similar, *i.e.* nickel content ~83 wt%, the TiO_2 ~5 wt% and the polymeric binder ~11 wt% in each PSE1, PSE2 and PIP-based printed films. The electrical properties, mechanical properties, particle size distribution, zeta

potential, thermal stability and flow properties of the other different ink formulations on the basis of the nickel powder, anatase TiO_2 and PSE1, PSE2 and PIP binders were not exhibited here is because these properties followed the same trend as those of the printed films from ink formulations in Table 4-1.

Table 4-1 Ink formulations with the different polymeric binders

Sample component	*PSE1-9 ink*	*PSE2-9 ink*	*PIP9 ink*
Ni powder	*70 wt%*	*70 wt%*	*78 wt%*
Anatase TiO_2	*5 wt%*	*5 wt%*	*5 wt%*
Specific binder	*25 wt%*	*25 wt%*	*17 wt%*

4.2 Results and discussion

4.2.1 Response of the electrical properties to the external force for the PSE1, the PSE2 and the PIP-based printed films

Figure 4.1 shows the variation in resistance as a function of the compression force for the PSE1-9, the PSE2-9 and the PIP9-based printed films. The three printed films have exhibited pressure electrically sensitive properties, as water-based printed films in Chapter 3. The electrical resistance of the printed films varied exponentially with increasing applied force. All of the three printed films were found to possess electrically insulating behaviour, when no compression was applied. After the increasing pressure was applied, the films changed from the insulating behaviour to the conductive characteristic. The performance changing from insulating to conductive is a result of the destruction of the percolation structure of the Ni-Polymer composites [1].

Regarding to the insulating property, the PIP9 printed film possessed this behaviour until larger external force, 0.5 N, was applied, comparing to the PSE1 and the PSE2-based films. This is because the insulating PIP-based polymer matrix is better binding with nickel fillers than the PSE1 and the PSE2 polymers, which can be seen in the morphologies and the particle distribution of the PIP-based film (see Section 4.2.2). The PSE1-9 and the PSE2-9 printed films behaved more like

electrically switching properties. The PIP9 printed film behaved controlled electrically sensing property. The distinct property for each printed film is owing to the nature of the used binding polymers (*i.e.* the mechanical property, the thermal property and the rheological property) that would be further discussed in the next section.

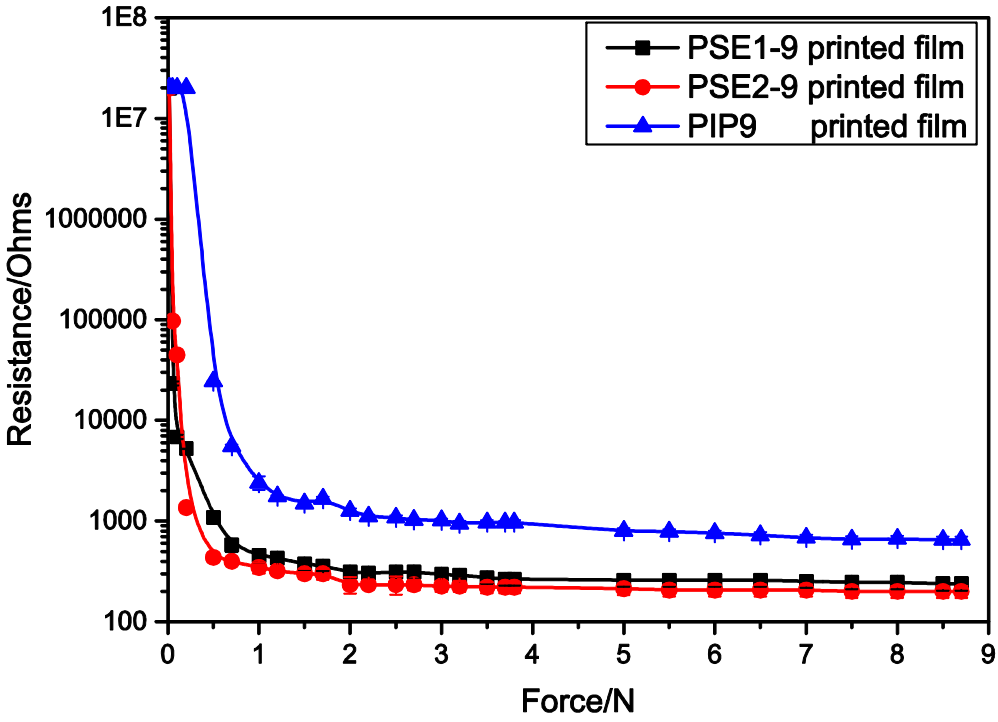

Figure 4.1 Variation in resistance as a function of compression for the PSE1-9, the PSE2-9 and the PIP9 printed films, of which containing the same nickel content (~83 wt%)

4.2.2 Morphologies of the PSE1, the PSE2 and the PIP printed films

Figure 4.2 to Figure 4.4 show the SEM micrographs of surfaces of the PSE1-9, the PSE2-9 and the PIP9 printed films which indicate that the films are heterogeneous and anomalous. It could be seen that the some continuous spheres and voids at the surface of the PSE1-9 and the PSE2-9 printed films. In the larger SEM magnifications (×10,000) of them, the white particles embedded in the polymer matrix and on the surface of nickel particles are TiO_2, in the diameter of approximately 200 nm. The nickel particles in the PSE1-9 and the PSE2-9 printed films are significantly increased comparing with the PIP9 film, which can be attributed to the strong intermolecular forces between nickel particles, *i.e.* van der

Waals attraction, π-π interaction and magnetic dipole-dipole interaction [2]. This nickel aggregates could induce the electrical instability, which resulted in larger errors of the resistance measurements (see Figure 4.1). However, the SEM images of the surfaces of the PIP9 printed film shows that the film is more continuous, more hermetic and less nickel spheres, comparing with the PSE1 and the PSE2 printed films. This remarkably better binding PIP polymeric matrix can be attributed to the electrically insulating property of PIP9 film until 0.5 N force was applied, as shown in Figure 4.1. It could be seen that some white particles and white particle aggregates at the surface of the PIP9 printed film, which are considered to be the TiO_2 particles due to their sizes.

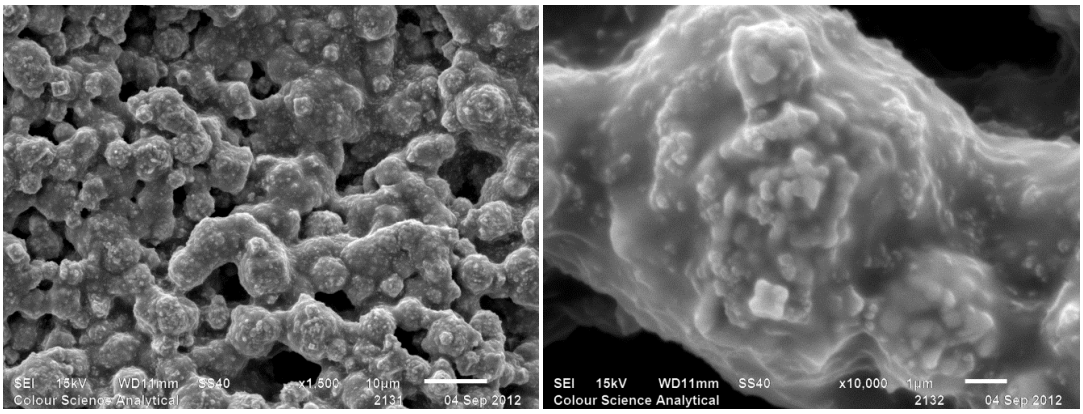

Figure 4.2 SEM micrographs of a surface of the PSE1-9 printed film at × 1500 (left) and × 10000 (right) magnifications

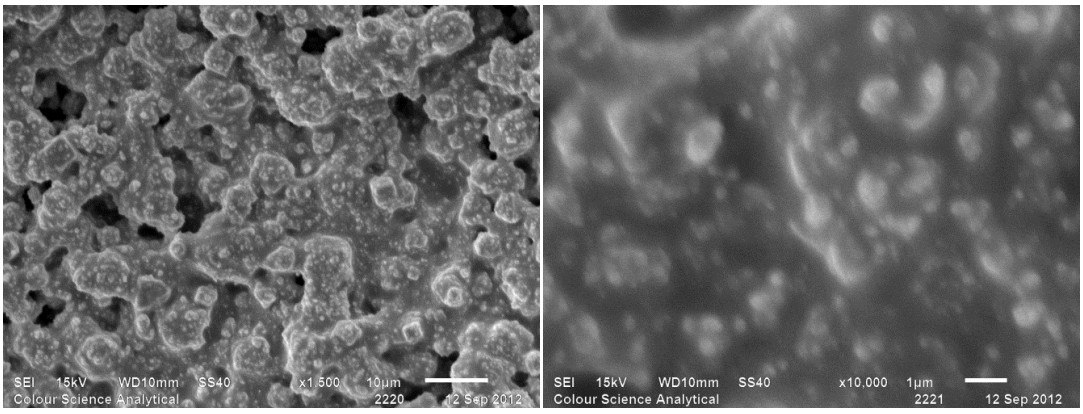

Figure 4.3 SEM micrographs of a surface of the PSE2-9 printed film at × 1500 (left) and × 10000 (right) magnifications

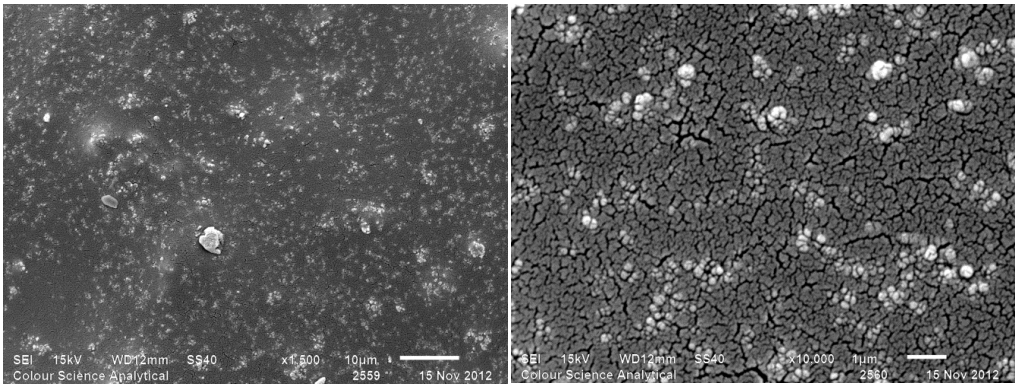

Figure 4.4 SEM micrographs of a surface of the PIP9 printed film at × 1500 (left) and × 10000 (right) magnifications

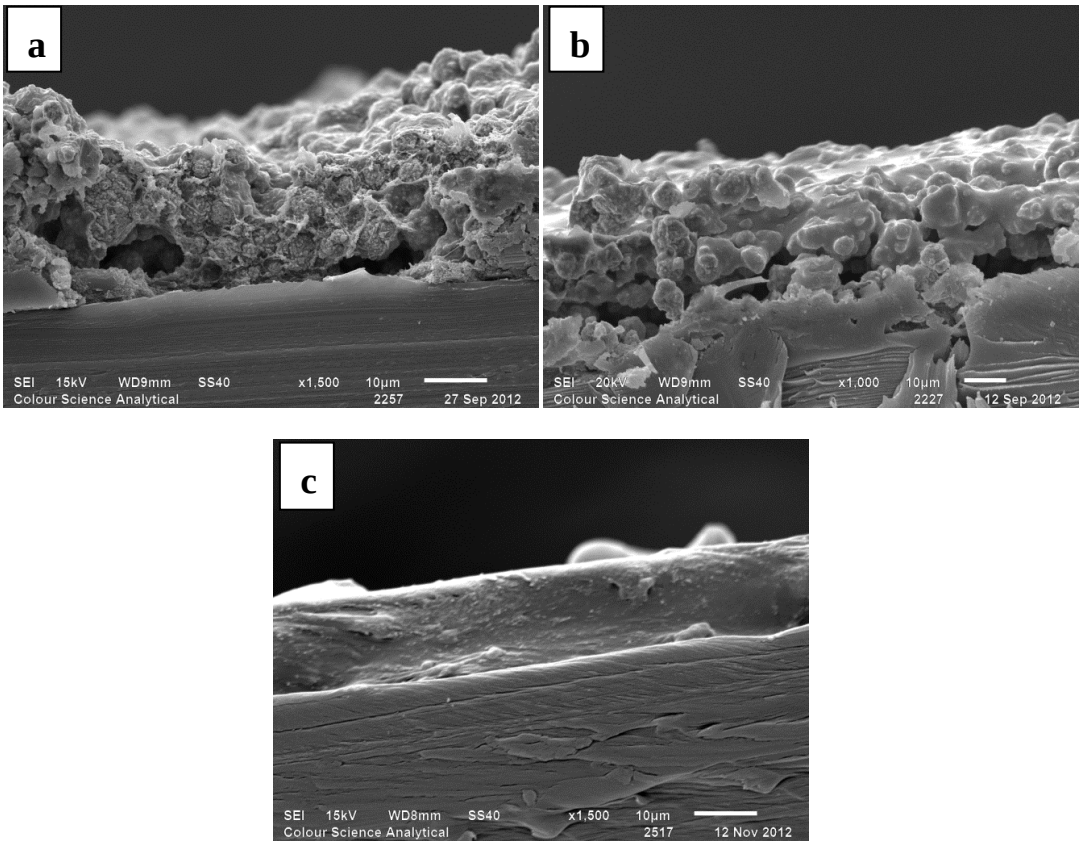

Figure 4.5 SEM micrographs of a cross-section of cross-sections of the (a) PSE1-9, the (b) PSE2-9 and the (c) PIP9 printed films

Figure 4.5 indicates the cross-section SEM image of the PSE1-9, the PSE2-9 and the PIP9 printed films, which have approximate thicknesses of 20 µm, 30 µm and 15 µm, respectively. The cross-section of the PIP9 printed film is smoother and more homogeneous than that of the PSE1-9 and PSE2-9 printed films. This reveals

that the PIP polymer is a better binding polymeric matrix with nickel particles, which caused the insulating property. There are a large number of nickel aggregates binding in and exposing on the PSE1-9 and the PSE2-9 printed films, which led to their lower critical percolation fractions comparing with that of PIP9 printed film. As a consequence, the PIP-based printed film behaved more like electrically sensing behaviour, however, the PSE1 and the PSE2-based printed films behaved more like electrically switching characteristics, as demonstrated in Figure 4.1.

It was reported that the Ni-Polymer composite systems exhibit core-shell structures of intercrosslinked networks, as shown in Figure 4.6 [3-8]. However, even though the three Ni-Polymer composite systems (the Ni-PSE1, the Ni-PSE2 and the Ni-PIP composites) are all display the core-shell like structures, the mechanical property, the electrical property, the thermal property and rheological property of different polymers based printed films are different.

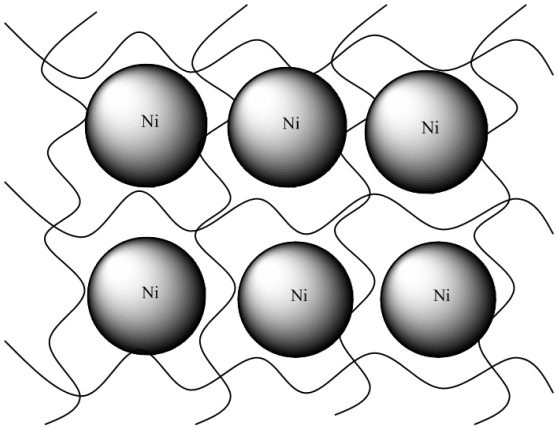

Figure 4.6 Schematic cross-section view of the core-shell structure of Ni-Polymer composite [3-8]. The curves and the spherical represent the polymer chains and the nickel particles, respectively

4.2.3 Particle size distributions of the PSE1, the PSE2 and the PIP-based inks

The particle size analysis data for the nickel powder and the TiO_2 powder in the PSE1 silicone-based binder (see Figure 4.7) indicate that the bulk of the spherical fused particle aggregates lie in a size range between 2 μm and 100 μm, with aggregates also being present (around 200 μm). This particle size range distribution

matches that obtained for the sample observed under the scanning electron microscope.

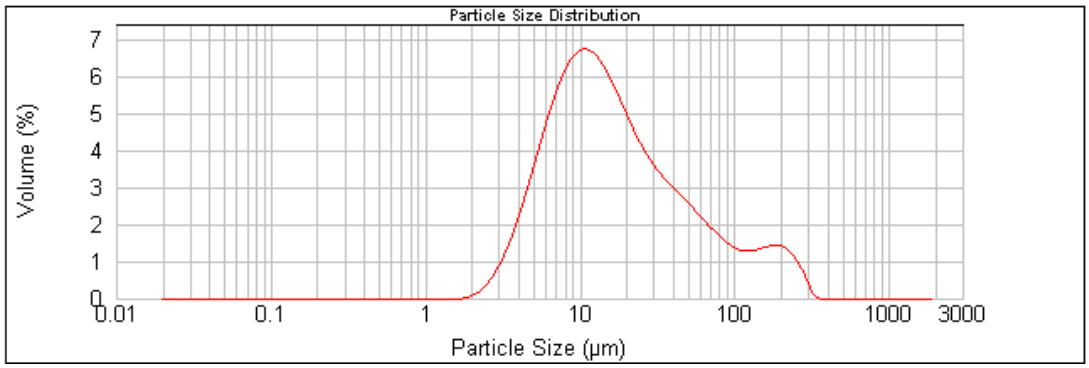

Figure 4.7 Particle size distribution graph of the nickel and the TiO_2 particles in the PSE1-based binder

Figure 4.8 shows the size distribution graph of the nickel particles and the TiO_2 particles in PSE2-based binder. It indicates that the bulk of the spherical fused particle aggregates lie in a size between 100 µm and 1000 µm. This means that there is a large number of particle aggregates, averagely fifty nickel particles in one aggregate, in the PSE2-based binder, because the average size of nickel particle is approximately 10 µm. This large number of nickel aggregates resulted in the electrical switching property under the pressure that was applied (see Figure 4.1).

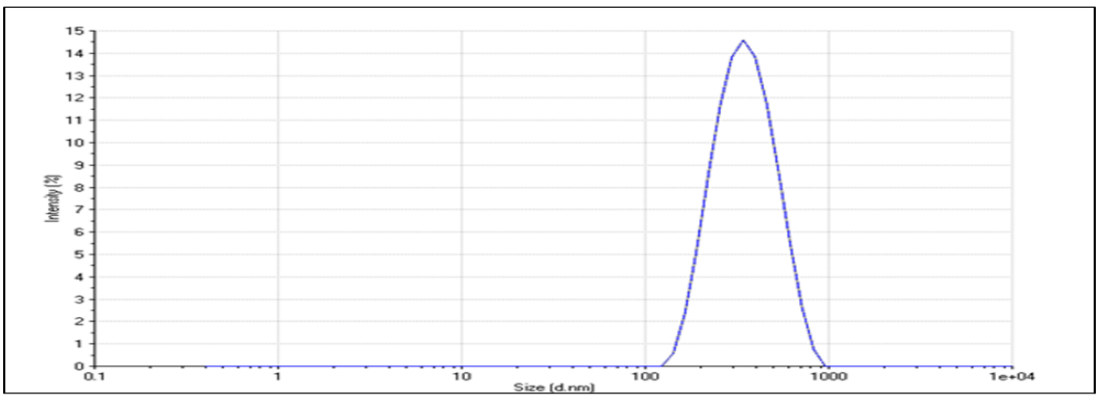

Figure 4.8 Particle size distribution graph of the nickel particles and the TiO_2 in the PSE2-based binder

Figure 4.9 displays size distribution of the nickel particles and the TiO_2 particles dispersed in the PIP-based binder. It indicates that the bulk of the spherical particle aggregates lie in a size range between 1 µm and 100 µm, which is consistent

with the particle size range of pure nickel powder. This means that the PIP polymer matrix separated and bound well nickel particles from each other, which resulted in the better insulating property under no pressure was applied and the more like electrically sensing behaviour under the pressure was applied (see Figure 4.9).

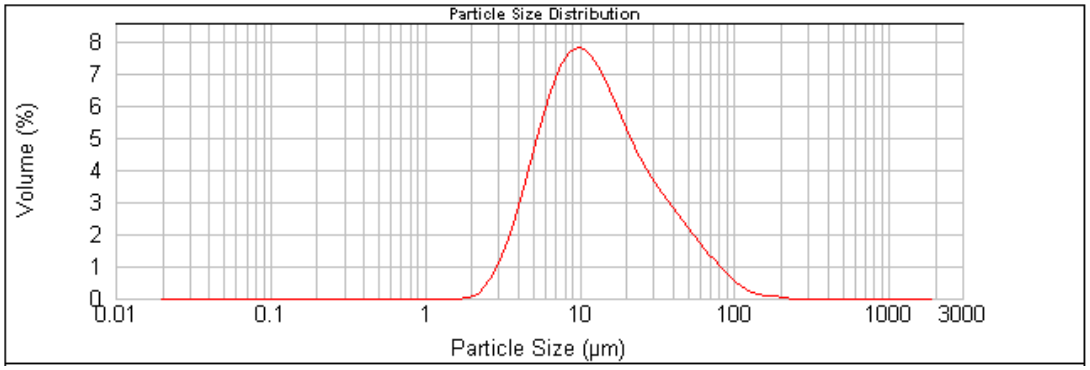

Figure 4.9 Particle size distribution graph of the nickel particles and the TiO_2 in the PIP-based binder

4.2.4 Zeta potential measurements for the PSE1, the PSE2 and the PIP-based inks

The stability of the pigments in different polymeric binders can be evaluated by examining the zeta potential analysis. Figure 4.10 shows the zeta potential measurements for the nickel particles and the TiO_2 particles dispersing in each of the PSE1, the PSE2 and the PIP polymeric binders. The pigments in the PIP-based binder has the greatest absolute zeta potential value, *i.e.* (-35.7 + 5.13) mV, indicates that the nickel particles and the TiO_2 particles formed the most stable suspension comparing to the other two. The pigments in the PSE2-based binder formed the least stable suspension (*i.e.* -23.6 + 4.82) mV. This stability results matched that obtained for the particle size distributions of the samples. The most stable suspension, PIP9 ink, caused the particle well separated from each other (see Figure 4.9), however, the least stable suspension, PSE2-9 ink, caused a large number of pigment particle aggregated together (see Figure 4.8).

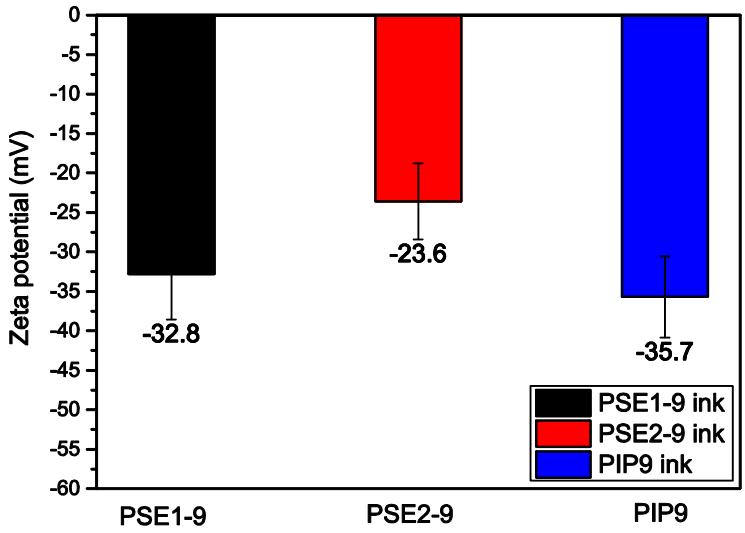

Figure 4.10 Zeta potential graphs for the PSE1-9, the PSE2-9 and the PIP9 inks

4.2.5 Thermal stability of the PSE1, the PSE2 and the PIP-based inks

Figure 4.11 shows the decomposition arsing during the TGA induced breakdown of the polymeric binders, the PSE1, the PSE2 and the PIP. Differences in the thermal stability can be seen between the three polymeric binders. The extent to which the PIP binder holds onto water was the greatest within the three binders. The overall thermal reactivity of the binders is similar. In the TGA profile of each binder, each thermogram indicates a curve which can be correlated to loss of water as the heating temperature was increasing up to around 155 °C, 130 °C and 175 °C for the PSE1 binder, the PSE2 binder and the PIP binder, respectively. This is then followed by any self-crosslinking reactions that take up to around 280 °C, 320 °C and 350 °C for the PSE1 binder, the PSE2 binder and the PIP binder, respectively. In the TGA profile of each binder, it is shown that the PIP binder has the greatest affinity to solvent components within the three binders. It was reported that the water molecules in a polymer could significantly reduce the breakdown of the electric field as the water molecules penetrate in the free space of the polymer chain [9, 10]. However, the PIP-based ink that has the greatest affinity to water did not behave as the most conducting printed film (see Figure 4.1) compared to the PSE1 and the PSE2 ones. This electrical performance implies that the size distribution of the nickel particles is the more significant factor than the extent of the water of the film impact the electrical property of a printed film. The decomposition curves, in Figure

4.11, for each polymeric binder suggest that the properties of each ink can vary with the temperature of drying or curing. An increase in the temperature can accelerate the polymeric binders curing and decomposing.

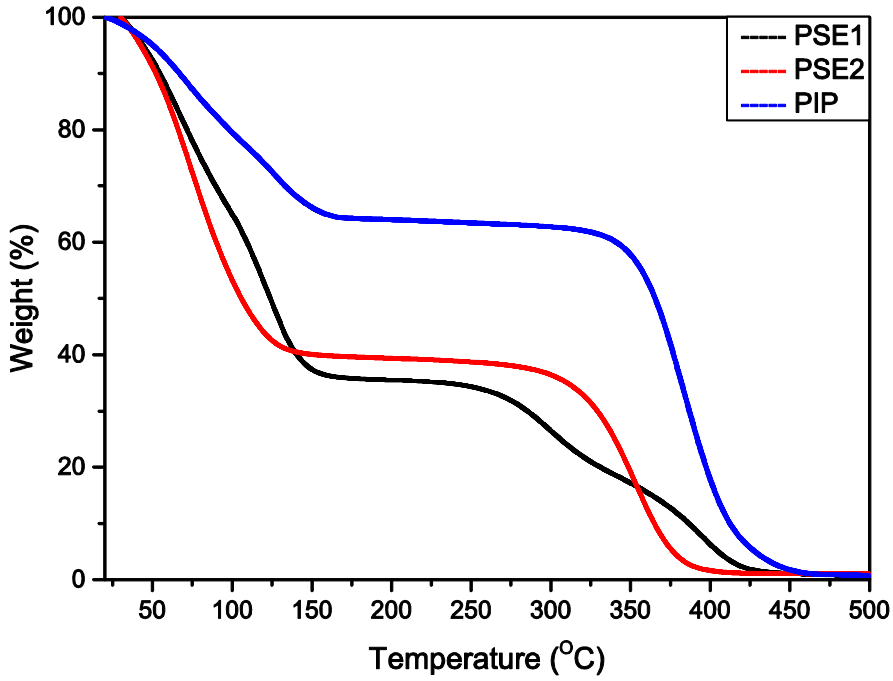

Figure 4.11 TGA analysis for PSE1, PSE2 and PIP polymeric binders, in which each binder sample was heated for 50 min from 0 °C to 500 °C

Table 4-2 Solid content for the each individual binder, the PSE1, the PSE2 and the PIP from TGA analysis

	PSE1 binder	*PSE2 binder*	*PIP binder*
Solid Content	*35.18%*	*38.98%*	*63.98%*
	at 155.04 °C	*at 133.34 °C*	*at 175.02 °C*

4.2.6 Viscosity/Flow characteristics of the PSE1, the PSE2 and the PIP-based binders

The flow patterns of the binder materials under highly controlled condictions relating to the applied shear stress, shear strain rate and temperature are important to monitor the rheological characteristics of the inks. Figure 4.12 shows that the various polymeric binders that were studied exhibited a shear thinning flow

character at 25 °C. The viscosities of the binders decrease with an increase in the shear rate. The shear thinning behaviour of the inks was more pronounced between shear rate values of 1 s^{-1} and 1000 s^{-1}. The value of the viscosity and the extent of shear thinning of one polymeric binder, at a particular value of shear rate, are different from another binder because of differences in the characteristics of the polymers.

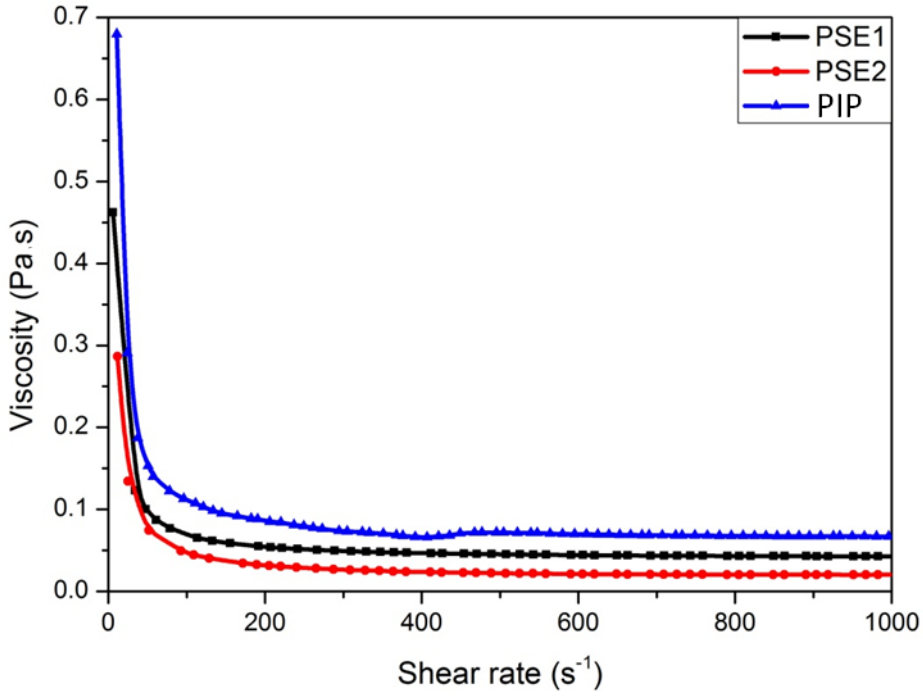

Figure 4.12 The relationship of viscosity and shear rate for each individual binder, the PSE1, the PSE2 and the PIP, at 25 °C

Figure 4.13 shows the result of the study of the viscosity *vs.* temperature relationships for the PSE1 ink, the PSE2 ink and the PIP ink, which indicates that the viscosity of the inks depend on temperature. It is shown that the curing of the inks commenced when the temperature reached approximately 60 °C. In the meantime, the formulation of the nickel particle aggregates and the TiO_2 particle aggregates was favoured when the temperature increased up to 60 °C. This therefore increases the resistance of the inks to flow and leads to a significant increase in viscosity. The overall data imply that during application of the inks, careful consideration needs to be given to the temperature at which the process is being conducted. If an undesirable change in viscosity occurs during application,

the ease of application and the overall properties of the inks can significantly be affected.

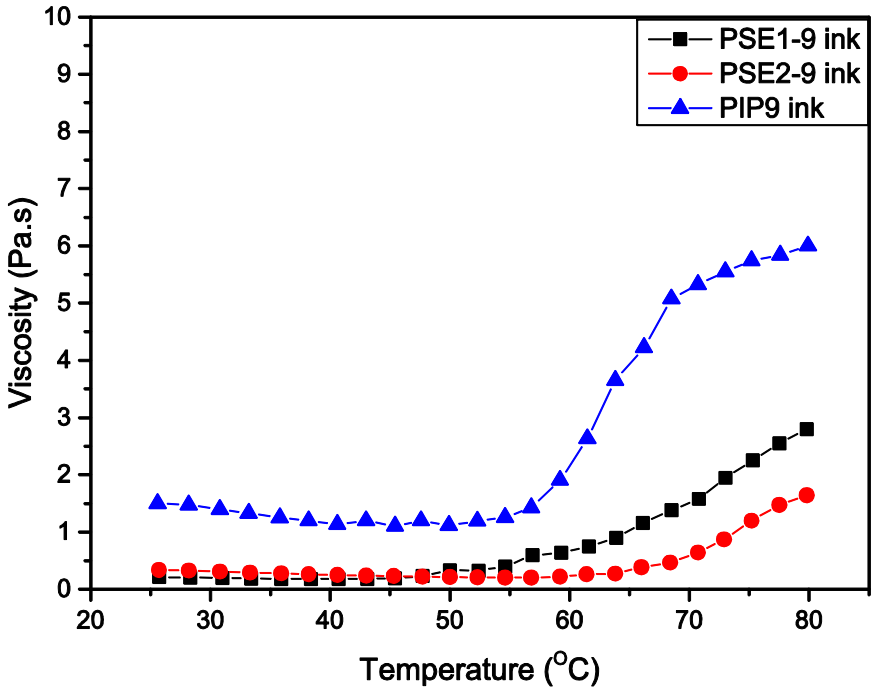

Figure 4.13 Viscosity vs. temperature profile of the different polymer based ink formulations

4.2.7 Mechanical properties of the PSE1, the PSE2 and the PIP-based printed films

It is known that the degrees of cross-linking can be used to evaluate whether the polymer is soft or rigid. The higher degree of the cross-linking network, the stiffer of the equivalent non-crosslinked polymer would be. On the contrary, the lower degree of the cross-linking network, the softer of the polymer is.

It is known that the variation of electrical resistance for a printed film under uniaxial compression is owing to the destruction of percolation channels of the Ni-Polymer composite. Therefore, deformation of elastic polymer matrix perpendicular in the applied force occurred [11]. Elastic modulus is a significant parameter to investigate a compression of a printed film. The elastic modulus values of each individual polymeric binder, the PSE1, the PSE2 and the PIP, and their printed films are shown in Figure 4.14 and Figure 4.15. The elastic modulus measurements for the PSE1, the PSE2 and the PIP printed films are dramatically increased by the

addition of the nickel powder and the TiO_2 powder. This is because the stiffer nickel filler and TiO_2 are able to reinforce the strength of the composite.

It is shown that the PIP binder is the most elastic polymer than the PSE1 and the PSE2 polymer (see Figure 4.14), which has the lowest elastic modulus value. The PIP polymer has a noncrystalline characteristic at room temperature, which leads to the low hardness and tensile strength [12]. It was reported that for the polysiloxane-based composites, the higher content of silanol group, the larger cohesive force of polymers, which resulted in an agglomeration of metal fillers [8]. In this case, the nickel particles and the TiO_2 particles in PSE2-based binder formed bulk aggregates owing to its larger silanol content, compared with those in PSE1-based binder (see Figure 4.2 and Figure 4.3). This then resulted in a lower elastic modulus of the PSE1 polymer than that of the PSE2 polymer.

As a consequence, elastic modulus of a polymer matrix for Ni-polymer composite has an important impact on the particle size distribution and the morphology of a printed film.

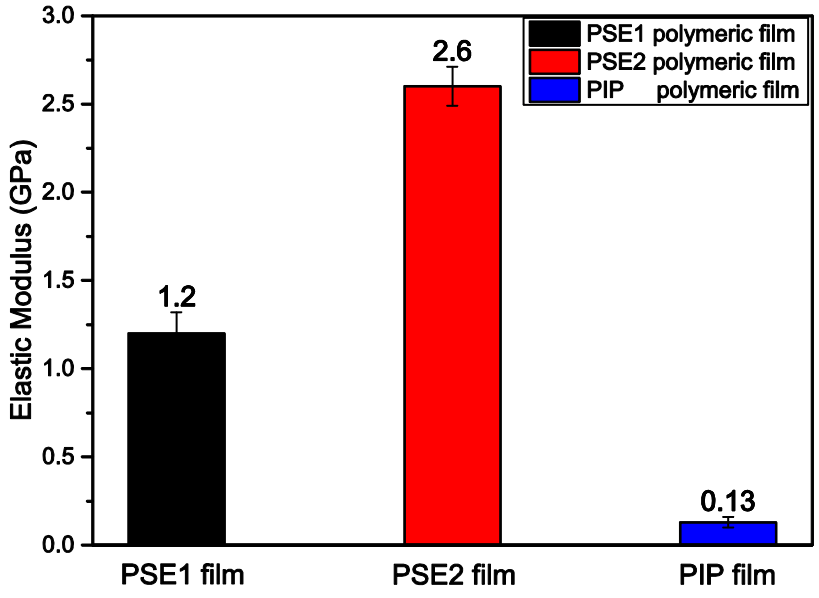

Figure 4.14 Elastic modulus for the PSE1-9 binder film, the PSE2-9 binder film and the PIP9 binder film

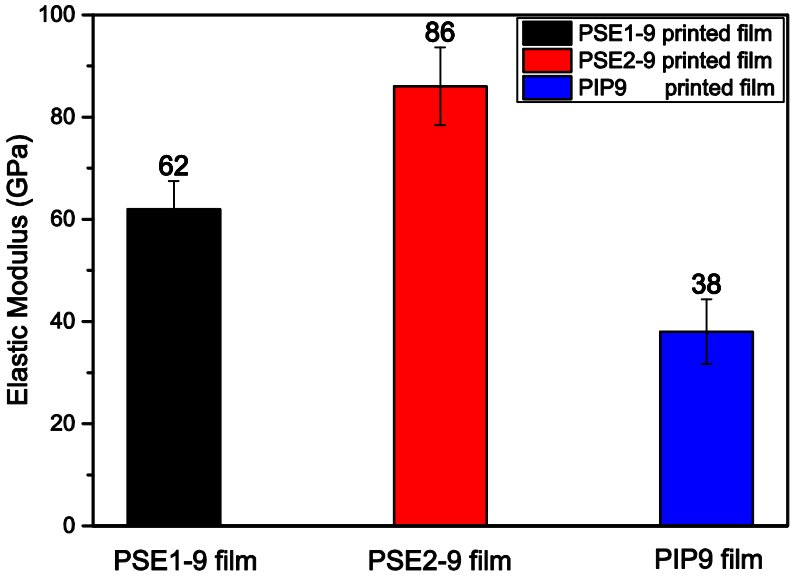

Figure 4.15 Elastic modulus for the PSE1-9 printed film, the PSE2-9 printed film and the PIP9 printed film

4.2.8 Conclusions

Ink formulations and printed films were successfully developed based on the filling of the nickel powder in the highly elastic polymeric matrix. The choice of polymeric binder has a significant effect on the rheological properties, the mechanical properties and the thermal properties of the inks, which resulted in the morphologies and the particle size distributions of the printed films.

The variation in electrical resistance was a function of the applied force of PSE1, PSE2 and PIP-based printed films. The printed films have exhibited pressure electrically sensitive properties as a QTC commercial material. The PIP-based printed film possessed insulating property behaviour at large external force was because the insulating polymer matrix was better binding better with nickel fillers than the PSE1 and the PSE2-based printed films. The PSE1 and the PSE2-based printed films behaved more like electrically switching properties. The PIP-based printed film behaved controlled electrically sensing properties. The distinct property for each printed film is owing to the nature of the used binding polymers, *i.e.* the mechanical property, the thermal property and the rheological property.

4.3 Modelling the electrical properties response to the external force for QTC printed films

Modelling the electrical properties response to the external force for the QTC printed film is focussed on the deformation of microstructure and properties of the Ni-polymer composite. From the previous results and discussion of the printed films, it is found that a conductive Ni-polymer composite can be analysed and affected by Ni diameter (r), Ni shape (s), Ni position (p), Ni conductivity (c) and flexibility of polymer (f). Thus, electrical resistance (R_f) of a printed film is a function of their parameters, $R_f = f$ (r, s, p, c, f). Therefore, the resistance regarding to strain is termed as $R_s = f$ (r_s, s_s, p_s, c_s, f_s). In order to address the model of the deformation of strain, a) a conductive model to describe the resistance of the Ni-polymer composite before and after a compression is employed, (b) a material model to convey the original and the deformed internal structures of the Ni-polymer composite [13], will be detailed in following sections.

4.3.1 Conductive models for a printed film

4.3.1.1 Percolation theory

Percolation theory was used to describe the physical properties of composite materials, such as electrical resistivity, permeabilities of diphasic material and thermal conductivity. The percolation theory illustrates the region in which the conductivity performance changes very quickly.

The percolation threshold describes the concentration of filler particles at which minimum value can achieve the behaviour with rapidly varying conductivity [14]. The electrical conductivity increases rapidly within a limited range of metal filler content. And this metal filler content is the percolation threshold of the material. When the metal filler content in a composite is low regarding to QTC inks, the conductive particles are either as isolated or aggregated and the polymeric matrix is nearly insulating. With an increase in the concentration of metal fillers, the isolated particles are more likely to be as clusters, resulting in a change from insulating to conductive of a composite. This critical concentration, V_c, is the percolation threshold of the composite. It is suggested that a thermodynamic composite is at the maximum sensitivity, which is the percolation threshold, under

the phase transition [15]. In order to determine the percolation threshold of a composite, a model of fixed positions of metal filler particles is stimulated.

Figure 4.16 shows the schematic view of nickel particles dispersed in a polymeric matrix. When the distance between nickel particles, d=0, the nickel spherical are physically contacted. In this case, a contacting conduction is involved. When d>0, the nickel particles in a polymeric matrix involves conduction via tunnelling. The printed film does not behave as electrically conductive when no pressure is applied. This means that the contacting conduction is not dominant in the generation of conductivity [16]. A nickel particle with diameter, d, surrounded by polymeric matrix, which resulted in a Ni-polymer composite with a diameter, D. The volume fraction of nickel powder in a printed film can be expressed as follows [16].

$$c = \frac{V_D * n_n}{V}$$

Equation 4-1 Volume fraction of the nickel powder in a printed film, in which V_D, n_n and V represent the volume of a Ni-polymer composite, the number of Ni-polymer composite and the total volume of a printed film, respectively

$$V_D = \frac{4}{3}\pi(\frac{D}{2})^3$$

$$n_n = \frac{V_n}{V_R} = \frac{V_n}{\frac{4}{3}\pi(\frac{r}{2})^3}$$

Equation 4-2 Volume of a Ni-polymer composite and the number of Ni-polymer composites in a printed film with volume V. V_R and V_n are the volume of a Ni-polymer composite with a diameter r and the total volume of Ni-polymer composites in a printed film

Then the Equation 4-1 and Equation 4-2 can be simplified as,

$$\frac{D}{r} = \sqrt[3]{\frac{V * c}{V_n}}$$

$$d = D - r$$

Therefore,

$$d = \left(\sqrt[3]{\frac{V * c}{V_n}} - 1 \right) * r$$

Thus,

$$\Delta d = d - d_0 = \left(\sqrt[3]{\frac{V * c}{V_n}} - \sqrt[3]{\frac{V_0 * c}{V_n}} \right) * r$$

Equation 4-3 The relationship of the distance between Ni-polymer composites and the volume change, in which the total volume fraction of the Ni-polymer composites, Vn, is a constant

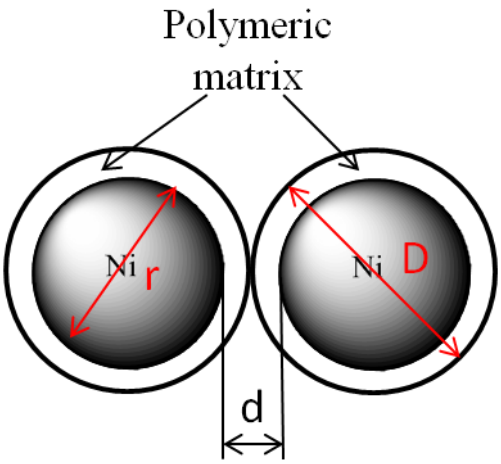

Figure 4.16 Schematic view of nickel particles in a polymeric matrix, in which r, D, and d represent the nickel diameter, Ni-polymer composite diameter and the distance between nickel particles, respectively

4.3.2 Response of electrical properties to the external compression

The electrical resistance of a printed film is a sum of the resistance of the conductive fillers and the resistance of the polymeric matrix. When the nickel particles are far away from each other, the printed film behaves an electrically insulator. When the

nickel particles are close enough, tunnelling conduction of the conductive fillers starts to occur. The dimensions and shapes of the Ni-polymer composite system will be varied under the external compression. The tunnelling current between two adjacent metal fillers at low applied voltage was proposed by Simmons [17], that is:

$$I = \frac{3a^2(2m\varphi)^{\frac{1}{2}}}{2d}\left(\frac{e}{h}\right)^2 V\, e^{\left(-4\pi d\sqrt{\frac{2m\varphi}{h^2}}\right)}$$

Equation 4-4 expresses the tunnelling current between two adjacent metal fillers at low applied voltage, where I is the current, a^2 is the effective cross-sectional area, m and e are the electron mass and charge mass, φ and d are the height and width of the potential barrier between two adjacent metal particles, h is the Plank's constant [17]

The electrical resistance of a printed film, R, have been derived from Zhang et al [18],

$$R = \frac{L}{S}\left(\frac{4\pi hd}{3a^2\gamma e^2}\right)e^{(2\gamma d)}$$

$$\gamma = 2\pi\sqrt{\frac{2m\varphi}{h^2}}$$

Equation 4-5 Electrical resistance of Ni-polymer composite, where L is the number of particles forming one tunnelling path, S is the total number of paths in a sample

The thickness and the average distance between two adjacent particles of a printed film will be reduced when an external compression is applied. Therefore, the value of resistance at a given pressure R can be derived [19],

$$R = R_0\frac{d_p}{d_0}e^{(2\gamma(d_p - d_0))}$$

$$d_p = d_0(1-\varepsilon) = d_0\left(1 - \frac{F}{AG}\right)$$

Equation 4-6 The relationship between the resistance of a composite and the applied compression, where R_0 is the original resistance at unstressed state, d_p and d_0 are the thickness of the interparticle insulating polymer under pressure and at unstressed state, respectively, ε is the elastic modulus of the polymeric matrix, F is the applied external force, A is the original cross-section area when the force is applied, G is the polymer compressive modulus

Therefore,

$$R = R_0\left(1 - \frac{F}{AG}\right)e^{(-2\gamma d_0 \frac{F}{AG})}$$

Equation 4-7 The derivatives from Equation 4-6 [19]

Lantada et al [20] has proposed a model for the electrical behaviour of QTC materials, which can also be employed to the other metal-polymer composite, therefore,

$$R(p,t,T) = R_0\sqrt{(\frac{T_0}{T})}$$

$$T_0 = \frac{1}{(1 + \frac{\varphi_0^2(\sinh(\gamma_0 d_0))^2}{4E(\varphi_0 - E)})}$$

$$\gamma_0 = 2\pi\sqrt{\frac{2m(\varphi_0 - E)}{h^2}}$$

Equation 4-8 The derivatives of the resistance of a Ni-polymer composite with respect to the ratio of the barrier, in which φ_0 is the initial height of the potential barrier and E is the energy of the electrons, T0 is the barrier transmission coefficient at the initial state.

Hence, the combination of Equation 4-7 and Equation 4-8 will be derived as [19],

$$R = R_0(\frac{1 + \frac{\varphi_0^2(\sinh(2\pi d\sqrt{\frac{2m(\varphi_0 - E)}{h^2}}))^2}{4E(\varphi_0 - E)}}{1 + \frac{\varphi_0^2(\sinh(2\pi d_0\sqrt{\frac{2m(\varphi_0 - E)}{h^2}}))^2}{4E(\varphi_0 - E)}})^2$$

$$\varphi = \varphi_0\left(1 - \frac{F}{AG}\right)$$

$$d = d_0\left(1 - \frac{F}{AG}\right)$$

Equation 4-9 The electrical resistance of a composite system under uniaxial compression

The nickel particles are spiky near-spherical. It is assumed that all the nickel particles are same sized spheres and packed in a cubic lattice [21].

$$d_0 = D(\sqrt[3]{\frac{\pi}{6\nu_f}} - 1)$$

Equation 4-10 The width of the potential barrier at the initial state correlates with the filler volume concentration

It was shown that the nickel particles were randomly distributed and not perfectly aligned on planes in the Ni-polymer composite. Therefore, the nickel particles were rearranged when a perpendicular force was applied onto the composite, which caused creations of extra tunnelling pathways throughout the sample. Under such a circumstance, the resistance of the printed film decreases exponentially with the external force, which follows the tunnelling conduction mechanism [19].

It is assumed that the variation of the thickness of the insulating polymer matrix between the particles depends only on the perpendicular direction of deformation on the composite sample. Hence, the width of the potential barriers along the perpendicular applied force can be derived as:

$$\boldsymbol{d_z = d_0(1+\varepsilon) = d_0\left(1+\frac{F}{AG}\right)}$$

$$\boldsymbol{d_{x.y} = \frac{d_0}{\sqrt{1+\varepsilon}} = \frac{d_0}{\sqrt{1+\frac{F}{AG}}}}$$

Equation 4-11 The derivation of the width of the potential barriers along the direction of the applied force and on the perpendicular ones (x,y), where ε is the tensile strain.

Therefore, combining Equation 4-6 and Equation 4-11, the resistance of a printed film can be expressed as below [19],

$$\boldsymbol{R = \frac{R_0}{2\sqrt{1+\frac{F}{AG}}} e^{(-2\gamma \frac{\sqrt{1+\frac{F}{AG}}-1}{\sqrt{1+\frac{F}{AG}}})}}$$

Equation 4-12 Theoretical model for the relationship between the resistance of the Ni-polymer composite and the applied force

The relationship between the electrical resistance and its corresponding applied force was fitted exponentially by Equation 4-12, as shown in Figure 4.17. It is shown that the resistance of the printed films, PSE1-9, PSE2-9 and PIP9, exponentially decreased with increasing applied force.

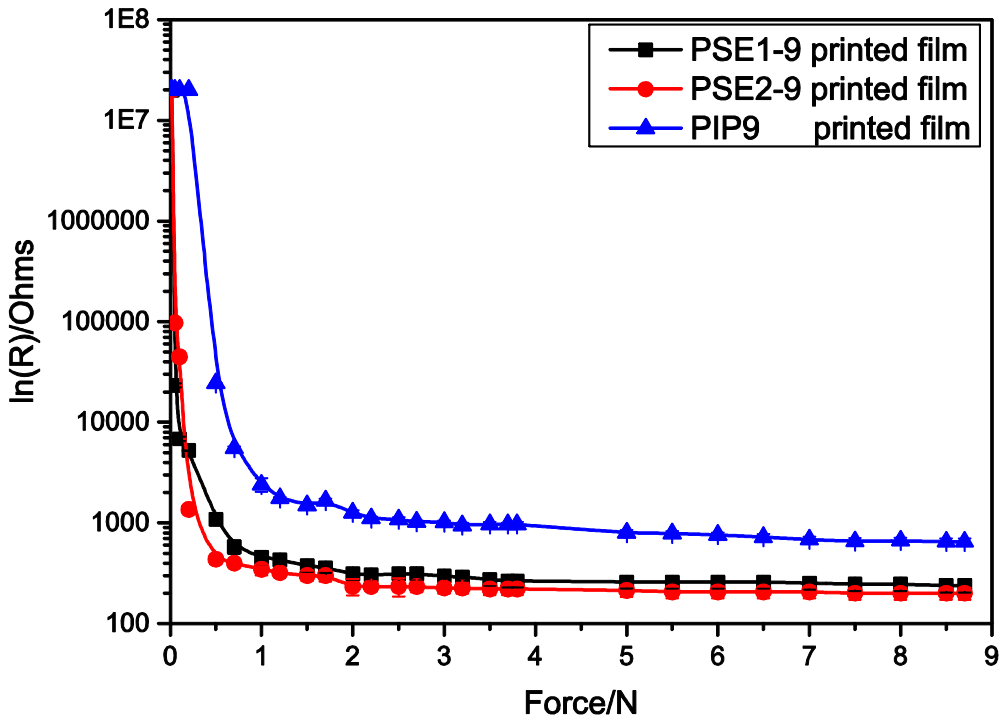

Figure 4.17 The relationship between the electrical resistance and applied force for the PSE1-9 film, the PSE2-9 film and the PIP9 film

The experimental results were:

$R_0 = 2\times10^7\ \Omega$,

$A = 4\pi*(0.5/2cm)^2 = 7.85\times10^{-5}m^2$,

$\varepsilon_{PSE1\text{-}9} = (62+5.8)$ GPa

$\varepsilon_{PSE2\text{-}9} = (86+6.7)$ GPa

$\varepsilon_{PIP9} = (38+5.6)$ GPa

In summary, the theoretical model arising from Equation 4-12 fitted well for the electrical-force profiles of the PSE1, the PSE2 and PIP-based printed films.

Reference

1. Knite, M., et al., *Polyisoprene—multi-wall carbon nanotube composites for sensing strain.* Materials Science and Engineering: C, 2007. **27**(5): p. 1125-1128.
2. Hou, Y., et al., *Size-controlled synthesis of nickel nanoparticles.* Applied Surface Science, 2005. **241**(1): p. 218-222.
3. Pathak, S., A. Sharma, and A. Khanna, *Value addition to waterborne polyurethane resin by silicone modification for developing high performance coating on aluminum alloy.* Progress in organic coatings, 2009. **65**(2): p. 206-216.
4. Sharifi, M., et al., *Toughened epoxy polymers via rearrangement of network topology.* Journal of Materials Chemistry A, 2014. **2**(38): p. 16071-16082.
5. Prabu, A.A. and M. Alagar, *Mechanical and thermal studies of intercross-linked networks based on siliconized polyurethane-epoxy/unsaturated polyester coatings.* Progress in organic coatings, 2004. **49**(3): p. 236-243.
6. Zhu, Q., et al., *Improving the lithium storage properties of Fe 2 O 3@ C nanoparticles by superoleophilic and superhydrophobic polysiloxane coatings.* Journal of Materials Chemistry, 2012. **22**(31): p. 15894-15900.
7. Yu, J., et al., *A MWCNT/polyisoprene composite reinforced by an effective load transfer reflected in the extent of polymer coating.* Macromolecules, 2012. **45**(6): p. 2841-2849.
8. Ono, S., et al., *Structure development in silica-filled rubber composites.* Polymer International, 1999. **48**(10): p. 1035-1041.
9. Bernal, A., I. Kuritka, and P. Saha, *Poly (vinyl alcohol)-poly (vinyl pyrrolidone) blends: Preparation and characterization for a prospective medical application.* Mathematical Methods and Techniques in Engineering and Environmental Science, 2014: **32**(4), p. 978-1.
10. Wang, Q., Z. Suo, and X. Zhao, *Bursting drops in solid dielectrics caused by high voltages.* Nature communications, 2012. **3**: p. 1157.
11. Knite, M., et al., *Polyisoprene-carbon black nanocomposites as tensile strain and pressure sensor materials.* Sensors and Actuators A: Physical, 2004. **110**(1): p. 142-149.
12. Kent, E. and F. Swinney, *Properties and applications of trans-1, 4-polyisoprene.* Industrial & Engineering Chemistry Product Research and Development, 1966. **5**(2): p. 134-138.
13. Pham, G.T., *Characterization and modeling of piezo-resistive properties of carbon nanotube-based conductive polymer composites*. 2008: ProQuest.
14. McLachlan, D.S., M. Blaszkiewicz, and R.E. Newnham, *Electrical Resistivity of Composites.* Journal of the American Ceramic Society, 1990. **73**(8): p. 2187-2203.
15. Knite, M., M. Ozolinsh, and A. Sternberg, *Electrooptical and electrostrictive PLZT ceramics light modulators for infrared.* Ferroelectrics, 1989. **94**(1): p. 67-72.
16. Han, B., B. Han, and X. Yu, *Experimental study on the contribution of the quantum tunneling effect to the improvement of the conductivity and piezoresistivity of a nickel powder-filled cement-based composite.* Smart Materials and Structures, 2009. **18**(6): p. 065007.

17. Simmons, J.G., *Electric tunnel effect between dissimilar electrodes separated by a thin insulating film.* Journal of Applied Physics, 1963. **34**(9): p. 2581-2590.
18. Zhang, X.W., et al., *Time dependence of piezoresistance for the conductor-filled polymer composites.* Journal of Polymer Science Part B: Polymer Physics, 2000. **38**(21): p. 2739-2749.
19. Stassi, S. and G. Canavese, *Spiky nanostructured metal particles as filler of polymeric composites showing tunable electrical conductivity.* Journal of Polymer Science Part B: Polymer Physics, 2012. **50**(14): p. 984-992.
20. Lantada, A.D., et al., *Quantum tunnelling composites: Characterisation and modelling to promote their applications as sensors.* Sensors and Actuators A: Physical, 2010. **164**(1): p. 46-57.
21. Wu, S., *Phase structure and adhesion in polymer blends: a criterion for rubber toughening.* Polymer, 1985. **26**(12): p. 1855-1863.

Khadka, P., J. Ro, H. Kim, I. Kim, J.T. Kim, H. Kim, J.M. Cho, G. Yun, and J. Lee, *Pharmaceutical particle technologies: An approach to improve drug solubility, dissolution and bioavailability.* asian journal of pharmaceutical sciences, 2014. **9**(6): p. 304-316.

Chapter 5. Preparation and characterisation of Ni, Cu, Fe, Zn and bronze-based inks

In this chapter, the suitability of four metal powders and one alloy powder for use in composite inks was investigated on the basis of the contribution by each metallic powder to the formulation, printability, rheology, conductivity and thermal properties of inks. The metal powders were characterised for their particle shape and morphology. The different powders were used individually to form a composite ink using PVP and PVP-S-based polymeric binders. The effects of the binder chemistry, the composition of the inks and the application conditions on the rheological, electrical, thermal properties of the inks were investigated. In particular, electrical-mechanical properties of different metallic powder-based ink films were laid emphasis on looking into.

Experimental procedures relevant to the work described in this chapter have been detailed in Chapter 2.

5.1 Materials

The polymeric binders poly(vinyl pyrrolidone) (PVP) and poly(vinylpyrrolidone-*co*-styrene) (PVP-S) were used in the ink formulations. The chemical properties of two binders were detailed in Chapter 2.

The substrate used to print each metallic powder-based ink was PET sheet that has detailed in Chapter 2. Relevant information on the different metallic powder samples is listed in Table 5-1.

5.2 Ink formulations

All of the inks used in this study were containing 50 wt% of the specified metallic powder and 50 wt% of the specified polymeric binder, PVP and PVP-S. Each ink was prepared following the specific procedure as detailed in Chapter 2. The ink formulation in each ink was followed the ratio 1:1 of metal powder to polymeric binder. The ink formulation here designed different from those in Chapter 3 and Chapter 4 was because the inks containing Cu and Bronze powders were too viscous to fabricate the inks. In order to compare different metal powder-based inks on the

same condition, the formulations were reduced regarding to 70 wt of Ni and 30 wt% of binder.

Table 5-1 Information on the different metallic powders used in formulations

Powder	*Supplier*	*Nature and characteristic*
Ni	*Vale Inco Europe Ltd,* *Swansea, West Glamorgan*	*This has a fine, spiky characteristic, which has electrical conductivity value of 14.3 Siemens/m. The particle size distribution ranges from 1 to 100 µm. Such nickel powders rarely become surface oxidised [4].*
Fe	*Sigma Aldrich Ltd, Gillingham, Dorset, UK*	*This iron powder has a fine characteristic and light grey colour, which has electrical conductivity value of 10.1 Siemens/m.*
Cu	*Echart UK Ltd, Unit C The Sidings Station Road Ampthill, Bedforeshirem, UK*	*This is a flaky material that was developed to be resistant to oxidation. This has electrical conductivity value of 58.5 Siemens/m.*
Zn	*Sigma Aldrich Ltd, Gillingham, Dorset, UK*	*This has non-flaky, non-spiky powder that is coarse in nature. This has electrical conductivity value of 16.6 Siemens/m.*
Bronze	*Echart UK Ltd, Unit C The Sidings Station Road Ampthill, Bedforeshirem, UK*	*This is a flaky powder, oxidation resistant which is heat treated. This has electrical conductivity value of 7.4 Siemens/m.*

5.3 Results and discussion

5.3.1 Morphology of the metal powders

The morphologies for the metallic powder particles are shown in Figure 5.1. Obviously, the nature of each powder particles and particle distribution is different from that exhibited by the others. The Ni powder can be seen to have spiky characteristic surface. The Fe powder can be considered to have "rod-like" spiky character. The Cu powder and the bronze powder are shown as flaky shape. In contrast to all the other metallic powders, the Zn particles are spherical. With these major particle differences between the powders, it can therefore be expected that shape effects and particle morphologies will dominate the flow characteristics of the various inks. Thus, for each ink, the rotation, transition, movement and alignment of the particles can govern its rheology. Furthermore, it was reported that the pigment shapes have a significant effect on the flexibility and durability of coatings, because they can determine how close the particles stay and the pathways of a crack propagating [2]. From the particle morphologies and particle shapes of the metallic powder, it could be assumed that the near-spherical spiky like nickel particles would have the most effective correlation with the polymer due to their large porosity and high roughness. The Cu powder and the bronze powder with flaky shapes would have the least correlation with the polymer owing to their limited and flat surface areas.

5.3.2 Rheological characteristics of the ink

The inks require suitable viscosity values and good rheological characteristics. Therefore, it is significant to monitor the flow patterns of the ink materials under highly controlled conditions relating to the applied shear stress, shear strain rate and temperature. Figure 5.2 and Figure 5.3 show that the various ink formulations that were studied exhibited a shear thinning flow character at 25 °C. The viscosities of the inks decrease with an increase in the shear rate. The shear thinning behaviour of the inks was more pronounced between shear rate values of 1 s^{-1} and 1000 s^{-1}. The value of the viscosity and the extent of shear thinning of one ink formulation, at a particular value of shear rate, are different from another ink because of differences

in morphology and distribution of the particulate metallic materials in the ink samples.

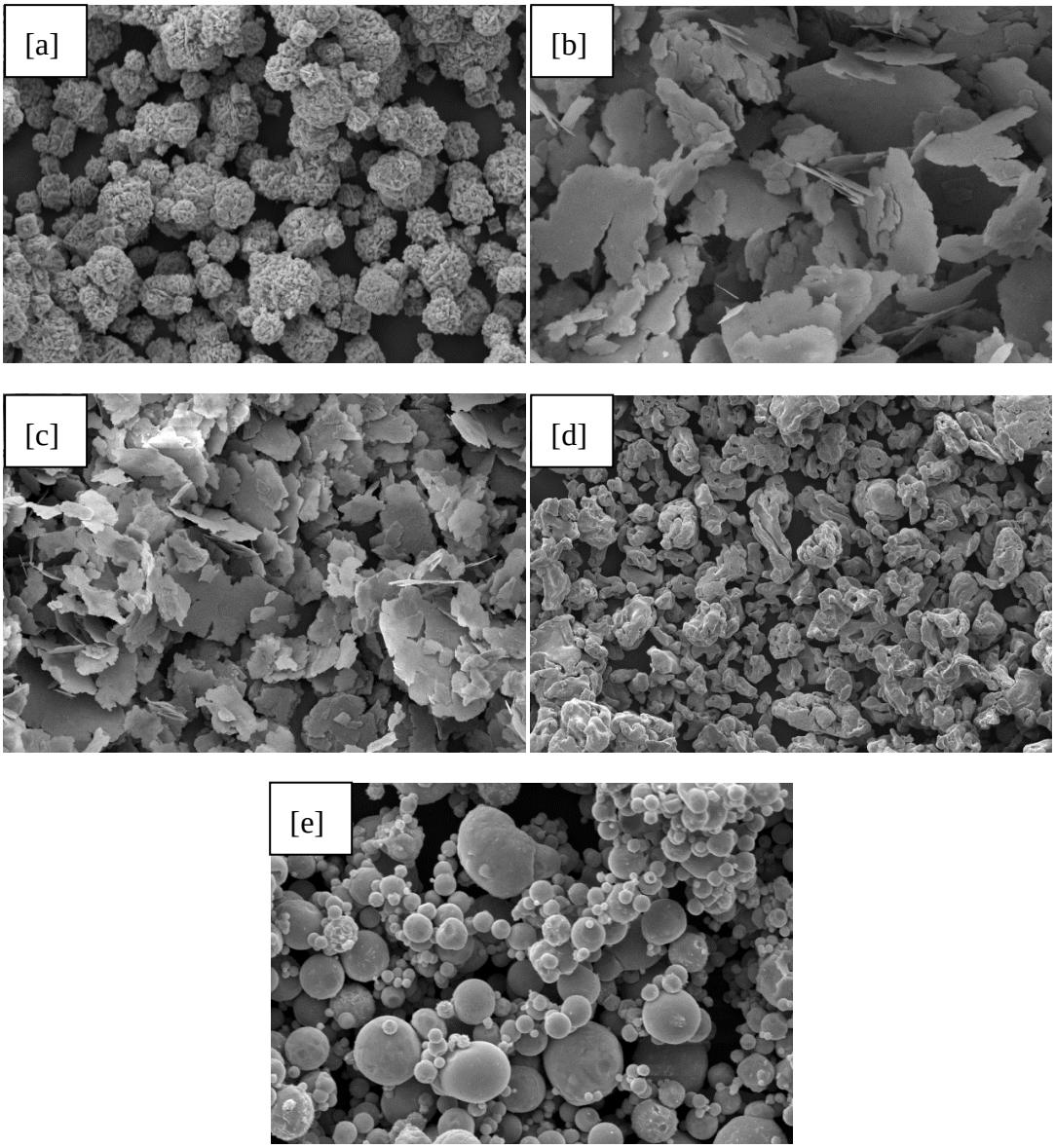

Figure 5.1 Morphologies of [a] Ni powder, [b] Cu powder, [c] Bronze powder, [d] Fe powder and [e] Zn powder under scanning electron microscope

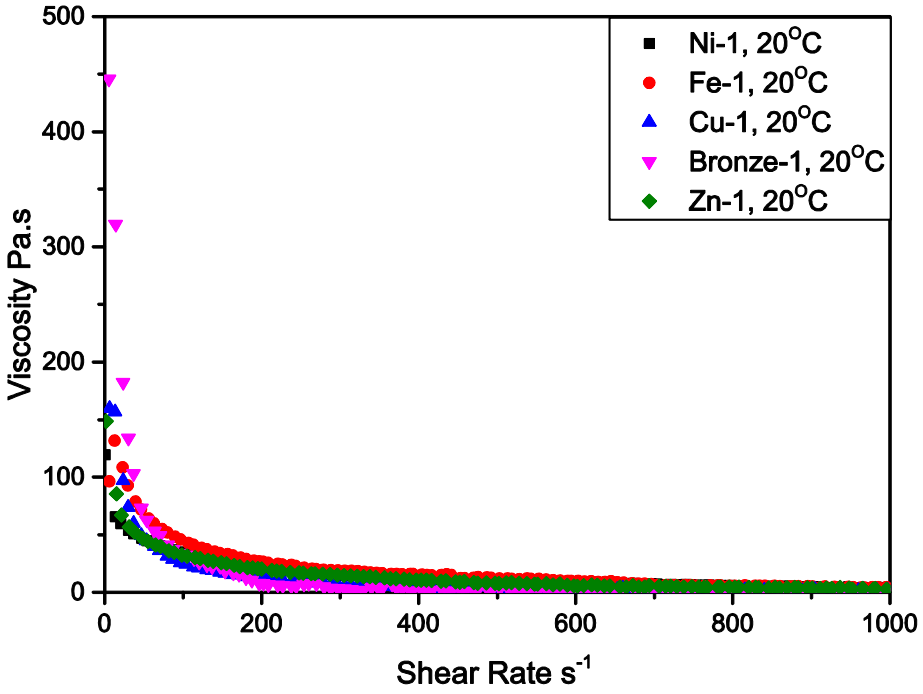

Figure 5.2 Rheological behaviour of viscosity and shear rate for the ink formulations containing PVP-based binder

Figure 5.3 and Figure 5.4 show the results of the study of the viscosity and temperature relationships, which indicates that the viscosity of the inks depend on temperature. The viscosity decreases with an increase in the heating temperature. Therefore, polymer section chains gliding pass one another more easily as the thermal energy is increased, through an increase in temperature. It is possible that the bronze powder-based ink shows a distinct viscosity *vs.* temperature behaviour because as the temperature was increased, it was quicker for its water component to be lost and for the binder polymer to build structure leading to an increase in viscosity.

Figure 5.3 shows a different pattern of viscosity *vs*. temperature compared with Figure 5.4. Apparently, this difference arises because the two sets of inks contained different polymeric binders. In the inks contain the PVP-S, as the heating temperature reached 60 °C, curing of the inks commenced. Also, it is possible that as the temperature of the ink formulations was increased up to 60 °C, the formulation of metallic powder aggregates was favoured. This therefore increases the resistance of the inks to flow and leads to a significant increase in viscosity. The overall data shows that during application of the inks, careful consideration needs to

be given to the temperature at which the process is being conducted. If an undesirable change in viscosity occurs during application, the ease of application and overall properties of the inks can significantly be affected.

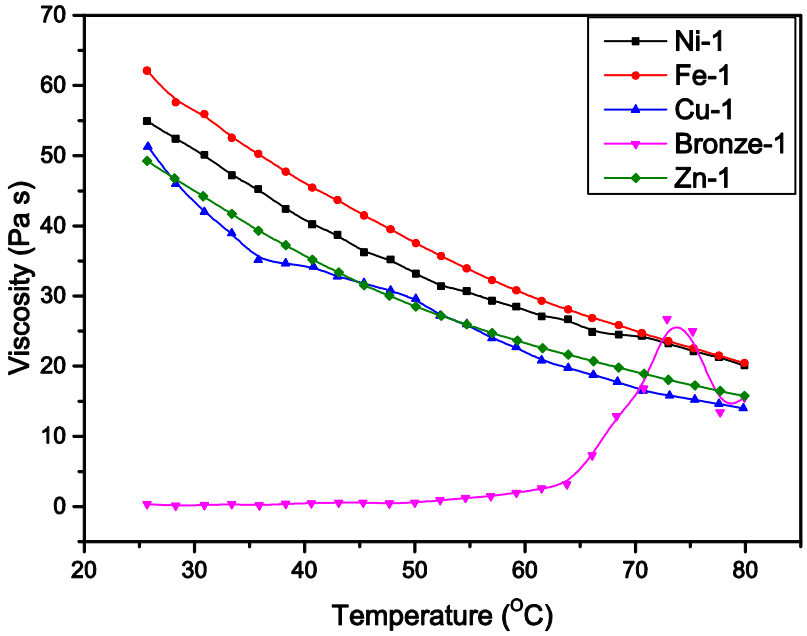

Figure 5.3 Viscosity vs. temperature profile of the different ink formulations, each containing the PVP polymeric binder

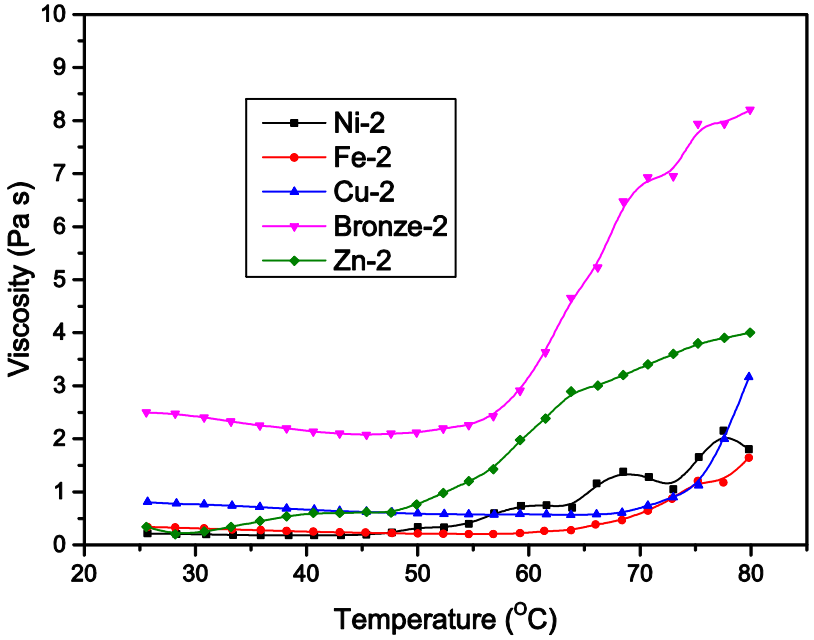

Figure 5.4 Viscosity vs. temperature profile of the different ink formulations, each containing the PVP-S polymeric binder

5.3.3 Electrical resistance properties of the inks

All of the ink prints that were formulated containing Cu powder, Bronze powder and Zn powder were found to possess electrically insulating behaviour. Up to 5 kg of compression that was applied to each of the printed films does not cause any conductivity in the materials. On the basis of the insulating property of these printed films, only the electrical properties of Ni powder-based printed films and Fe powder-based printed films were further investigated.

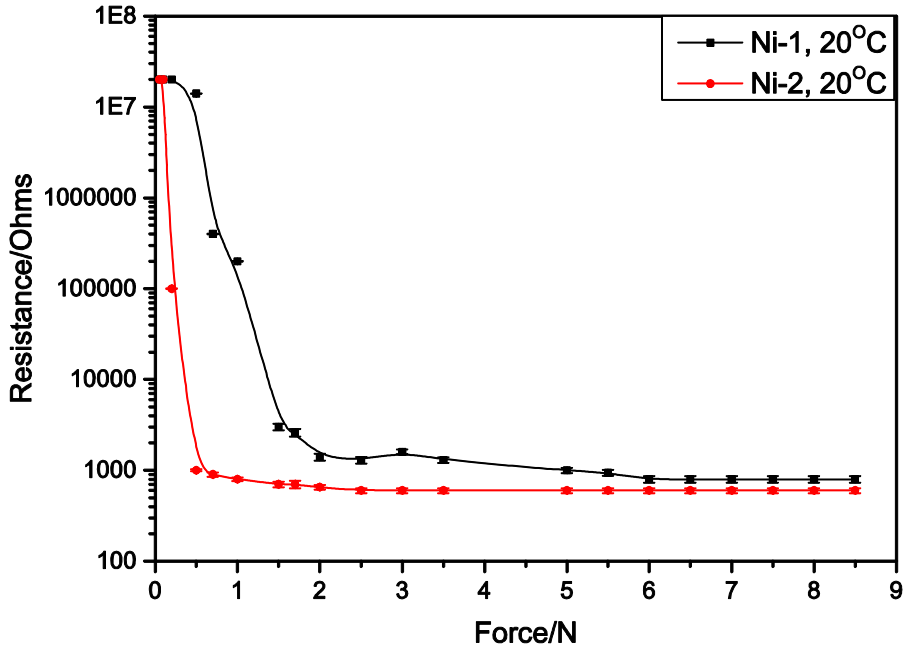

Figure 5.5 Electrical properties of Ni powder-based inks that containing PVP binder and containing PVP-S binder

Both the Ni powder-based ink prints and the Fe powder-based inks have exhibited pressure electrically sensitive properties, as shown in Figure 5.5 to Figure 5.7. As a result, the electrical resistance of the printed films changes exponentially with increasing applied force. However, both printed films were electrically insulating when no pressure was applied to their surfaces. After the increasing pressure was applied, the printed films changed from insulating behaviour to conductive characteristic. Ni-1 based printed films showed controlled electrically sensing behaviour and Ni-2 based printed films behave more like electrically switching materials. Electrical sensing behaviour means that the resistance gradually changes with an increasing force. Electrical switching behaviour means

that the resistance rapidly changes with increasing force. The two contrasting behaviour shown by two Ni powder-based printed films arises because of the nature of the polymeric binders that two inks contain, *i.e.* PVP and PVP-S. The characteristics of the two different polymeric binders (PVP and PVP-S) are discussed in the next section.

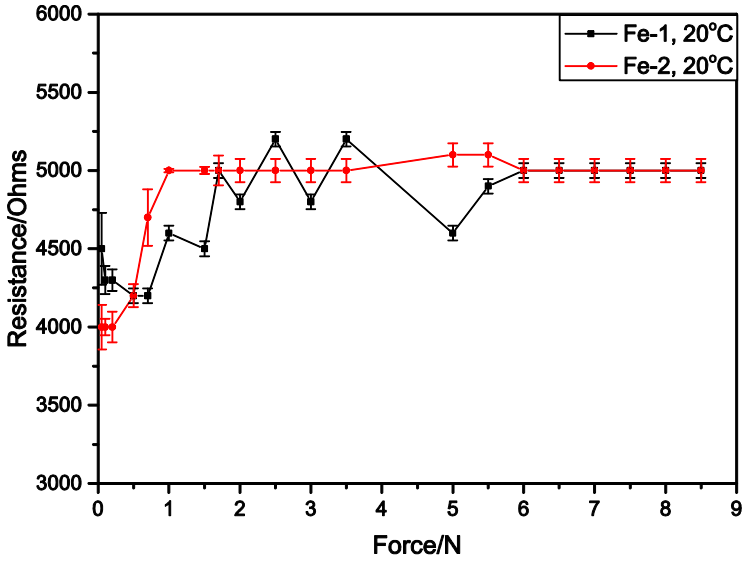

Figure 5.6 Electrical properties of Fe powder-based inks that containing PVP binder and containing PVP-S binder

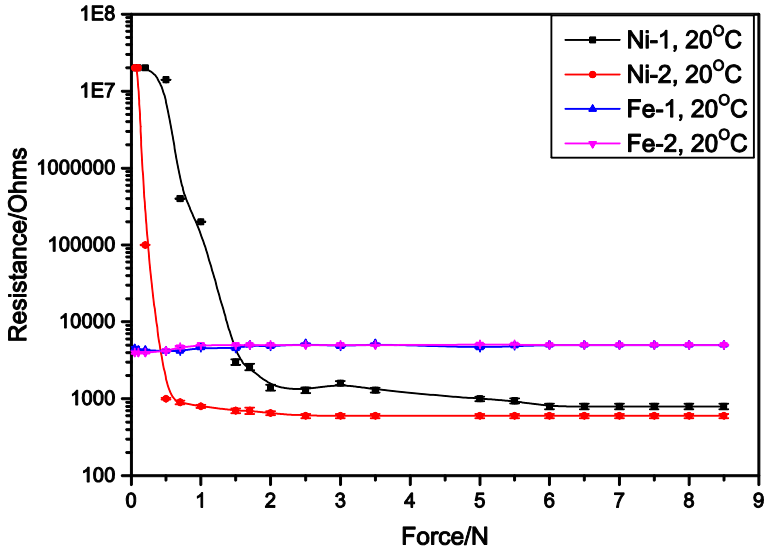

Figure 5.7 Comparisons of electrical properties of Ni powder-based printed films and the Fe powder-based printed films, which containing PVP binder and containing PVP-S binder

Both Fe powder-based printed films have shown that the electrical properties of the printed films change with the applied force. The printed films have behaved electrically conductive when no pressure was applied. However, the resistance values have fluctuated with changing applied forces. This is because of the characteristics of the metallic Fe powder in comparison to the Ni powder material and difference shown the particles of each material as discussed with respect to Figure 5.1.

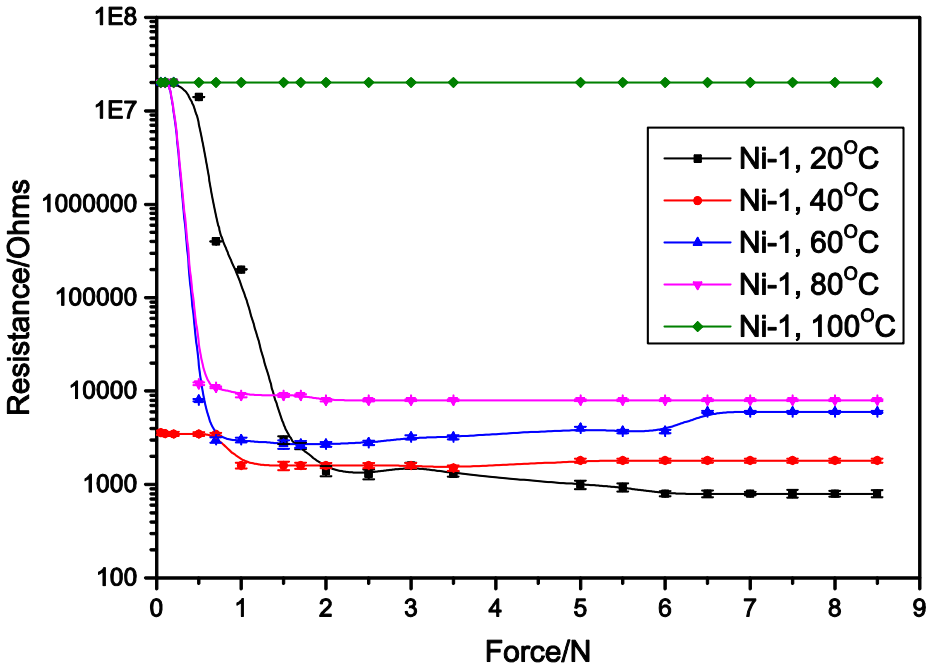

Figure 5.8 Resistance vs. force plots for the printed films that contained Ni powder and that were dried at different temperatures. Each contains the PVP polymeric binder

With respect to Figure 5.8 and Figure 5.9, the temperature at which the printed films were dried has an effect on the electrical characteristics of the inks. Drying the printed films at 100 °C makes them less conductive (highest values of resistivity) compared to the conductivity of the printed films after drying at 20 °C. In particular, after drying at 100 °C, the Ni-1 printed film has lost its switch characteristic as can be seen by the linearity of the Ni-1 printed film plot, in Figure 5.8. It can be said that the higher the drying temperature, the less flexible are the ink prints and as such the electrons in the print have lesser ability to move and generate current.

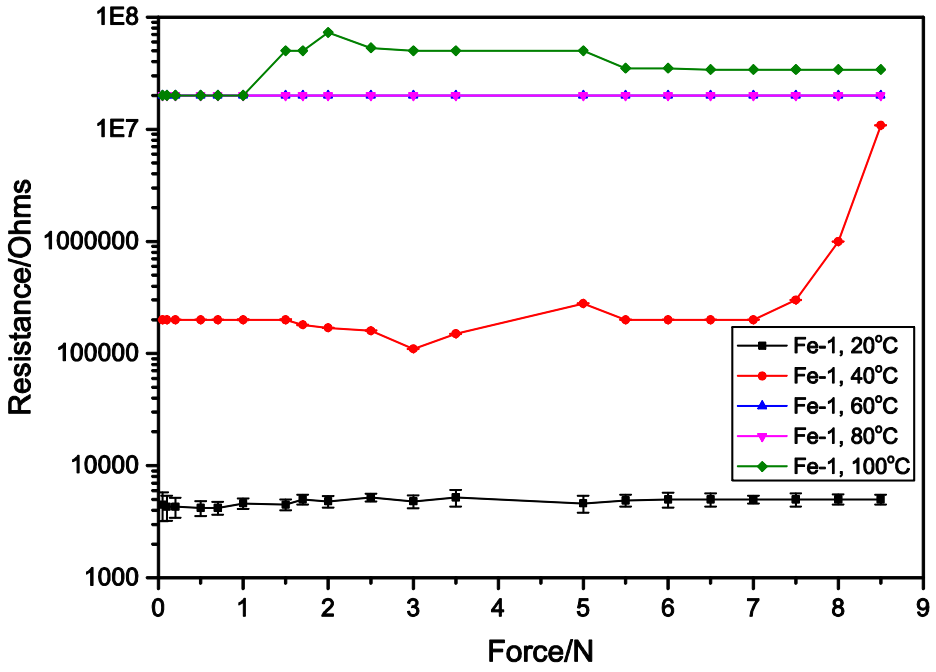

Figure 5.9 Resistance vs. force plots for the printed films that contained Fe powder and that were dried at different temperatures. Each contains the PVP polymeric binder

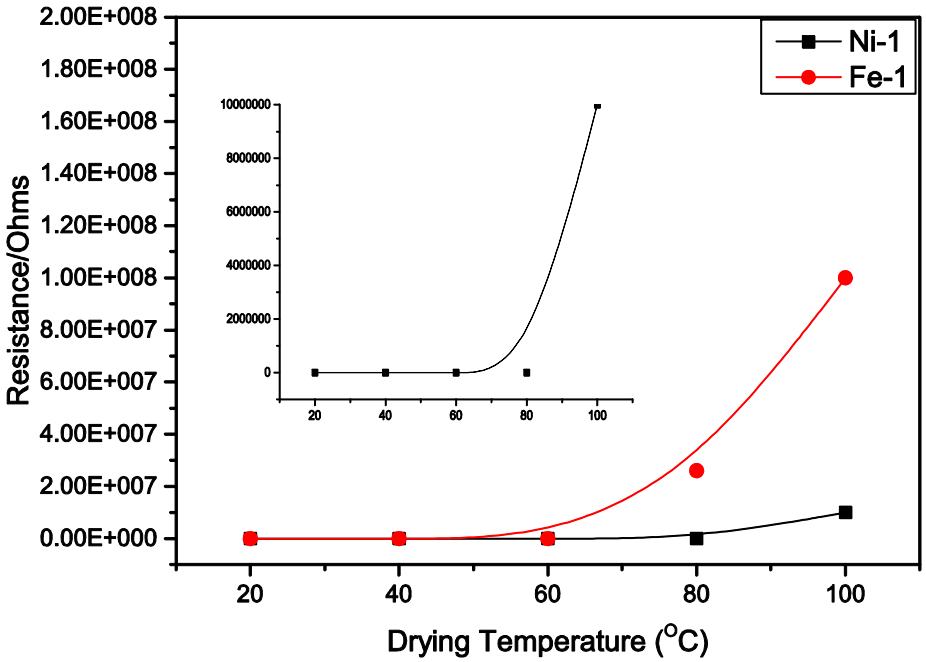

Figure 5.10 Plot of the relationship between resistance and drying temperature, from printed films that were formulated containing either with Ni powder or with Fe powder. Both inks contain the PVP polymeric binder

As shown in Figure 5.10, the resistivity of the printed films increases exponentially with an increase in the drying temperature. This associated with an increase in the extent of drying in the inks as the temperature was increased. Therefore, as more structure was formed in the inks, as the temperature increases, the ability/mobility of the electrons is affected. The results show that for any intended application, the temperature at which the inks are dried is of paramount importance. This choice of temperature will not only affect the conductivity of the inks, but will also affect their mechanical properties such as the flexibility. Also, producing ink prints with too much hardness and reduced flexibility might cause cracks or gaps in the printed films which will in turn restrict the movement of the electrons in such inks.

5.3.4 Thermal properties of the PVP and the PVP-S-based inks

Decomposition arising during the TGA induced breakdown of the polymeric binders is shown in Figure 5.11. Differences in the thermal stability can be seen between the two polymeric binders. The extent to which the PVP-S binder holds onto water was greater than that shown by the PVP polymeric binder. The overall thermal stability of the binders is similar. In the TGA profile of each binder, each thermogram indicates a curve which can be correlated to loss of water as the heating temperature was increased up to around 100 °C and 150 °C for PVP binder and for PVP-S binder, respectively. This is then followed by any self-crosslinking reactions that take place up to around 400 °C. Comparison of the self-crosslinking curve in Figure 5.11, for each polymeric binder with Figure 5.10 will suggest that the properties of each ink can vary with the temperature of drying or curing.

It was discussed with respect to Figure 5.3 and Figure 5.4, that, the rheological properties of the ink formulations can be affected by the temperature of flow or temperature of application. Considering the fact that PVP-S polymeric binder has shown greater affinity to solvent components (Figure 5.11) and has a less intense endothermic peak (Figure 5.12, 80 °C to 200 °C), this can allow greater extent of structure formation in those inks containing the PVP-S binder in comparison to those containing the PVP binder. This therefore resulted in differences in viscosity *vs.* temperature trends between the two sets of inks. This

point can be explored further where application temperatures on such inks are intended to be studied in more details.

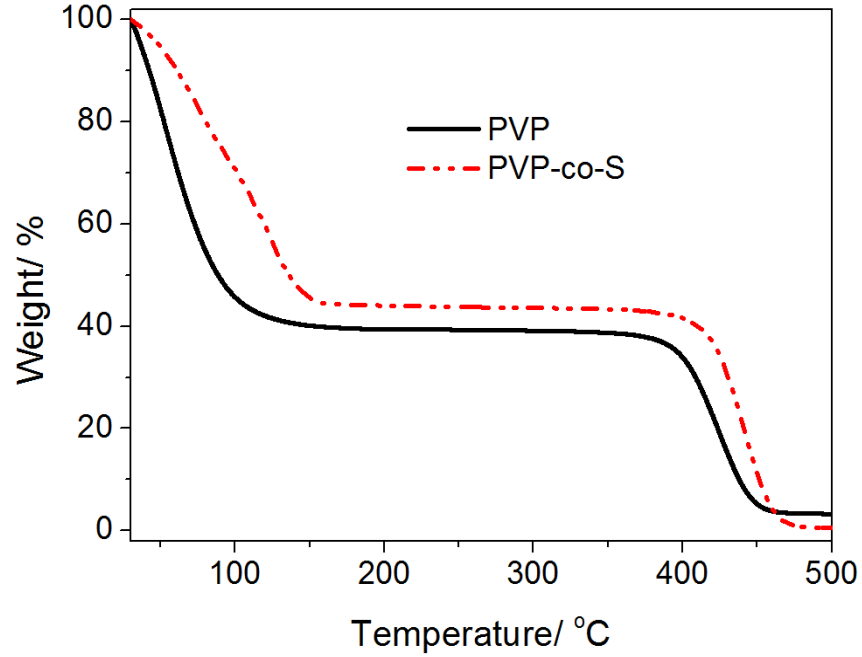

Figure 5.11 TGA, 10 °C/min plots of the polymeric binders that were used in formulating the inks, PVP binder and PVP-S binder

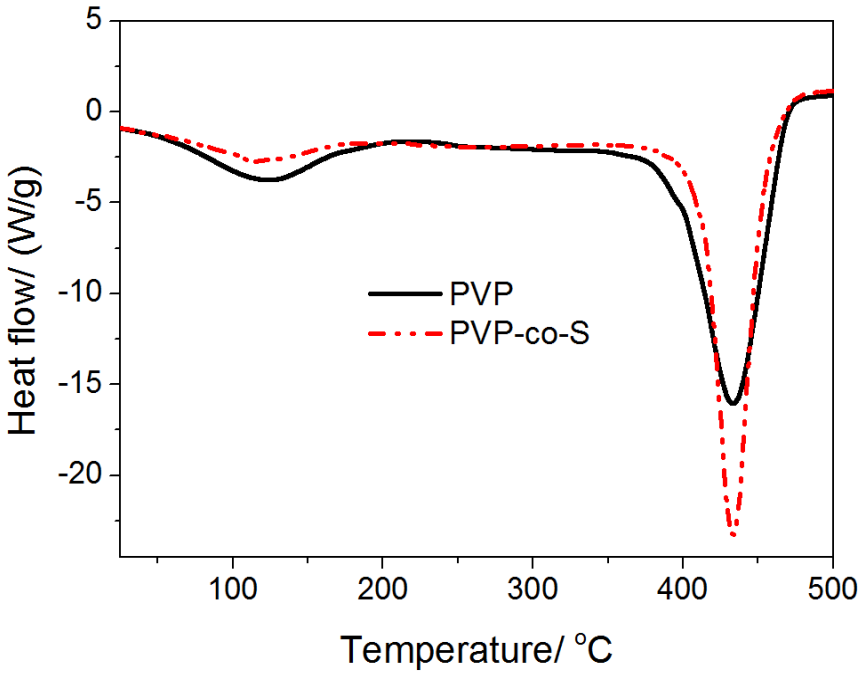

Figure 5.12 DSC, 10 °C/min plots of the polymeric binders that were used in formulating the inks, PVP binder and PVP-S binder

The problems that can be encountered when using the inks on PET substrate include spreading problem and blistering of thick films. With respect to some of the inks that were formulated containing the Fe powder, applied onto the two substrates, delamination of the printed films was encountered. Since the inks were formulated containing water as solvent, the aspects of dried ink delamination can be related to the wetting character of the inks on the surface of the substrates. Water has a surface tension value of 72 mNm^{-1} and PET substrate is known to have low surface energy values. However, the wettability of the inks on the PET substrates can be enhanced by employing appropriate surface energy pre-treatment procedures [159].

From the drop test measurements, the contact angle of water on PET was found to be 73.5°. In contrast, the contact angle of the same solvent on the carbon board substrate was 50°. A proportion of the ink on the carbon board substrate must be adsorbed during the wetting process and this must have enhanced the overall adhesion of the inks on the substrate.

5.4 Conclusions

Ink formulations and printed inks were successfully developed based on the use of different options of metallic powder particles. The choice of polymeric binder has a significant effect on the rheological properties of the inks but had limited effect on the electrical properties of the inks. The choice of polymeric binder in formulation and the choice of substrate in application also affect the printed film property. The electrical properties of the Ni powder containing printed films and the Fe powder containing printed films depend on the temperature at which the inks were dried. Conductivity of the inks generally decreased with an increase in the drying temperature. None of the inks that were formulated on the basis on the Cu, the bronze and the Zn metallic powders showed any desirable electrical conductivity properties. Such inks electrically insulated and were not found to have any potential for use in pressure sensitive electrical devices in contrast to those inks that were formulated and applied based on the Ni metallic powder and the Fe metallic powder.

Reference

1. Gündüz, G., *Chemistry, Materials, and Properties of Surface Coatings: Traditional and Evolving Technologies*. 2015: **54**(9), p: 134 – 156.

2. Wolf, R. and A.C. Sparavigna, *Role of plasma surface treatments on wetting and adhesion.* Engineering, 2010. **2**(06): p. 397.

Chapter 6. Conclusions and Future Work

The work of this thesis formulated a range of screen printable functional inks, each containing a combination of conductive spiky-like nickel particles, three grades of semiconducting titanium dioxides particles and several water-based binders. A number of pressure-sensitive printed films from the formulated inks were successfully developed. In order to understand these electrical properties, printability, rheology, thermal stability and mechanical properties of a printed film on the basis of the contribution by each component to the formulation were carefully investigated. The results showed that the printed film behaved as an insulator in the absence of an external compression, even when the nickel filler content was well above the expected percolation threshold. The electrical resistance of the printed film decreased, up to 10 orders of magnitude, with an increase in external compression. This dramatic resistance variation was explained by the quantum tunnelling mechanism and percolation mechanism, which were mainly dependent on the distribution of the nickel particles and nickel aggregates, the nickel loading, the morphology of the nickel particles and the elasticity of a polymer matrix.

The electrical properties of screen printable printed films have been successfully altered by the addition of TiO_2. The loading of TiO_2 had a significant effect on modifying the printed films from being electrically switching to showing electrically sensing behaviour. This has also assisted the printed films to have electrically insulating property when no pressure was applied. It was found that the anatase form of TiO_2 had a significant effect on the electrical properties of the final printed films due to its large specific surface area.

Moreover, a model of the response of the electrical properties to the external compression for the printed QTC films had been successfully developed, which permitted quantification of the relationship between the electrical property and the structure of the composite. This model was the most applicable to the printed composite film for the prediction of the electrical-mechanical property of the nickel particles randomly dispersed in a polymeric matrix.

Ink formulations and printed inks were successfully developed based on the use of different options of metallic powder particles. The choice of polymeric binder has a significant effect on the rheological properties of the inks but had limited effect on the electrical properties of the inks. The choice of polymeric binder in formulation and the choice of substrate in application also affect the printed film property. The electrical properties of the Ni powder containing printed films and the Fe powder containing printed films depend on the temperature at which the inks were dried. Conductivity of the inks generally decreased with an increase in the drying temperature. None of the inks that were formulated on the basis on the Cu, the bronze and the Zn metallic powders showed any desirable electrical conductivity properties. Such inks electrically insulated and were not found to have any potential for use in pressure sensitive electrical devices in contrast to those inks that were formulated and applied based on the Ni metallic powder and the Fe metallic powder. However, the Fe-based printed film did not behave any similarity as the QTC commercial material.

A number of areas were outlined throughout the thesis as opportunities for future work. The most significance of this included investigation of electrical properties of different ink formulations and binding polymer types that used to further investigate the relationship between metal fillers and polymers. For the further work, it might involve the study of the contribution of the extent of the surface treatment on electrical-mechanical properties of printed films. Also, the addition of different additives might use to optimise the electrical properties of printed films regarding to employ them in different applications.